Carbon Nanofibers as Catalyst Support for Noble Metals

Marjolein Toebes

ISBN 90-393-3588-5

Cover lay-out by Jan den Boesterd, AV-dienst, Faculteit Scheikunde, Universiteit Utrecht

Drukkerij Ponsen & Looijen, Wageningen

Carbon Nanofibers as Catalyst Support for Noble Metals

Kooldraden als Dragermateriaal voor Edelmetaalkatalysatoren

(met een samenvatting in het Nederlands)

Proefschrift

ter verkrijging van de graad van doctor aan de Universiteit Utrecht
op gezag van de Rector Magnificus, Prof. Dr. W.H. van Gispen, ingevolge het
besluit van het College voor Promoties in het openbaar te verdedigen op
maandag 9 februari 2004 des middags te 14:30 uur

door

Marjolein Lizette Toebes

geboren op 23 juli 1975, te Winterswijk

Promotoren: Prof. dr. ir. K.P. de Jong
Faculteit Scheikunde, Universiteit Utrecht

Prof. dr. ir. D.C. Koningsberger
Faculteit Scheikunde, Universiteit Utrecht

Co-promoter: Dr. A.J. van Dillen
Faculteit Scheikunde, Universiteit Utrecht

The research described in this thesis was financially supported by the Council for Chemical Sciences of the Netherlands Organization for Scientific Research with financial aid from the Netherlands Technology Foundation (CW/STW 349-5357).

**Never mistake knowledge for wisdom.
One helps you make a living; the other
helps you make a life.**

Sandra Carey

Promotiecommissie

Promotoren:	Prof. dr. ir. K.P. de Jong (Universiteit Utrecht) Prof. dr. ir. D.C. Koningsberger (Universiteit Utrecht)
Co-promoter:	Dr. A.J. van Dillen (Universiteit Utrecht)
Leescommissie:	Prof. dr. F.H.P.M. Habraken (Universiteit Utrecht) Prof. dr. J.J. Kelly (Universiteit Utrecht) Prof. dr. H.N.W. Lekkerkerker (Universiteit Utrecht)
Overige leden:	Dr. J.H. Bitter (Universiteit Utrecht) Prof. dr. ir. L. Lefferts (Universiteit Twente) Dr. H. Oevering (DSM Research)

Contents

1

General Introduction

Introduction

According to the definition of Berzelius a catalyst is a substance that accelerates the establishment of a chemical equilibrium without itself being consumed [1]. Nowadays, catalysts have a significant impact on society as they are used for the efficient and environmentally benign preparation of useful and valuable products. Supported metal catalysts are important both from an industrial and a scientific point of view. They are used, amongst others, in processes such as catalytic reforming, hydrotreatment, polymerization reactions and hydrogenations. In general, these catalysts consist of nanosized metal particles deposited on an oxidic support, the metal particles expose the active sites whereas the support acts as an anchor for these particles, thus preventing sintering. In addition, the support can in some cases contribute to a certain extent to the reaction network.

The major part of the (industrially) utilized support materials are refractory oxides, like silica (SiO_2) and alumina (Al_2O_3) because these materials are porous, thus have a large accessible surface, are mechanically strong and thermally stable. Moreover, they can be shaped into macroscopic dimensions [2], which is required for application in industrial reactors. Oxidic supports and the application of an active phase on these materials have been investigated extensively and a large number of methods have been developed to produce catalysts with reproducible catalytic properties. Initially, naturally occurring oxides like Kieselguhr (diatomite, amorphous silica) [3] and zeolitic minerals [4] were used. For example, the common Fischer-Tropsch catalyst used during World War II to produce transport fuels from CO/H_2 mixtures was based on cobalt supported on Kieselguhr [5,6]. Later on, synthetic oxide supports such as silica gel and γ-alumina were used. Advanced microporous (zeolite-type materials) and, since the 1990s, ordered mesoporous solids (*e.g.* MCM-41 and SBA-15) also comprise a class of oxidic supports with emerging significance [2,4].

Recently, carbon supports have attracted much interest. Carbon materials are often used because of their high surface area and chemical inertness, which is of special importance in strongly basic and acidic environments. For gas-phase applications the high thermal stability related to the high melting point is of relevance. In addition, the possibility to oxidize the support to CO_2 makes an easy recovery of the metal from the spent carbon-based catalyst possible [2,7]. However, knowledge of carbon supports and the preparation of carbon-supported catalysts is relatively limited. Due to their favorable costs and high surface area the most commonly used carbon supports are activated carbons. These materials are produced from natural materials such as coconut shells or wood, consequently they contain impurities and display an inhomogeneous texture. Because of this, control during the application of the active components and their use in catalysis is limited [2,7-9].

Notably for catalysis well-defined, pure carbon supports and suitable preparation methods are indispensable. Carbon materials that do not suffer from the above-mentioned drawbacks

are synthetic carbon compounds such as carbon nanofibers (CNF), carbon nanotubes (CNT), single-walled carbon nanotubes (SWNT) and highly ordered pyrolytic graphite (HOPG). Especially CNF can be produced at relatively low costs with a high yield and are therefore suitable as catalyst support material [10]. They can be prepared in a reproducible manner, with tunable properties, making these fibers a support with great potential. However, a fundamental understanding of either the preparation of CNF-supported metal catalysts and insight in their catalytic behavior is still lacking.

Aim of the research described in this thesis is to prepare CNF-supported platinum and ruthenium catalysts with different support properties (*viz.* oxygen groups) and to gain insight in the influence of these support properties on catalyst activity and selectivity during hydrogenation reactions.

In this chapter some background information will be given concerning the key issues of the preparation and testing of metal/CNF catalysts in the selective hydrogenation of cinnamaldehyde. First, we will deal with the nomenclature, the history and synthesis of CNF. In addition, the possibilities of tuning the properties of CNF will be discussed. Next, a brief overview of catalyst preparation methods suitable for the reproducible synthesis of CNF-supported noble metal catalysts will be given.

A sensitive test reaction is needed in which the influence of the catalyst properties on activity and selectivity can be observed. We have chosen for the selective hydrogenation of cinnamaldehyde. A brief literature survey on the mechanism and the effect of the type of metal, the metal particle size and the type of support in the hydrogenation of cinnamaldehyde over carbon-supported catalysts will be presented in this chapter.

Carbon nanofibers

Nomenclature

The nomenclature of CNF and related materials is ambiguous. Therefore the names for these compounds used in this thesis are clarified and various synonyms are given. The three main types of CNF-related materials are shown in Figure 1. In carbon nanofibers (CNF) the graphitic planes are oriented at an angle to the central axis, thus exposing graphite edge planes. Alternative names for this material are fishbone CNF, herringbone CNF, carbon filaments and carbon fibrils. Besides the CNF in which the graphite planes are stacked in a “fishbone” way, also other graphitic orientations, such as “ribbon” and “platelet” are reported in literature [11]. The second type are the carbon nanotubes (CNT). In CNT the graphitic planes run parallel to the central axis, implying that in this compound only basal planes are exposed. These materials are also referred to as multi-walled carbon nanotubes (MWNT) or parallel carbon nanofibers. If the fiber consists of only one graphene sheet that is oriented in a parallel way to the fiber axis it is called a single-walled carbon nanotube (SWNT).

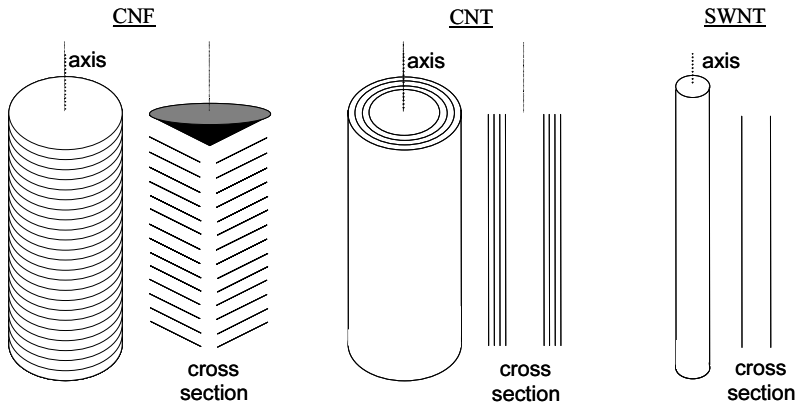

Figure 1. Schematic presentation of carbon nanofibers (CNF), multi-walled carbon nanotubes (CNT) and single-walled carbon nanotubes (SWNT).

History and applications

The history of graphitic carbon nanofibers (CNF) goes back to more than a century. The first patent describing the production of carbon filaments was already published in 1889 [12]. For the first 80 years of the last century the growth of CNF was mainly considered a nuisance. The fibers were often formed in metal-based catalysts used for the conversion of carbon-containing gases, like in Fischer-Tropsch syntheses or steam reforming reactions. The metals used in these reactions catalyze CNF growth. Besides the loss of catalyst activity and the deterioration of catalyst pellets also the metallic reactor walls can be damaged severely. Therefore, detailed studies on the nucleation and growth of CNF were carried out in those early days in order to prevent the formation of fibers during industrial processes [10].

Starting from the 1980s researchers realized the potential of CNF [13] and CNT [14] as unique materials suitable for various applications. As a consequence, research also focused on controlling the growth and properties of CNF instead of suppressing CNF formation. Nowadays, CNT are commercially applied for the prevention of electrostatic charging of cling films and other polymer objects [10]. Currently, a lot of research is focused on the use of CNF and CNT as catalyst support material (*vide infra*).

Growth of CNF

The production of reactive carbon intermediates from a carbon source is a crucial step in the synthesis of CNF. This can be achieved by activation of graphite by laser vaporization [15], by electric arc-discharge [16,17] or by the dissociation of a carbon-containing gas (*e.g.* CH_4, CO and C_2H_4) on the surface of a suitable metal catalyst like Ni, Fe or Co [10,18-23]. Only with the latter route, the catalytic synthesis route, very pure carbon nanofibers can be produced in large quantities, while tuning of physico-chemical properties like surface structure, mean diameter, density and morphology is possible.

The mechanism of the catalytic growth of CNF has been studied for a long period of time. Although consensus has been reached with respect to the different growth steps [10], still

uncertainties exist about some details.

A schematic representation of the mechanism of steady-state growth of fishbone-type fibers is given in Figure 2 and is based on the review by De Jong and Geus [10]. Carbon-containing gases are decomposed on the metal surface. During this process carbon atoms are deposited on the surface with the concomitant release of gaseous products like molecular hydrogen, carbon dioxide and water, depending on the carbon-containing gas used. The carbon atoms dissolve in and diffuse through the bulk of the metal particle, although some contribution of surface diffusion cannot be excluded. The carbon atoms are precipitated in the form of a CNF consisting of graphite layers at the other side of the metal particle. The thermodynamic driving force for CNF production is the formation of graphite out of carbon containing gas [10,24].

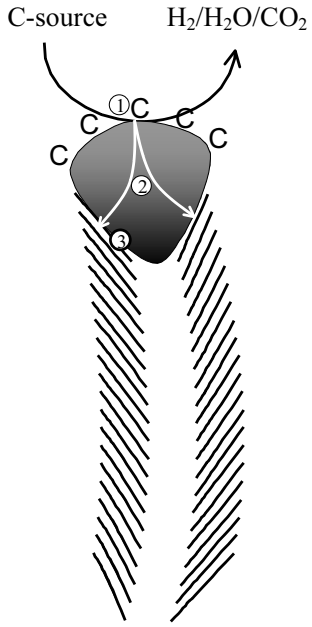

Figure 2. Schematic representation of the catalytic growth of a CNF using a gaseous carbon-containing gas. Step ①, decomposition of carbon-containing gases on the metal surface. Step ②, carbon atoms dissolve in and diffuse through the bulk of the metal. Step ③, precipitation of carbon in the form of a CNF consisting of graphite [10].

The diameter of the resulting fibers is usually in the range of 15-50 nm and is to some extent controlled by the size of the metal particles from which the CNF start to grow [18,22].

Up to now a major disadvantage of applying CNF has been the production of this material in sufficient large quantities at reasonable costs. However, these drawbacks might be overcome due to the development of fluidized bed technology for large-scale production [10,25]. Production-cost estimates have shown that CNF might be obtained at costs less than 10 US$/kg when grown in large volumes in a fluidized bed [10].

Potential of CNF as catalyst support

Potentially CNF have unique properties for use as catalyst support material. They have a relatively large and accessible external surface area (100 - 200 m^2/g), a graphitic structure, they do not contain impurities (such as sulfur or other inorganic impurities) and they are chemically inert. CNF used in this study have a diameter of 20-30 nm and because the fibers interweave during growth, larger bodies containing meso- and macropores are obtained. So, no micropores are present that at forehand can give rise to diffusion problems of reactants and/or products. All these features are essential, especially for use in the liquid-phase.

Certain characteristics of the fibers can be tuned by adaptation of the synthesis conditions (T, P and time), choice of the growth metal, the metal particle size, the support and the carbon source. The first variable is the orientation of the graphitic planes in either a fishbone (CNF) or a parallel way (CNT) [26,27]. Secondly, the fiber diameter and length can be tailored. Also the macroscopic structure that arises from interweaving of the fibers is tunable, which influences the strength and accessibility of the CNF bodies [10,24].

After growth of the CNF the non-polar surface of the graphitic CNF can be changed by the introduction of oxygen-containing groups by treatment of this material with an oxidizing agent, *e.g.* nitric acid. These groups ensure wettability with water and other polar solvents and enable the anchoring of an active phase or its precursor [7,9,28,29]. The precise nature of carbon-oxygen structures has not been entirely established, but the results of many studies using FT-IR spectroscopy, Boehm-titrations and TPD measurements demonstrate that several types of surface oxygen groups can be distinguished [7,9,28,30], as shown in Figure 3.

These oxygen-containing surface groups can be acidic, neutral and basic in nature. In water, depending on the pH, they can be neutral, negatively or positively charged. At $pH>pH_{IEP}$ (iso-electric point ≈ 2-3) the carbon surface, covered by deprotonated acidic carboxylic groups, will mainly adsorb cations from the precursor solution; whereas at $pH<pH_{IEP}$ chiefly anions will be adsorbed [7,31]. Thus, when preparing a supported catalyst, one needs not only physically accessible sites but also affinity towards the metal precursor. Electrostatic repulsion between the charged surface and the ionic catalyst precursors may be stronger than the non-specific attractive dispersion forces, resulting in a loss of dispersion [7].

The use of CNF and related materials as catalyst support has been investigated before. Commonly used metals like Pt, Pd, Ru, Fe, Co and Ni have been applied on CNT or CNF and tested in various reactions, such as in selective hydrogenations (Table 1).

In order to study the effect of the surface properties of CNF on the catalytic behavior of CNF-supported noble metal catalysts a reproducible preparation procedure is required that results in a catalyst with a homogeneous distribution of small metal particles displaying a narrow particle size distribution. Most of the catalysts listed in Table 1 do not meet these requirements. Therefore a suitable preparation method will be discussed in the next paragraph.

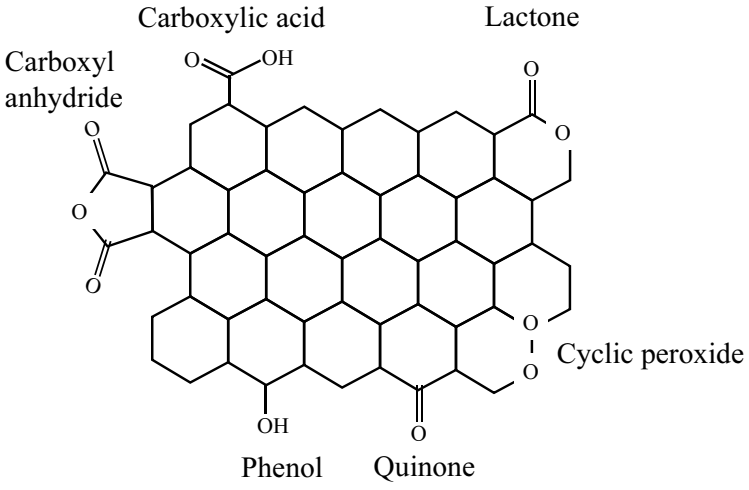

Figure 3. Different types of oxygen-containing surface groups on graphitic carbon, adapted from [30].

Table 1. Survey of catalysts prepared on a CNF support or related material.

Metal	Support	Preparation method	Test reaction	Ref.
Pt	CNF*	impregnation	n-hexane skeletal reactions	[11]
	CNF*	impregnation	fuel cell methanol oxidation	[32]
Pd	CNT	ion exchange	nitrobenzene hydro#	[24]
	CNT	deposition reduction	nitrobenzene hydro	[33]
	CNF	impregnation	cinnamaldehyde hydro	[34,35]
Pt/Ru	CNF	adsorption	fuel cell methanol oxidation	[36]
	CNT	adsorption	-	[37]
Ru	CNT	adsorption	cinnamaldehyde hydro	[38]
	Fullerene (C_{60})	impregnation	2-cyclohexenone hydro	[39]
	Fullerene (C_{60})	impregnation	cinnamaldehyde hydro	[40]
Fe	CNT	impregnation	ethylene hydro	[20]
	CNT	impregnation	Fischer-Tropsch	[41]
	CNT	deposition precipitation	Fischer-Tropsch	[41]
Co	CNT	impregnation	cyclohexanol dehydro	[42]
Ni	CNF	impregnation	methane decomposition	[43]
	CNF*	impregnation	crotonaldehyde hydro	[44]
	CNF*	impregnation	1-butene and 1,3-butadiene hydro	[27,45]
	CNT	electroless plating	-	[46]
	CNF	homogeneous deposition precipitation	-	[47]

* CNF with various graphitic orientations (ribbon, platelet)

(de)hydro = (de)hydrogenation

Preparation of noble metal catalysts using ion exchange

In literature various methods have been presented to apply an active phase on CNF and related materials, mostly incipient wetness impregnation [*e.g.* 34,40,42,45], but also wet impregnation/adsorption [*e.g.* 38], ion exchange [*e.g.* 24] and electroless plating [*e.g.* 46]. Using adsorption Planeix *et al.* [38] have applied 0.2 wt% ruthenium on CNT, resulting in relatively large ruthenium particles ranging from 3 to 7 nm. When nickel (5 wt%) is deposited on CNF *via* incipient wetness impregnation, particles in the range of 2-22 nm with an average size of 8 nm are found [27]. Using ion exchange, however, Hoogenraad *et al.* [24,33] have succeeded in the application of small palladium particles (1-1.5 nm) on CNF with a maximum metal loading of 3 wt%. Therefore, for the preparation of CNF-supported noble metal catalysts for liquid-phase applications with a relatively low metal loading displaying

both a high dispersion and a narrow particle-size distribution, ion exchange seems the best option. However, catalysts prepared using this method sometimes suffer from inhomogeneities in the metal distribution as will be discussed in more detail later on. Here, we briefly review the key steps in the ion exchange procedure to overcome this problem.

Ion exchange allows for the introduction of a precursor (ion) from aqueous solution onto a support in a controlled way and is usually followed by drying, calcination and reduction steps. The term ion exchange is used to describe processes where ionic species are attracted (electrostatically) to charged sites on the support surface [30]. It is still uncertain which step in the procedure is predominantly responsible for the ultimate size and distribution of the metal particles. Nonetheless, the distribution of the precursor of the active component as accomplished in the exchange step determines to a large extent the final result. The maximum loading depends on the number and nature of the adsorption sites, the pH of the solution, the speciation of the precursor species and the presence of other competing species that may adsorb on the same sites [2].

Several mechanisms for the adsorption of precursor ions from solution onto the support surface can be found in literature. Spieker and Regalbuto [48] have extensively studied the adsorption of chloroplatinic acid onto alumina and developed the Revised Physical Adsorption (RPA) model. Their model implies that adsorption is based purely on physical (coulombic) and not on chemical interactions. This type of adsorption is also referred to as the formation of outer-sphere complexes. The precursor ions are adsorbed on the surface according to a Langmuir adsorption isotherm with a maximum adsorption capacity resembling a closed-packed monolayer of adsorbates retaining one or several hydration shells. The RPA model can also be applied to carbon supports with some minor revisions to reflect the more complex chemistry of the carbon surface [49].

Another way of creating an interaction between a transition metal precursor complex and the surface is a true ionic exchange. Adsorbed complexes in electrostatic interaction with the surface can substitute some of the original ligands by ‘surface ligands’. The resulting inner-sphere complexes are then chemically bonded to the surface [50,51].

As mentioned before, next to the exchange step in the preparation, which is important to obtain an atomic distribution of the metal precursor over the support, the subsequent drying, calcination and reduction steps are also crucial for the preparation of a highly dispersed catalyst. For example, De Graaf *et al.* [52] have shown that a very low heating rate during calcination is essential to obtain small platinum particles in zeolite Y using ion exchange.

The above could lead to the conclusion that with the ion exchange technique precursor species can be applied easily and that dispersions will be high, provided that the number of adsorption sites and the strength of interaction are high. But reality is different, predominantly with porous support bodies. If the interaction between the precursor and the support is strong and adsorption is fast, ion exchange often results in inhomogeneous distributions, especially when a precursor has to be applied in amounts lower than that corresponding to saturation [2]. On their way into the support body the precursor ions become

mainly adsorbed in the outer layer of the support and an eggshell distribution results, which is not always desired. A well-known example of this phenomenon is the preparation of Pt/γ-Al_2O_3 catalysts by ion exchange using chloroplatinic acid as precursor. In this case a homogeneous distribution over the support body can only be obtained if hydrochloric acid is added to the impregnate: due to the competitive adsorption of $PtCl_6^{2-}$ and Cl^- ions the platinum precursor penetrates deeper into the support body and a reasonable distribution is obtained [2]. Even with the carefully prepared EUROPT-1 catalyst, *i.e.* Pt/SiO_2 prepared *via* ion exchange using $Pt(NH_3)_4^{2+}$ with a loading of 6.3 wt%, some inhomogeneities in the distribution were observed [53]. In part of the samples platinum particles were clustered together like the fruit in a bunch of grapes and sometimes areas of silica were observed with no platinum particles at all.

We therefore explored an alternative technique for the deposition of noble metals on CNF to further improve the homogeneity of the resulting catalysts. Subsequently, the performance of these catalysts was tested in the hydrogenation of cinnamaldehyde.

Selective hydrogenation of cinnamaldehyde

The selective hydrogenation of α,β-unsaturated aldehydes is an important area in the fine chemical industry. These conjugated molecules contain an olefinic bond (C=C) as well as a carbonyl group (C=O). Cinnamaldehyde (3-phenyl-2-propenal) is an example of such an α,β-unsaturated aldehyde. The selective hydrogenation of the carbonyl group yielding the unsaturated alcohol is of special interest, because of the importance of these alcohols in the preparation of compounds used in perfumes, flavorings and pharmaceuticals. For instance, cinnamyl alcohol is utilized as a modifier in berry, nut and spice flavor systems and used in blossom compositions [54,55].

The selectivity in this reaction can be tuned by, amongst others, choice of the active metal and the nature of the support in such a way that a shift occurs from the thermodynamically more favorable saturated aldehyde towards the desired unsaturated alcohol [56].

A few review papers have been published with respect to group 8-10 metal catalysts in the hydrogenation of α,β-unsaturated aldehydes using oxidic supports [56-60]. In the next paragraphs a summary of the literature on carbon-supported catalysts with Pt, Pd, Rh and Ru as the active metal in the hydrogenation of cinnamaldehyde will be given. Several parameters that influence the selectivity and activity of the reaction will be discussed. First, the reaction scheme and relevant modes of adsorption will be presented.

Reaction network

A reaction network of the commonly observed intermediates and products for the hydrogenation of cinnamaldehyde (CALD) is shown in Figure 4. The main products are

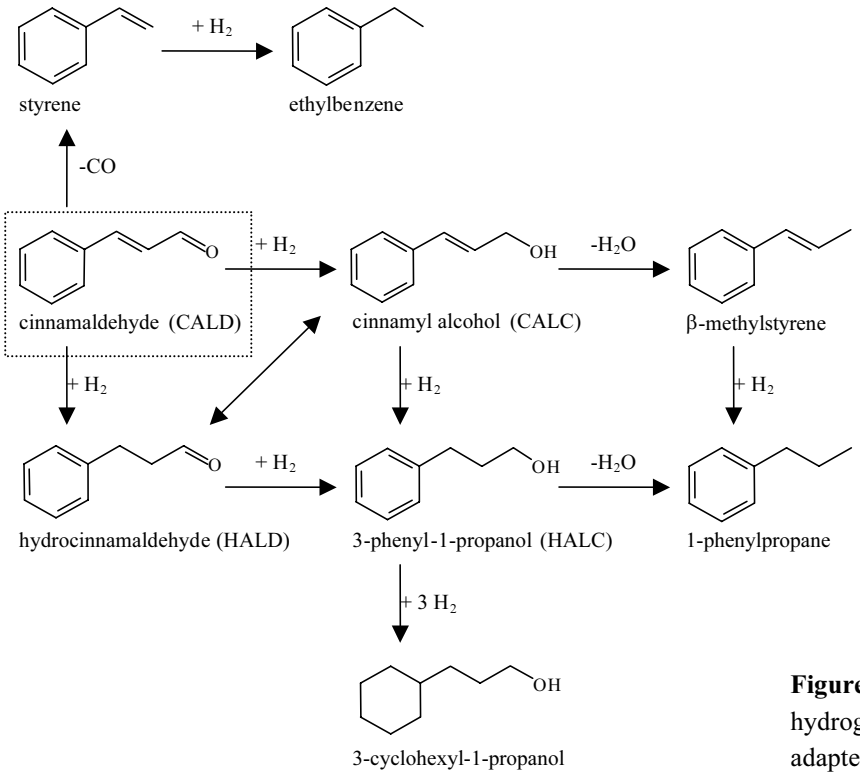

Figure 4. Reaction network for the hydrogenation of cinnamaldehyde, adapted from [56].

cinnamyl alcohol (CALC), hydrocinnamaldehyde (HALD) and 3-phenyl-1-propanol (hydrocinnamyl alcohol (HALC)). These products can undergo further chemical transformations such as decarbonylation, isomerization hydrolysis and hydrogenation [56]. Moreover, when short chain alcohols like ethanol and *iso*-propanol are used as a solvent in this reaction condensation of cinnamaldehyde with the alcohol can also occur, resulting in the formation of acetals and ethers (not shown).

It is assumed that the adsorption mode of cinnamaldehyde is the main factor determining the selectivity of the hydrogenation reaction. Cinnamaldehyde can bind to a metal surface *via* the C=O group, the C=C group or *via* both functional groups. Figure 5 shows commonly distinguished adsorption modes of α,β-unsaturated aldehydes. The η_1 on top, the η_2 di-σ_{CO} and the η_2 π_{CO} modes yield the cinnamyl acohol upon hydrogenation, whereas the η_2 di-σ_{CC}, η_2 π_{CC} and the η_4 or η_2 di-π modes yield hydrocinnamaldehyde [56,61,62].

Group 8-10 metal properties

Palladium and rhodium display a rather poor selectivity towards cinnamyl alcohol [34,35,63]. Palladium catalysts are very active in the hydrogenation of the C=C bond, since the η_4 adsorption mode is favored [62]. The most commonly used metals for cinnamaldehyde hydrogenation are platinum and ruthenium. These metals have an intermediate selectivity to cinnamyl alcohol. However, the selectivity can be enhanced by, amongst other factors, the type of support and the metal particle size and morphology. The main trend in activity observed for carbon-supported Pd, Pt, Rh and Ru catalysts is in the order Pd>Rh>Ru≈Pt,

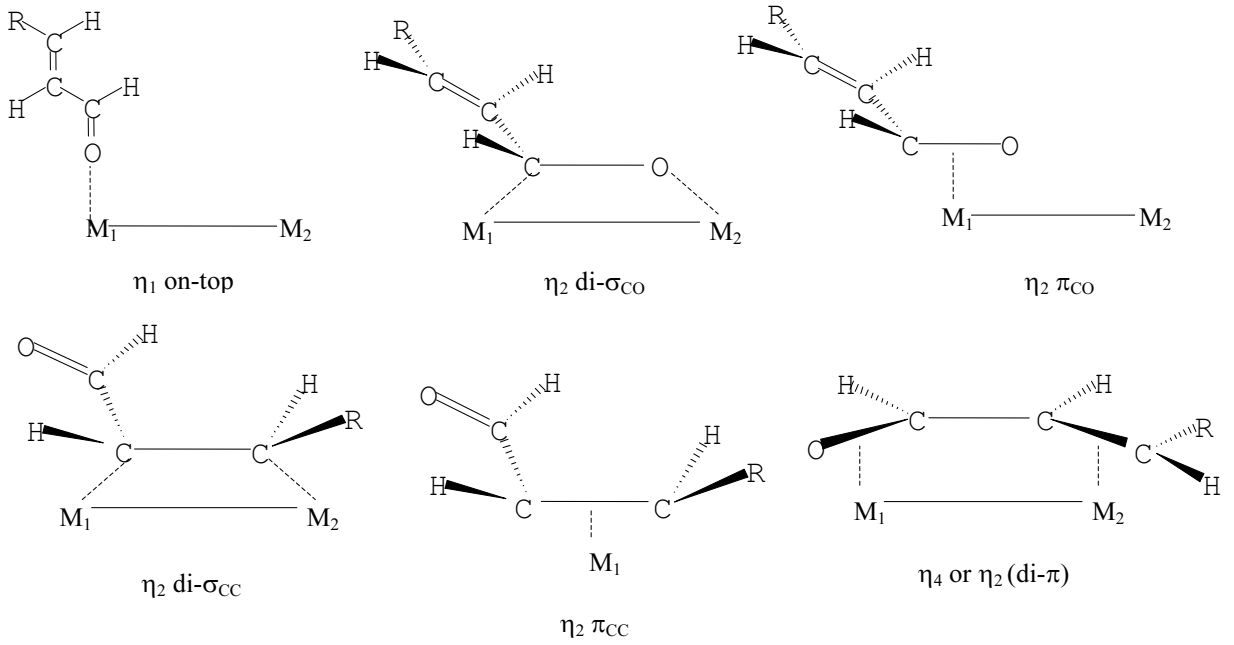

Figure 5. Adsorption modes of α,β-unsaturated aldehydes [56,61,62].

which is related to the values of the adsorption coefficients [63]. Selectivities to the unsaturated alcohol, on the other hand, were in the order Pt>Ru>Rh>Pd [63,64]. Especially because of their tunable selectivities we have focused on platinum and ruthenium as the active phase.

Particle size effect

The metal particle size can have a significant influence on the selectivity of the hydrogenation of cinnamaldehyde over carbon-supported catalysts. It is observed that with increasing metal particle size the selectivity towards cinnamyl alcohol increases. This improvement of the selectivity is due to the lower probability of C=C bond activation compared to C=O bond activation. Two explanations are given for this effect.

Delbecq and Sautet [62] showed with theoretical calculations that the adsorption mode is strongly dependent on the structure of the metal surface. On Pt(111) cinnamaldehyde would prefer η_2 di-σ_{CO} adsorption, resulting in hydrogenation of the C=O bond, while on Pt(100) hydrogenation of the C=C and C=O bonds is equally preferred and on Pt(111)-steps adsorption of the C=C bond dominates. By making larger particles the Pt(111) face is exposed preferrentially, thereby increasing the selectivity towards the unsaturated alcohol.

In a second explanation the particle size effect is interpreted as a result of steric constraints originating from the phenyl group in cinnamaldehyde. On a flat metal surface (large particles) the cinnamaldehyde molecule cannot adsorb parallel to the metal surface because of repulsion of the aromatic ring. Therefore this ring tilts away from the metal surface, thus protecting the C=C bond. On particles smaller than 2-3 nm this steric repulsion is not or hardly present, implying that the C=C bond can be hydrogenated as well [56,63].

Support

Several carbon support materials, like activated carbon, graphite, carbon black, CNF and CNT are used in the selective hydrogenation of cinnamaldehyde. A metal-support effect is observed when ordered carbon supports, like graphite, CNF and CNT are used. In many cases these support materials were more selective towards cinnamyl alcohol than non-graphitic ones. Graphitic carbons are known for their electrical conductivity, which is closely related to the structure of its delocalized π-bonds. The mobility of the delocalized π-electrons in these materials is best in the planes of the structure. The π-electrons of the graphitic planes can give rise to an elevation of the density of states (DOS) of metal particles that are located at steps or edges. This raised DOS decreases the probability of C=C bond adsorption due to repulsion, thereby increasing the selectivity towards the unsaturated alcohol [56,63]. For CNF this effect will probably be less pronounced than for *e.g.* CNT because of the orientation of the graphitic planes and hydrogen atoms at the external edges of the CNF structure.

Coloma *et al.* [65,66] emphasized the importance of oxygen-containing surface groups on carbon supports. In their study on the gas-phase hydrogenation of crotonaldehyde over platinum on activated carbon catalysts they found an increased selectivity to the alcohol with a larger amount of oxygen-containing groups present on the carbon surface. Later on, Bachiller-Baeza *et al.* [64] contradicted the influence of oxygen groups on the hydrogenation of crotonaldehyde over graphite-supported platinum and ruthenium catalysts. In both studies relatively large particles in the range of 3-10 nm were used and the metal particle sizes of the samples with different concentrations of oxygen-containing surface groups were not the same. This demonstrates that more insight into the role of the oxygen-containing surface groups on the catalytic performance of carbon-supported catalysts can only be gained when a well-defined catalyst system is available. This requires a well-defined carbon support without contaminants or micropores, small metal particles with a narrow particle size distribution and a tunable number of oxygen-containing surface groups.

Support effects in catalysis

Although it is undisputable that under certain conditions the support can influence the catalytic properties of the active phase, the origin of this phenomenon is still under debate [67-70]. In this paragraph two causes of support effects that are probable in metal on carbon systems will be discussed.

The first type of support effect has been extensively investigated by Koningsberger and coworkers [71-74] and concerns metal-oxidic support interactions, which influence the electronic structure of the metal. It has been well-established that the reaction rates of hydrogenation and hydrogenolysis reactions of hydrocarbons over supported Pt catalysts are enhanced when the Pt particles are supported on oxidic supports with a lower electron density on the support oxygen. The origin of this support effect is ascribed to a shift of the Pt DOS to

a higher energy (lower binding energy) on supports with a high electron density on the support oxygen and to a lower energy on supports with a lower electron density on the support oxygen. The changes in the electronic structure within supported Pt particles will affect the strength of chemisorption of adsorbates such as CH_x and H_2 on the surface, thereby influencing the catalytic behavior [74]. This metal-support interaction can be found in catalytic systems with metal particles smaller than 2 nm and with relatively large differences in electron density of the support oxygen for catalytic reactions that take place predominantly on the metal (*e.g.* hydrogenolysis of neopentane).

It is common knowledge, however, that not all reactions run exclusively over the metal. An extreme example of this is bifunctional catalysis, in which sites of the support as well as the metal take part in the catalytic process. For alkane hydro-isomerization an acidic zeolite is used onto which a metal has been deposited. The metal particles exhibit hydrogenation/ dehydrogenation activity, whereas the acidic sites of the support exhibit isomerization and cyclization properties. Similar support effects are known in which the support is involved in the overall catalytic process. Part of the activity can be due to conversion over specific support sites or support sites play an important role in the mode of adsorption of the reactant. Burch and Flambard were the first describing an interfacial metal-support interaction [75,76]. They observed that titania-supported nickel catalysts containing large particles not in SMSI (strong metal-support interaction) state had a fifty times higher specific activity in CO hydrogenation than silica-supported nickel catalysts. It is proposed that new active sites, created at the metal-support interface, are responsible for the high specific activity of these catalysts for the CO/H_2 reaction. Also for gold on titania catalysts the metal-support interface plays an essential role in CO oxidation. Neither bulk gold nor titania is active for CO oxidation, while gold on titania is one of the most active catalysts. In this reaction oxygen probably adsorbs on vacancy sites of titania whereas CO adsorbs on gold [77,78]. For CO_2/CH_4 reforming over zirconia-supported platinum catalysts, Bitter *et al.* [79] proposed that platinum atoms on the support-metal perimeter determine the activity and that CO_2 is activated on the support *via* carbonate species in the proximity of platinum to react with methane that is adsorbed on the metal.

In this thesis, we examine whether (and how) CNF as a support material influences the catalytic performance of the CNF-supported noble metal catalysts in the hydrogenation of cinnamaldehyde. Conditions are advantageous, since our starting material is a well-defined CNF support, onto which we can apply highly dispersed platinum and ruthenium particles.

Scope and outline of this thesis

Aim of the work described in this thesis has been the exploration of the potential of CNF as catalyst support material, notably for platinum and ruthenium, and its role in the performance of these catalysts in hydrogenation reactions. A prerequisite for such a study was

to make well-defined CNF-supported catalysts available. Therefore, very pure CNF were produced with a uniform diameter. For the application of noble metals a reproducible preparation procedure has been designed, resulting in a homogeneous distribution of small metal particles with a narrow particle size distribution.

In **Chapter 2** research aiming at a further extension of our knowledge of the formation of uniform CNF using various nickel catalysts is described. It turned out that the nickel particle size as well as the nature of the carbon-containing gas significantly affect the CNF growth process. We demonstrate that uniform CNF with a small average diameter (25 nm) can be grown from a silica-supported, highly dispersed nickel catalyst and a carbon-containing gas of relatively low reactivity, like CH_4 or CO/H_2. Before applying the active phase the inert and non-polar CNF have to be activated in boiling nitric acid or an HNO_3/H_2SO_4 mixture in order to introduce oxygen-containing groups on the CNF surface, *i.e.* to introduce polar sites. **Chapter 3** deals with the effect of this acid treatment on the structure and texture of CNF and both the total number of oxygen groups and the number of acidic oxygen-containing groups introduced are determined. It is shown that the graphite-like structure of the treated fibers remains intact, however, specific surface area and pore volume increase with the severity of the oxidation treatment. With acid-base titrations, XPS and TGA-MS it is demonstrated that both the total oxygen content as well as the number of acidic groups are a function of the type of oxidizing agent used and the treatment time. In **Chapter 4** a literature review on the synthesis of supported palladium catalysts is given. This review focuses on the chemistry of catalyst synthesis, relevant support properties and case studies for oxide- and notably carbon-supported catalysts. The results of this literature survey on carbon supports give direction to the synthesis of CNF-supported platinum and ruthenium catalysts, as described in **Chapter 5**. In this chapter, the preparation of CNF-supported platinum and ruthenium catalysts by two different ion exchange techniques, one at constant pH of ~ 6 (ion exchange) and one in which the pH is gradually increased from 3 to 6 by the hydrolysis of urea (HDP method) is presented. With both synthesis techniques homogeneously distributed, highly dispersed and thermally stable metal particles were obtained with an average particle size of 1-2 nm. A remarkable finding was that with the HDP method substantial higher metal loadings (+ 100%) can be obtained. The work described in **Chapter 6** demonstrates the surprisingly strong influence of oxygen-containing surface groups on the activity and selectivity of CNF-supported ruthenium catalysts in the hydrogenation of cinnamaldehyde. The overall activity strongly increases with a decreasing number of oxygen-containing groups, along with a shift in selectivity from cinnamyl alcohol to hydrocinnamaldehyde. In **Chapter 7** we extended this work to CNF-supported platinum catalysts in the hydrogenation of cinnamaldehyde. For this catalyst system the effect of the surface oxygenates turns out to be even more pronounced than for the ruthenium catalysts. The observed activity of the catalyst with a small number of oxygen support groups is one of the highest reported in literature for this reaction and the intrinsic activity is even larger, as internal diffusion limitations slow down the reaction rate of

this catalyst. With XPS and H_2-chemisorption no clear evidence has been found for oxygen in the support indirectly influencing the catalytic behavior by changing the electronic properties of the platinum particles. A model including both Langmuir-Hinshelwood kinetics and mass transfer effects is presented in **Chapter 8** to establish whether differences in the number of oxygen support groups can be related with changes in certain kinetic parameters. Results suggest that hydrogenation becomes assisted by adsorption of the benzene ring of cinnamaldehyde on the non-polar CNF support surface after removal of the oxygen surface groups. Finally, in **Chapter 9** a summary of the results of the previous chapters is given and some concluding remarks are presented.

References

1. J.J. Berzelius, Ann. Chim. Phys. 61 (1836) 146.
2. E.B.M. Doesburg, K.P. de Jong, J.H.C. van Hooff, J.W. Geus and J.A.R. van Veen, Stud. Surf. Sci. Catal. 123 (1999) Chapter 9 and 10.
3. R.K. Iler, The Chemistry of Silica – Solubility, Polymerization, Colloid and Surface Properties, and Biochemistry, John Wiley & Sons, Inc. New York (1979) Chapter 1.
4. E.M. Flanigen, Stud. Surf. Sci. Catal. 137 (2001) 11.
5. F. Fischer and H. Tropsch, Brennstoff-Chem. 4 (1923) 276.
6. F.R. van den Berg, Ph.D. thesis, Utrecht University (2001) Chapter 1.
7. F. Rodriguez-Reinoso, Carbon 36 (1998) 159.
8. R.L. Augustine, Heterogeneous Catalysis for the Synthetic Chemist, Marcel Dekker, Inc., New York (1996) Chapter 13.
9. R.J.J. Jansen, Ph.D. thesis, Delft University (1994) Chapter 1.
10. K.P. de Jong and J.W. Geus, Catal. Rev.-Sci. Eng. 42 (2000) 481.
11. R.T.K. Baker, K. Laubernds, A. Wootsch and Z. Paál, J. Catal. 193 (2000) 165.
12. T.V. Hughes and C.R. Chambers, US Patent 405,480 (1889).
13. J.W. Geus and J.W. Linowski, US Patent 4,855,091 (1989).
14. H.G. Tennent, US Patent 4,663,230 (1987).
15. A. Thess, R. Lee, P. Nikolaev, H.J. Dai, P. Petit, J. Robert, C.H. Xu, Y.H. Lee, S.G. Kim, A.G. Rinzler, D.T. Colbert, G.E. Scuseria, D. Tomanek, J.E. Fischer and R.E. Smalley, Science 273 (1996) 483.
16. S. Iijima, Nature 354 (1991) 56.
17. T.W. Ebbensen and P.M. Ajayan, Nature 358 (1992) 220.
18. N.M. Rodriquez, J. Mater. Res. 8 (1993) 3233.
19. R.T.K. Baker, Carbon 27 (1989) 315.
20. N.M. Rodriquez, M.-S. Kim and R.T.K. Baker, J. Phys. Chem. 98 (1994) 13108.

21. J.W. Geus, A.J. van Dillen and M.S. Hoogenraad, Mat. Res. Soc. Symp. Proc. 368 (1995) 87.
22. R.T.K. Baker, Carbon Fibers, Filaments and Composites, NATO ASI Series, Kluwer, Dordrecht, (1990) 405.
23. D.L. Trimm, Catal. Rev.-Sci. Eng. 16 (1977) 155.
24. M.S. Hoogenraad, Ph.D. thesis, Utrecht University (1995).
25. V.N. Parmon, G.G. Kuvshinov, V.A. Sadykov and V.A. Sobyanin, Stud. Surf. Sci. Catal. 119 (1998) 677.
26. N.M. Rodriquez, A. Chambers and R.T.K. Baker, Langmuir 11 (1995) 3862.
27. A. Chambers, T. Nemes, N.M. Rodriquez and R.T.K. Baker, J. Phys. Chem. B 102 (1998) 2251.
28. H.P. Boehm, Adv. Catal. 16 (1966) 179.
29. T.G. Ros, A.J. van Dillen, J.W. Geus and D.C. Koningsberger, Chem. Eur. J. 8 (2002) 1151.
30. R. Schlögl, M. Che, O. Clause and C. Marchilly, Preparation of Solid Catalysts, Wiley-VCH, Weinhein, (1999) Chapter 3 and 4.
31. J.P. Brunelle, Pure Appl. Chem. 50 (1978) 1211.
32. C.A. Bessel, K. Laubernds, N.M. Rodriguez and R.T.K. Baker, J. Phys. Chem. B 105 (2001) 1115.
33. M.S. Hoogenraad, R.A.G.M.M. van Leeuwarden, G.J.B. van Breda Vriesman, A. Broersma, A.J. van Dillen and J.W. Geus, Stud. Surf. Sci. Catal. 91 (1995) 263.
34. C. Pham-Huu, N. Keller, L.J. Charbonniere, R. Ziessel and M.J. Ledoux, Chem. Commun. (2000) 1871.
35. C. Pham-Huu, N. Keller, G. Ehret, L.J. Charbonniere, R. Ziessel and M.J. Ledoux, J. Mol. Catal. A Chem. 170 (2001) 155.
36. E.S. Steigerwalt, G.A. Deluga, D.E. Cliffel and C.M. Lukehart, J. Phys. Chem. B 105 (2001) 8097.
37. S. Hermans, J. Sloan, D.S. Shephard, B.F.G. Johnson and M.L.H. Green, Chem. Commun. (2002) 276.
38. J.M. Planeix, N. Coustel, B. Coq, V. Brotons, P.S. Kumbhar, R. Dutartre, P. Geneste, P. Bernier and P.M. Ajayan, J. Am. Chem. Soc. 116 (1994) 7935.
39. T. Braun, M. Wohlers, T. Belz, G. Nowitzke, G. Wortmann, Y. Uchida, N. Pfänder and R. Schlögl, Catal. Lett. 43 (1997) 167.
40. M. Lashdaf, A. Hase, E. Kauppinen and A.O.I. Krause, Catal. Lett. 52 (1998) 199.
41. E. van Steen and F.F. Prinsloo, Catal. Today 71 (2002) 327.
42. Z.-J. Liu, Z.-Y. Yuan, W. Zhou, L.-M. Peng and Z. Xu, Phys. Chem. Chem. Phys. 3 (2001) 2518.

43. S.K. Shaikhutdinov, L.B. Avdeeva, B.N. Novgorodov, V.I. Zaikovskii and D.I. Kochubey, Catal. Lett. 47 (1997) 35.
44. F. Salman, C. Park and R.T.K. Baker, Catal. Today 53 (1999) 385.
45. C. Park and R.T.K. Baker, J. Phys. Chem. B 102 (1998) 5168.
46. L.M. Ang, T.S.A. Hor, G.Q. Xu, C.H. Tung, S.P. Zhao and J.L.S. Wang, Carbon 38 (2000) 363.
47. J.H. Bitter, M.K. van der Lee, A.G.T. Slotboom, A.J. van Dillen and K.P. de Jong, Catal. Lett. 89 (2003) 139.
48. W.A. Spieker and J.R. Regalbuto, Chem. Eng. Sci. 56 (2001) 3491.
49. J.R. Regalbuto, M. Schrier, X. Hao, W.A.Spieker, J.G. Kim, J.T. Miller and A.J. Kropf, Stud. Surf. Sci. Catal. 143 (2002) 45.
50. J.-F. Lambert and M. Che, J. Mol. Catal. A Chem. 162 (2000) 5.
51. C. Lepetit and M. Che, J. Mol. Catal. A Chem. 100 (1995) 147.
52. J. de Graaf, A.J. van Dillen, K.P. de Jong and D.C. Koningsberger, J. Catal. 203 (2001) 307.
53. J.W. Geus and P.B. Wells, Appl. Catal. 18 (1985) 231.
54. M. Arai, A. Obata, K. Usui, M. Shirai and Y. Nishiyama, Appl. Catal. A Gen. 146 (1996) 381.
55. T. Birchem, C.M. Pradier, Y. Berthier and G. Cordier, J. Catal. 146 (1994) 503.
56. T. Vergunst, Ph.D. thesis, Delft University (1999).
57. B. Coq and F. Figueras, Coord. Chem. Rev. 178-180 (1998) 1753.
58. P. Gallezot and D. Richard, Catal. Rev.-Sci. Eng. 401 (1998) 81.
59. P. Kluson and L. Cerveny, Appl. Catal. A Gen. 128 (1995) 13.
60. U.K. Singh and M.A. Vannice, Appl. Catal. A Gen. 213 (2001) 1.
61. V. Ponec, Appl. Catal. A Gen. 149 (1997) 27.
62. F. Delbecq and P. Suatet, J. Catal. 152 (1995) 217.
63. A. Giroir-Fendler, D. Richard and P. Gallezot, Stud. Surf. Sci. Catal. 41 (1998) 171.
64. B. Bachiller-Baeza, A. Guerrero-Ruiz and I. Rodriguez-Ramos, Appl. Catal. A Gen. 192 (2000) 289.
65. F. Coloma, A. Sepúlveda-Escribano and F. Rodríguez-Reinoso, Appl. Catal. A Gen. 123 (1995) L1.
66. F. Coloma, A. Sepúlveda-Escribano, J.L.G. Fierro and F. Rodríguez-Reinoso, Appl. Catal. A Gen. 150 (1997) 165.
67. R.L. Augustine, Heterogeneous Catalysis for the Synthetic Chemist, Marcel Dekker, Inc., New York (1996) Chapter 9.
68. S.J. Tauster, S.C. Fung, R.T.K. Baker and J.A. Horsley, Science 211 (1981) 1121.
69. G.C. Bond, Stud. Surf. Sci. Catal. 11 (1982) 1.
70. G.C. Bond and R. Burch, Catalysis 6 (1983) 27.

71. D.E. Ramaker, J. de Graaf, J.A.R. van Veen and D.C. Koningsberger, J. Catal. 203 (2001) 7.
72. D.C. Koningsberger, J. de Graaf, B.L. Mojet, D.E. Ramaker and J.T. Miller, Appl. Catal. A. Gen. 191 (2000) 205.
73. B.L. Mojet, J.T. Miller, D.E. Ramaker and D.C. Koningsberger, J. Catal. 186 (1999) 373.
74. D.C. Koningsberger, M.K. Oudenhuijzen, J. de Graaf, J.A. van Bokhoven and D.E. Ramaker, J. Catal. 216 (2003) 178.
75. R. Burch and A.R. Flambard, J. Catal. 78 (1982) 389.
76. R. Burch and A.R. Flambard, Stud. Surf. Sci. Catal. 11 (1982) 193.
77. M. Haruta, S. Tsubota, T. Kobayashi, M.J. Genet and B. Delmon, J. Catal. 144 (1993) 175.
78. J.-D. Grunwaldt and A. Baiker, J. Phys. Chem. B 103 (1999) 1002.
79. J.H. Bitter, K. Seshan and J.A. Lercher, J. Catal. 171 (1997) 279.

2

Impact of the Structure and Reactivity of Nickel Particles on the Catalytic Growth of Carbon Nanofibers

Abstract

Catalytically grown, fishbone carbon nanofibers (CNF), are prepared by the decomposition of carbon-containing gases (CH_4, CO/H_2 or C_2H_4/H_2) over a silica-supported nickel catalyst and an unsupported nickel catalyst at 550 °C. It turns out that both the nickel particle size and the nature of the carbon-containing gas significantly affect the CNF growth process. We demonstrate that at the chosen temperature small supported nickel particles need a carbon-containing gas with a relatively low reactivity, like CH_4 or CO/H_2, to produce CNF. The resulting fishbone CNF have a uniform and small diameter (25 nm). The CNF thus synthesized hold great potential, *e.g.* as catalyst support material. However, the large unsupported nickel particles only produce CNF using a reactive carbon-containing gas, like C_2H_4/H_2. The CNF thus obtained show a variety of morphologies with a large range of diameters (50-500 nm). The CNF yield is a subtle interplay between the nickel particle size and consequently the exposed crystal planes on the one hand and the reactivity of the carbon-containing gas on the other.

Introduction

Carbon nanofibers-related materials have gained increasing attention in the last few years due to their high strength, chemical purity and chemical inertness, which features make them ideally suitable for use as a catalyst support [1-3]. The two most encountered forms are the carbon nanofibers (CNF) and the carbon nanotubes (CNT). In the CNF the graphite planes are oriented at an angle to the central axis, thus exposing graphite edge sites. If the graphite planes are oriented parallel to the central axis, like in the CNT, only basal graphitic planes are exposed.

Because CNF consist of carbon, a carbon-containing gas is needed for the synthesis of these materials. The production of reactive carbon intermediates from this carbon-containing gas is a crucial step in the synthesis procedure. This can be achieved by activation of graphite by laser vaporization [4], electric arc-discharge [5,6] or by the dissociation of a carbon-containing gas on the surface of a metal catalyst like Ni, Fe or Co [1-3,7-10]. The latter route, which is called catalytic synthesis, is the only technique with which one can produce very pure CNF in large quantities, while tuning of physico-chemical properties like surface structure, diameter and morphology is possible.

The relevance of carbon materials is clearly envisioned by their application as a support in various catalytic processes, especially selective hydrogenations. The catalytic performance of the carbon (graphite, activated carbon) supported catalysts can be tuned by a change of the features of the support, like the amount of oxygen-containing surface groups [11,12] the accessibility of the support [13,14] and the degree of carbon ordering [15]. We expect a similar influence of the support on the performance of a metal/CNF catalyst. However, the preparation of uniform CNF with defined properties, like diameter and macroscopic porosity, is not well understood. The most important parameters which influence these properties are the nature of the metallic catalyst particles and that of the carbon-containing gas [1,9,16-27]. Although effects of promotors have been described as well [28,29].

Variations in the choice of the metal and the growth temperature can alter the ordering of the graphite planes from parallel (CNT) to fishbone (CNF) [16,17]. CNT can be grown, especially using CO, from iron [16] and cobalt particles [18] as well as from nickel at elevated temperatures [19]. CNF are mainly obtained when using nickel and nickel-iron alloy catalysts with methane as the carbon-containing gas [20-22].

As stated, the dissociation of a carbon-containing gas on a metal surface is a key step in the production of catalytically-grown CNF. It is noted that the dissociation rate of carbon-containing gases is, among other things, dependent on the detailed surface structure of the metal, thus influencing the CNF growth process [23-26]. For example, Ni(110) and Ni(100) [23] surfaces are much more active for methane dissociation than the Ni(111) surface [25,26].

The particle size of the metal can affect the characteristics of the CNF as well. The diameter of the nanofibers is controlled by the size of the metal particles from which the nanofibers start to grow [1,9,16]. This allows us to tune the diameter of the CNF. Previous

studies have revealed that CNF can be produced with surface areas of up to 300 m^2/g [27], which is comparable to the surface areas commonly reported for selective hydrogenation catalysts [13].

Due to the diversity of the applied reaction conditions in the above-mentioned studies, it is difficult to directly compare the obtained results with respect to the tuning of the CNF. To our best knowledge, no systematic study has been carried out on the influence of the metal particle size of the growth catalyst and the nature of the carbon-containing gas on the CNF growth and their physico-chemical properties, like diameter and textural properties.

In this paper, we present the results of our study on the catalytic decomposition of several carbon-containing gases (CH_4, CO/H_2 and C_2H_4/H_2) on a silica-supported nickel catalyst and on an unsupported nickel catalyst. It turns out that the combination of the nickel particle size and the nature of the carbon-containing gas significantly affects the CNF growth process. We demonstrate that small supported nickel particles need a carbon-containing gas with a relatively low reactivity, like CH_4 or CO/H_2, to produce CNF. The resulting fishbone CNF have a uniform and small diameter. However, the large unsupported nickel particles only produce CNF using a reactive carbon-containing gas, like C_2H_4/H_2. The CNF thus obtained show a variety of morphologies with a large range of diameters.

Experimental

Preparation of growth catalysts

Silica-supported nickel catalysts with a metal loading of 20 wt% were prepared by deposition precipitation using the hydrolysis of urea at 90 °C [30,31]. Silica (8.5 g, Degussa Aerosil 200) was suspended in 1 L of demi-water at 90 °C and mechanically stirred at 1000 rpm. Nickel nitrate hexahydrate (10.55 g, Acros 99%) was added and the pH was adjusted to 3-4 using nitric acid (Merck p.a.). Subsequently, 6.95 g urea (Acros p.a.) was introduced. After 16 h of reaction, the mixture was cooled to room temperature and filtered. The residue was washed three times with demi-water, followed by drying at 120 °C for 16 h. Finally, a sieve fraction of 425-850 μm of the catalyst precursor was calcined in static air at 600 °C (5 °C/min) for 3 h. The calcined samples were stored in static air for further use.

Unsupported nickel was synthesized from nickel carbonate, precipitated from a nickel nitrate solution using ammonium bicarbonate (Aldrich 99%) at room temperature and a pH of about 9.0. [22]. Nickel nitrate (24.77 g) was dissolved in 1 L demi-water and the solution was mechanically stirred at 1000 rpm. Subsequently solid ammonium bicarbonate (~ 25 g) was added until the supernatant was colorless. After filtering, the precipitate was treated likewise the supported catalyst, except that calcination was carried out at 500 °C.

CNF growth

A weighed sample (100 mg) of the nickel growth catalyst, loaded in a spherical quartz vessel with a porous quartz plate at the bottom, was reduced in a flow of 20% hydrogen in argon (flow rate 100 ml/min). The temperature was raised to 700 °C for Ni/SiO_2 (5 °C/min) and 500 °C for the unsupported Ni sample (5 °C/min) and kept at these levels for 2 h. After the reduction the reactor was brought at the desired reaction temperature, maintaining 20% hydrogen in argon flow.

Subsequently, synthesis gas (20% CO, 7% H_2), methane (20 % CH_4) or an ethene/hydrogen mixture (20% C_2H_4, 7% H_2) balanced with Ar was passed through the reactor for 10 h to grow CNF. The total flow was always 100 ml/min. After 10 h, the sample was cooled down to room temperature under an argon stream. During the growth, the conversion of the gases was assessed by gas chromatography analysis using an HP5890A gas chromatograph equipped with a 12ft Porapack Q column. The following equation was used for the determination of the carbon deposition rate:

$$\text{rate} = \frac{(C_0 - C_{offgas} - C_{byproducts}) * 12.01}{g_{Ni}} \qquad \left(\frac{g_C}{g_{Ni} * h} \right)$$

where C_0 is the feed rate of carbon (mol/h), C_{offgas} the rate of unconverted feed (mol/h), $C_{byproducts}$ the rate of gaseous carbon-containing byproducts formed during CNF growth (mol/h) and g_{Ni} the amount of nickel in grams used for the CNF growth. This results in a C-deposition rate expressed in gram carbon per gram nickel per hour.

To remove the growth catalyst, *i.e.* SiO_2 and non-encapsulated nickel, from the CNF after the growth process, the fibers are subsequently refluxed in 1M KOH solution and concentrated HCl for 1 h. After this treatment the sample was filtered, thoroughly washed with demi-water and dried in air at 120 °C.

Characterization

The growth catalysts and the produced fibers were examined in a Philips CM-200 FEG transmission electron microscope (TEM) operated at 200 kV. After suspending in ethanol under ultrasonic vibration, samples were brought onto a holey carbon film on a copper grid. Scanning electron microscopy (SEM) was performed using a Philips XL30 FEG apparatus. Specific surface areas (BET) and pore volumes of the growth catalysts and the CNF were calculated from nitrogen physisorption data measured at –196 °C with a Micromeritics ASAP 2400 apparatus. Prior to the physisorption experiments the samples were evacuated at 200 °C for at least 16 h. XRD patterns were recorded at room temperature with a Nonius PDS 120 powder diffractometer system equipped with a position-sensitive detector with a 2θ range of 120 ° using Co $K\alpha_1$ (λ=1.78897 Å) radiation.

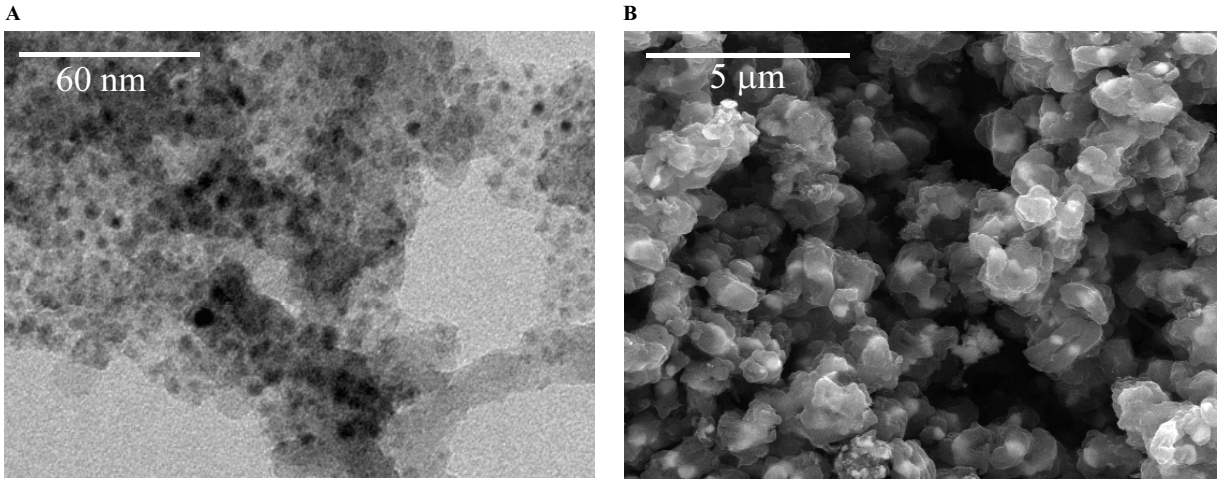

Figure 1. (A) TEM micrograph of reduced Ni/SiO_2; (B) SEM micrograph of the reduced unsupported Ni catalyst.

Results

Electron micrographs of both growth catalysts used in this study are shown in Figure 1. It can be clearly seen that the nickel particle size (the dark spots) in the Ni/SiO_2 catalyst is small (d 5-10 nm) with a narrow size distribution. The unsupported nickel catalyst consists of micrometers-sized conglomerates of 50-1000 nm particles. The nickel particle sizes were also determined by XRD by an analysis of the line broadening of the Ni(111), (200), (220) and (311) reflections, see Figure 2. The NiO phase observed with XRD is formed when the reduced nickel catalyst is exposed to the air prior to the XRD measurement. This phase is not present while growing CNF. For the Ni/SiO_2 catalyst line broadening analysis of the Ni reflections leads to similar sizes as found with the TEM, which indicates that the nickel particles are small single crystals.

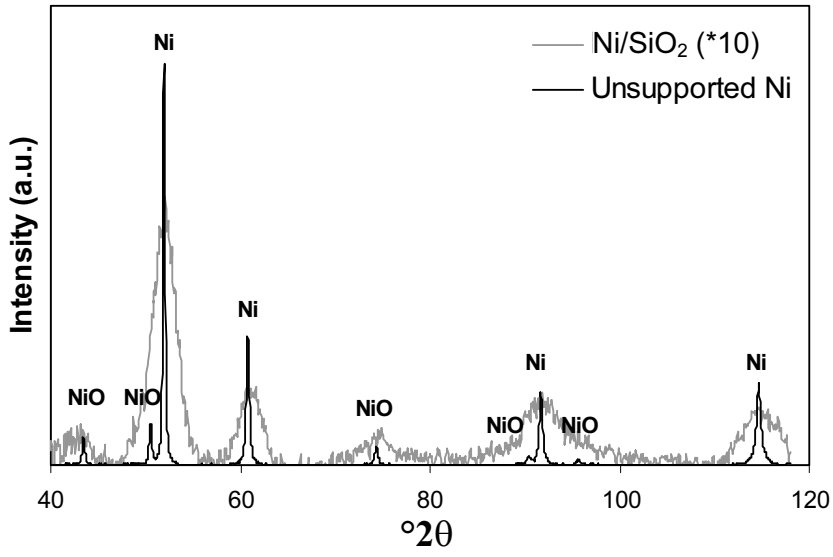

Figure 2. XRD patterns of reduced Ni/SiO_2 and of the reduced unsupported Ni catalyst.

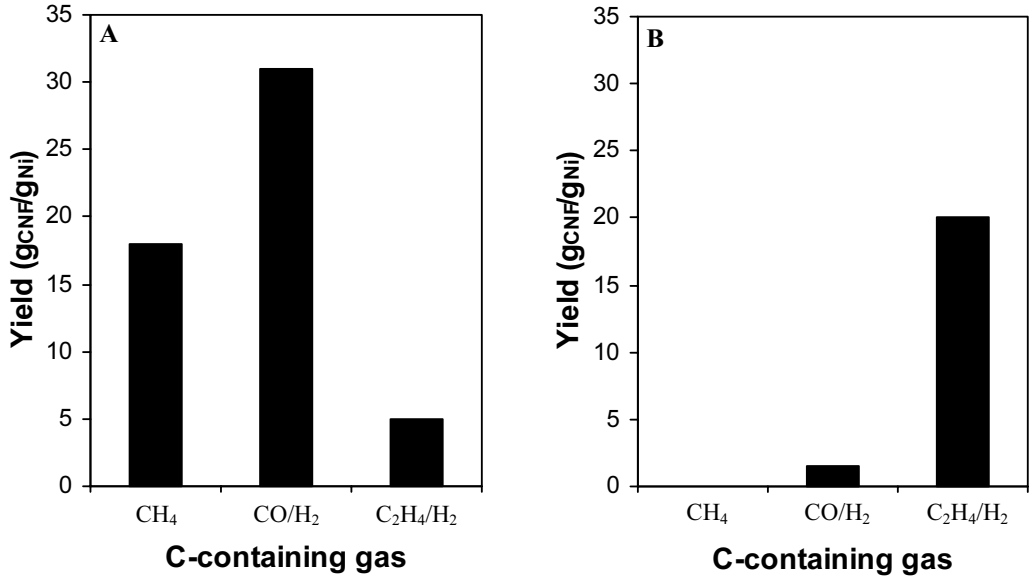

Figure 3. Yield of CNF as a function of the carbon source used: (A) Ni/SiO_2 at 550 °C; (B) unsupported Ni at 550 °C.

On the other hand, for the unsupported Ni, XRD leads to d > 50 nm. Probably also small crystallites are present because the peaks are slightly broadened at the bottom. The particles (50-1000 nm) as shown with SEM (Figure 1) most likely are highly polycrystalline.

From both Ni catalysts, CNF were grown using different carbon-containing gases. The amounts of CNF grown in 10 h with these catalysts in the respective carbon-containing gases are shown in Figure 3. It can be seen that over this period of time Ni/SiO_2 is most effective in growing CNF from CH_4 (18 g_{CNF}/g_{Ni}) and CO/H_2 (31 g_{CNF}/g_{Ni}) while unsupported Ni is most effective for CNF growth from C_2H_4/H_2 (20 g_{CNF}/g_{Ni}). Evidently, the CNF yield depends on the combination of the type of nickel catalyst and the carbon-containing gas.

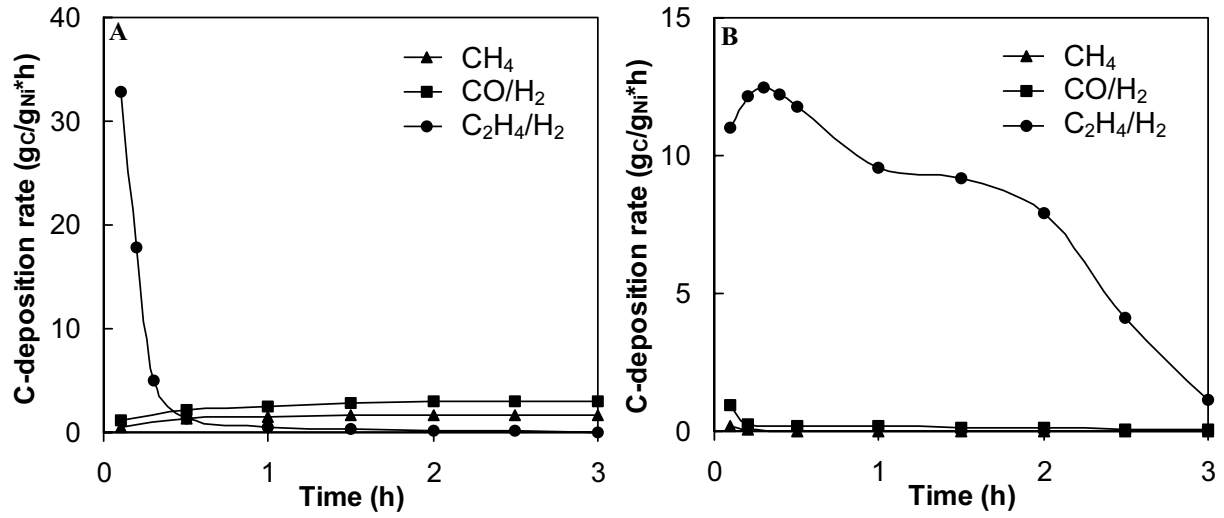

Figure 4. Conversion of different carbon sources with a flow of 20 ml/min (total flow 100 ml/min) at 550 °C and 1 bar over: (A) Ni/SiO_2; (B) unsupported Ni.

Table 1. Some physico-chemical features of CNF grown at 550 °C from Ni/SiO_2, 20% $CO/7\%$ H_2 and unsupported Ni catalyst, 20% $C_2H_4/7\%$ H_2.

	S_{BET} (m^2/g)	V_{micro} (ml/g)	V_{meso} (ml/g)	d_{pore} (nm)
CNF (Ni/SiO_2 CO/H_2)	214	0.01	0.41	10
CNF (Ni C_2H_4/H_2)	54	0.01	0.10	70

To examine how this yield is brought about we monitored the course of the deposition in time. The results are summarized in Figure 4. When CNF were grown with the use of Ni/SiO_2 from CH_4 and CO/H_2, the carbon deposition rate increased somewhat and reached a steady-state, which leads to a high yield after 10 h. When, however, C_2H_4/H_2 was used a high initial deposition rate was observed which dropped rapidly to zero already within 30 min. Obviously, the catalyst deactivated completely. With the unsupported Ni catalyst the situation is rather different. With CH_4 and CO/H_2 low initial conversions were measured. These conversions diminished fast, which explains the negligible yields, even after 10 h on stream. The unsupported catalyst turned out to be more active and the activity more stable with C_2H_4/H_2, however, also in this case the catalyst deactivated completely albeit at a lower rate. The apparently high yield, as shown in Figure 3B had already been attained within the first period of 3h.

The CNF produced with the gases giving the highest yields after 10 h, thus for the Ni/SiO_2 catalyst, the fibers grown out of CO/H_2 and for the unsupported Ni catalyst the CNF originating from C_2H_4/H_2 are investigated in more detail. Figure 5 displays the SEM images of these CNF. Uniform and small diameter (25 nm) CNF had been grown from CO/H_2 using the Ni/SiO_2 catalyst. In contrast to this, unsupported Ni and C_2H_4/H_2 resulted in large diameter CNF with a broad diameter distribution (50-500 nm). XRD showed that both types of CNF consisted of graphitic carbon.

The textural properties of both types of CNF were investigated by means of nitrogen physisorption. The results are summarized in Table 1. The small diameter CNF exhibited a

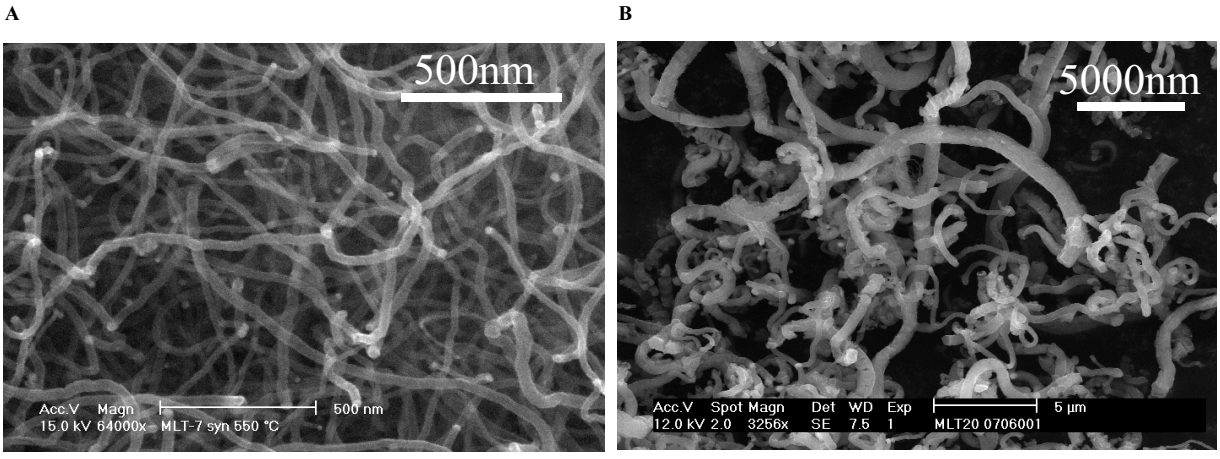

Figure 5. SEM: (A) CNF grown using Ni/SiO_2 and 20% $CO/7\%$ H_2 at 550 °C; (B) CNF produced by unsupported Ni and 20% $C_2H_4/7\%$ H_2 at 550 °C.

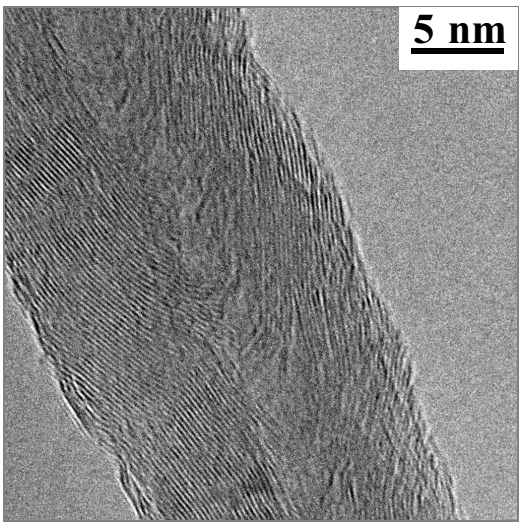

Figure 6. TEM image of CNF grown using Ni/SiO_2 and 20% CO/7% H_2 at 550 °C [32].

high specific surface area (214 m^2/g) and a high mesopore volume (0.41 ml/g). The large diameter CNF, on the other hand, had a lower surface area (54 m^2/g) and mesopore volume (0.10 ml/g). The pore distributions, derived from the desorption isotherm, differed for both types of CNF. The small diameter CNF had a narrow pore size distribution with an average diameter of 10 nm. A broad pore diameter distribution was found for the large diameter CNF with an average pore diameter of 70 nm. From the corresponding t-plots for both types a low

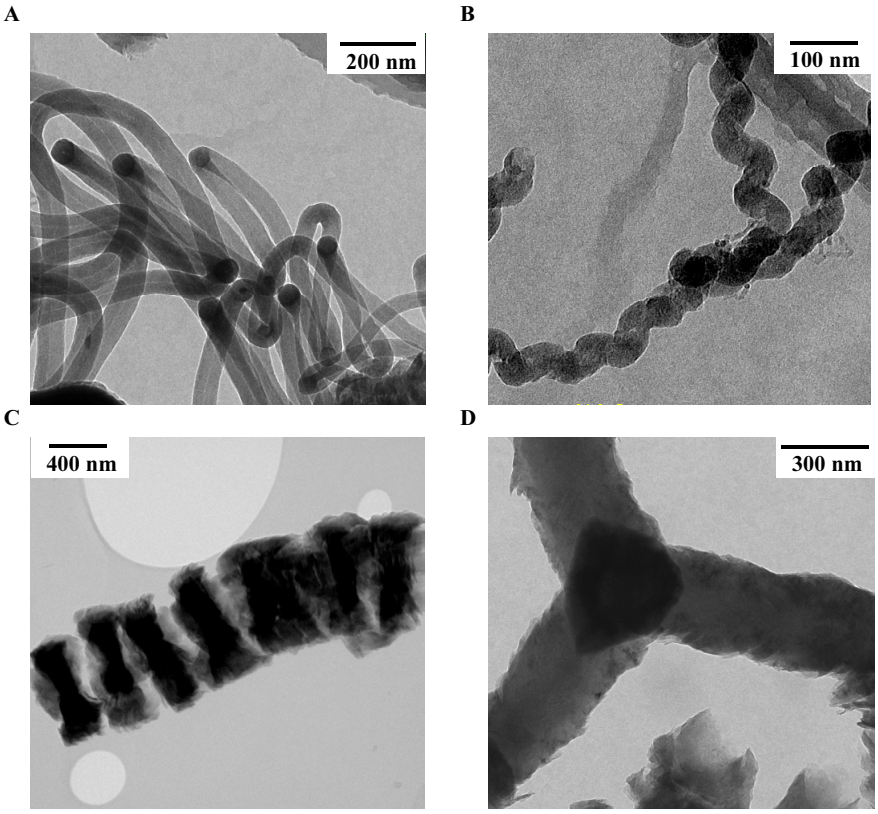

Figure 7. (A-D) TEM images of CNF produced by unsupported Ni and 20% C_2H_4/7% H_2 at 550 °C.

but not negligible micropore volume of 0.01 ml/g was derived, probably originating from the surface roughness of the fibers.

TEM pictures of the CNF grown from the supported and the unsupported catalyst are presented in Figure 6 and 7. These pictures clearly show the difference in the diameters of the CNF. With the small diameter CNF (Figure 6 [32]) the individual lattice planes of the graphite lattice are visible ordered in the fishbone structure. In contrast to the small diameter CNF, the large diameter CNF are very heterogeneous. Besides fishbone type of fibers with perfect graphitic ordering, also less ordered platelet type of fibers and some helical [33,34] and multidirectional [35,36] fibers are found (Figure 7A-D). These large diameter CNF are too thick to make acquisition of micrographs with higher magnification meaningful.

Discussion

The mechanism of the catalytic growth of CNF has been studied over a long period of time. Although consensus has been reached with respect to the different growth steps [3], still uncertainties exist about some details. A schematic representation of the mechanism of steady-state growth is given in Figure 8 and is based on the review of De Jong and Geus [3].

The first step is the decomposition of carbon-containing gases on the metal surface. In this process carbon atoms are deposited on the surface with the concomitant release of gaseous products like molecular hydrogen, carbon dioxide and water depending on the carbon-containing gas used. In the second step the carbon atoms dissolve in and diffuse through the bulk of the metal particle, although some contribution of surface diffusion cannot be excluded. The final step is the precipitation of the carbon in the form of a CNF consisting of graphite at the other side of the metal particle. The thermodynamic driving force of the CNF production is the formation of graphite out of carbon-containing gas. The above-mentioned steps show that

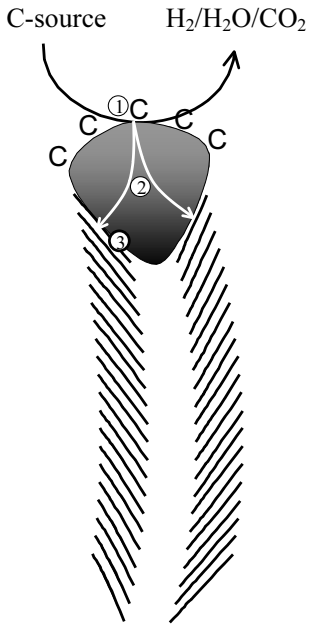

Figure 8. Schematic representation of the catalytic growth of a CNF using a gaseous carbon-containing gas. Step ①, decomposition of carbon-containing gases on the metal surface. Step ②, carbon atoms dissolve in and diffuse through the bulk of the metal. Step ③, precipitation of carbon in the form of a CNF consisting of graphite [3].

the steady-state growth process is a delicate balance between the dissociation of the carbon-containing gases, carbon diffusion through the particle, and the rate of nucleation and formation of graphitic layers [3,20].

Addition of hydrogen is required when C_2H_4 and CO is used to balance the amount of carbon atoms in the CNF growth process. Hydrogen reduces the amount of carbon atoms formed and can therefore prevent encapsulation and thus deactivation of the catalyst.

Our study clearly demonstrates, see Figures 3 and 4, that the CNF yield within a certain period of time strongly depends on the type of catalyst as well as on the nature of the carbon-containing gas. From the small supported nickel particles large amounts of CNF are grown from CH_4 and from CO/H_2 at an almost constant, moderate rate over the entire period of 10 h.

As already mentioned above, the mechanism of CNF growth is a delicate process. When the balance between dissociation, diffusion and segregation is disturbed, the CNF growth stops. Since with the Ni/SiO_2 catalyst and C_2H_4/H_2 a high initial rate is observed followed by fast deactivation, we have to conclude that the diffusion of the C-atoms through the metal particle and the fiber formation cannot keep up with the C-atom supply at the surface, resulting in encapsulation of the nickel particles by a layer of carbon. No clean metal surface is left to dissociate the carbon-containing gas and hence the fiber growth stops. The C-deposition rates with CH_4 and CO/H_2 are slowly increasing in the first hour, *i.e.* activation occurs, after which more or less a steady-state is reached. This shows that with these two gases the CNF growth is a balanced process, which holds for a long period of time.

With the unsupported nickel catalyst with none of the used gases a steady-state production of CNF is observed. CH_4 is not converted at all, CO/H_2 shows only initially some activity, while C_2H_4/H_2 deactivates the catalyst within 3 h, not withstanding the fact, that the activity is high and close to constant for 2 h. How to explain, to start with, the different behavior of the catalysts with respect to CH_4 and CO/H_2?

We are convinced that this difference originates from the difference in nickel particle size, and with this, with the different types of lattice planes exposed. From literature it is well known that the type of exposed lattice plane significantly affects the rate of hydrocarbon decomposition [23-26]. Because this decomposition is the first step in the growth process of the fiber too, this must also hold for the rate of CNF growth when the rate of decomposition becomes rate determining.

It has been reported [8,21], that small particles from which CNF have been grown, usually are more or less spherical/conical, which implies that more open, high-index planes are exposed. These planes are active for dissociation, even of CH_4, the least reactive compound at 550 °C. With larger particles the most stable, low-index plane(s) dominate the gas-solid interface [37,38], which means that only more reactive hydrocarbons, like C_2H_4, are dissociated.

With the small nickel particles we found with C_2H_4/H_2 a rather high initial carbon deposition rate, which was rapidly followed by deactivation due to encapsulation. This initial rate is much higher indeed than those measured with CH_4 and CO/H_2, probably as a result of

the high reactivity of C_2H_4. As we stated earlier, ultimately nucleation and fiber formation cannot keep up with the rate of hydrocarbon dissociation, due to which encapsulation occurs.

With the large, unsupported particles, however, we observed that the growth process remained for even 2 h at a surprisingly high level. From Figure 1 we concluded that the nickel particles of the unsupported catalyst are sized in the range of 50 - 1000 nm but are conglomerated to even much larger units. Furthermore, XRD results make it even questionable whether the smallest particles as observed were monocrystalline. Undoubtedly, from the start of the process, carbon is deposited on all exposed surfaces, which rapidly diffuses into the bulk. Probably from the smallest particles of the conglomerates fibers start to grow because of these units diffusion paths are the shortest.

In Figure 7A a bundle of fibers is shown with diameters of about 50 nm, a size close to that, formed from the small supported nickel particles. Striking is the observation that from each of these particles a pair of fibers had formed. Such a phenomenon we never have observed with the small particles of a supported catalyst.

A tentative explanation of the deviating behavior of the 50 nm particles is that the particles consist of two monocrystalline units, from each of which a fiber has grown. Probably, these nickel particles had been expelled from the conglomerated units because of stress forces brought about by dissolution of large amounts of carbon. It is very well possible that, if nucleation of the fibers occurred close to each other, *e.g.* on both sides of the interface between the monocrystalline regions, defects in the graphitic layers became introduced, which caused the helical growth [33,34] of the fibers, see Figure 7B.

With SEM no large metal conglomerates could be found after CNF growth, only small metal fragments are observed. Obviously the process of fragmentation and the continuously formation of fresh metal surfaces is the explanation for the relatively long period of time the growth of fibers could continue. Only after 2 h the growth rate decreased and after 3 h no fresh surfaces were formed anymore and termination of the fiber formation occurred.

The above given explanations may also hold for the formation of the multidirectional fibers [35,36] as shown in figure 7D. Only in this case the nickel particle is much larger and probably consists of at least several monocrystalline domains. The formed graphitic planes probably originate from more than one monocrystalline region, due to which many defects are built in, causing the variable diameter and roughness of the fibers.

The most peculiar type of fiber is shown in figure 7C. The thickness of the fiber, about 700 nm, indicates that in this case it must have grown from a highly polycrystalline surface from which nucleation and piling up of the layers took place rather irregularly. Possibly a pulse-like change of layer orientation and variation in fiber diameter occurred.

Conclusions

In this study, we have demonstrated that a continuous production of CNF is only possible when carbon deposition, diffusion, nucleation and growth are in a subtle balance. This can be achieved with the small nickel particles of the supported catalyst in combination with a carbon-containing gas with a relatively low inclination for dissociation, *i.e.* CH_4 and CO/H_2 at 550 °C. The small metal particles expose high-index planes, which avoid termination of the growth process. With the more reactive C_2H_4/H_2 mixture, diffusion of carbon and nucleation cannot keep up with the carbon deposition, due to which encapsulation rapidly terminates the growth process.

With the unsupported nickel particles termination in case of C_2H_4/H_2 is delayed due to formation of fresh metal surfaces as a result of fragmentation of the large conglomerates. A variety of fiber types is formed of which only the fibers grown from the small particles are more or less regular. Because most of the particles are large, low-index planes, incapable of dissociation of CH_4 and CO/H_2, dominate the gas-metal interface and fiber formation is not possible at the chosen conditions.

References

1. N.M. Rodriquez, J. Mater. Res. 8 (1993) 3233.
2. R.T.K. Baker, Carbon 27 (1989) 315.
3. K.P. de Jong and J.W. Geus, Catal. Rev.-Sci. Eng. 42 (2000) 481.
4. A. Thess, R. Lee, P. Nikolaev, H.J. Dai, P. Petit, J. Robert, C.H. Xu, Y.H. Lee, S.G. Kim, A.G. Rinzler, D.T. Colbert, G.E. Scuseria, D. Tomanek, J.E. Fischer and R.E. Smalley, Science 273 (1996) 483.
5. S. Iijima, Nature 354 (1991) 56.
6. T.W. Ebbensen and P.M. Ajayan, Nature 358 (1992) 220.
7. N.M. Rodriquez, M.-S. Kim and R.T.K. Baker, J. Phys. Chem. 98 (1994) 13108.
8. J.W. Geus, A.J. van Dillen and M.S. Hoogenraad, Mat. Res. Soc. Symp. Proc. 368 (1995) 87.
9. R.T.K. Baker, Carbon Fibers, Filaments and Composites NATO ASI Series, Kluwer, Dordrecht (1990) 405.
10. D.L. Trimm, Catal. Rev.-Sci. Eng. 16 (1977) 155.
11. F. Coloma, A. Sepúlveda-Escribano, J.L.G. Fierro and F. Rodríguez-Reinoso, Appl. Catal A Gen. 150 (1997) 165.
12. B. Bachiller-Baeza, A. Guerrero-Ruiz and I. Rodríguez-Ramos, Appl. Catal. A Gen. 192 (2000) 289.
13. A. Giroir-Fendler, D. Richard and P. Gallezot, Stud. Surf. Sci. Catal. 41 (1988) 171.

14. C. Pham-Huu, N. Keller, G. Ehret, L.J. Charbonniere, R. Ziessel and M.J. Ledoux, J. Mol. Catal. A Chem. 170 (2001) 155.
15. P. Gallezot and D. Richard, Catal. Rev-Sci. Eng. 40 (1998) 81.
16. N.M. Rodriquez, A. Chambers and R.T.K. Baker, Langmuir 11 (1995) 3862.
17. A. Chambers, T. Nemes, N.M. Rodriquez and R.T.K. Baker, J. Phys. Chem. B 102 (1998) 2251.
18. J.-F. Colomer, P. Piedigrosso, I. Willems, C.Cournet, P. Bernier, G. Van Tendeloo, A. Fonseca and J.B. Nagy, J. Chem. Soc., Faraday Trans. 94 (1998) 3753.
19. P. Chen, H.-B. Zhang, G.-D. Lin, Q. Hong and K.R. Tsai, Carbon 35 (1997) 1495.
20. M.S. Hoogenraad, Ph.D. thesis, Utrecht University (1995).
21. E. Boellaard, P.K. de Bokx, A.J.H.M. Kock and J.W. Geus, J. Catal. 96 (1985) 481.
22. R.T.K. Baker, M.S. Kim, A. Chambers, C. Park and N.M. Rodriquez, Stud. Surf. Sci. Catal. 111 (1997) 99.
23. I. Alstrup, J. Catal. 109 (1988) 241.
24. M. Audier, A. Oberlin and M. Coulon, J. Crystal Growth 55 (1981) 549.
25. F.C. Schouten, E.W. Kaleveld and G.A. Bootsma, Surf. Sci. 63 (1977) 1.
26. F.C. Schouten, O.L.J. Gijzeman and G.A. Bootsma, Surf. Sci. 87 (1979) 460.
27. M.-S. Kim, N.M. Rodriquez and R.T.K. Baker, Mat. Res. Soc. Symp. Proc. 368 (1995) 99.
28. C. Menini, C. Park, R. Brydson and M.A. Keane, J. Phys. Chem. B. 104 (2000) 4281
29. C.D. Tan and R.T.K. Baker, Catal. Today 63 (2000) 3.
30. A.J. van Dillen, J.W. Geus, L.A.M. Hermans and J. van der Meijden, Proc. 6th Int. Congr. Catal. 2 (1977) 677.
31. L.A.M. Hermans and J.W. Geus, Stud. Surf. Sci. Catal. 3 (1979) 113.
32. W. Teunissen, Ph.D. thesis, Utrecht University (2000).
33. M.S. Kim, N.M. Rodriguez and R.T.K. Baker, J. Catal. 134 (1991) 253.
34. S. Amelinckx, X.B. Zhang, D. Bernaerts, X.F. Zhang, V. Ivanov and J.B. Nagy, Science 265 (1994) 635.
35. M.T. Tavares, C. Bernardo, I. Alstrup and J.R. Rostrup-Nielsen, J. Catal. 100 (1986) 545.
36. H. Terrones, T. Hayashi, M. Munoz-Navia, M. Terrones, Y.A. Kim, N. Grobert, R. Kamalakaran, J. Dorantes-Davila, R. Escudero, M.S. Dresselhaus and M. Endo, Chem. Phys. Lett. 343 (2001) 241.
37. N.M. Rodriguez, Mol. Nanostruct., Proc. Int. Wintersch. Electron. Prop. Novel Mater. (1998) 495.
38. V.I. Zaikovskii, V.V. Chesnokov and R.A. Buyanov, Appl. Catal. 38 (1988) 41.

3

The Influence of Oxidation on the Texture and the Number of Oxygen-Containing Surface Groups of Carbon Nanofibers

Abstract

The effect of liquid-phase oxidation on the texture and surface properties of carbon nanofibers has been studied using XRD, TEM, SEM, N_2-physisorption, TGA-MS, XPS and acid-base titrations. Oxidation was performed by refluxing the nanofibers in HNO_3 and mixtures of HNO_3/H_2SO_4 for different times. The graphite-like structure of the treated fibers remained intact, however, the specific surface area and the pore volume increased with the severity of oxidation treatment. For the first time it is shown that the most predominant effect that gives rise to these textural modifications is the opening of the inner tubes of the fibers. Moreover, it is demonstrated that both the total oxygen content (O/C=0.02-0.07 at/at) as well as the number of acidic groups (1-3 nm^{-2}) are a function of the type of oxidizing agent used and the treatment time. The total oxygen content of the oxidized samples turns out to be substantially higher than can be accommodated in the form of oxygen-containing groups at the exterior surface.

Introduction

Carbon materials are widely used, *e.g.* as adsorbent, as catalyst support and for structural reinforcement of polymers. Often mentioned advantages are their high surface area and chemical inertness. Among the many types of carbons, activated carbon is still the most commonly used. However, more recently, carbon nanofibers (CNF), carbon nanotubes (CNT) [1-3] and related materials have attracted interest. These graphite-like CNF are grown from decomposition of carbon-containing gases on small metal particles. They have unique textural and mechanical properties and contain neither micropores nor impurities.

The hydrophobic and inert nature of the as-grown graphite-like CNF can be unfavorable for some applications. Nevertheless, by treatment in *e.g.* an oxidizing acid, oxygen-containing surface groups can be introduced thus enhancing the wettability for polar solvents such as water and making the surface more reactive [4-7]. The precise nature of these carbon-oxygen structures is not entirely established, but the results of many reported studies using FT-IR, Boehm-titrations and TPD demonstrate that several types of surface-oxygen groups can be distinguished [4-6]. The number of oxygen-containing surface groups is highly dependent on the way of preparation. A critical survey of methods for the determination of these groups on carbon has been given by Boehm *et al.* [8]. In contact with aqueous solutions depending on the pH, negatively, neutral and positively charged surface sites exist [4].

These oxygen-containing surface groups are formed not only by reaction with oxidizing gases (*e.g.* O_2, O_3 and CO_2) but also by treatment with aqueous solutions of HNO_3, H_2SO_4 or H_2O_2. In this study aqueous solutions of HNO_3 and mixtures of HNO_3/H_2SO_4 have been used. In these solutions the nitronium ion, NO_2^+, is able to attack aromatic compounds, which is probably the first step in the introduction of oxygen-containing surface groups. Therefore the severity of the oxidation treatment depends both on the treatment time and the concentration of NO_2^+, which increases in the order HNO_3 < 1:1 HNO_3/H_2SO_4 < 1:3 HNO_3/H_2SO_4 [7,9,10].

Over the years, the effect of oxidation of classical carbon supports, such as activated carbon, carbon black, graphite and graphite-like materials has been extensively studied. For example, He *et al.* [11] have reported on the structure of graphite oxide prepared by treating graphite with aqueous oxidizing agents. More recently, studies on the oxidation of CNT have been reported [2,7,12-15]. Results show that treatment of CNT in oxidizing acids results in opening of the inner tubes [12,14,15]. Hoogenraad *et al.* [2] treated CNT in HNO_3 to introduce surface oxygen groups, largely carboxylic- or carbonyl groups, to enable the application of Pt- and Pd-complexes *via* ion exchange. The iso-electric point (IEP) of 2.3 after treatment was found to be indicative of the presence of carboxylic groups.

Up to now the effect of surface oxidation on the texture and surface properties of fishbone CNF has only scarcely been described. Darmstadt *et al.* studied the (12 h) oxidation of CNF (diameter ~ 200 nm) in boiling HNO_3 [16]. They claim that not only the surface became affected; also the ordering of the graphite-like structure in the bulk was decreased.

Nonetheless, from the work of Ros *et al.* where the oxidation treatment of CNF in the liquid-phase (HNO_3 and HNO_3/H_2SO_4) had been confined to 2 h it appeared that the macroscopic structure as well as the graphite-like structure of the fibers was preserved [7]. During oxidation, first the formation of carbonyls occurs, which later on are converted into carboxyls and carboxylic anhydrides. Also ether-type oxygen groups in the graphite layers are formed. Ros *et al.* [7] stated that the formation of oxygen-containing surface groups occurs mainly at defect sites on the CNF surface. Unfortunately, in their work only the total number of oxygen groups is quantified.

Here, we report on the effects of surface oxidation of small diameter (20-30 nm) fishbone CNF. XRD and TEM were used to investigate the graphite-like structure of untreated and oxidized CNF. To examine the possible changes in the texture of the CNF N_2-physisorption and SEM were utilized. Moreover TGA-MS, XPS and titrations were used to determine the total oxygen content and the number of acidic surface groups. The thermostability of the surface oxides was studied by titration, TGA-MS and XPS measurements of oxidized samples thermally treated in N_2 at 573, 773 and 973 K.

Experimental

Carbon nanofiber growth

For the growth of CNF, 20 wt% Ni/SiO_2 was prepared by homogeneous deposition precipitation (HDP) as described by van Dillen *et al.* [17] using silica (Degussa, Aerosil 200), nickel nitrate (Acros), and urea (Acros). After filtering and washing, the catalyst precursor was dried at 393 K and calcined in static air at 873 K (5 K/min) for 2 h.

One gram of the Ni-catalyst precursor was placed in a quartz reactor and prior to the fiber growth reduced *in situ* for 2 h in a flow of a mixture of H_2 (80 ml/min) and N_2 (320 ml/min) at 1 bar and 973 K (heating rate 5 K/min). Next, the CNF were grown at 823 K in a mixture of CO (80 ml/min), H_2 (28 ml/min), and Ar (292 ml/min) for 24 h. Typically, a CNF yield of 10 g was obtained. A more detailed description of the preparation of the growth catalyst and the growth of the CNF can be found elsewhere [3].

Surface oxidation of carbon nanofibers

In Table 1 the samples together with their identification codes and the different treatments are listed. After growth all the CNF samples, except for the untreated sample CNF#1, were refluxed for 1 h in a 1 M KOH solution in order to remove the silica support. CNF sample #2 was obtained after subsequent treatment in boiling HCl, to remove exposed nickel metal particles. All the other samples were, after KOH treatment, refluxed in concentrated HNO_3 (#3 and #4) or in a mixture of HNO_3/H_2SO_4 (#5 and #6) for different times for activation and for removal of exposed nickel. Typically, 10 g CNF was refluxed in 200 ml solution.

Table 1. Identification codes and treatment conditions of the various carbon nanofiber samples.

Code	Base treatment	Acid treatment	N_2 treatment (2 h)
#1	-	-	-
#2	reflux 1 h 1M KOH	reflux 1 h conc HCl	-
#3	reflux 1 h 1M KOH	reflux 0.5 h conc HNO_3	-
#4	reflux 1 h 1M KOH	reflux 2 h conc HNO_3	-
#5	reflux 1 h 1M KOH	reflux 0.5 h conc HNO_3/H_2SO_4 1:1	-
#6	reflux 1 h 1M KOH	reflux 0.5 h conc HNO_3/H_2SO_4 1:3	-
#4 573 K N_2	reflux 1 h 1M KOH	reflux 2 h conc HNO_3	573 K
#4 773 K N_2	reflux 1 h 1M KOH	reflux 2 h conc HNO_3	773 K
#4 973 K N_2	reflux 1 h 1M KOH	reflux 2 h conc HNO_3	973 K

Subsequently, the CNF were washed thoroughly with demi-water and dried in air at 393 K for 16 h.

Heat treatment in N_2 of oxidized carbon nanofibers

In order to investigate the thermostability of the oxygen-containing groups on the CNF surface, samples of the CNF oxidized in HNO_3 for 2 h (#4) were heat-treated in flowing nitrogen for 2 h at 573, 773 and 973 K (#4 573, #4 773 and #4 973).

Carbon nanofiber characterization

Transmission electron microscope (TEM) images were obtained using a Philips CM-200 FEG operated at 200 kV. After suspending in ethanol under ultrasonic vibration, samples were brought onto a holey carbon film on a copper grid.

A Philips XL-30 Field Emission Gun (FEG) scanning electron microscope was used to obtain SEM images.

Texture analyses were performed with N_2-physisorption at 77 K, up to a pressure of 1 bar. From the N_2-physisorption data, obtained with a Micromeritics ASAP 2400 apparatus, BET surface area, total mesopore volume and micropore volume (t-plot) were derived. Prior to physisorption measurements, the samples were evacuated at 473 K for at least 16 h.

X-ray diffraction (XRD) patterns were recorded at room temperature with an Enraf Nonius PDS 120 powder diffractometer system equipped with a position-sensitive detector with a 2θ range of 120 ° using Co $K\alpha_1$ (λ=1.78897 Å) radiation.

The amount of carbon burned-off during oxidation is determined by weighing dried CNF samples before and after the oxidation treatment.

The number of acid sites of the oxidized CNF after the various treatments was determined by performing direct acid-base titrations. Since grinding of the mesoporous CNF samples before the titration experiments did not influence the results, it was concluded that transport

restrictions did not interfere. Samples of 20-40 mg of untreated and oxidized CNF were stirred with 25 ml of a solution containing 0.1 M NaCl (supporting electrolyte) and 0.1 mM oxalic acid in demi-water, acidified to pH=3 with HCl. This composition was found by optimization to give the most reproducible results. While stirring, pure nitrogen was flushed through the reactor and 10 mM NaOH was added dropwise from a buret with a rate of 0.05 ml/min. The pH was monitored using a combined pH electrode PHC 4406. All acid sites with a $pK_a < 7.5$ were measured. It is likely that in the pH range of 3-7.5 only the carboxylic groups are probed. The accuracy of this method was found to be within 10%.

The total number of oxygen-containing groups was measured using thermogravimetric analysis (TGA) on a Netzsch STA-429 thermobalance. The gases evolved were monitored by a Fisons Thermolab quadropole mass spectrometer, through a capillary situated directly above the sample cup. Samples (20-100 mg) were heated in Ar (60 ml/min) at a rate of 5 K/min to 1123 K.

XPS data were obtained with a Fisons ESCALAB 210I-XL and a Vacuum Generators XPS system. Al Kα X-ray radiation was utilized, employing an anode current of 20 mA at 15 and 10 keV respectively. The pass energy of the analyzer was set at 70 eV for the Fisons apparatus and 50 eV for the Vacuum Generators XPS. The samples were measured without grinding of the CNF skeins.

Results and Discussion

In Figure 1A an SEM picture of an untreated CNF sample (CNF#1) is shown. The fibers with an average diameter of about 25 nm are interwoven, forming porous skeins in the micrometer range. The lighter spots in the image, two of them are indicated by arrows, are nickel particles from which the fibers had been grown. Figure 2 displays a TEM image of untreated CNF (CNF#1), showing the individual lattice planes of the graphite-like lattice, ordered predominantly in the fishbone structure thus exposing the edges of the graphene sheets. In contrast to what might be concluded from this image, Ros *et al.* [18] mentioned that

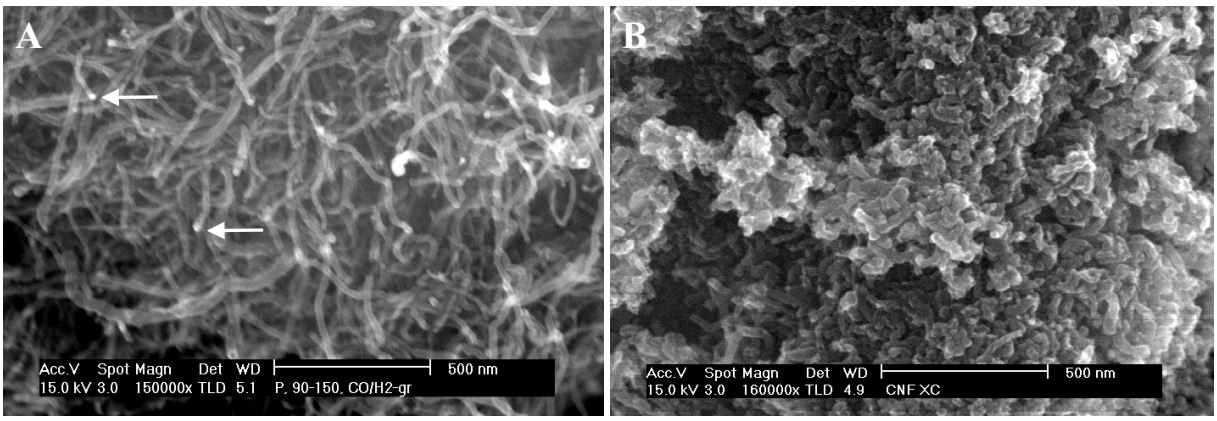

Figure 1. SEM image of (A) CNF#1 and (B) CNF#6.

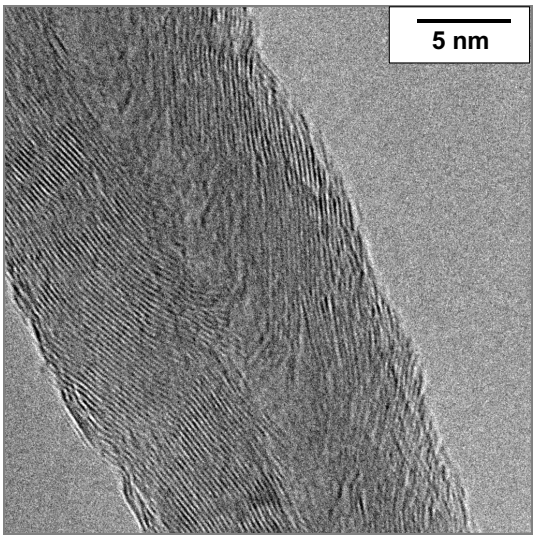

Figure 2. TEM image of untreated carbon nanofibers (CNF#1).

the ordering in the graphene sheets and their stacking in as-grown CNF is far from ideal. Regions of high defect concentrations alternate with defect-poor regions, which are presumably more sensitive to oxidation. Also Nijkamp stated that untreated CNF display a significant amount of defects, such as two planes coinciding to one, bending planes, planes more or less parallel to the fiber axis and plane ends parallel to the fiber surface [19].

Graphite-like structure of carbon nanofibers

The effect of the various oxidation treatments on the graphite-like structure of all CNF samples has been studied using XRD and TEM. In Figure 3 the diffraction patterns are shown. Untreated CNF#1 distinctly shows diffraction peaks of graphite-like carbon, next to diffraction peaks of nickel. These diffraction patterns demonstrate that the subsequent treatments in acid did not affect the integrity of the graphite-like structure, since the carbon peak positions and widths are unaltered. The set of patterns also demonstrates the removal of (part of the) nickel present after the growth of the fibers. TEM examination showed that

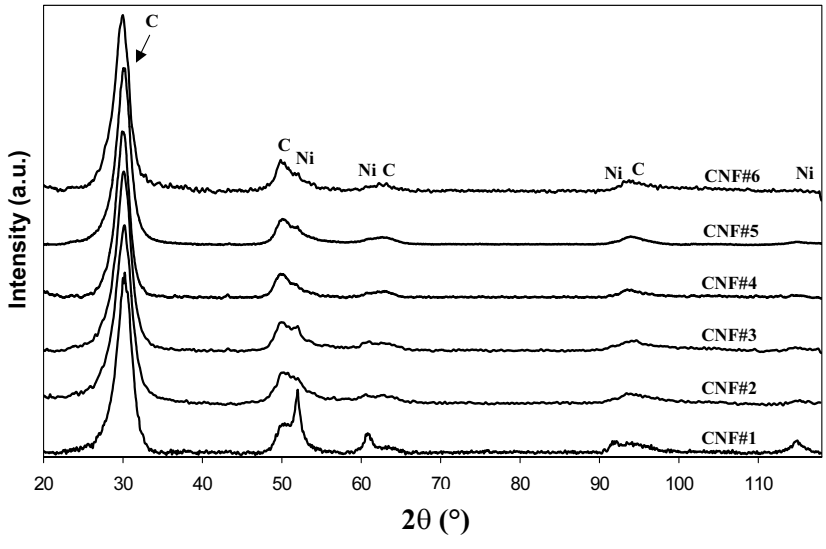

Figure 3. X-ray diffraction patterns of untreated and treated carbon nanofibers.

Table 2. Burn-off (%) due to various oxidation treatments.

Samples	Burn-off (%)
CNF#1	n.d.
CNF#2	n.d.
CNF#3	2.4
CNF#4	3.1
CNF#5	3.7
CNF#6	22.3

n.d. not determined

graphitic envelopes encapsulate the remaining nickel. Moreover, TEM images of the samples (not shown) indicate that the characteristics of the CNF remained the same, *i.e.* the graphite-like structure is still intact and no change in average diameter is observed. So, both techniques prove that the graphite-like structure was unaffected after the oxidation.

Texture of carbon nanofibers

The textural properties of CNF#1 to #6 were investigated by means of N_2-physisorption and SEM. Furthermore, the carbon burn-off percentage after the various acid treatments was measured (Table 2). Oxidizing CNF in HNO_3 or 1:1 HNO_3/H_2SO_4 (CNF#3 to #5) results in a weight loss of 2-4 wt %, which can be chiefly explained by the removal of non-encapsulated nickel. Oxidation in 1:3 HNO_3/H_2SO_4 (CNF#6) for 0.5 h results in a considerable weight loss of 22%. This sample required a substantially longer filtration time than the other samples. Probably plugging of the 200 nm pores of the filter occurred. After treatment in this acid mixture for 2 h hardly any fibers remained.

The SEM images of CNF#2 to #4 are very similar to the SEM image of CNF#1 shown in Figure 1A. The macroscopic structure of CNF#5 and especially that of CNF#6, however, is much more dense and the fibers are considerably shorter (Figure 1B).

The weight loss and the SEM images after treatment in 1:3 HNO_3/H_2SO_4 indicate a partial destruction of the fibers. The original, mainly macroporous skeins of long and interwoven fibers have been converted into a more dense packing of short fiber fragments. Treatment in 1:1 HNO_3/H_2SO_4 also results in fragmentation, but to a significantly lower extent. This is confirmed by the much smaller weight loss upon treatment of CNF#5 compared to that of CNF#6. SEM images of the various samples show that the fragments have about the same average diameter as that of the untreated fibers, which strongly suggests that the original long fibers are broken up perpendicular to the length axis. Treatment of the fibers with a strong oxidizing agent ultimately leads to complete oxidation and consumption of defect-rich regions in the CNF, leaving the short fragments. Other investigators have reported on the breaking up of CNT [12,14,15,20] and SWNT [21] into smaller fragments by liquid-phase oxidation.

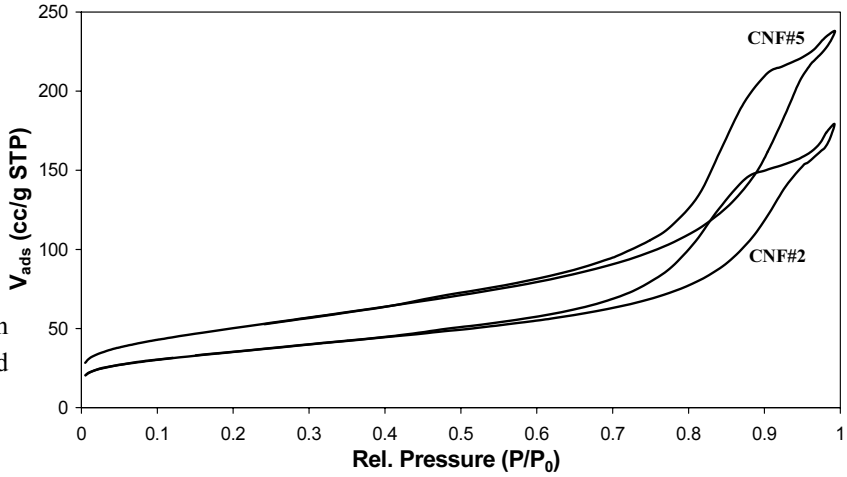

Figure 4. Adsorption-desorption isotherm of N_2 of CNF#2 and CNF#5.

To obtain more information on the effect of the pretreatment on the structure of the CNF, N_2-physisorption experiments were performed on CNF#1 to #6. As representative examples, the adsorption-desorption isotherms of two CNF samples, one before and one after oxidation (CNF#2 and #5), are given in Figure 4. The derived values of S_{BET}, total pore volumes and micropore volumes of all samples are summarized in Table 3. The isotherms are characteristic of multilayer adsorption/desorption accompanied by capillary condensation in relatively large mesopores, causing a hysteresis loop. The shape of the hysteresis loops indicates a distribution of cylindrical pores open at both sides. From the corresponding t-plots a very low micropore volume of 0.01 ml/g can be derived for all samples. An increase in the total surface area is noticed with increasing severity of the oxidation treatment, roughly coinciding with a proportional increase in pore volume of the material, as can be seen in Table 3.

Corrected for the silica support, a specific surface area of 130 m^2/g can be calculated for non-treated CNF (CNF#1). With increasing oxidation time of the same acid and/or increasing the oxidation power of the acid, the surface area gradually rises to 194 m^2/g. The pore volume of CNF#1 to #5 increased from 0.21 to 0.38 cm^3/g. For CNF#6, however, a slightly lower pore volume was found. This decrease might be correlated with the strong fragmentation and the associated more dense packing of the fibers as demonstrated with SEM.

Samples CNF#1 up to #5 exhibited a relatively narrow pore size distribution with an average diameter of about 12 nm. In Figure 5 pore size distributions of CNF#2 and #5 are plotted as representative examples. Only with CNF#6 a somewhat broader pore diameter distribution was found with an average pore diameter of 8 nm. For the calculations of the pore size distributions the BJH (Barret-Joyner-Halenda) method has been applied, using the desorption branch of the nitrogen isotherms. Above ~4 nm diameter this method gives reliable pore size distributions based on the Kelvin equation, valid from 2 nm. However, in the 2-4 nm region artifacts can arise due to the closure of the hysteresis loop.

All oxidative treatments led to both an increase of specific surface area and pore volume, taking the respective values of CNF#2 as the base for comparison. The increase of specific

Table 3. Some physico-chemical features of carbon nanofibers before and after the various oxidation treatments.

Sample	S_{BET} (m^2/g)	V_{pore} total (cm^3/g)
CNF#1	137*	0.21
CNF#2	138	0.25
CNF#3	156	0.30
CNF#4	186	0.36
CNF#5	183	0.38
CNF#6	194	0.32

* S_{BET} after correction for still present silica support is ~130 m^2/g

surface area can be ascribed to three effects: fragmentation, surface roughening and opening of the inner tubes of the fibers. Fragmentation of the long fibers into shorter fragments of the same diameter hardly increases the specific surface. Taking into account the dimensions of the original fibers and that of the fragments as can be estimated from SEM images, we calculated that this effect is confined to about 10% in the case of CNF#6, the sample with the most and the shortest fragments.

Another explanation can be found in roughening of the fiber surface due to oxidative treatments. Shaikhutdinov *et al.* [22] earlier investigated the roughness of the surface of CNF. They utilized scanning tunneling microscopy (STM) to study the height differences on the surface of fishbone CNF and found considerable surface roughness factors of 4-5. The CNF used in our study presumably also have a rough surface. From the average diameter of the fibers of 25 nm an external surface area of 71 m^2/g can be derived, assuming a carbon density of 2.25 g/cm^3 and closed fibers. For CNF#2 a S_{BET} of 138 m^2/g is found and for CNF#6, the most oxidized CNF, 194 m^2/g. This implies that the surface area is 2 to 3 times larger than one would expect. From TEM, however, no evidence for enhanced surface roughness of the oxidized samples has been observed. Since only a small increase in surface area is observed from CNF#1 to CNF#2, it can be concluded that the changes in texture are not caused by the KOH treatment but can be ascribed to the treatment in oxidizing acids.

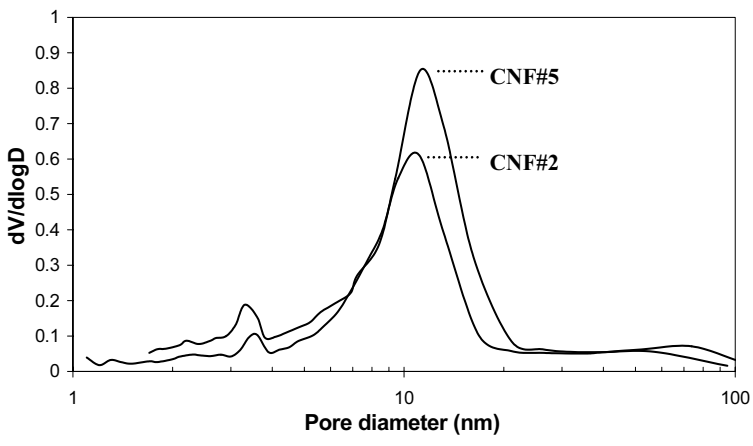

Figure 5. Pore size distributions of CNF#2 and #5.

As most likely explanation for the increased surface area due to oxidation, opening of the inner tubes of the fibers remains. From literature it is known that CNT can be opened by boiling them in oxidizing acids, thereby making their inner tubes accessible [12,14,15,20]. If CNF are oxidized extensively, the nickel particles on top of the fibers might be extracted and carbon from the center of the fiber can be removed, which could result in the formation of an inner tube with a diameter of several nanometers. Moreover, the fibers can be broken up at defect-rich areas, leading to opening of the fiber fragments. An argument that strongly supports this explanation is that a significant increase in pore volume is found going from sample CNF#1 to CNF#5 (Table 3) along with a proportional increase in surface area.

The difference in total pore volume of CNF#5 and CNF#2 is 0.13 cm^3/g. Calculations using an average fiber diameter of 25 nm and an average inner tube diameter of 12 nm, taken from the pore size distribution plots, show that opening of ~65% of the CNF can give rise to this increase in pore volume, while an increase in surface area of 43 m^2/g has to be expected. A difference in S_{BET} between CNF#5 and CNF#2 of 45 m^2/g was found with nitrogen physisorption (Table 3). These calculations support the supposition that opening of part of the inner tubes of CNF upon oxidation occurs.

From the adsoption-desorption isotherms it was concluded that filling of cylindrical pores very likely caused the hysteresis. Cylindrical pores indeed suggest the opening of the CNF, while the pores between the fibers are far from cylindrical. At first sight, the fact that no significant changes in the pore size distributions of CNF#2 to CNF#5 are found, while the majority of the inner tubes become accessible, is surprising. This might be explained by assuming that at maximum 35% of the CNF#2 fibers is already accessible for N_2-physisorption.

Studies of our group on the deposition of metals on CNF convincingly provide proof for the opening of the fibers. TEM tilt series have shown that part of the metal (Ni, Pd, Co) can be deposited in the inner tubes of oxidized CNF [23].

Number of oxygen-containing surface groups

A direct acid-base titration technique using NaOH was performed to determine the number of

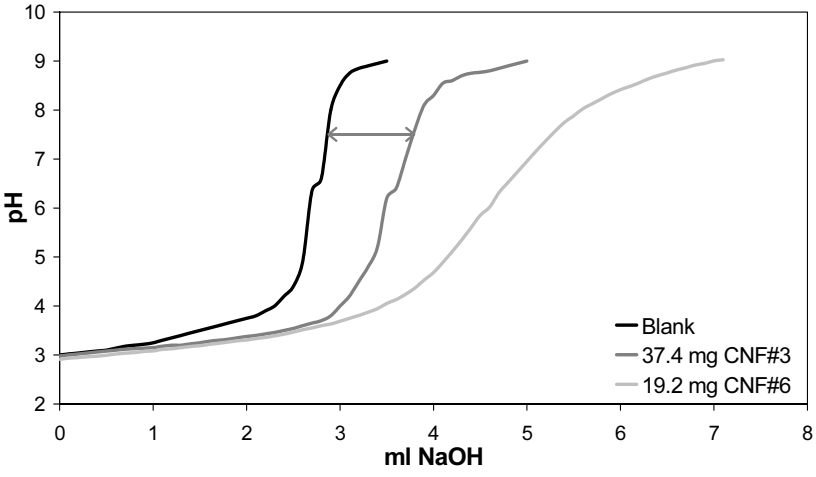

Figure 6. Titration curves of blank, CNF#3 and CNF#6.

Table 4. Titration, XPS and TGA-MS (corrected for phys. water) results of carbon nanofibers after different treatments.

Sample	Titration		TGA-MS		XPS	
	Acidic oxygen-containing surface groups/nm^2	O atoms/nm^2	Weight loss (%)	O atoms/nm^2	O/C atomic ratio	O atoms/nm^2
CNF#1	-	-	<0.5	<1.2 ± 0.2	0.016	2.3 ± 0.3
CNF#2	-	-	-	-	0.023	3.4 ± 0.5
CNF#3	1.0 ± 0.1	2.0 ± 0.2	4.0	8.3 ± 0.6	-	-
CNF#4	1.4 ± 0.1	2.8 ± 0.2	5.7	9.8 ± 0.8	0.069	9.6 ± 1.4
CNF#5	1.5 ± 0.2	3.0 ± 0.4	6.4	9.8 ± 0.8	-	-
CNF#6	3.3 ± 0.3	6.6 ± 0.6	9.2	12.3 ± 1.1	-	-
CNF#4 573 K N_2	1.0 ± 0.1	2.0 ± 0.2	3.7	6.3 ± 0.5	0.038	5.3 ± 0.8
CNF#4 773 K N_2	0.2 ± 0.02	0.4 ± 0.04	3.3	5.6 ± 0.5	0.032	4.4 ± 0.7
CNF#4 973 K N_2	~0.03 ± 0.003	~0.06 ± 0.01	1.8	3.0 ± 0.3	0.017	2.3 ± 0.3

surface groups exhibiting a pK_a<7.5. Titration curves obtained with samples CNF#3 and #6 are displayed as examples in Figure 6. In Table 4 the numbers of acidic oxygen-containing surface groups of the different samples as measured by titration are given. CNF#1 and #2 could not be measured reliably. Since these samples were too hydrophobic, they could not be dispersed in water properly. The titration experiments demonstrate that an increase in severity of the oxidation results in an increase in the number of acidic surface sites, from 1.0 on CNF#3 to 3.3 acidic oxygen groups/nm^2 on CNF#6. Assuming that all acidic oxygen groups are carboxylic groups the number of oxygen atoms/nm^2 is also calculated (Table 4).

XPS measurements were done to establish the amount of oxygen in the subsurface (2-3 nm) of the CNF. In Table 4 the O/C atomic ratios of most of the CNF samples are given. Results obtained with this technique confirm an increase in oxygen concentration with increasing severity of the oxidation treatment. Part of the oxygen present in CNF#1 must be due to the presence of silica from the growth catalyst in this sample. However, in CNF#2 the silica has been removed meaning that the O/C ratio of 0.023 as found demonstrates that non-oxidized CNF do already contain some oxygen, probably taken up during the fiber growth from CO/H_2 or is due to reaction with oxygen or water during storage. The O/C ratios are converted to oxygen atoms/nm^2 using a model of Gijzeman [24]. The error in the numbers is estimated to be about 15 %. These results (Table 4) show that fibers oxidized in HNO_3 for 2 h (CNF#4) contain 9.6 O atoms/nm^2. This implies that ca 5-10 oxygen-containing groups are present per nm^2, which is rather high. Values up to 1-3 groups/nm^2, as we found by titration,

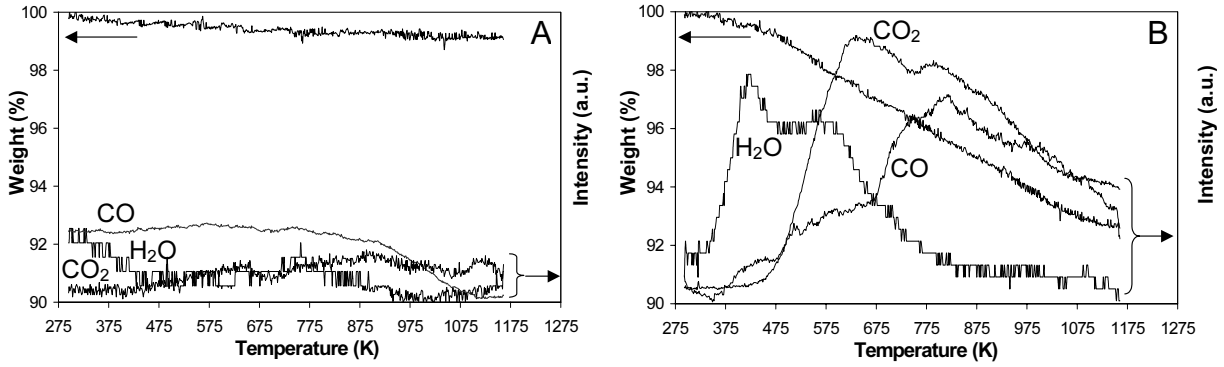

Figure 7. TGA-MS patterns in Ar: (A) CNF#1 and (B) CNF#5.

seem to be much more realistic [6]. An explanation for this discrepancy can be found by assuming that oxygen atoms are not present solely at the exterior surface, but also are built in in the subsurface of the fibers [7,11].

TGA-MS was used to study the amount of oxygen in the bulk as well as at the surface of the CNF samples. The total weight loss up to 1123 K is related to the total amount of oxygen present in the CNF and from the mass signals as function of the temperature information about the types of surface groups can be obtained. In Figure 7 typical TGA-MS temperature patterns of CNF#1 and CNF#5 are displayed. Weight loss of the untreated sample CNF#1 is relatively small, about 1 %, as can be seen in Figure 7A. Only small amounts of H_2O, CO and CO_2 are formed during heating, meaning that untreated hydrophobic CNF (CNF#1) contain small amounts of thermally removable oxygen and physisorbed water.

From Figure 7B it is evident that due to the treatment in 1:1 HNO_3/H_2SO_4 substantial amounts of oxygen had been taken up in CNF#5. Up to 1123 K a total weight loss of 7.5 % was measured, which confirms the results of Ros *et al.* [7] obtained with oxidized CNF and CNT. The TGA-MS patterns of CNF#4 and CNF#6 are very similar to that of CNF#5 (Figure 7B), is it that the total weight losses increase from CNF#1 to #6.

From the literature it is known that the water peak around 423 K can be ascribed to evolved physisorbed water [7,25]. The second peak at 523 K might originate from carboxylic anhydrides formed from neighboring carboxyl groups. CO_2 evolution around 623 K is attributed to the decomposition of carboxylic groups [6,7,25,26] and CO_2 evolving at still higher temperatures originates from carboxylic anhydrides and/or lactones [7,25-27]. For the CO evolution profile the assignment is less certain. CO could originate amongst others from phenol, carbonyl, quinone, ether and anhydride groups [7,8,25,26].

TGA-MS demonstrates that treatment of the fibers in HNO_3 for 0.5 h, CNF#3, already results in the formation of a significant amount of oxygen-containing groups. However in the CO and CO_2 patterns no distinct maxima are measured making assignment difficult. Weight loss profiles of CNF#4 up to #6 are very alike and are therefore discussed together. The CO_2 patterns demonstrate the presence of carboxyl and anhydride groups on their surface, decomposing from ~473 to 750 K and higher temperatures.

Water evolved preceding the CO and CO_2 evolution, arises from physisorbed water. To enable quantification of the loss of weight due to evolution of oxygen-containing compounds, weight loss due to removal of physisorbed water should be subtracted from the total weight loss. The corrected weight losses of all CNF samples are listed in Table 4. It may be concluded that weight loss is related to the severity of the oxidation treatment. With CNF#1 a weight loss of <0.5% was found, while for the oxidized samples CNF#3 to #6 weight losses of 4.0, 5.7, 6.4 and 9.2 % were measured respectively. When it is assumed (see [7]) that CO and CO_2 evolve in a ratio of 1:1, that weight loss exclusively originates from decomposition of oxygen-containing groups and the BET surface areas are taken, the number of oxygen atoms/nm^2 can be calculated. The results are given in Table 4. The error margins are estimated by assuming CO/CO_2 ratios of 1:2 and 2:1. Untreated CNF (CNF#1) contains <1.2 oxygen atoms/nm^2. Dependent on the severity of the oxidation treatment 8.3 to 12.3 oxygen atoms/nm^2 are found. As discussed earlier concerning our XPS results it is not likely that all these groups are localized at the surface. Probably oxygen is also built in in the outer 2-3 nm of the fibers [7,11]. Our results are in agreement with values found in literature. Hoogenraad *et al.* [2] found a weight loss of more than 10% for CNT treated in HNO_3 for 2 h and Ros *et al.* [7] found weight losses up to 7% for oxidized CNF.

With titration, XPS and with TGA-MS we found an increase in the amount of oxygen with the severity of the oxidation treatment. Using titration, the lowest numbers are found, because with this technique only the acidic groups ($pK_a < 7.5$) at the exterior surface can be measured. The number of oxygen atoms as determined using XPS and TGA-MS are comparable when the error margins are taken into account. From this we can conclude that besides acidic groups on the CNF surface, oxygen is built in the outer 2-3 nm of the fibers and no significant amounts of oxygen are incorporated in the bulk of the CNF during oxidation. It is also likely that some non-acidic groups are present at the surface of the CNF.

Thermostability of oxygen-containing surface groups

To study the thermal stability of the acidic oxygen-containing surface groups CNF#4 was heat-treated in flowing N_2 at 573, 773 and 973 K for 2 h. The results as given in Table 4 show a decrease of the number of acidic groups/nm^2 as determined using acid-base titrations, from 1.4 to respectively 1.0, 0.2 and 0.03 after heat treatment at the respective temperatures. These results show that only a small part of the acidic groups decomposes below 573K. After treatment at 773K, the majority of the acidic groups had been removed from the surface. This is in accordance with our TGA-MS results, showing that the decomposition of the carboxylic groups occurred in the range 473-750K. Treatment in nitrogen at 973K eliminated almost all acidic oxygen-containing groups from the surface. In the literature it is reported that below this temperature acid sites are destroyed and basic surface oxides can be formed when the carbon surface comes into contact with air after cooling [4-6,8].

In Table 4 also the oxygen contents of the heat-treated samples as measured with XPS and TGA-MS are given. With both techniques a gradual decrease in the oxygen amount with

temperature was observed. The numbers indicate that part of the oxygen groups is easily decomposed, since after treatment at 573 K a significant part of the oxygen atoms/groups had been removed. Most interesting is that TGA-MS results indicate that after treatment at 973 K for 2 h 3.0 oxygen atoms/nm^2 remained and with XPS it was found that 2.3 oxygen atoms/nm^2 survived this heat treatment. This shows that some very thermostable oxygen is present and/or new basic surface oxides are formed upon exposure to oxygen. These groups might play an important role in the prevention of sintering of metal particles in CNF-supported catalysts at high temperatures [28].

Conclusions

Small diameter, fishbone carbon nanofibers (CNF) (Ø ~ 25 nm) were oxidized in HNO_3 and mixtures of HNO_3/H_2SO_4 for 0.5 and 2 h. Results demonstrate that the graphite-like structure remained intact after the different oxidation treatments. However, the texture of the CNF is significantly altered. Specific surface area and pore volume increased with the severity of the treatment. We have shown that these changes in texture are mainly due to opening of the inner tubes of the CNF.

Furthermore, we showed that both the total oxygen content and the number of acidic oxygen-containing surface groups can be tuned by variation of the treatment time and by the type of acid or acid mixture used. Besides acidic oxygen groups (1-3 groups/nm^2) at the CNF exterior surface that are formed upon oxidation, also oxygen is built in in the subsurface layer (2-3 nm) of the fibers

Treatment of CNF oxidized in HNO_3 for 2 h in an inert atmosphere at 973 K leads to almost complete decomposition of the acidic oxygen-containing groups. However, non-acidic oxygen groups are still present on/in the CNF, showing that some very thermostable oxygen remains and/or new basic surface oxides are formed upon exposure to air.

References

1. K.P. de Jong and J.W. Geus, Catal. Rev.-Sci. Eng. 42 (2000) 482.
2. M.S. Hoogenraad, Ph.D. thesis, Utrecht University (1995).
3. M.L. Toebes, J.H. Bitter, A.J. van Dillen and K.P. de Jong, Catal. Today 76 (2002) 33 / Chapter 2 of this thesis.
4. F. Rodriguez-Reinoso, Carbon 36 (1998) 159.
5. R.J.J. Jansen, Ph.D. thesis, Delft University (1994).
6. H.P. Boehm, Adv. Catal. 16 (1966) 179.
7. T.G. Ros, A.J. van Dillen, J.W. Geus and D.C. Koningsberger, Chem. Eur. J. 8 (2002) 1151.

8. H.P. Boehm, Carbon 40 (2002) 145.
9. A.I. Vogel, Textbook of Practical Organic Chemistry, Longman, Green and co, London (1957) 523.
10. H.G.M. Edwards and V. Fawcett, J. Mol. Struct. 326 (1994) 131.
11. H. He, J. Klinowski, M. Fortser and A. Lerf, Chem. Phys. Lett. 287 (1998) 53.
12. H. Hiura, T.W. Ebbesen and K. Tanigaki, Adv. Mater. 7 (1995) 275.
13. D. Chattopadhyay, I. Galeska and F. Papadimitrakopoulos, Carbon 40 (2002) 985.
14. S.C. Tsang, Y.K. Chen, P.J.F. Harris and M.L.H. Green, Nature 372 (1994) 159.
15. Y.-H. Li, S. Wang, Z. Luan, J. Ding, C. Xu and D. Wu, Carbon 41 (2003) 1057.
16. H. Darmstadt, L. Summchen, J.-M. Ting, U. Roland, S. Kaliaguine and C. Roy, Carbon 35 (1997) 1581.
17. A.J. van Dillen, J.W. Geus, L.A.M. Hermans and J. van der Meijden, Stud. Surf. Sci. Catal. 2 (1977) 677.
18. T.G. Ros, A.J. van Dillen, J.W. Geus and D.C. Koningsberger, Chem. Phys. Chem. 3 (2002) 209.
19. M. Nijkamp, Ph.D. thesis, Utrecht University (2002).
20. C.-H. Li, K.-F. Yao and J. Liang, Carbon 41 (2003) 858.
21. J. Liu, A.G. Rinzler, H. Dai, J.H. Hafner, R.K. Bradley, P.J. Boul, A. Lu, T. Iverson, K. Shelimov, C.B. Huffman, F. Rodríguez-Macías, Y.-S. Shon, T.R. Lee, D.T. Colbert and R.E. Smalley, Science 280 (1998) 1253.
22. Sh.K. Shaikhutdinov, Kinet. Catal. 36 (1995) 549.
23. F. Winter, G.L. Bezemer, C. van der Spek, J.D. Meeldijk, A.J. van Dillen and K.P. de Jong, to be published.
24. O.L.J. Gijzeman, unpublished results.
25. S. Haydar, C. Moreno-Castilla, M.A. Ferro-Garcia, F. Carrasco-Marin, J. Rivera-Utrilla, A. Perrard and J.P. Joly, Carbon 38 (2000) 1297.
26. A.E. Aksoylu, M. Madalena, A. Freitas, M. Fernando, R. Pereira and J.L. Figueiredo, Carbon 39 (2002) 175.
27. M. Domingo-García, F.J. López Garzón and M.J. Pérez-Mendoza, J. Colloid Interface Sci. 248 (2002) 116.
28. M.L. Toebes, F.F. Prinsloo, J.H. Bitter, A.J. van Dillen and K.P. de Jong, J. Catal. 214 (2003) 78 / Chapter 6 of this thesis.

4

Synthesis of Supported Palladium Catalysts

- a Review -

Abstract

The synthesis of supported palladium (Pd) catalysts is reviewed with emphasis on the chemistry of catalyst synthesis, oxidic and carbon support properties and case studies in the period 1990-2000. For the application of Pd onto oxidic supports aqueous precursor solutions are frequently used. The charge of the Pd precursor and the iso-electric point of the support are important properties since they affect both the dispersion and the distribution over large support bodies during synthesis. With carbon supports direct reduction of Pd precursors may occur, giving rise to large metallic Pd particles. Using the latter support lyophilicity can to a large extent affect Pd emplacement. For the application of Pd on both oxidic and carbon supports sol-gel, deposition-precipitation, deposition-reduction, ion exchange and impregnation methods have been used. In general, it turns out that the thermal treatment often dominates the primary application of the Pd-precursor in establishing the ultimate metal dispersion. Thermal treatment in an inert atmosphere at temperatures not exceeding 773 K prior to reduction is beneficial for the Pd dispersion. Furthermore, it is concluded that gas-phase reduction leads to smaller Pd particles than liquid-phase reduction. In our opinion large progress in the development of highly loaded thermostable Pd-catalysts can be made by utilizing deposition-precipitation techniques in combination with anchoring sites on the support.

Introduction

Solid supported catalysts are complex assemblies, the preparation of which is a challenging task. Even when it is known which active sites and other features are needed to make a catalyst effective for a specific application, its preparation, generally from simple precursors, is often complicated and laborious. Minor adjustments of the preparation conditions can already have a significant influence on the delicate balance of conflicting demands: a high activity, a high selectivity and a long lifetime [1].

A high activity of a supported catalyst often calls for a large active surface area and thus for small particles, *i.e.* a high dispersion of the active phase. Because small particles, especially small metal particles, tend to sinter already at relatively low temperatures, they are generally applied onto a pre-existing support material, which itself has a large surface area and a high thermostability [2]. Suitable and therefore frequently used support materials are alumina, silica and carbon, all compounds with high melting and decomposition temperatures. Important (physical) characteristics like texture (specific surface area, pore size distribution and pore volume), density and mechanical strength can be established for these types of supports.

A complication is that catalyst particles must have a prescribed size and shape to be applicable in a specific reactor type and/or for separation from liquid-phase reaction media by filtration or centrifugation. Shaping of a support material implies, however, that a large surface area can only be attained when support bodies are highly porous, which might conflict with the desired thermal stability. Moreover, narrow and long pores might hinder transport of reactants and/or products, which generally is undesirable. Furthermore, a high porosity might bring along a decreased mechanical strength, causing the formation of fines and loss of (expensive) catalytic material.

For most catalyzed reactions the combined chemical properties of the active phase and the support bring about the catalytic functionality. Even when the support material only serves as an anchor to keep the catalytically active species separated, these species have to interact to some degree and in some way with the support. As a result of the support interaction, the nature of which remains still largely unknown, the performance of supported catalysts strongly depends on the morphology and dispersion of the active particles and, with metal catalysts, on the electronic properties of the metal [3,4].

An overview of the literature learns that, although a growing number of contributions deal with supported palladium catalysts, there is only little focus on the preparation processes of these catalysts. Generally, an earlier developed procedure is somewhat optimized, with the catalytic reaction as the ultimate test. Studies on the various steps in a synthesis route, separately and in the sequence of the total procedure, are relatively scarce.

Here, we survey the preparation of palladium catalysts supported on some oxidic and carbon materials. In this review we follow the general survey on supported catalyst preparation as given earlier by Augustine [5]. This approach enables us to confine ourselves

mainly to contributions of the last decade. We will concentrate on those contributions, which give experimental details on the preparation, thus enabling scientific interpretation.

In the section on the chemistry of catalyst synthesis we deal with surface properties of oxidic and carbon supports, which influence the interactions of the support with precursor compounds, notably during the first step of most synthesis routes. In the section 'catalyst synthesis – case studies' we first review the state of the art with respect to the preparation of Pd catalysts on oxidic supports, mainly of Pd on silica and alumina, and subsequently we focus on the application of Pd onto carbon supports. We conclude this review with some general remarks.

The chemistry of catalyst synthesis

Preparation of supported catalysts generally involves contacting a (porous) pre-shaped support with a solution (most often aqueous) of a suitable precursor of the active component, which is converted into the active component in one of the subsequent preparation steps. Only when a sufficiently high interaction between the support and Pd-precursor exists at this stage of the procedure, ultimately the wished distribution and high dispersion of the active component can be achieved. If there is poor interaction notably during removal of the solvent, *i.e.* during drying, an unwanted re-distribution of the precursor might occur leading to egg-shells and broad particle size distributions of the active component [1]. The interaction between the solvated precursors and the support surface as modified by the solvent is generally of an electrostatic nature. First, we will briefly deal with solvated precursors. Next, we will concentrate on the interaction between solvent and support surface and on adsorption sites suitable for interaction with precursors.

Precursor solutions

Solvation of metal cations in water leads to the formation of partially covalent bonds between the cation and the water ligands. Charge transfer from filled orbitals of the water ligands to the central metal ion raises the positive charge on the hydrogen atoms of the coordinated water molecules. This process increases their acidic character and promotes hydrolysis. In a general form the hydrolysis reaction is expressed by:

$$xM^{+} + y\,H_2O \quad \rightleftharpoons \quad M_x(OH)_y^{(x-y)+}(aq) + yH^{+} \quad (K_{xy})$$

This reaction reflects that, depending on the nature of the cation, besides monomeric also oligonuclear species can be formed. With cations of a very high charge proton abstraction from the hydroxide ligand may even occur and oxo species are formed [6,7].

The Pd^{2+} ion favors the formation of square planar PdL_4 complexes and in water, with no other complexing ligands present, exclusively $Pd(H_2O)_4^{2+}$ exists in solutions with a pH< 1. For this ion a pK_a of 2.3 has been measured. At pH > 1 polynuclear palladium species are gradually formed as described by Bönneman *et al.* [8] for solutions of palladium nitrate. Didillon *et al.* [9] investigated the formation of colloidal PdO particles by hydrolysis of a palladium nitrate solution. At pH values of 2 and 2.8 they obtained particles of 1.8-1.9 nm. Acidification of a basic solution of pH = 12 down to pH = 1.8 resulted in the same small particles of 1.7-1.8 nm. These findings are interesting for the preparation of supported catalysts with well-defined palladium particle sizes.

In view of the (surface) chemistry of the oxidic and carbon supports cationic or anionic palladium precursor ions have to be available in a pH range of ~3 to ~9. The complex $Pd(NH_3)_4^{2+}$ ion, is stable in neutral and moderately basic environments and the NH_3-ligands as well as some remaining nitrate ions can simply be removed from the loaded support by heating. The most utilized negatively charged palladium complex is $PdCl_4^{2-}$, which is stable in neutral and acidic solutions, provided that the Cl^-/Pd^{2+} ratio is high enough to avoid hydrolysis. Generally a solution of $PdCl_2$ in diluted hydrochloric acid is used.

Many authors make use of neutral palladium complexes that interact, generally from a non-polar environment, with specific surface sites of the supports. Most often the acetylacetonate complex of palladium, $Pd(C_5H_7O_2)_2$ or simply $Pd(acac)_2$, in inert solvents like benzene or toluene is used. Another precursor is $Pd(C_3H_5)_2$, which is generally dissolved in pentane. This allylic complex is highly reactive towards water and hydroxylated surfaces.

Oxidic supports

The surface of most oxides is hydroxylated or becomes hydroxylated upon contact with liquid water or water vapor. The nature of the surface hydroxyl groups has been identified by IR spectroscopy. The OH stretch region of most oxides contains several bands corresponding to different types of surface groups [10,11]. Roughly, these hydroxyl groups can be classified as acidic, neutral and basic (Brønsted-sites). In addition, coordinatively unsaturated metal sites (c.u.s.) can be present, which may act as Lewis-acidic centers [1]. The lower the OH stretching frequency for a given support, the more acidic its character. With γ-alumina three bands are present, as shown in Figure 1, which can be assigned to specific surface OH configurations. The high-frequency band is due to single bonded, basic hydroxyl groups, whereas the other bands correspond to more acidic, bridged hydroxyl groups. With silica the sharp band at 3740 cm^{-1} is ascribed to isolated and presumably also to geminal hydroxyls, while the broader band at lower wavenumbers is due to the presence of hydroxyl groups exhibiting hydrogen bonding [11].

Van Veen *et al.* [12] revealed that many $M(acac)_n$ complexes show a well-defined reactivity towards the surface groups of γ-alumina. Acetylacetonate-complexes, stable in the presence of H^+ and OH^-, such as those of palladium, platinum and cobalt, only react with the c.u.s. sites, and can thus be used to probe the nature of the surface sites oxidic supports.

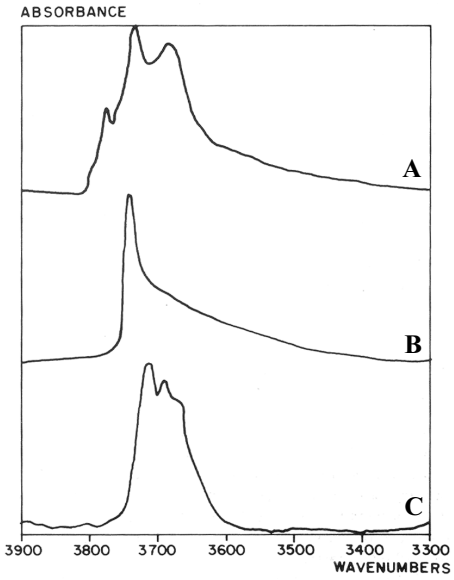

Figure 1. IR-spectra (OH stretch region) of (A) γ-Al_2O_3, (B) SiO_2 and (C) TiO_2, reproduced with permission [1].

When dispersed in aqueous solutions the surface of particles of mineral amphoteric oxides such as silica and alumina becomes generally charged. Charging occurs as a result of (de)-protonation, as described by equation (1) for neutral and positively charged surfaces and by equation (2) for neutral and negatively charged surfaces.

$$M—OH + H^+ \rightleftharpoons M—OH_2^+ \qquad (1)$$

$$M—OH \rightleftharpoons M—O^- + H^+ \qquad (2)$$

In which M is Si, Al, Ti, *etc.*

The charged surface in combination with the charged layer around the particle is called the electrical double layer. The pH value at which the net surface charge is zero is referred to as the point of zero charge (PZC) or often loosely the iso-electric point (IEP).

At pH values below its IEP an oxidic particle tends to adsorb compensating anions like $PdCl_4^{2-}$. At pH values above its IEP, the surface acquires a net negatively charge and cations like $Pd(NH_3)_4^{2+}$ can be adsorbed [13].

From the above discussion it follows that the pH of the precursor solution determines the nature as well as the amount of charged surface sites and, thus, the number of counter ions that can be adsorbed. Therefore it is important to know the evolution of the surface charge as a function of pH. In Table 1 a number of IEP values of support materials are given. It is important to realize that the actual IEP value of a support material can deviate somewhat from the values given in the table because of specific pretreatments and the presence of contaminations. For example, Vordonis *et al.* revealed that the IEP and the concentration of charged surface groups at each pH can be regulated by the temperature and by 'doping' the support with ions like Li^+, Na^+ and F^- [14].

Table 1. Iso-electric points of various oxides, adapted from [13].

Type	Oxide	IEP	Adsorption
Acidic	Sb_2O_3	<0.4	Cations
	WO_3	<0.5	
	SiO_2	1.0-2.0	
Amphoteric	MnO_2	3.9-4.5	Cations or Anions
	SnO_2	~5.5	
	TiO_2	~6	
	γ-Fe_2O_3	6.5-6.9	
	ZrO_2	~6.7	
	CeO_2	~6.75	
	α,γ-Al_2O_3	7.0-9.0	
Basic	Y_2O_3	~8.9	Anions
	α-Fe_2O_3	8.4-9.0	
	ZnO	8.7-9.7	
	La_2O_3	~10.4	
	MgO	12.1-12.7	

Suspended in aqueous solutions basic OH groups will be involved primarily in type (1) reactions and acidic hydroxyl groups in type (2) reactions. Of the oxides of interest here, γ-alumina contains predominantly basic hydroxyl groups, with IEP ≈ 8. Silica is acidic, with IEP ≈ 2. At pH values above the IEP the surface is negatively charged and will therefore adsorb cations. Below the IEP the support surface will be positively charged and anionic species can adsorb [1,15]. As an example the extent of adsorption of $Pd(NH_3)_4^{2+}$ on silica as a function of the pH as measured by Contescue *et al.* [16] is shown in Figure 2.

Carbon Supports

Materials

In addition to oxidic materials, carbon supports are very important in catalysis. Carbon materials are often used because of their large surface areas and chemical inertness, in

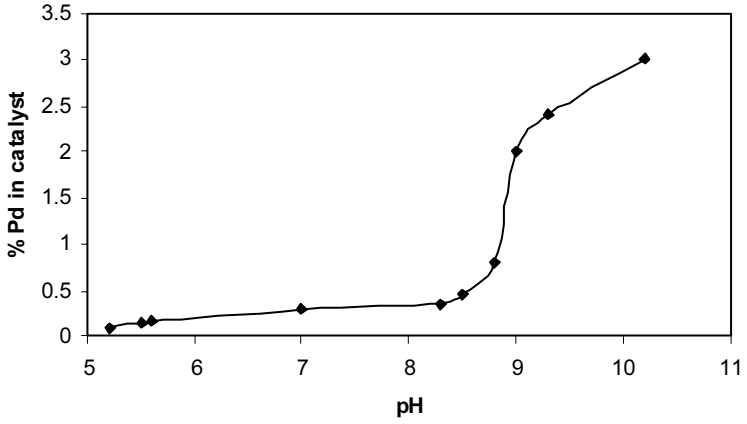

Figure 2. Effect of impregnation pH on the extent of $Pd(NH_3)_4^{2+}$ adsorption on silica, adapted from [16].

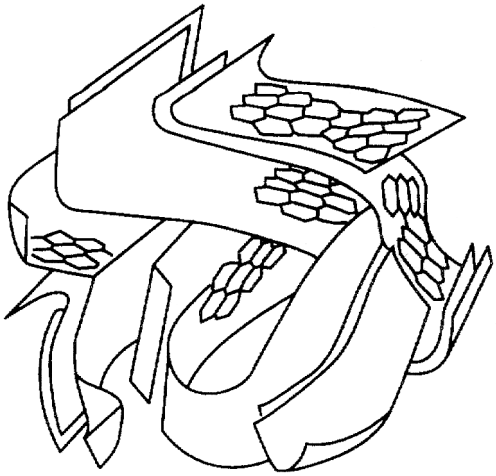

Figure 3. Schematic representation of the structure of activated carbon, reproduced with permission [19].

particular in strong alkaline and acid environments. For gas-phase applications its high thermal stability, related to a high melting point, is of relevance. Especially for the production of noble metal catalysts, carbon is a suitable support material due to the easy reclaim of the metal by burning off the carbon. However, the chemical inertness of carbon can sometimes be a disadvantage. The low reactivity of the surface makes it difficult to deposit metals and therefore a pretreatment of the carbon in an oxidizing environment is generally used to introduce oxygen-containing surface groups, which enhance interaction with the metal (precursor) [1,17]. This will be discussed in more detail in the next section.

Of the many types of carbons, activated carbon is still most commonly used as absorbent and catalyst support, because of its large surface area (500-1200 m^2/g) and low costs. It is produced by pyrolysis of natural or synthetic organic polymer materials. Natural materials like wood, coconut shells or fruit pits are used most often. During pyrolysis the carbon material is activated by air or steam treatment to increase the accessibility of the carbon surface. After activation the carbon still contains a large range of elements, such as hydrogen, oxygen and because of its adverse effect on catalysis: sulfur. The texture of activated carbon is extremely complex since it involves macropores, mesopores, as well as micropores [1,5,17,18]. Figure 3 shows an average structure of activated carbon, consisting of aromatic sheets and strips, containing various slit-shaped voids, *i.e.* the micropores [19]. Both during the application of the active component and during catalysis this complex texture results in poor control and reproducibility [1,17,18].

Carbon molecular sieves (CMS) are a special type of activated carbon. The slit-shaped and almost uniform micropores of these materials are used for *e.g.* separation of air or benzene from cyclohexane. An advantage of CMS as a catalyst support over zeolites is that CMS can be prepared with larger pore volumes and the pore size can be easily adjusted. Another difference between CMS and zeolites is the geometry of the micropores: in zeolites the pores are comprised of channels and cavities, whereas in CMS the pores are slit-shaped, which influences their accessibility [17,20].

Carbon blacks are carbonic products obtained from thermal decomposition or incomplete combustion of hydrocarbons. They are commercially available with a wide range of surface areas and porosities. Structures ranging from non-porous, highly ordered and homogeneously graphitized carbon black to highly porous aggregates with surface areas up to 1500 m^2/g are available [1,17,21].

In contrast to activated carbon and carbon black, graphite is a highly crystalline material composed of stacked planes of aromatic rings 0.335 nm apart, as depicted in Figure 4. This material originates from carbon treated at high temperature. The electronic character of the stacked aromatic systems makes it possible for certain atoms or molecules to slip between the layers, either accepting or donating electrons from/to the carbon system, a process referred to as intercalation [1,5]. Except for this interplanar area, graphite particles are essentially non-porous, and as a result graphite is not commonly used as a catalyst support. However, after an oxidation treatment the edges of the planes contain, amongst others, acidic functional groups which enable adsorption of cationic precursors of the active phase from neutral and basic media.

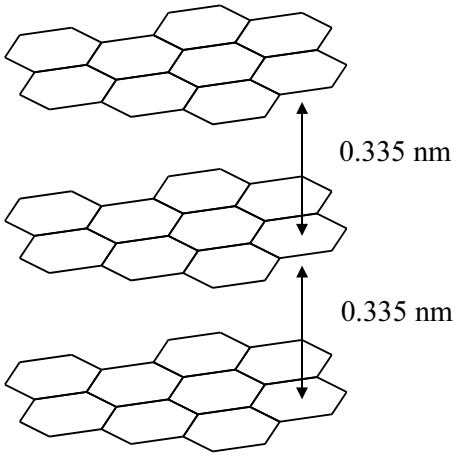

Figure 4. Layer structure of graphite, adapted from [5].

An emerging type of carbon support materials is carbon nanofibers. These fibers with a diameter between 10-50 nm are grown from decomposing carbon-containing gases (*e.g.* CH_4, CO, C_2H_4) over small metal particles of similar sizes. Carbon atoms are generated on the free metal surface and diffuse subsequently through the particle after which they are converted into a graphite-like fiber by segregation processes. By proper choice of the synthesis conditions (temperature, gas and metal used) the morphology of the fiber can be either of the fishbone type (CNF, exposed edge planes) or the parallel type (CNT, exposed basal planes), see Figure 5. Potentially these materials have unique properties for use as catalyst support. They have a large surface area (10-200 m^2/g) and possess neither micropores nor impurities (such as sulfur or other inorganic matter) [1,22,23]. A major disadvantage for the application of carbon nanofibers for catalytic purposes was their limited availability and high production costs. However, recently these drawbacks were overcome by the development of fluidized bed technology for large-scale production [23,24]. Lately De Jong and Geus have written an extensive review about the synthesis and applications of carbon nanofibers [23].

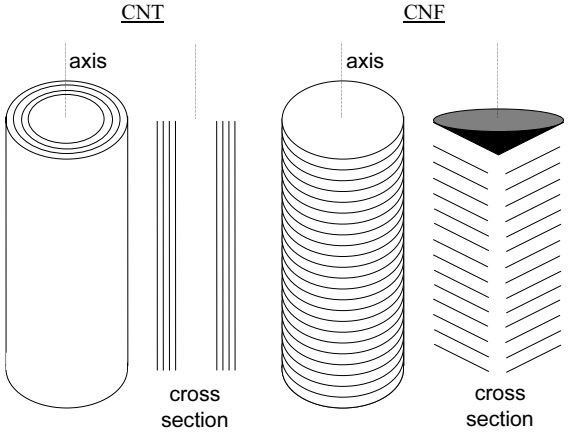

Figure 5. Schematic view of carbon nanotubes (CNT) and carbon nanofibers (CNF), redrawn from [22].

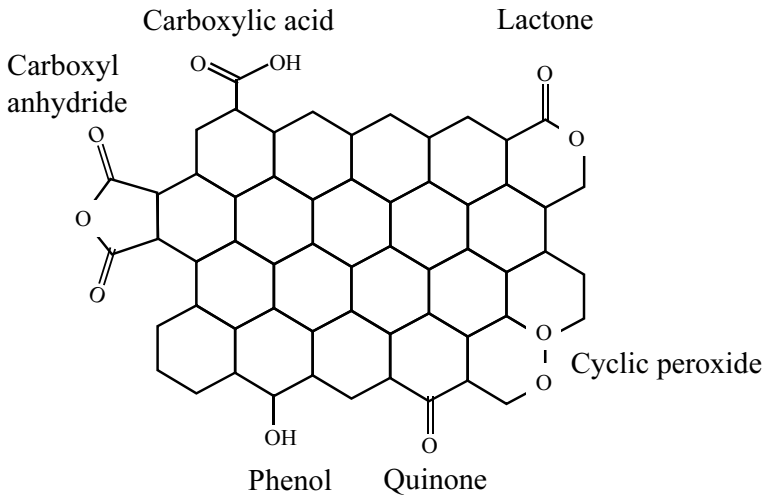

Figure 6. Different types of oxygen-containing surface groups on graphitic carbon, adapted from [27].

Surface chemistry

Oxygen-containing surface groups are by far the most important groups influencing the surface characteristics and adsorption behavior of activated carbon. On activated carbon these groups are always present, although their amount is highly dependent on the way of preparation. They are formed not only by reaction with oxygen, but also from reaction with other oxidizing gases (such as ozone or carbon dioxide) and solutions containing nitric acid, hydrogen peroxide or hypochlorite. The precise nature of carbon-oxygen structures is not entirely established, but the results of many studies using FT-IR spectroscopy, Boehm-titrations and TPD measurements demonstrate that several types of surface-oxygen groups can be distinguisted [17,18,25], as shown in Figure 6. In addition, treatment of carbon does not only introduce oxygen groups, but can also affect the bulk carbon chemistry. Darmstadt *et al.* reported that when catalytically grown carbon nanofibers are treated in nitric acid (373 K, 12 h) pores are formed and the ordering of the graphitic structure decreases [26]. Carbon nanofibers have small diameters (10-200 nm), as a result a treatment of 12 hours induces severe modifications. When the treatment is confined to 1-2 hours the bulk carbon properties are not affected [22].

The oxygen-containing surface groups can be divided in acidic, neutral and basic ones. This implies that the carbon surface may have different amounts and types of oxygen surface groups and, consequently, both negatively and positively charged surface sites can exist in aqueous solution, depending on the pH. At $pH>pH_{IEP}$ the carbon surface, covered by

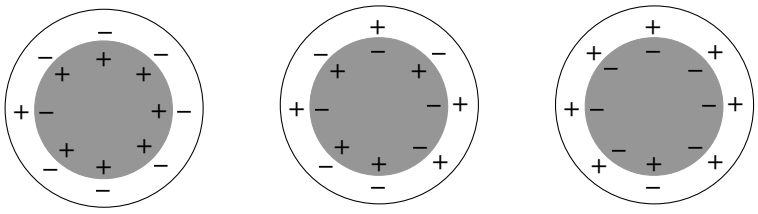

Acidic medium ($pH < pH_{IEP}$) | $pH = pH_{IEP}$ | Basic medium ($pH > pH_{IEP}$)

Figure 7. Schematic representation of the amphoteric character of carbon, adapted from [17].

deprotonated acidic groups, will attract cations from solution; at $pH<pH_{IEP}$ it will attract anions [13,17]. This is illustrated in Figure 7. When preparing a supported catalyst, one needs not only physically accessible sites but also chemical reactivity towards the metal precursor. The electrostatic repulsion between the charged surface and the ionic catalyst precursor may be stronger than the non-specific dispersion forces of attraction. This results in a loss of catalyst dispersion. The catalyst dispersion is optimal when the entire carbon surface is accessible, *i.e.* when there is electrostatic attraction between the positively charged surface (below pH_{IEP}) and the catalyst precursor anions or *vice versa* [17].

Carboxylic, quinone and lactone groups are acidic. Because of their negative charge they enhance the interaction between the carbon surface and positively charged metal precursors. Furthermore, they decrease the hydrophobicity of the carbon material, thus making the surface more accessible for aqueous metal precursor solutions [17,27-29]. Suh *et al.* have proven for Pd on activated carbon that the metal dispersion increases with increasing amounts of surface oxygen groups [30]. Phenols, carbonyls and ethers are weakly acidic to neutral. Prado-Burguete *et al.* found that these oxygen groups increase both the interaction of the metal precursor and the resulting metal particles with the support, thus minimizing sintering [29]. Carbons heated in oxygen always contain basic sites next to acidic ones. A carbon surface is freed from all surface groups by heating to around 1273 K in vacuum or in an inert atmosphere and when it is subsequently contacted with oxygen after cooling basic surface oxides are formed. Boehm *et al.* concluded that basic surface groups are localized at the same edges as acidic groups, although their quantity is lower. The basicity of graphitic carbon is explained in terms of the π sites of the graphite basal plane interacting with water, as shown in the reaction below.

$$C_\pi + 2\ H_2O \longrightarrow C_\pi H_3O^+ + OH^-$$

Increase of the amount of basic sites on the basal plane surface will both enhance the electrostatic attraction with metal anion complexes (*e.g.* C_π-H_3O^+ - $PdCl_4^{2-}$) and diminish repulsive interactions (*e.g.* COO^- - $PdCl_4^{2-}$), thus increasing the dispersion [17,18,25,31-33]. Leon y Leon *et al.*, for example, described the basicity of carbon in terms of pyrone-type structures, in which two non-neighboring oxygen atoms constitute one basic site. These two atoms are proposed to be located in two different rings of a graphitic layer, thus favoring resonance-stabilization of the positive charge [31].

Nitrogen is not always present on carbons, but it can be introduced. Ammonia is often used for the preparation of these nitrogen-containing carbons. Although characterization of the nitrogen groups is difficult (oxygen and nitrogen functional groups coincide in IR), it is assumed that amides, imides and lactams are created around 473 K in flowing NH_3. At higher temperatures in an inert atmosphere these nitrogen-containing groups convert to pyridines and pyrroles [17,18,32].

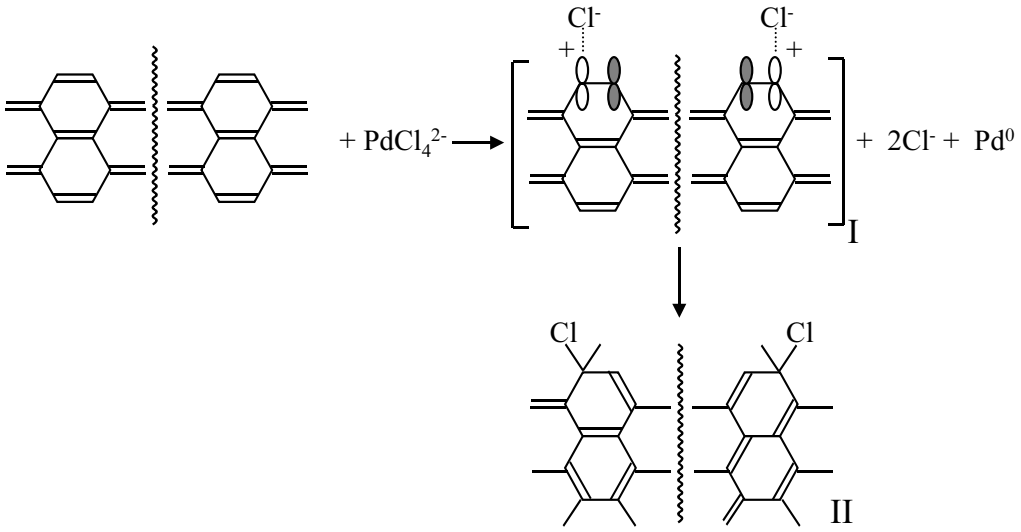

Figure 8. Scheme representing the adsorption of Cl^- anions to compensate for the number of electrons consumed from the carbon to reduce palladium [36].

Precursor-surface interactions

From the last paragraph it is clear that oxygen surface groups play a very important role in the dispersion of the active phase. The exact nature of the interaction between palladium precursors and oxygen groups is not fully clear, however. In order to gain more information on the fundamental interactions between palladium (precursor) and carbon Mojet *et al.* [34] performed an XAFS study on the preparation of a carbon fiber-supported palladium catalyst. This study showed that no oxygen is present in the first coordination shell of palladium after ion exchange of $[Pd(NH_3)_4](NO_3)_2$. Secondly, the XAFS data pointed to a strong metal-carbon interaction before and after reduction, responsible for anchoring of the metal particles to the carbon surface after reduction. Although a direct Pd-O contribution could not be detected, oxygen might be situated at a slightly longer distance. Probably the carboxylic groups on the surface and the π-system of the support stabilize the well-dispersed precursor complex. This work will be discussed in more detail later on. Also Ryndin *et al.* did not find indications for interactions between Pd(II) ions and oxygen-containing surface groups [35], which was to be expected, since the metal precursor they used ($PdCl_4^{2-}$) was negatively charged, as were the oxygen surface groups. These findings necessitate a further investigation of the precise role and interaction of oxygen groups with metal precursors.

Simonov *et al.* have done extensive research on the chemical processes, which occur when H_2PdCl_4 from aqueous solution is adsorbed on the surface of graphite-like carbon materials [36,37]. They found that adsorption proceeds *via* two competitive pathways: reduction to form metallic Pd particles (process 1) and formation of π-complexes of $PdCl_2$ with C=C fragments of the carbon matrix (process 2):

$$PdCl_2/C + 2HCl \underset{(2)}{\rightleftharpoons} H_2PdCl_4 + C \underset{(1)}{\rightleftharpoons} Pd^0/C + 2Cl^-/2C^{\oplus} + 2HCl$$

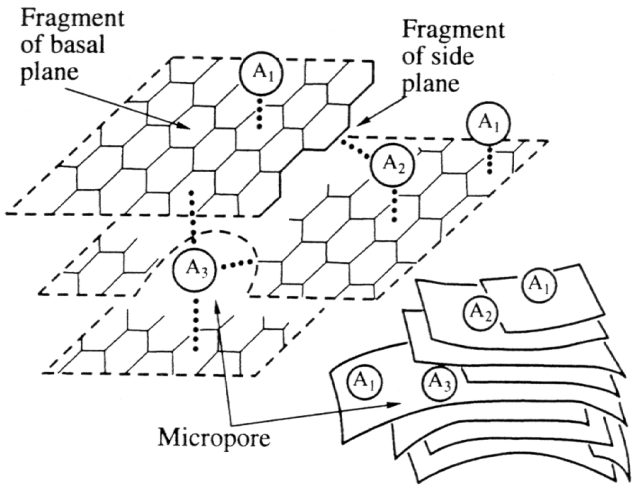

Figure 9. Probable positions of irreversible (A_3), strong (A_2) and weak (A_1) adsorption of H_2PdCl_4 on the surface of carbon, reproduced with permission [37].

The first process takes place near the exterior surface of the carbon particles. Reduction of palladium occurs as a result of the high reducing power and the conductivity of graphitic carbon. Because no evolution of carbon oxides is observed upon palladium reduction, carbon oxidation is excluded as electron donating process. Simonov *et al.* state that Pd(II) ions are discharged by the "electron gas" of carbon accompanied by adsorption of Cl^- ions. $C^{\oplus}$ is a positively charged "hole" which appears at the carbon surface when Pd(II) is reduced. Cl^- anions compensate this charge through the formation of an electric double layer at the carbon surface. This process is illustrated in Figure 8 [36]. The spontaneous reduction of H_2PdCl_4 results in Pd^0 particles with a broad size range of 6-100 nm [36,37].

Process (2) takes place on the entire surface of the support and results in a uniform distribution of adsorbed $PdCl_2$ particles (1.6-1.8 nm). An XPS study on H_2PdCl_4 adsorption on oxidized carbons revealed that Pd(II) complexes with oxygen-containing ligands are not formed. $PdCl_2$ is adsorbed on the carbon surface resulting in the formation of π-complexes with the C=C fragments of the carbon network. On the carbon surface at least three types of adsorption sites occur: weak (A_1, basal plane), strong (A_2, edge plane) and very strong or irreversible (A_3, micropores), as shown in Figure 9. When carbon is treated to increase the amount of oxygen-containing surface groups, A_2 and A_3 sites disappear. During drying Pd(II) compounds migrate over the surface to form small clusters. The centers of agglomeration are the surface steps, due to the high adsorption potential of these regions [35,37,38]. This is schematically represented in Figure 10.

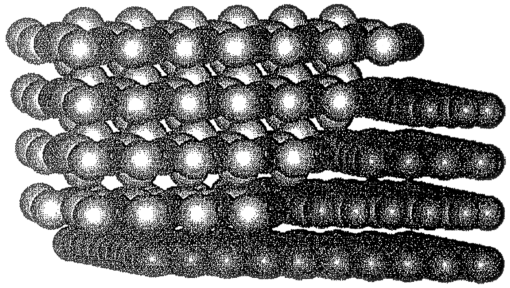

Figure 10. $PdCl_2$ agglomeration on carbon surface steps, reproduced with permission [38].

In their review Simonov *et al.* summarize the factors determining the $PdCl_2/Pd^0$ ratio in adsorbed compounds: the chemical nature of the support surface, its textural characteristics and grain sizes and the conditions for the deposition of palladium compounds (especially pH and composition of the gas-phase) [37]. These variables will be discussed further in the section on 'carbon-supported catalysts: impregnation and drying'

Catalyst synthesis – case studies

In our survey of the literature we will use the classification as given by Augustine [5] and other authors in the field [39,40]. This classification is mainly based on the first step in the procedure during which the active component(s) and the support are combined. Unfortunately, although this approach seems straightforward, it sometimes appeared difficult to unambiguously label a number of synthesis descriptions in the literature.

Oxide-supported catalysts

Co-precipitation

In the first step of the co-precipitation procedure a compound is formed which is the precursor of both the active component and the support. Using a sol-gel López *et al.* prepared Pd/SiO_2 catalysts by heating a mixture of an aqueous alcoholic solution of tetraethoxysilane and either an aqueous solution of $PdCl_2$ or an ammoniacal $Pd(NH_3)_2Cl_2$ solution [41,42]. The palladium-silica precipitate was extensively dried at 343-373 K for 12 h and calcined for 4 h at 723 K. Subsequent reduction at 723 K for 4 h resulted in Pd loadings below 0.5 wt% albeit with a high dispersion of Pd over silica, which exhibited a large surface area of around 800 m^2/g. TEM and chemisorption characterizations demonstrated the presence of Pd particles smaller than 1 nm with a narrow size distribution. At higher loadings particle sizes became comparable to results obtained with the impregnation technique.

Zou and Gonzalez investigated the thermal stability of silica-supported Pd catalysts prepared by the sol-gel method [43]. They mainly used mixtures of $Pd(acac)_2$ and tetraethoxysilane in ethanol, *sec*-butanol or acetone. By fine-tuning the reaction conditions, the relative amounts of reactants and the nature of the solvent, they succeeded in the production of a catalyst with small average particle sizes and average pore diameters, which suppress sintering of palladium up to 923 K. With TEM and H_2 chemisorption Pd particles of 2.4-3 nm were shown to be present (BET surface area of the catalyst was 650 m^2/g). In oxygen the Pd particles appeared to be stable, but in hydrogen sintering occurred at 923 K, probably as a result of a mechanism involving Pd hydride.

Kim *et al.* [44] used the sol-gel technique for the synthesis of Pd-alumina three-way catalysts and studied the influence of the pH on the features of the ultimate catalysts. They stirred a mixture of a basic (ammonia) or acidified (nitric acid) aqueous solution of aluminum

iso-propoxide and a $Pd(acac)_2$ solution in acetone for 5 h at 323 K. After drying at ambient temperature for 24 h and calcination at 773 K for 24 h the catalysts were reduced. Differences in the reducibility of the two samples were observed. The catalyst prepared at the highest pH required the highest reduction temperature, *i.e.* 573 K. NMR measurements indicated that the palladium ions interact preferentially and strongly with tetrahedrally coordinated aluminum ions, present in basic environments. This catalyst showed also the highest Pd dispersion, the most homogeneous Pd distribution and the highest BET surface area. These findings underline the conclusions of Lecloux and Pirard [45] that the sol-gel process, applied to catalyst syntheses, requires particular, well-defined conditions in order to control the morphology of the resulting solids.

With a somewhat modified approach Schneider *et al.* [46] produced highly porous palladium-titania aerogels. They re-dispersed preformed titania gels and added different Pd precursor solutions followed by drying under supercritical conditions. The best results were obtained with palladium acetate, although also with this precursor rather large Pd particles were obtained (at least 20 nm) depending on calcination and reduction temperature.

A general procedure for the production of highly loaded palladium catalysts *via* co-precipitation was presented by Fujitani *et al.* [47]. They prepared a precipitate by addition of an aqueous solution of Na_2CO_3 to a solution containing both a nitrate precursor of the support metal, in this case gallium, and a palladium precursor. After aging at 343 K for 1 h and washing, the residue was dried overnight in static air at 383 K, calcined at 623 K for 2 h and reduced at 523 K. Unfortunately, no specification of the palladium dispersion was given.

Deposition-precipitation

For a general introduction to this synthesis technique we refer to the work of Geus *et al.* [2,48] and De Jong [49]. Deposition-precipitation can be used to produce catalysts with a variety of supports. Augustine and O'Leary prepared, *e.g.* 1% Pd/MgO by addition of an aqueous $Pd(NO_3)_2$ solution to a stirred slurry of the support in an aqueous NaOH solution [50]. After washing, the residue was dried overnight at 383 K and subsequently reduced in hydrogen: up to 673 K the palladium dispersion (40 %) was found to be independent of the reduction temperature. With CeO_2 as the support material Shen *et al.* demonstrated, using XPS [51], EXAFS [52] and chemisorption measurements [53], that the above procedure leads to large amounts of Pd^{2+} ions on the support surface, even after reduction at 773 K. Obviously, the high pH values applied give rise to a strong interaction of the metal ions with the surface. Interestingly, catalysts prepared with $PdCl_2$ as a precursor show a significant higher ion-concentration than catalysts prepared from the nitrate salt.

Deposition-reduction

In the deposition-reduction technique one starts with a suspension of the support material in a precursor solution of the metal of interest. By introduction of a reducing agent the metal is directly applied onto the support [54,55]. This procedure is especially suitable for the

production of noble metal catalysts, because of the favorable reduction potentials. Fogassy *et al.* deposited palladium directly on silica, alumina and carbon black, up to a loading of 10%, by addition of the reducing agent sodium formate to a boiling suspension of the supports in an aqueous K_2PdCl_4 solution at pH 10-11. Unfortunately, no characteristics of the obtained catalysts were presented [56].

An interesting procedure, called "controlled colloidal synthesis", has been developed by Beck *et al.* [57]. Control was effected by restricting the reduction of the palladium precursor to a well-designed solid/liquid interfacial layer on a silica support. They postulated that by using a proper binary liquid system for the suspension of the support, good separation can be achieved between the adsorption layer and the liquid-phase for one of the two components. If one of the reaction partners is soluble only in one component, or this component itself is the reducing agent, the reduction is localized. As a binary mixture they used ethanol/toluene (6/94), ethanol also being the reducing agent. The support was silica and Pd-acetate (in toluene) was the precursor. Although the average Pd dispersions and particle sizes did not differ appreciably from those obtained *via* the normal impregnation route, TEM results revealed sharper size distributions. Furthermore, it appeared that reduction is a rather slow process. As a result the mean particle size could be readily controlled by varying the reduction time: *viz.* 6 nm after 1.5 h and 26 nm after 12 h, as determined with CO adsorption.

A similar but less well-controlled procedure was used by Farrauto *et al.* [58], who obtained 4 wt% palladium on zirconia, titania, ceria and alumina catalysts by dry impregnation of these supports with a solution of $Pd(NO_3)_2$, followed by the addition of hydrazine to form metallic palladium. Bond and Rawle [59] used the same reduction method for the production of 4-5 wt% Pd/SiO_2 catalysts using H_2PdCl_4 and $Pd(NO_3)_2$ as the palladium precursors. With the nitrate precursor a dispersion of 13 % was obtained, whereas with the acidified chloroplatinic precursor a dispersion of only 5% could be attained. A last example of fixation by reduction has been given by Ilinitch *et al.* [60]. For the production of γ-Al_2O_3 supported Pd and Pd-Cu catalysts as well as membranes loaded with these metals they used sodium borohydride ($NaBH_4$) as the reducing agent at room temperature.

Photo-deposition

Recently, an example of the photo-deposition procedure for the production of palladium catalysts has been given by Amalric-Popescu and Boszon-Venduraz, who deposited metallic Pd particles onto SnO_2 by irradiating a suspension of this support in an aqueous solution of $Pd(NO_3)_2$ [61]. Rather large particles (4.5 nm) were formed, as determined by XRD line broadening. With silica and alumina supports this method is not viable.

Impregnation / ion exchange

In most scientific studies wet or dry impregnation or ion exchange is used for the production of supported Pd catalysts. For a detailed description of these techniques we refer to Augustine [5] and Schwartz [39].

Sivaraj *et al.* [62] prepared a series of Pd catalysts on alumina supports (aluminum hydroxide ($Al(OH)_3$) calcined at different temperatures) *via* $Pd(NH_3)_4^{2+}$ and/or $PdCl_4^{2-}$ exchange. With acid-base titrations they found that the pH_{IEP} shifted from 7.6 after calcination at 673 K to 8.7 after treatment at 1173 K. More importantly the exchange site concentration decreased from 6.3 to 3.0 sites/nm^2. Cordi and Falconer pre-calcined their alumina support samples at 873 K to dehydrate the alumina support and to remove contaminants from the surface before loading with an aqueous solution of $PdCl_2$ by dry impregnation [63]. Zou and Gonzalez [64] treated their silica support with dilute nitric acid in order to remove traces of alkali metal ions. The importance of such a treatment, especially in scientific research, was revealed by Prins *et al.* [65,66] who demonstrated that the impurities commonly found in commercial silicas are sometimes effective catalyst promoters, as in their case for the synthesis of methanol from syngas over Pd/SiO_2 catalysts. Other authors aim at the formation of a specific support phase before applying palladium species. An example is the formation of δ-Al_2O_3 from a commercial γ- Al_2O_3 material by calcination at 1273 K for 6 h [67]. Similar pre-treatments might also be important in view of the (temperature) conditions of the catalytic process under study. We found that in preparations *via* ion exchange with non-aqueous precursor solutions a pre-calcination is generally executed. The importance of such a treatment has been demonstrated by Van Veen *et al.*: with $Pd(acac)_2$ as the precursor the rate of exchange with dehydroxylated surfaces is substantially higher than with hydroxylated surfaces [12]. With γ-Al_2O_3 extrudates the obtained catalysts showed egg-shell distributions, whereas with a hydroxylated support an even distribution was obtained.

When the palladium precursor is applied by ion exchange and/or wet impregnation it has to be taken into account that the rate of extraction from solution is controlled by the limited rate of adsorption and often, with macroscopic porous support bodies, by pore diffusion. Unfortunately, in most publications information concerning the period of interaction is lacking. One of the exceptions is the work by Neyertz and Volpe, who measured the removal of $Pd(acac)_2$ from γ-Al_2O_3/toluene suspensions under well-defined conditions [68]. At room temperature equilibration of 0.5 g precalcined support samples in an excess of a 0.03 M solution of $Pd(acac)_2$ in toluene took about 80 minutes.

A good method for the preparation of Pd/SiO_2 catalysts (~1.5 wt%) using ion exchange in aqueous solutions is given by Zou and Gonzalez [64]. They applied a period of 12 h for interaction with $Pd(NH_3)_4^{2+}$, thereby keeping the suspension with the pre-calcined silica support (Cab-O-Sil M-5, surface area 200 m^2/g) at a pH value of 9 to maximize the 'metal-support' interaction. After heat-treatment in an inert gas and reduction at 673 K they obtained Pd dispersions as high as 70%. Another suitable exchange procedure involves the interaction of palladium acetylacetonate, $Pd(acac)_2$, or similar complexes, dissolved in, *e.g.* benzene or toluene, with alumina supports. Most authors follow the procedures presented by Boitiaux *et al.* [69] and Van Veen *et al.* [11,12].

After ion exchange the loaded samples can be separated from the excess liquid-phase by filtration or centrifugation. Zou and Gonzalez [64] filtered their suspension and washed the

residue in order to remove the weakly adsorbed precursor. Goetz *et al.* [70] and Pisanu and Gigola [71] dried unwashed samples in their ion exchange syntheses of various $Pd/\alpha\text{-}Al_2O_3$ catalysts (0.09, 0.2 and 0.3 wt%). Only at 0.09 wt% loading high palladium dispersions of about 50% were obtained after reduction in hydrogen at 573 K. Notably, Venezia *et al.* underline the importance of the washing step to avoid the formation of large palladium particles in the final reduction step due to the presence of an excess of palladium precursor [72].

After wet impregnation, despite the sometimes high Pd-loadings, the solvent is removed by evaporation at room temperature or at higher temperatures, whether or not under decreased pressure, leaving all of the components in the dried precursor and taking the risk of formation of undesired egg-shell distributions of the active phase [73,74]. The drying procedure can severely influence the ultimate distribution of the active component, especially with macroscopic, porous support bodies [75]. When the impregnated precursor is only weakly interacting with the pore walls outward transport of the palladium precursor during drying is hardly avoidable. Some authors chose for a slow drying procedure: most of the solvent is removed under decreased pressure at room temperature, after which the sample is further dried at elevated temperatures. Most authors dried their samples "overnight" in static air at a temperature between 353 and 393 K, without further explanation of the chosen conditions. It is beyond the scope of this review to further discuss the process of drying. Here we limit ourselves to the statement that no scientific study on the drying of supported palladium catalyst precursors has been published up to now.

In a next step of the synthesis procedure the dried supported precursor is generally heat-treated in air (calcination) or in an inert atmosphere before, in the final step, palladium is converted into the metallic state, almost always in a flow of hydrogen. In many papers this heat treatment step as well as the subsequent reduction step are better documented than the foregoing steps. By using different treatment conditions, *e.g.* durance and temperature, a number of authors were able to obtain palladium catalysts with different particle sizes and dispersions in order to measure the influence of these parameters on the selectivity and activity of a defined hydrogenation reaction. Zou and Gonzalez [64] studied the heat treatment variables which affect the properties of Pd/SiO_2 catalysts prepared *via* dry impregnation under optimized conditions with $Pd(NH_3)_4(NO_3)_2$ as the precursor and Cab-O-Sil M-5 (surface area 200 m^2/g) as the support. All heat treatments were followed by the same reduction procedure at 673 K. They found that heat treatments in hydrogen at temperatures up to 673 K without pretreatment in oxygen resulted in poor dispersions of 10-20%, as measured with H_2 and CO chemisorption as well as with TEM, probably as a result of hydride formation. Pretreatment in oxygen at 373, 473 and 573 K led to substantially higher dispersions of around 40 % for all temperatures. Pretreatment in argon or helium resulted in the highest dispersions of about 70 %. Oxidation of the reduced catalysts at 573 K and re-reduction at 673 K did not change the palladium dispersion.

Łomot *et al.* demonstrated that the palladium dispersion strongly depends on the loading. With exactly the same treatment in oxygen and reduction in hydrogen, both at 573 K, their 1.45 wt% Pd/γ-Al_2O_3 catalyst showed a dispersion of 62 % whereas for the 0.39 wt% catalyst a dispersion of 91% was measured (CO chemisorption) [76]. Furthermore it was speculated that at reduction temperatures as high as 873 K Pd-Al species are formed at the metal-support interface, which influences the catalytic properties in the reforming of *n*-hexane and its branched isomers. Burch and Urbano found that the atmosphere and durance of the pretreatment hardly influence the resulting dispersions (around 20%) of 4 wt% Pd/alumina catalysts (manufactured using the incipient wetness technique with $Pd(NO_3)_2$ as the precursor salt) when the subsequent reduction is executed at 773 K [77]. This reduction temperature is so high that possible differences introduced during the pretreatment step became leveled out.

It is generally accepted that with pretreatments in oxygen-containing atmospheres the temperature has to be chosen below the decomposition temperature of the formed palladium oxide phase to avoid sintering as a result of the weaker interaction of metallic Pd particles with the support. A convincing example of the dependence of the ultimate Pd dispersion on the calcination temperature has been presented by Papaefthimiou *et al.* [78]. They calcined a series 0.3 wt% loaded Pd/γ-Al_2O_3 catalysts at temperatures in the range between 773 and 1073 K with increments of 50 K, and found a fall of the dispersion from 100% obtained after calcinations at 773 K to only 4% after treatment at 1073 K. The most severe decrease was observed going from 1023 to 1073 K, probably due to thermal decomposition of PdO.

The decomposition temperature, however, is found to depend on the nature of the support material as demonstrated by Farrauto *et al.* [58]. Using thermal gravimetric measurements they found for 4 wt% Pd catalysts (prepared using reduction-precipitation and precalcination in air at 773 K) that the highest decomposition temperature was obtained with PdO/Al_2O_3 (1083 K) and the lowest with PdO/ZrO_2 (955 K). XRD line broadening results showed that the decomposition was accompanied by sintering. An interesting observation has been reported by Cordi and Falconer: a 3 wt% Pd/Al_2O_3 catalyst reduced at 573 K exhibited re-dispersion of the metal during a subsequent treatment in helium at 773 K [63].

The nature of the palladium precursor also influences the ultimate dispersion, as has been demonstrated by Seoane at al. [79]: after calcination in a stream of air at 623 K and reduction in hydrogen at 523 K, their 0.3 wt% Pd/α-Al_2O_3 catalyst *ex* nitrate exhibited a dispersion of ~22%, whereas the 0.3 wt% catalyst *ex* chloride exhibited a dispersion of only 8 %. The results were found to be almost independent on the reduction temperatures.

Earlier we reported the work of Didillon *et al.* [9], in which the formation of colloidal palladium oxide particles from acidic palladium nitrate solutions by an alkaline solution is described. These authors demonstrated that the colloidal PdO suspensions containing particles of 1.8-1.9 nm can be used for the production of catalysts with well-defined palladium dispersions *via* the dry impregnation technique. After drying, reduction was performed at 423 K. Although the authors did not observe significant sintering at this temperature no information is available concerning the resistance towards sintering of such

systems at higher temperatures. Nevertheless, the described procedure may be interesting especially when very well-defined palladium dispersions are desired.

The above survey demonstrates that many factors influence the ultimate dispersion of a catalyst. With high loadings it is always more difficult to attain and maintain high dispersions, because it is impossible to bind all the precursor species strongly and with a high dispersion to the support. Of course, the 'critical' loading up to which sintering can readily be suppressed will depend on the nature, the structure and the pretreatment of the support as well as on the nature of the precursor and the synthesis procedure.

Carbon-supported catalysts

Deposition-precipitation

Jin *et al.* [80] used pitch-based activated carbon fibers as a support material onto which palladium (5 wt%) was deposited. The fibers had been activated by a treatment in 70% nitric acid at 353 K for 3 h to introduce oxidic surface groups. The Pd/C catalysts were prepared by alkaline hydrolysis of palladiumchloride, resulting in the deposition of $Pd(OH)_2$ on the carbon surface, followed by a liquid-phase reduction using formaldehyde as a reducing agent. The metal dispersions thus obtained ranged from 55% to 77%. Farkas *et al.* [81] also deposited palladium on carbon using deposition-precipitation. Instead of carbon fibers they used graphite, carbon black and activated carbon, pretreated with HCl, O_2/N_2 or HNO_3. The palladium precursor, K_2PdCl_4, was added to an aqueous suspension of the support and the pH of this suspension was adjusted to 10-11 by addition of a KOH solution. Precipitated $Pd(OH)_2$ was reduced by HCOONa or H_2. The effects of the type of support, pretreatment and reduction procedure on the Pd dispersion of the resulting catalysts are presented in Table 2. From the table it can be concluded that reduction by hydrogen results in a much higher dispersion than reduction by HCOONa. With only the dispersion data available it is not possible to determine whether a broad or small particle size distribution was present.

Table 2. Effect of support activation and reduction procedure on Pd dispersion, adapted from [81].

Support	**S_{BET} (m^2/g)***	**% Pd dispersion (H_2 chemisorption)**	
		Reduction H_2	Reduction HCOONa
Activated carbon, HCl	1000	48	10
Activated carbon, O_2/N_2	1130	41	20
Activated carbon, HNO_3	910	50	20
Graphite	8.4	48	20
Carbon black	36	43	10

* As reported in literature. For microporous supports, however, S_{BET} is only a relative measure and has no physical meaning.

Deposition-reduction

Another method to apply palladium on carbon is deposition-reduction. Hoogenraad *et al.* [82] used this method to deposit palladium on carbon nanotubes (surface area = 230 m^2/g). Their method consisted of four steps: pretreatment of the tubes in boiling nitric acid (65%, 10-30 min), suspension of the treated nanotubes in water and in the third step addition of an aqueous solution of $Pd(NH_3)_4Cl_2$. Finally, a formaldehyde solution was injected to reduce the palladium ions. The precipitation and reduction of palladium were performed under a nitrogen atmosphere. After reduction the suspension was filtered and dried in an inert atmosphere at room temperature. Additional drying of the loaded carbon nanotubes involved heating up to 353 K (5 K/h), and cooling, both also in inert atmosphere. This procedure of slow heating was performed to avoid sintering. The resulting 2.5 wt% Pd/C catalysts were characterized with TEM and XRD. In the fresh catalyst no palladium species could be observed on the carbon nanotubes. Only after reduction in hydrogen at 523 K palladium particles with a mean size of 4 nm could be detected. The size of the particles increased during prolonged reduction due to sintering. When air had not been excluded during preparation and drying the extent of sintering turned out to be higher. Probably, the palladium particles became reoxidized in the presence of oxygen, which enhanced their mobility and sintering. Another parameter studied by Hoogenraad *et al.* was the effect of pretreatment of the carbon nanotubes. It was found that hardly any palladium was deposited onto the tubes when the carbon tubes had not been pretreated in nitric acid. Pretreatment of the support for only 10 min in HNO_3 appeared to be sufficient to obtain a maximal Pd loading (~2.5-3 wt%). Surface oxygen groups thus created either anchor the palladium precursor directly to the surface or make the initially hydrophobic tubes more accessible for the aqueous precursor.

Heal and Mkayula [83] used deposition-reduction for the preparation of 5 wt% palladium on activated carbon catalysts. In a suspension of activated carbon they reduced an aqueous solution of Na_2PdCl_4 with either sodium hypophosphite or formaldehyde. The activated carbon samples had been pretreated in several ways: oxidation in air (burn-off), with nitric acid or with furfuryl alcohol to block the micropores. Reduction with sodium hypophosphite resulted in smaller particles than with formaldehyde. Burn-off (15-25%) was advantageous for the palladium dispersion, probably caused by an increase of the surface heterogeneity. Nitric acid treatment resulted in larger Pd particles whereas preferential blocking of carbon micropores by furfuryl alcohol had no effect. Furthermore, it was found that the reduction-deposition technique yields catalysts with metal particles located mainly inside wider pores. Apparently, liquid-phase reduction is so fast that penetration into small pores is not possible.

Yang *et al.* [84] performed deposition-reduction with a $Pd(NO_3)_2$ precursor, but they used an alternative procedure for activation of the support. Instead of creating oxygen-containing surface groups, they preadsorbed halogen ions. First, activated carbon was immersed in a halide solution (NaCl, KBr, NaI) and halogen ions were adsorbed on the carbon for at least 10 h. After separation of the supernatant liquor a $Pd(NO_3)_2$ solution was added. After some hours of precipitation or complexation of Pd^{2+} ions with halogen ions the synthesis mixture was

reduced with hydrazine. Thus obtained results were compared with results obtained with non-preadsorbed supports. The preadsorption of different halogen ions on carbon resulted in significant differences in the ultimate Pd^0 particle size distribution. With Cl^- preadsorption some of the Pd particles grew much larger than without preadsorption, whereas Br^- ions resulted in smaller and more uniform particles. With I^- the Pd particle size was considerably reduced (2-6 nm) and a very uniform particle size distribution was obtained. Yang *et al.* concluded that functional ion preadsorption on a support is an efficient method for the preparation of highly dispersed Pd/C catalysts. The most important advantage is the possibility to select functional ions or groups based on the interaction between metal precursors and these functional ions. This fine-tuning is not possible when an oxidative pretreatment is used.

Impregnation and drying

Gurrath *et al.* [85] have thoroughly investigated the preparation of palladium on activated carbon catalysts using incipient wetness impregnation. The carbon supports (produced from peat, coconut shell and pyrolyzed hydrocarbons) were subjected to treatments with either oxygen, hydrogen, chlorine or ammonia at elevated temperatures in order to obtain catalyst supports with different pore structures and surface properties. Palladium was applied using anionic (H_2PdCl_4 in water), neutral ($Pd(OAc)_2$ in acetone) and cationic ($[Pd(NH_3)_4](NO_3)_2$) precursor complexes to study the difference in interaction. These complexes were introduced into the pores of the supports by incipient wetness impregnation, with the Pd concentration of the solutions adjusted to obtain a metal loading of 100 μmol per gram of support. After impregnation the samples were dried in an oven at 380 K, followed by outgassing in vacuum at the same temperature. Subsequently the samples were reduced in pure hydrogen with a heating rate of 20 K/min.

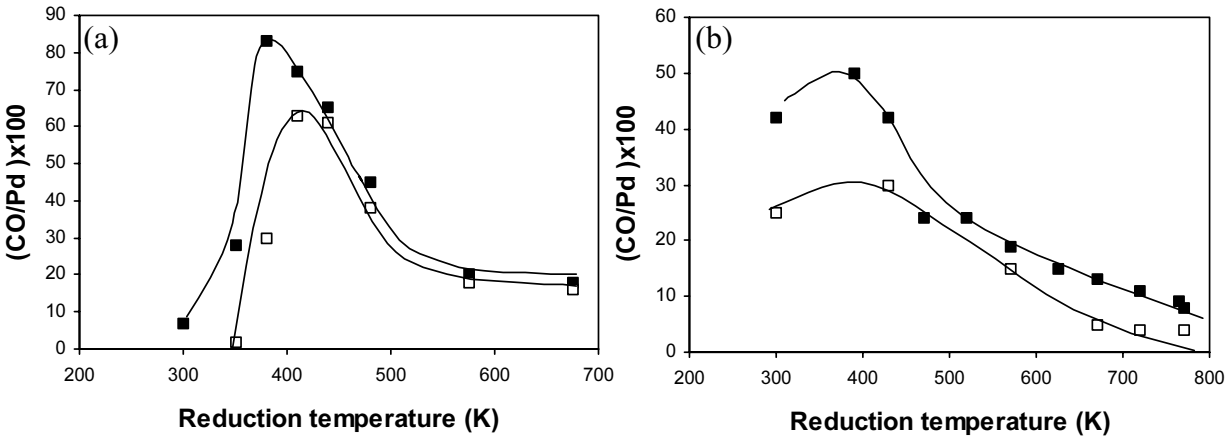

Figure 11. Dispersion values (CO/Pd) as a function of reduction temperature (treatment with H_2 for 1 h): (a) for H_2PdCl_4 on Anthralur-HT; (b) $[Pd(NH_3)_4](NO_3)_2$ on Norit-ox. The metal loadings were 50 μmol/g (open symbols) and 200 μmol/g (filled symbols), redrawn from [85].

As expected, treatment with oxygen resulted in supports with a significantly larger number of acidic groups, at the expense of the number of basic groups. The pretreatments in chlorine, hydrogen and ammonia led to the opposite effect. All treatments caused only small changes in the porous structure of the carbons. However, the results of CO chemisorption measurements on the supported Pd catalysts proved to be strongly dependent on the reduction temperature. Figure 11a shows a relatively small amount of CO uptake with H_2PdCl_4 as the precursor and after H_2 reduction at room temperature. However, catalysts prepared from the tetra-ammine complex and which have been reduced at room temperature showed a larger uptake of CO (Figure 11b). With both catalysts a strong decrease of the palladium dispersion was always observed upon reduction above 420 K, due to sintering of the metal.

In comparison to the reduction temperature, the nature of the palladium precursor complex and the pretreatment of the carbon support had a less pronounced effect on the ultimate metal dispersion. This behavior is rather unexpected, because the work of Brunelle [13] learns that the final dispersion of the metal is to a large extent determined by electrostatic repulsion and attraction forces between charged supports and anionic, neutral and cationic metal precursors.

The use of the tetra-ammine complex tends to result in the poorest dispersions (2-31%). Gurrath *et al.* [85] ascribe this observation to direct reduction of the adsorbed $Pd(NH_3)_4^{2+}$ complex with hydrogen. A mobile $Pd(NH_3)_2H_2$ species is formed, which results in easy agglomeration. When the Pd complex is thermally decomposed under helium first, higher dispersions are obtained. No general trends for the Pd dispersion as a function of the pretreatment procedure could be detected, partially because the nature of the Pd precursor influences the results as well. Several explanations have been given for the limited effects of the carbon surface groups on the Pd dispersion of the catalysts studied in this work. Thermal decomposition of surface groups is not a valid explanation, since this process occurs only at temperatures exceeding 470 K. However, some compensating phenomena can occur. Two possibilities will be given here. The first explanation relates to surface sites capable of anchoring metal complexes and stabilizing the supported metal against sintering. If, for instance, carboxylic surface groups are destroyed by a heat treatment with ammonia, the Pd complex may become adsorbed as a result of ligand exchange with newly created N-containing groups, which are present on the modified surface. As a consequence, the Pd dispersion can be the same after this treatment. Secondly, catalysts pass through several stages during preparation. An influence of the carbon treatment in one stage of the preparation process might be counteracted in subsequent steps. Another important influence on Pd dispersion is the presence of micropores in activated carbons. Gurrath *et al.* found that the small and square planar $PdCl_4^{2-}$ ions can penetrate deeper into smaller pores than the bulkier $Pd(NH_3)_4](NO_3)_2$ and trimeric $[Pd(OAc)_2]_3$ precursors.

Krishnankutty *et al.* [86-88] also investigated the effect of the nature of the Pd precursor and carbon pretreatment on the preparation of Pd/C catalysts by incipient wetness impreg-

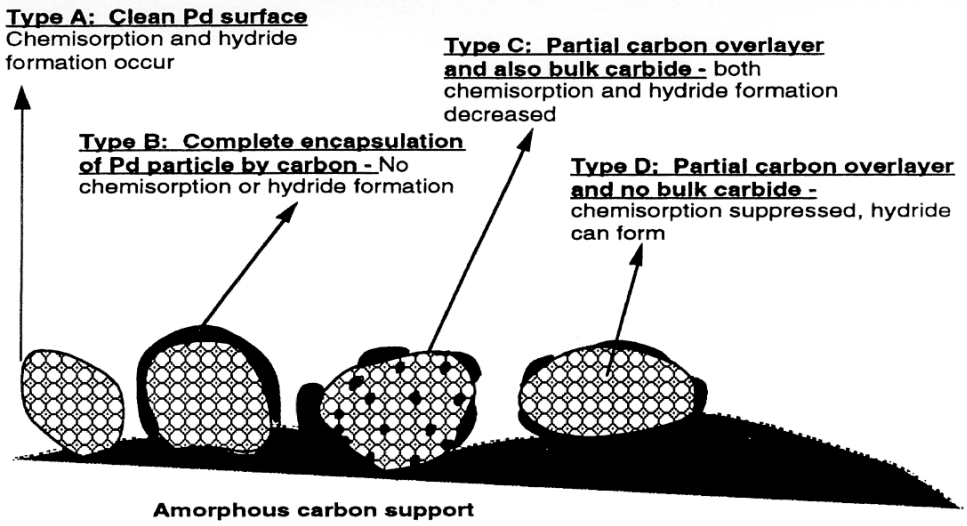

Figure 12. Palladium particles with various extents of carbon surface coverage and/or bulk carbide formation, reproduced with permission [88].

nation. Carbon black was given a high temperature pretreatment under flowing H_2 (C-HTT-H_2) or Ar (C-HTT-Ar) for 16 h at 1223 K to remove sulfur and oxygen from the surface. A pretreated C-HNO_3 sample was prepared by boiling a portion of the C-HTT-Ar sample in 65% HNO_3 for 6 h. An incipient wetness impregnation method under nitrogen was used to prepare 3 wt% Pd/C catalysts. $Pd(acac)_2$ dissolved in water-free THF to produce Cl-free catalysts and $PdCl_2$ dissolved in water were used as precursors. After reduction an expansion of the Pd lattice, suppressed hydrogen chemisorption and decreased hydride formation were observed, pointing to the presence of interstitial carbon or carbon covering the Pd surface. Carbon from the $Pd(acac)_2$ precursor was found to contaminate both the bulk and the surface of Pd crystallites in Pd/C catalysts during a standard hydrogen reduction at 573 K. This carbon could be removed by calcination in oxygen. Krishnankutty *et al.* proposed a model in which a Pd/C catalyst could contain a mixture of Pd particles (type A, B, C and D) with various extents of carbon coverage, as shown in Figure 12 [88]. Phenomena observed during dispersion measurements on the catalysts can be explained by the presence of Pd particles of type C (containing a partial carbon overlayer and bulk carbide). Therefore it is of great importance to subtly remove carbon from the surface of the palladium particles when the dispersion of Pd/C catalysts prepared with $Pd(acac)_2$ is determined with chemisorption.

After reduction at 573 K fairly narrow Pd particle size distributions were obtained for all catalysts prepared with $Pd(acac)_2$, irrespective of carbon pretreatment. Pd/C-AS, Pd/C-HTT-H_2 and Pd/C-HTT-Ar have similar Pd particle sizes of 3.5-4.3 nm, although Pd/C-HNO_3 displayed a slightly larger size, *viz.* 6.3 nm. This small increase, probably due to the smaller surface area of the C-HNO_3 support, shows that small Pd particles are not preferentially stabilized by oxygen-containing surface groups of the support. Because the $Pd(acac)_2$ precursor is a neutral species an advantageous interaction between the precursor and the negatively charged support surface is not expected. Broader particle size distributions and

large Pd particles up to 45 nm were obtained with the $PdCl_2$ precursor. These findings have to be ascribed to sintering of Pd particles (*ex* $PdCl_2$) at higher temperatures.

A substantial amount of research has been devoted to the influence of the palladium chloride precursor during incipient wetness impregnation. The work of Gurrath and Krishnankutty was already described and below the most important results of other authors using $PdCl_2$ [38,89-93] have been summarized. Moroz *et al.* [38] extended the work of Simonov *et al.* using incipient wetness impregnation on carbon black. As shown in Table 3 incipient wetness impregnation of H_2PdCl_4 on carbon results in a high $PdCl_2/Pd^0$ ratio. After drying 60% of the original amount of $PdCl_2$ is present in the form of small, highly dispersed clusters (<1.8 nm in size). XRD RED (radial electronic density distribution) analysis shows a Pd-C distance, as a result of the earlier mentioned preference of $PdCl_2$ clusters to coordinate near carbon surface steps.

A special type of carbon support material was used by Teunissen [90]. She used magnetic, graphite-coated nickel-iron alloy particles (average size 25 nm) as a catalyst support. The magnetic properties of the support particles allow fast and simple catalyst recovery from liquid media. After incipient wetness impregnation with H_2PdCl_4 Electron Probe Analysis

Table 3. Factors determining the $PdCl_2/Pd^0$ ratio in carbon-supported catalysts prepared *via* impregnation with aqueous solutions of H_2PdCl_4, adapted from [37].

$PdCl_2$ high	**Pd^0 high**
1. Powdered carbon support	1. Granulated support
2. Low temperature	2. High temperature
3. The presence of ligands that decrease the $E^0_{Pd2+/Pd}$ value (excess HCl)	3. The absence of ligands that decrease $E^0_{Pd2+/Pd}$ value in the H_2PdCl_4 solution
4. The presence of electrolytes with lyophilic anions (SO_4^{2-})	4. The presence of electrolytes with surface active anions (ClO_4^-)
5. The presence of additional oxidants (O_2, H_2O_2)	5. No other oxidants (inert)
6. Fast penetration of Pd(II) ions into the pores of carbon (high conc. H_2PdCl_4, incipient wetness impregnation or adsorption from solution under vigorous stirring)	6. Slow penetration of Pd(II) ions into the carbon pores (low conc. H_2PdCl_4 and excess solvent)
7. High coverage of the carbon surface by palladium compounds	7. Low coverage of the carbon surface by palladium compounds
8. Low electric capacity of the double electrical layer (DEL) of carbons (low surface area of carbon support or oxidized surface)	8. High electrical capacity of carbon DEL (large surface area carbon support, no oxidation of carbon support)

showed a homogeneous distribution of palladiumchloride over the sample. HRTEM images of the reduced Pd on C/NiFe catalyst displayed the presence of 3 to 4 nm-sized palladium particles. It turned out that activation of the carbon coating was not necessary to anchor the palladium complexes.

An important topic when using impregnation for catalyst preparation is the distribution of the precursor over the macroscopic support bodies. Four types of distribution are shown in Figure 13. Each of these distributions has advantages and disadvantages. If a reaction is diffusion-limited, an "egg-shell" catalyst, containing the active component at the outer parts of the support, would be most efficient. If no diffusion-limitations occur a uniform distribution is usually preferred. "Egg-white" and "egg-yolk" types are desirable if the reaction medium contains a catalyst poison: the exterior part of the support can absorb the poison and the catalyst remains active for a longer time [1,5]. Bianchi *et al.* [94,95] have reported a method for the preparation of a 5 wt% egg-white Pd/C catalyst. They used activated carbon as a support, which was impregnated with H_2PdCl_4. During the adsorption process (15 min) the vessel was sonificated. Subsequently the samples were reduced by addition of Na-formiate at 353 K. Counter-diffusion between impregnate and reducing agent brought about the egg-white distribution.

It is not possible to extensively review all precursors. Therefore a short description of the most frequently applied palladium precursor complexes, next to H_2PdCl_4, and the resulting catalysts will be given below. Hermans *et al.* [96] synthesized palladium-based carboxylate-type compounds for impregnation on active carbon. The selected precursors correspond to the general compositions $Pd(O_2CR)_2$, $Pd(O_2CR)_2L_2$ or $Pd(O_2CR)_2L'$, with R = CH_3, C_2H_5 or C_6H_5, L = pyridine or diethylamine and L' = 2,2'-bipyridine or 1,10-phenanthroline. 5 wt% Pd/C catalysts were prepared by impregnation of solutions of these complexes in water, benzene or acetone, followed by drying and thermal activation under nitrogen. After activation only metallic palladium was detected, indicating that decomposition of these complexes results in complete reduction of the metal. All catalysts prepared in benzene were found to have high Pd dispersions, whereas impregnation with water or acetone as the solvent resulted in poorly dispersed catalysts. An explanation for this phenomenon is the occurrence of disadvantageous interactions between the (non-polar) support and the precursor solvent. The interaction with acetone and water can probably be improved by creating additional oxygen surface groups on the support, which make the support more hydrophilic. Also the palladium/ligand ratio of the polydentate precursor complexes appears to play an important

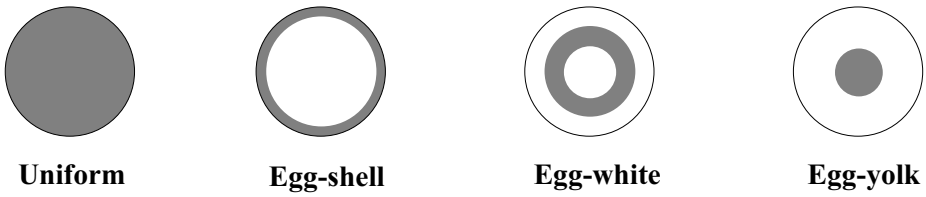

Figure 13. Distributions of active phase over support bodies, adapted from [1].

role in the preparation of the catalysts, since these complexes can have a monomeric as well as a trimeric structure. The presence of monomeric structures results in higher dispersions compared to catalysts preparations with trimeric species.

Other palladium precursors used are allylic Pd complexes ($(C_3H_5)Pd(C_5H_5)$) [35], palladium acetate ($Pd(Oac)_2$) [28], palladium acetylacetonate ($Pd(acac)_2$) [97] and polynuclear palladium hydroxide complexes ($Pd(OH)_n^{(2-n)+}$) [37]. All precursors give monomodal, 1-2 nm-sized Pd particles except the $Pd(acac)_2$ precursor, with which the catalyst is pyrolysed at high temperatures (873-1673 K) probably causing strong sintering. It is difficult to compare the various precursors because there are many variations in the preparation procedures (drying, calcination and reduction).

Adsorption/ion exchange

The precursor most often used for the preparation of Pd/C catalysts *via* adsorption is H_2PdCl_4 (*i.e.* $PdCl_2$ in HCl). Simonov *et al.* have extensively studied the interaction of H_2PdCl_4 with different types of carbon supports and the parameters influencing the palladium dispersion [35-37,98-100]. The four key steps involved in the synthesis of Pd/C catalysts using adsorption are adsorption, washing, drying and reduction. A detailed description of the chemistry of the interaction of Pd and carbon is found in section on 'precursor-surface interactions'.

Simonov *et al.* reported on the room temperature adsorption of H_2PdCl_4 on carbon support materials from an aqueous 0.01 M solution under a controlled atmosphere (He, air or O_2) [36]. A Sibunit carbon support (graphite-like, 500 m^2/g) [101,102], pretreated by boiling for 3 h in water or in an aqueous mixture of 15% HCl and 5% HF, was used. Adsorption onto powdered support was performed in a static reactor under strong stirring of the suspension, whereas adsorption onto granulated supports was accomplished through circulative impregnation. After adsorption (1-3 h) the support was filtered, washed and dried in vacuum at 323 K. The Pd content of the samples was 2.0 wt%. Both methods yielded catalysts containing large (6-100 nm), non-uniform metallic Pd particles assembled on the external surface and small (1-3 nm), uniform $PdCl_2$ clusters evenly distributed over the surface [36]. Factors influencing the $PdCl_2/Pd^0$ ratio are summarized in Table 3.

Besides the above-mentioned influences on the $PdCl_2/Pd^0$ ratio, the dispersion of the metallic palladium particles was found to be determined by at least three factors: support particle size, preliminary washing of the support with acid and the composition of the gas atmosphere. The average size of the metal particles increased with increasing carbon particle size, due to a relative decrease of external surface. Obviously, the concentration of sites responsible for the formation of metal nuclei decreased when the oxygen partial pressure in the gas atmosphere was increased. Thus, oxygen not only reduces the quantity of metal phase formed, but also decreases the number of sites at which nucleation of metallic Pd occurs. Ash removal from the support by acid washing enlarged the Pd particles too, due to a decreased amount of nucleation sites. XRD and HRTEM results show that the metallic Pd particles are

spherical and that their average size was about 1.5-2 times larger than their crystallite size which indicates that the particles display polycrystalline behavior [36].

The drying procedure has a significant influence on the properties of Pd/C catalysts as well. Fast drying (heating with solvent evaporation) causes a small increase in the amount of Pd^0, due to thermal decomposition of $PdCl_2$ complexes. Slow drying (storing impregnated carbon in air for a long time), however, decreases the amount of Pd^0, because metal particles dissolve under the action of O_2 and HCl. During drying Pd(II) compounds migrate over the carbon surface to the micropores and the most disordered regions on the surface and interact with each other, giving rise to agglomeration. The centers of $PdCl_2$ agglomeration, *i.e.* the surface steps that interact with the $(PdCl_2)_n$ clusters both chemically *via* π-bonds and epitaxially, are shown in Figure 10. Another consequence of solvent removal is surface coverage of some Pd^0 and Pd(II) particles by fragments of the carbon framework. This phenomenon is caused by "graphitization" of carbon around crystallites and by the ability of palladium to interact epitaxially with carbon networks [37].

According to Simonov *et al.* the origin of the metal particles in the final Pd/C catalyst may be dual: some are formed at the initial stage during impregnation of carbon with H_2PdCl_4 (primary Pd^0, 6-100 nm) and other particles appear only when $PdCl_2$ is reduced (secondary Pd^0) [37]. Reduction with hydrogen at 523 K does not change the size distribution of primary Pd^0. Highly dispersed (1-5 nm) particles of secondary Pd^0 are formed during reduction of surface π-complexes and $(PdCl_2)_n$ clusters. Oxygen-containing surface groups do not affect the ability of Pd^0 particles to sinter, apparently because these groups are decomposed or reduced under the reduction conditions (H_2, 523 K) in the presence of Pd^0. The average size of the secondary Pd^0 particles strongly depends on the presence of strong adsorption sites on the support (A_2, edge sites, see Figure 9) and on the interaction of the catalyst precursor with the support. Due to the co-existence of two routes for the formation of Pd^0 particles a bimodal particle size distribution is observed for the Pd/C catalyst [37]. Benedetti *et al.* [103] confirmed this bimodal size distribution using a comparable preparation method. In conclusion, in order to obtain high Pd dispersions it is very important to choose conditions that surpress the formation of primary Pd^0 and increase the amount of secondary Pd^0.

Fenelonov *et al.* [100] extended the research on Pd/C catalysts to another carbon support, namely carbon nanofibers. Because of the similar electronic properties of graphitic Sibunit material and graphitic carbon nanofibers it can be assumed that the same processes take place when H_2PdCl_4 is adsorbed. The only major difference between the two types of carbon support is the absence of A_3 absorption sites in carbon nanofibers, because of the absence of micropores. Fenelov *et al.* concluded that carbon nanofibers are capable of stabilizing the finely dispersed Pd phase, due to a strong interaction between the palladium precursor and the fiber support.

Other authors also reported on H_2PdCl_4 adsorption onto carbon supports [83,103,104]. Albers *et al.* [104] prepared Pd catalysts (5 wt%) on activated carbon and carbon black. The

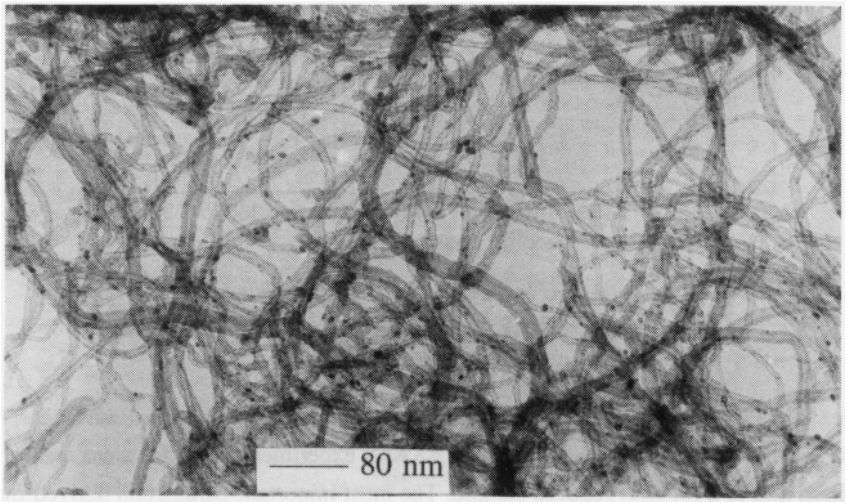

Figure 14. TEM micrograph of reduced palladium on carbon tubes [22].

supports were used both in their original state and after a treatment with hydrochloric acid to reduce the ash and impurity content. It appeared that the treatment with acid enhanced the Pd dispersion and narrowed the Pd particle size distribution in the resulting catalysts.

In the literature on the preparation of palladium on carbon catalysts cation exchange is only described on negatively charged (oxygen-containing surface groups) carbon supports. We found no literature describing anion exchange on basic (positively charged) carbon supports. The most widely applied cationic precursors are palladium ammine complexes. They are used in two forms, *viz.* the $Pd(NH_3)_4(NO_3)_2$ [22,34,90,105,106] and the $Pd(NH_3)_4Cl_2$ complex [22,83,105,107].

In our group extensive investigations have been carried out on the preparation of palladium on carbon nanotube (CNT) catalysts using the ion exchange technique [22,34,105]. Hoogenraad *et al.* utilized CNT (surface area of 225 m^2/g) grown out of an iron on alumina catalyst. The tubes were activated by boiling in concentrated nitric acid (10-120 min). Subsequently, the tubes were washed with water and dried for one hour in air at 393 K. A weighted amount of the activated and dried support was suspended in water, the pH of which had been adjusted to a value of 5-6. Then an aqueous solution of a palladium-precursor ($Pd(NH_3)_4(NO_3)_2$, $Pd(NH_3)_4Cl_2$ or H_2PdCl_4) was injected under stirring. After this procedure the suspension was filtered and dried at 353 K for 12 h in air or under nitrogen atmosphere. From thermogravimetric measurements the amount of oxygen-containing sites was found to increase linearly with pretreatment times up to 120 min. Nevertheless, activation for 10 min appeared to be sufficient to get a maximum loading. Prolonged activation turned out to increase the number of surface groups, but not the final loading. The pH_{IEP} of treated CNT was 2.3. Therefore, the cationic palladium complexes ($Pd(NH_3)_4^{2+}$) should interact favorably with the support. The authors found that with non-pretreated tubes palladium did not adsorb onto the surface of the nanotubes. Ion exchange with palladium chloride resulted in the precipitation of large particles (50-100 nm) of $Pd(OH)_2$ separate from the support. Apparently, at a pH of around 5.5, which was attained by addition of a small amount of sodium hydroxide, the Cl/Pd ratio was too low to avoid hydrolysis. With the palladium

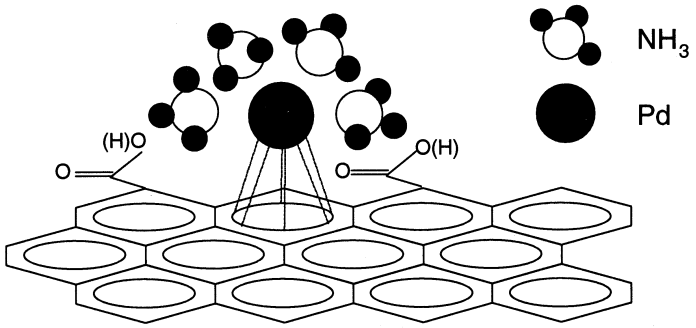

Figure 15. Schematic representation of the interaction of a palladium tetra-ammine complex with a carbon nanotube surface (dried catalyst) [22].

ammine precursors nucleation of insoluble palladium species in the bulk of the solution was not observed. TEM images and XRD patterns of dried samples (3 wt%) did not show the presence of palladium particles. After a 2 h reduction in hydrogen at 523 K some sintering occurred, leading to the formation of very small palladium particles (1 to 1.5 nm), as can be seen in Figure 14. These results were obtained with both $Pd(NH_3)_4(NO_3)_2$ and $Pd(NH_3)_4Cl_2$. When filtering and drying was executed in air instead of nitrogen, much larger particles (30-50 nm) were found. Decomposition of the ammine complexes proceeded at lower temperatures in air, resulting in mobile palladium species that coalesced. Hoogenraad *et al.* [22,34,105] tried to gain information on the interaction of ionic palladium complexes and palladium metal atoms with the CNT surface using *in situ* EXAFS. In the dried sample no Pd-O contributions were observed. However they measured a Pd-C coordination number of 6. It was concluded that palladium ions interact directly with the graphitic surface of the tubes. Nevertheless, oxygen-containing surface groups must participate in these interactions, since adsorption of palladium on the surface did not take place without these groups. A schematic representation of the proposed interaction, involving oxidic surface groups, is shown in Figure 15. After reduction the Pd-Pd coordination number is 8. This number corresponds to a particle size of 1-1.5 nm, which is in agreement with TEM observations.

Summarizing, the most important factor when using ion exchange for the deposition of palladium on carbon is a large amount of ion-exchangeable sites on the carbon surface [22,83,106].

Conclusions

- The synthesis of supported palladium catalysts has been reviewed, focusing on the chemistry of catalyst synthesis, relevant support properties and case studies for oxide- and carbon-supported catalysts.
- Aqueous Pd precursor solutions may consist of $Pd(H_2O)_4^{2+}$ at pH<1, while colloidal PdO is formed at higher pH values. In catalyst syntheses ligand-stabilized precursors are

frequently used; in particular $Pd(NH_3)_4^{2+}$ and $PdCl_4^{2-}$. With non-aqueous precursor solutions $Pd(acac)_2$ is often applied.

- The precursor-support interaction during synthesis is advantageously rationalized by considering for oxides the iso-electric point in combination with the precursor ion charge. Silica and alumina are at present the most important supports for Pd catalysts.
- With carbon supports it turns out that additionally one has to consider the direct reduction of the Pd-precursor by the carbon support, which gives rise to large Pd particles. Furthermore, the lyophilicity of carbon may affect catalyst synthesis. Activated carbon is most extensively used, whereas carbon nanofibers/nanotubes also show great potential related to tailoring of surface properties, good accessibility and high mechanical strength.
- For the preparation of oxide-supported Pd catalysts sol-gel techniques can be used, yielding Pd particles of 1 nm at low loadings. However, ion exchange and impregnation are most often used. In general, careful washing after the adsorption process and calcination prior to reduction are beneficial to obtain high Pd dispersions.
- For carbon-supported catalysts is has been found that a thermal pretreatment often has a large effect on the Pd dispersion. Furthermore, thermal treatment in an inert atmosphere prior to reduction is also essential to obtain a high Pd dispersion.
- From this literature review some general rules for the thermal pretreatment of Pd catalyst precursors can be derived. High Pd dispersions call for decomposition of the precursor in an inert atmosphere and reduction temperatures should not exceed 423 K. Furthermore it is found that gas-phase reductions lead to higher dispersions than liquid-phase reductions.
- The challenge to develop supported Pd catalysts that display high dispersions at high loadings has hardly been addressed up till now. We feel that deposition-precipitation, in combination with the generation of anchoring sites on the support, could be a very promising technique to achieve this goal [108].

References

1. E.B.M. Doesburg, K.P. de Jong, J.H.C. van Hooff, J.W. Geus and J.A.R. van Veen, Stud. Surf. Sci. Catal. 123 (1999) Chapter 9 and 10.
2. L.A.M. Hermans and J.W. Geus , Stud. Surf. Sci. Catal. 3 (1979) 113.
3. A.Yu. Stakheev and L.M. Kustov, Appl. Catal. A Gen. 188 (1999) 3.
4. B.L. Mojet, J.T. Miller, D.E. Ramaker and D.C. Koningsberger, J. Catal. 186 (1999) 373.
5. R.L. Augustine, Heterogeneous Catalysis for the Synthetic Chemist, Marcel Dekker, Inc., New York (1996) Chapter13.

6. C.F. Baes and R.E. Mesmer, The Hydrolysis of Cations, John Wiley & Sons, Inc., New York (1976).
7. D.T. Richens, The Chemistry of Aqua Ions, John Wiley & Sons, Ltd., Chichester (1997).
8. H. Bönneman, W. Brijoux, R. Brinkmann. E. Dinjus, T.Joußen, R. Fretzen and B. Korall, J. Mol. Catal. 74 (1992) 323.
9. B. Didillon, E. Merlen, T. Pagès and D. Uzio, Stud. Surf. Sci. Catal. 118 (1998) 41.
10. H.P. Boehm and H. Knözinger, Catalysis Vol. 4, Springer-Verlag, Berlin (1983) 39.
11. J.A.R. van Veen, J. Colloid Interface Sci. 12 (1988) 214.
12. J.A.R. van Veen, G. Jonkers and W.H. Hesselink, J. Chem. Soc., Faraday Trans. 85 (1989) 389.
13. J.P. Brunelle, Pure Appl. Chem. 50 (1978) 1211.
14. L. Vordonis, A. Akratopulu, P.G. Koutsoukos and A. Lycourghiotis, Stud. Surf. Sci. Catal. 31 (1987) 309.
15. Z. Sojka and M. Che, Colloids and Surfaces A 158 (1999) 165.
16. C. Contescue, C. Sivaraj and J.A. Schwartz, Appl. Catal. 74 (1991) 95.
17. F. Rodriguez-Reinoso, Carbon 36 (1998) 159.
18. R.J.J. Jansen, Ph.D. thesis, Delft University (1994) Chapter 1.
19. H.F. Stoeckli, Carbon 28 (1990) 1.
20. Z. Hu and E.F. Vansant, Carbon 33 (1995) 561.
21. R. Leboda, A. Lodyga and A. Gierak, Mater. Chem. Phys. 51 (1997) 216.
22. M.S. Hoogenraad, Ph.D. thesis, Utrecht University (1995) Chapter 2 and 7.
23. K.P. de Jong and J.W. Geus, Catal. Rev.-Sci. Eng. 42 (2000) 482.
24. V.N. Parmon, G.G. Kuvshinov, V.A. Sadykov and V.A. Sobyanin, Stud. Surf. Sci. Catal. 119 (1998) 677.
25. H.P. Boehm, Adv. Catal. 16 (1966) 179.
26. H. Darmstadt, L. Summchen, J.-M. Ting, U. Roland, S. Kaliaguine and C. Roy, Carbon 35 (1997) 1581.
27. R. Schlögl, M. Che, O. Clause and C. Marchilly, Preparation of solid catalysts, Wikey-VCH, Weinheim, (1999) Chapter 3 and 4.
28. S.V. Gurevich, P.A. Simonov, A.S. Lisitsyn, V.A. Likholobov, E.M. Moroz, A.L. Chuvilin and V.N. Kolomiichuk, React. Kinet. Catal. Lett. 41 (1990) 211.
29. C. Prado-Burguete, A. Linares-Solano, F. Rodriguez-Reinoso and C. Salinas-Martinez de Lecea, J. Catal. 115 (1989) 98.
30. D.J. Suh, T.-J. Park and S.-K. Ihm, Carbon 31 (1993) 427.
31. C.A. Leon y Leon, J.M. Solar, V. Calemma and L.R. Radovic, Carbon 30 (1992) 797.
32. H.P. Boehm, Carbon 32 (1994) 759.
33. S.S. Barton, M.J.B. Evans, E. Halliop and J.A.F. MacDonald, Carbon 35 (1997) 1361.

34. B.L. Mojet, M.S. Hoogenraad, A.J. van Dillen, J.W. Geus and D.C. Koningsberger, J. Chem. Soc., Faraday Trans. 93 (1997) 4371.
35. Y.A. Ryndin, O.S. Alekseev, P.A. Simonov and V.A. Likholobov, J. Mol. Catal. 55 (1989) 109.
36. P.A. Simonov, A.V. Romanenko, I.P. Prosvirin, E.M. Moroz, A.I. Boronin, A.L. Chuvilin and V.A. Likholobov, Carbon 35 (1997) 73.
37. P.A. Simonov, S.Y. Troitskii and V.A. Likholobov, Kinet. Catal. 41 (2000) 255.
38. E.M. Moroz, P.A. Simonov, S.V. Bogdanov and A.L. Chuvilin, Mater. Sci. Forum 321-324 (2000) 1074.
39. J.A. Schwartz, Chem. Rev. 95 (1995) 477.
40. C. Perego and P. Villa, Catal. Today 34 (1997) 281.
41. T. López, M. Morán, J. Navarrete, L. Herrera and R. Gómez, J. Non-Cryst. Solids 147-148 (1992) 753.
42. T. López, M. Asomoza, P. Bosch, E. Garcia-Figueroa and R. Gómez, J. Catal. 138 (1992) 463.
43. W. Zou and R.D. Gonzalez, Appl. Catal. A Gen. 126 (1995) 351.
44. D.H. Kim, S.I. Woo and O.Yang, Appl. Catal. B Environ. 26 (2000) 285.
45. A.J. Lecloux and J.P. Pirard, J. Non-Cryst. Solids 225 (1998) 146.
46. M. Schneider, M. Wildberger, M Maciejewski, D.G. Duff, T. Mallát and A. Baiker, J. Catal. 148 (1994) 625.
47. T. Fujitani, M. Saito, Y. Kanai, T. Watanabe, J. Nakamura and T. Uchijima, Appl. Catal. A Gen.125 (1995) L199.
48. A.J. van Dillen, J.W. Geus, L.A.M. Hermans and J. v.d. Meijden, Proc. 6th Int. Congr. Catal. (1976) 677.
49. K.P. de Jong, Stud. Surf. Sci. Catal. 63 (1991) 19.
50. R.L. Augustine and S.T. O'Leary, J. Mol. Catal. A Chem. 95 (1995) 277.
51. W.-J. Shen and Y. Matsumura, J. Mol. Catal. A Chem. 154 (2000) 165.
52. W.-J. Shen, Y. Ichihashi, M. Okumura and Y. Matsumura, Catal. Lett. 64 (2000) 23.
53. W.-J. Shen and Y. Matsumura, Phys. Chem. Chem. Phys. 2 (2000) 1519.
54. K.P. de Jong and J.W. Geus, Appl. Catal. 4 (1982) 41.
55. K.P. de Jong, Current Opinions in Solid State & Materials Science 4 (1999) 55.
56. G. Fogassy, L. Hegedűs, A. Tungler, A. Lévai and T. Máthé, J. Mol. Catal. A Chem. 154 (2000) 237.
57. A. Beck, H. Horváth, A. Szűcs, Z. Schay, Z.E. Horváth, Z. Zsoldos, I. Dékány and L. Guczi, Catal. Lett. 65 (2000) 33.
58. R.J. Farrauto, J.K. Lampert, M.C. Hobson and E.M. Waterman, Appl. Catal. B Environ. 6 (1995) 263.
59. G.C. Bond and A.F. Rawle, J. Mol. Catal. 109 (1996) 261.

60. O.M. Ilinitch, L.V. Nosova, V.V. Gorodetskii, V.P. Ivanov, S.N. Trukhan, E.N. Gribov, S.V. Bogdanov and F.P. Cuperus, J. Mol. Catal. A Chem. 158 (2000) 237.
61. D. Amalric-Popescu and F. Boszon-Venduraz, Catal. Lett. 64 (2000) 125.
62. C. Sivaraj, C. Contescu and J.A. Schwartz, J. Catal. 132 (1991) 422.
63. E.M. Cordi and J.L. Falconer, J. Catal. 162 (1996) 104.
64. W. Zou and R.D. Gonzalez, Catal. Lett. 12 (1992) 73.
65. A. Gotti and R. Prins, J. Catal. 175 (1998) 302.
66. A.F. Gusovius, T.C. Watling and R. Prins, Appl. Catal. A Gen. 188 (1999) 187.
67. C. Chang and T.C. Chou, Appl. Catal. A Gen. 156 (1997) 193.
68. C. Neyertz and M. Volpe, Coll. Surf. A 136 (1998) 63.
69. J.P. Boitiaux, J. Cosyns and S. Vasudevan, Proc. 3th Int. Symp. Scientific Bases for the Preparation of Heterogeneous Catalysts, Elsevier, Amsterdam (1982) 123.
70. J. Goetz, M.A. Volpe, A.M. Sica, C.E. Gigola and R. Touroude, J. Catal. 153 (1995) 86.
71. A.M. Pisanu and C.E. Gigola, Appl. Catal. B Environ. 20 (1999) 179.
72. A.M. Venezia, A. Rossi, D. Duca, A. Martorana and G. Deganello, Appl. Catal. A Gen. 125 (1995) 113.
73. H. Gao and R.J. Angelici, J. Mol. Catal. A Chem. 149 (1999) 63.
74. K. Muto, N. Katada and M. Niwa, Appl. Catal. A Gen. 134 (1996) 203.
75. M. Kotter and L. Riekert, Stud. Surf. Sci. Catal. 3 (1979) 51.
76. D. Łomot, W. Juszczyk and A. Karpiński, Appl. Catal. A Gen. 155 (1997) 99.
77. R. Burch and F.J. Urbano, Appl. Catal. A Gen. 124 (1995) 121.
78. P. Papaefthimiou, T. Ioannides and X.E. Verykos, Appl. Catal. B Environ. 13 (1997) 175.
79. X.L. Seoane, P.C.L. l'Argentiere, N.S. Fígoli and A.A. Arcoya, Catal. Lett. 16 (1992) 137.
80. H. Jin, S.-E. Park, J.M. Lee and S.K. Ryu, Carbon 34 (1996) 429.
81. G. Farkas, L. Hegedus, A. Tungler, T. Mathe, J.L. Figueiredo and M. Freitas, J. Mol. Catal. A Chem. 153 (2000) 215.
82. M.S. Hoogenraad, R.A.G.M.M. van Leeuwarden, G.J.B. van Breda-Vriesman, A. Broersma, A.J. van Dillen and J.W. Geus, Stud. Surf. Sci. Catal. 91 (1995) 263.
83. G.R. Heal and L.L. Mkayula, Carbon 26 (1988) 815.
84. Y. Yang, Y. Zhou, C. Cha and W.M. Carroll, Electrochim. Acta 38 (1993) 2333.
85. M. Gurrath, T. Kuretzky, H.P. Boehm, L.B. Okhlopkova, A.S. Lisitsyn and V.A. Likholobov, Carbon 38 (2000) 1241.
86. N. Krishnankutty and M.A. Vannice, J. Catal. 155 (1995) 312.
87. N. Krishnankutty and M.A. Vannice, J. Catal. 155 (1995) 327.
88. N. Krishnankutty, J. Li and M.A. Vannice, Appl. Catal. A Gen. 173 (1998) 137.

89. M.G. Musolino, C. Milone, G. Neri, L. Bonaccorsi, R. Pietropaolo and S. Galvagno, Stud. Surf. Sci. Catal. 108 (1997) 239.
90. W. Teunissen, Ph.D. thesis, Utrecht University (2000), Chapter 5.
91. B. Czajka and P. Kirszensztejn, J. Therm. Anal. Calorim. 55 (1999) 619.
92. E.J.A.X. van de Sandt, A. Wiersma, M. Makkee, H. van Bekkum and J. A. Moulijn, Appl. Catal. A Gen. 173 (1998) 161.
93. A. Wiersma, E.J.A.X. van de Sandt, M.A. den Hollander, H. van Bekkum, M. Makkee and J.A. Moulijn, J. Catal. 177 (1998) 29.
94. C.L. Bianchi, R. Carli, C. Fontaneto and V. Ragaini, Stud. Surf. Sci. Catal. 91 (1995) 1095.
95. C.L. Bianchi, R. Carli, C. Fontaneto and V. Ragaini, Ultrason. Sonochem. 4 (1997) 317.
96. S. Hermans, M. Wenkin and M. Devillers, J. Mol. Catal. A. Chem. 136 (1998) 59.
97. H. Tamai, Y. Kataoka, F. Nishiyama and H. Yasud, Carbon 38 (2000) 899.
98. P.A. Simonov, E.M. Moroz, A.L. Chuvilin, V.N. Kolomiichuk, A.I. Boronin and V.A. Likholobov, Stud. Surf. Sci. Catal. 91 (1995) 977.
99. P.A. Simonov, A.V. Romanenko, I.P. Prosvirin, G.N. Kryukova, A.L. Chuvilin, S.V. Bogdanov, E.M. Moroz and V.A. Likholobov, Stud. Surf. Sci. Catal. 118 (1998) 15.
100. V.B. Fenelonov, L.B. Avdeeva, O.V. Goncharova, L.G. Okkel, P.A. Simonov, A.Y. Derevyankin and V.A. Likholobov, Stud. Surf. Sci. Catal. 91 (1995) 825.
101. Y.I. Yermakov, V.F. Surovikin, G.V. Plaksin, V.A. Semikolenov, V.A. Likholobov, L.V. Chuvilin and S.V. Bogdanov, React. Kinet. Catal. Lett. 33 (1987) 435.
102. E.M. Moroz, S.V. Bogdanov and V.A. Likholobov, React. Kinet. Catal. Lett. 47 (1992) 311.
103. A. Benedetti, L. Bertoldo, P. Canton, G. Goerigk, F. Pinna, P. Riello and S. Polizzi, Catal. Today 49 (1999) 485.
104. P. Albers, R. Burmeister, K. Seibold, G. Prescher, S.F. Parker and D.K. Ross, J. Catal. 181 (1999) 145.
105. M.S. Hoogenraad, M.F. Onwezen, A.J. van Dillen and J.W. Geus, Stud. Surf. Sci. Catal. 101 (1996) 1331.
106. W. Teunissen, A.A. Bol and J.W. Geus, Catal. Today 48 (1999) 329.
107. E. Theodoridou, A.D. Jannakoudakis, P.D. Jannakoudakis, N. Pagalos, J.O. Besenhard, C.I. Donner and M. Wicher, Electrochim. Acta 38 (1993) 793.
108. K.P. de Jong and J.W. Geus, Stud. Surf. Sci. Catal. 116 (1983) 111.

5

Preparation of Carbon Nanofiber-Supported Platinum and Ruthenium Catalysts

Comparison of Ion Exchange and Homogeneous Deposition Precipitation

Abstract

Carbon nanofiber (CNF)-supported platinum catalysts have been prepared using $Pt(NH_3)_4(NO_3)_2$ as precursor by two different ion exchange techniques, one at a constant pH and one in which the pH is gradually and homogeneously increased from 3 to 6 by hydrolysis of urea. The latter method resembles the procedure of homogeneous deposition precipitation (HDP). Characterization of the CNF support was performed by acid-base titration, TGA-MS and XPS and for the various platinum catalysts TEM, H_2-chemisorption and XRF/ICP-AES were utilized. With both synthesis techniques, from diluted precursor solutions, homogeneously distributed, highly dispersed and thermally stable metal particles were obtained with an average particle size of 1-2 nm. With the HDP method for the Pt/CNF catalysts a linear relationship between the number of acidic oxygen-containing groups on the surface of activated CNF and the metal loading has been found. For the highest loaded catalyst a platinum/adsorption site ratio of 0.5 was established, corresponding to about 0.7 $Pt(NH_3)_4^{2+}$ molecules/nm^2. Furthermore it has been established that with this procedure higher platinum loadings (~4 wt%) can be achieved that with the ion exchange procedure (<2 wt%). The HDP method using $RuNO(NO_3)_3(H_2O)_2$ also turned out to be suitable for the preparation of small (1-2 nm) uniform ruthenium particles on CNF with a high thermostability.

Introduction

Supported noble metal catalysts often are prepared *via* aqueous routes, mainly ion exchange. The term ion exchange is used to describe processes where ionic species interact electrostatically with charged sites on the support surface [1]. It is still uncertain which step in the preparation procedure is chiefly responsible for the ultimate size and distribution of the metal particles, but the distribution of the precursor of the active component as accomplished in the exchange step to a large extent determines the final result. The maximum metal loading depends amongst other factors on the number and nature of the adsorption sites, the pH of the solution, the speciation of the precursor and the presence of competing species that may adsorb on the same sites [2]. Sometimes, using ion exchange with porous oxidic support bodies inhomogeneous distributions have been reported, especially with loadings smaller than saturation and fast and strong adsorption of the precursor on the support [2,3].

Several adsorption mechanisms can be found in the literature. Regalbuto *et al.* [4] have extensively studied the adsorption of chloroplatinic acid onto alumina and developed the Revised Physical Adsorption (RPA) model. This model implies that in the adsorption process only physical interactions are involved and is therefore also referred to as the formation of outer-sphere complexes. The precursor ions are adsorbed on the surface according to a Langmuir adsorption model with a maximum coverage of a closed packed layer of adsorbate species, retaining one or several hydration shells. With some minor revisions to account for the more complex chemistry of the carbon surface the RPA model can also be applied to carbon supports [5].

Another way of considering interaction between precursor species and the surface involves ion exchange. An electrostatic interaction of adsorbed complexes with the surface can bring about an exchange of the original ligands by surface ligands. The resulting inner-sphere complexes are chemically bonded to the surface [6,7].

For the production of highly loaded and highly dispersed metal/oxide catalysts the homogeneous deposition precipitation technique (HDP) has been developed [8-10]. In HDP the active phase or its precursor is deposited onto an existing support by slowly and homogeneously introducing the precipitating agent in such a way that nucleation in the solution itself is avoided. This process of “surface precipitation” can be considered as a process in which next to the adsorption stage nucleation of a precursor compound occurs. These nuclei gradually grow and high loadings can be attained. To avoid nucleation in the bulk of the solution, locally high degrees of super saturation must be prevented. Generally hydrolysis of urea, added to the suspension of the support, is used to effectuate a slow and homogeneous increase of the hydroxyl concentration. From extensive research on the mechanism of HDP of nickel on silica supports it was found that during HDP surface compounds like 1:1 Ni-phyllosilicates are formed [8,9,11,12]. This procedure has been used with success to produce numerous highly loaded, thermally stable and highly dispersed catalysts. It is striking that even with graphite-like carbon nanofibers (CNF) as the support,

which is unable to form a mixed surface compound, highly loaded catalysts with relatively small metal particles can be obtained [13].

Nevertheless, the chemical inertness of graphite-like CNF brings along considerable difficulties in the application of the (precursor of the) active phase *via* wet chemical routes [14]. Because of the hydrophobic character of 'as synthesized' CNF their wettability is poor and interaction with dissolved polar precursor species is low. To tackle this problem the hydrophilic nature of the fibers can be raised by surface oxidation. Pretreatment of CNF with oxidizing agents, *e.g.* nitric acid, results in the formation of polar oxygen-containing surface groups, which can be acidic, neutral or basic in nature [15-18]. Because of the dissociation of carboxyl groups, the point of zero charge (pzc) is decreased from pH ~5 of the untreated fibers to pH ~2-3 [19-22]. Introduction of these groups increases the ion exchange capacity too, which is important in view of the attainable loadings with precursor species.

The evolution of surface charge as a function of the pH is important in view of the loading process using both HDP and ion exchange. In this respect oxidic surfaces behave strikingly different from (activated) carbon surfaces. According to Brunelle [23] the charge of, *e.g.* a silica surface (pzc ~ 2) remains close to zero from pH 1 to 7 and only becomes substantial above pH 7. With carbon supports, the zeta potential as a function of the pH develops rather differently [21,23]. From a pH value of 2-3 charging of the surface rapidly increases but at a pH of around 5 a constant level is reached, indicating that all the available adsorption sites have dissociated. This difference is related to the difference in the nature of the adsorption sites, *i.e.* carboxylic groups for carbon and hydroxyl groups for oxides.

Although many studies in literature can be found dealing with platinum deposited on carbon [amongst others 24-28], fundamental research on the preparation of carbon-supported platinum catalysts is rather scarce [5,29-35]. In our research on the application of platinum on CNF we have compared the results obtained with an HDP method with that obtained with ion exchange (IE) and we have investigated the extent of interaction between the dissolved metal precursor and the CNF support. To gain more insight in the relation between the ultimate metal loading, particle size distribution, thermal stability and the number of adsorption sites, we prepared CNF support samples with different numbers of oxygen-containing groups and studied the results obtained with the loading procedures. Additionally, we prepared CNF-supported ruthenium catalysts according to the HDP method.

Experimental

Carbon nanofiber growth

For the growth of CNF a 20 wt% Ni/SiO_2 catalyst was prepared by homogeneous deposition precipitation (HDP) as described by van Dillen *et al.* [8] using silica (Degussa,

Aerosil 200), nickel nitrate (Acros) and urea (Acros). After filtering the catalyst precursor was dried at 393 K and calcined in static air at 873 K (heating rate 5 K/min) for 2 h.

Prior to the fiber growth 1 g of Ni-catalyst precursor, placed in a quartz fixed bed reactor, was reduced *in situ* for 2 h in a flow of a mixture of H_2 (80 ml/min) and N_2 (320 ml/min) at 1 bar and 973 K (heating rate 5 K/min). Next, the CNF were grown at 823 K in a mixture of CO (80 ml/min), H_2 (28 ml/min) and Ar (292 ml/min) for 24 h. A more detailed description of the growth catalyst and the growth of the CNF can be found elsewhere [36].

Activation and pretreatment of carbon nanofibers

All CNF samples were refluxed for 1 h in a 1 M KOH solution in order to remove the silica support. Subsequently, the CNF were refluxed in concentrated nitric acid for removal of non-encapsulated nickel and activation and washed thoroughly with demi-water. The activation and pretreatment process was varied to study the effect of type and number of oxygen-containing groups at the surface of the CNF during the application of the active phase (Table 1). Some CNF samples were refluxed in HCl instead of HNO_3 to remove non-encapsulated nickel without introduction of oxygen-containing groups. CNF were activated in HNO_3 for 0.5, 1 and 2 h, resulting in increasing amounts of oxygen groups. Furthermore CNF were utilized that, after oxidation in HNO_3 for 2 h, were treated in N_2 at 973 K to remove (part of) the surface oxides.

Table 1. Sample codes, preparation conditions and metal content determined by XRF of the various CNF-supported catalysts after reduction at 473 K.

Sample name	CNF treatment	Metal precursor	Intake (wt%)	Metal (wt%)	Method	Heat treatment in N_2
RuCNFCl	KOH, 2 h HNO_3	$RuCl_3.nH_2O$	5.0	n.d.	HDP	-
RuCNF	KOH, 2 h HNO_3	$RuNO(NO_3)_3.nH_2O$	5.0	5.0	HDP	-
RuCNF573	KOH, 2 h HNO_3	$RuNO(NO_3)_3.nH_2O$	5.0	5.0	HDP	573 K
RuCNF773	KOH, 2 h HNO_3	$RuNO(NO_3)_3.nH_2O$	5.0	5.0	HDP	773 K
RuCNF973	KOH, 2 h HNO_3	$RuNO(NO_3)_3.nH_2O$	5.0	5.0	HDP	973 K
PtCNF	KOH, 2 h HNO_3	$Pt(NH_3)_4(NO_3)_2$	5.0	3.4-4.3	HDP	-
PtCNF573	KOH, 2 h HNO_3	$Pt(NH_3)_4(NO_3)_2$	5.0	3.4-4.3	HDP	573 K
PtCNF773	KOH, 2 h HNO_3	$Pt(NH_3)_4(NO_3)_2$	5.0	3.4-4.3	HDP	773 K
PtCNF973	KOH, 2 h HNO_3	$Pt(NH_3)_4(NO_3)_2$	5.0	3.4-4.3	HDP	973 K
PtCNF-A	KOH, 0.5 h HNO_3	$Pt(NH_3)_4(NO_3)_2$	5.0	2.7	HDP	-
PtCNF-B	KOH, 1 h HNO_3	$Pt(NH_3)_4(NO_3)_2$	5.0	3.6	HDP	-
PtCNF-C	KOH, 1 h HCl	$Pt(NH_3)_4(NO_3)_2$	5.0	0.0	HDP	-
PtCNF-D	KOH, 2 h HNO_3, N_2 973 K	$Pt(NH_3)_4(NO_3)_2$	5.0	0.5	HDP	-
PtCNF-10	KOH, 2 h HNO_3	$Pt(NH_3)_4(NO_3)_2$	10.0	4.8	HDP	-
PtCNF-IE-293	KOH, 2 h HNO_3	$Pt(NH_3)_4(NO_3)_2$	5.0	1.4	IE-293K	-
PtCNF-IE-363	KOH, 2 h HNO_3	$Pt(NH_3)_4(NO_3)_2$	5.0	1.8	IE-363K	-

n.d. = not determined

Synthesis of carbon nanofiber-supported platinum and ruthenium catalysts

Platinum (intake 5 wt%) was deposited as follows. A suspension of 1 g CNF in 250 ml demi-water was acidified to pH=3 with nitric acid and heated up to 363 K under inert atmosphere. Subsequently, 0.08 g urea (Acros) and 0.10 g $Pt(NH_3)_4(NO_3)_2$ (Aldrich) were added under vigorous stirring. The pH of the slurry was monitored to follow the process. After the pH had reached a constant value (pH ~ 6, 363 K), the loaded CNF were filtered and washed thoroughly with demi-water, dried at 353 K in a nitrogen flow and reduced in H_2 at 473 K for 1 h (heating rate = 5 K/min). In addition also a Pt/CNF catalyst with an intended loading of 10 wt% has been prepared using this procedure.

For reasons of comparison 5 wt% Pt/CNF catalysts were prepared by means of an ion exchange. 0.10 g $Pt(NH_3)(NO_3)_2$ was dissolved in 250 ml at 293K or at 363 K. Then 1.0 g of activated CNF was added to the solution under vigorous stirring. The pH of the solution was adjusted using a diluted ammonia solution in such a way that a pH of ~6 was established after the addition of CNF. After 18 h the suspension was filtered, washed and finally dried at 353K. The whole procedure was carried out in N_2 atmosphere.

Ruthenium (intake 5 wt%) was deposited on the fibers as follows. A suspension of 5 g oxidized CNF in 250 ml demi-water was acidified to pH=0.5 with nitric acid and heated up to 363 K. Subsequently, 1.56 g urea (Acros) and 0.82 g $RuNO(NO_3)_3(H_2O)_2.nH_2O$ (Acros) or 0.73 g $RuCl_3$ (Acros) were added under vigorous stirring. The pH of the slurry was monitored to follow the process. After the pH had reached a constant value (pH ~ 6, 363 K), the loaded CNF were filtered and washed thoroughly with demi-water, dried at 393 K and reduced in H_2 at 473 K for 1 h (heating rate = 5 K/min).

In order to investigate the thermostability of both the ruthenium and the platinum catalysts, samples of the freshly reduced catalysts were heat-treated in an N_2 flow for 2 h at 573, 773 and 973 K. The description of catalysts treatments together with the identification codes are listed in Table 1.

Catalyst and carbon nanofiber characterization

The number of acid sites of the differently pretreated CNF was determined with standard acid-base titrations. For this purpose 20-40 mg of oxidized CNF was stirred with 25 ml of a solution containing 0.1 M NaCl and 0.1 mM oxalic acid in demi-water, acidified to pH =3 with HCl. While stirring, pure nitrogen was bubbled through the slurry and 10 mM NaOH was added dropwise from a buret until the endpoint (pH = 7.5) had been reached.

The total number of oxygen-containing groups was measured using thermogravimetric analysis on a Netzsch STA-429 thermobalance. The gases evolved were monitored by a Fisons Thermolab quadropole mass spectrometer, through a capillary situated directly above the sample cup. Samples (20-100 mg) were heated in Ar (60 ml/min) at a rate of 5 K/min up to 1123 K and maintained at that temperature for 1 h.

XPS analyses were performed on a Fisons ESCALAB 210I-XL and a Vacuum Generators XPS system. Al Kα X-ray radiation was utilized, employing an anode current of 20 mA at 15 and 10 keV, respectively. The pass energy of the analyzer was set at 70 eV for the Fisons apparatus and 50 eV for the Vacuum Generators XPS. The fibers were measured without grinding of the CNF skeins.

The various CNF samples and the CNF-supported ruthenium and platinum catalysts were examined in a Philips CM-200 FEG TEM and a Tecnai 20 FEG TEM both operated at 200 kV. After suspending in ethanol under ultrasonic vibration the samples were brought onto a holey carbon film on a copper grid.

TPR measurements were performed with a TPDRO 1100 instrument from Thermo Quest CE Instruments. A sufficient amount of sample (~ 0.02 g) was placed in a fixed bed reactor for analysis. A flow containing 5% hydrogen and 95% argon (HoekLoos) was passed downward through the catalyst bed at a rate of 20 ml/min (STP). From the dried flow (molsieves) the hydrogen consumption was measured as a function of temperature (heating rate = 10 K/min) using a tungsten thermal conductivity detector.

Textural analysis was performed with N_2-physisorption at 77 K, up to a pressure of 1 bar. From the N_2-physisorption data, obtained with a Micromeritics ASAP 2400 apparatus, the BET surface area, the total mesopore volume and the micropore volume were derived. Prior to the physisorption experiments the samples were evacuated at 473 K for at least 16 h.

Ruthenium loadings were determined using inductively coupled plasma emission spectrometry on a Vista AZ CCD simultaneous ICP-AES. The platinum loadings were determined by means of XRF on a Philips PW 1480. Before analysis the Pt/CNF samples were pressed into tablets using a methyl methacrylate binder. Besides the platinum loading also the residual nickel content of the samples after acid treatment was determined. It turned out that already after refluxing CNF in HNO_3 for 0.5 h of the initial amount of ~3 wt% only 0.5 wt% was left.

Hydrogen chemisorption measurements were performed using a Micromeritics ASAP 2010C. Before the chemisorption measurements, each sample was dried in a flow of He at 393 K for 1 h, and reduced in flowing H_2 (flow rate = 50 ml/min STP) at 473 K for 2 h, heating rate 5K/min. After reduction the catalyst was degassed for 2 h at 10^{-1} Pa at the reduction temperature in order to eliminate chemisorbed hydrogen and water. The isotherms were measured at 308 K. The H/M ratios are based on the amounts adsorbed at zero pressure found by extrapolation of the linear part of the isotherm. Calculations are made with the total amount of adsorbed hydrogen. Estimated average particle sizes and dispersions are based on spherical geometry and an adsorption stoichiometry of $H/M_s = 1$. The average metal particle size, d (nm), was calculated from:

$$d * D = 10^{21} \frac{M * 6 * \rho_{site}}{\rho_{metal} * N}$$

where D is the dispersion, M is the atomic weight (Ru = 101.07 g/mol, Pt = 195.09 g/mol),

ρ_{site} is the ruthenium surface site density (16.3 Ru atoms/nm^2, 12.5 Pt atoms/nm^2), ρ_{metal} is the metal density (Ru 12.3 g/cm^3, Pt 21.45 g/cm^3) and N is Avogadro constant (6.022*10^{23} mol^{-1}) [37].

Results and Discussion

Characterization of the support

The CNF are of the fishbone type, meaning that the graphene sheets are oriented at an angle to the central axis [14]. After treatment with nitric acid for 2 h the fibers remain non-microporous and show a surface area of 186 m^2/g. X-ray diffraction and transmission electron microscopy showed that the graphite-like structure of the CNF had not been affected during activation. SEM revealed an average fiber diameter of 25 nm with a narrow diameter distribution.

The number of acidic oxygen-containing groups on the CNF samples after the various activation treatments as determined with titration as well as XPS and TGA-MS results are reported in Table 2. As measured by titration, oxidation with concentrated HNO_3 for 0.5 and 2.0 h resulted in 1.0 and 1.4 acid sites/nm^2 respectively and heat treatment up to 973 K in removal of almost all acidic oxygen-containing groups. XPS measurements were executed to establish the amount of oxygen in the outer layer (2-3 nm) of the carbon fibers. Activation of CNF in HNO_3 for 2 h resulted in an O/C ratio of 0.069 and after treatment at 973 K an O/C ratio of 0.017 remained. The O/C atomic ratios can be converted into a number of oxygen atoms/nm^2 using a model of Gijzeman [38]. These results (Table 2) show that fibers oxidized in HNO_3 for 2 h would expose 9.6 O atoms/nm^2 and 2.3 O atoms/nm^2 after heat treatment. Since oxygen-containing groups contain one or two oxygen atoms, this implies that after activation according to the XPS results about 5-10 oxygen-containing groups would be present per nm^2 when it is assumed that all oxygen is located at the exterior surface. Values up to 1-3 groups/nm^2, as earlier proposed by Boehm, seem to be more realistic [17].

Table 2. Number of oxygen atoms/nm^2 on CNF surface and specific surface area in m^2/g as a function of activation treatment as determined with acid-base titration, XPS and TGA-MS.

Treatment	S_{BET} (m^2/g)	Titration		XPS		TGA-MS	
		Acid site /nm^2	O atoms/nm^2	O/C at/at	O atoms/nm^2	Weight loss (%)	O atoms/nm^2
KOH, 0.5 h HNO_3	156	1.0 ± 0.1	2.0 ± 0.2	-	-	4.0	8.3 ± 0.6
KOH, 2 h HNO_3	186	1.4 ± 0.1	2.8 ± 0.2	0.069	9.6 ± 1.4	5.7	9.8 ± 0.8
KOH, 2 h HNO_3, N_2 973 K	172	~0.03 ± 0.003	~0.06 ± 0.006	0.017	2.3 ± 0.3	1.8	3.0 ± 0.3

An explanation for this discrepancy could be found in the assumption that oxygen atoms are not exclusively present at the surface, but also are built in in the subsurface (2-3 nm) graphene sheets [18,39]. TGA-MS was used to establish the number of thermally removable oxygen atoms from the surface and the bulk of the activated CNF. When all oxygen atoms were considered to be located at the surface a concentration was found of 8.3 and 9.8 atoms/nm^2 after oxidation in HNO_3 for respectively 0.5 and 2 h. After treatment at 973 K this concentration drops to 3.0 O atoms /nm^2. The number of oxygen atoms as determined using XPS and TGA-MS is comparable when the error margins are taken into account. From these results and from earlier work [40] it is concluded that after treatment at 973 K oxygen is not present throughout the carbon support, but is mainly located in the outer 2-3 nm of the fibers. These results also show that upon treatment at 973 K in N_2 some very thermostable non-acidic groups remain, whereas acidic groups are hardly detected. For a more detailed investigation on the effects of oxidation of CNF we refer to [40] and to Chapter 3.

The number of acidic groups of the CNF treated in HNO_3 for 2 h could give rise to a ruthenium loading of at most 4.2 wt% using ion exchange, when it is assumed that the metal precursor species use one site for adsorption and no polymeric ruthenium species are present. With these assumptions for platinum it should be possible to obtain a loading of maximally 8.2 wt%.

Synthesis and characterization of the Pt/CNF catalysts

For the synthesis of CNF-supported platinum catalysts (intake 5 wt%) we started with the HDP method, utilizing $Pt(NH_3)_4(NO_3)_2$ as the precursor salt and activated CNF (2 h HNO_3) (PtCNF). From the TPR results of the dried PtCNF a reduction temperature of 473 K could be derived. A number of PtCNF catalysts were prepared in this way. The actual metal loading of these catalysts after reduction, determined using both ICP and XRF, turned out to be in the range 3.4-4.3 wt% (Table 1).

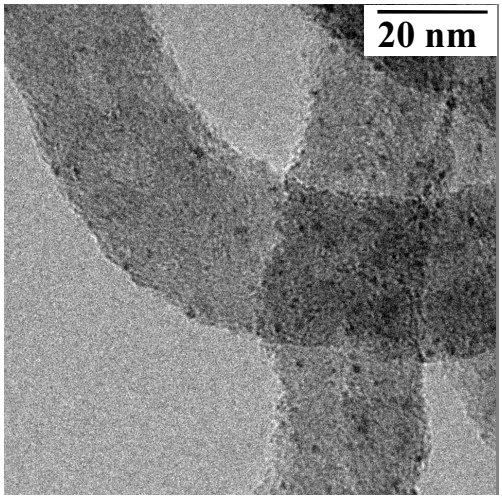

Figure 1. TEM image of PtCNF after reduction at 473 K.

In Figure 1 a TEM image of the PtCNF catalyst after drying and reduction at 473K is displayed. Platinum particle sizes are in the range 1-2 nm. The dispersion calculated from hydrogen chemisorption is 0.79, indicating platinum particles with an average size of 1.4 nm.

The final loading of PtCNF was considerably below the intake loading of 5 wt%. Using the number of acidic oxygen groups available (1.4 groups/nm^2) we calculated a loading of 8.2 wt% based on a one-to-one exchange, so a loading of 5 wt% should have been feasible. To verify this

result we also prepared a catalyst *via* the HDP method with an increased intake platinum loading of 10 wt% (PtCNF-10). The final platinum loading of PtCNF-10 was found by XRF analysis to be only 4.8 wt% (Table 1). In Figure 2 a TEM image of PtCNF-10 after reduction at 473 K is shown. In this catalyst platinum is well dispersed over the surface of the CNF, particles in the narrow range 1-2 nm are observed. These results show that with the HDP method using $Pt(NH_3)_4(NO_3)_2$ as the precursor salt small and homogeneously distributed platinum particles can be obtained. However, the attained metal loading is smaller than the calculated one-to-one adsorption loading for both ion exchange and the HDP method. This can be due to the low platinum concentrations (~10^{-3} M) used throughout this work leading to incomplete exchange. Another reason for this difference could be found in a platinum/site ratio of 0.5. In this case a platinum loading of 4.1 wt% as a maximum can be expected, which is close to the loadings found for these catalysts.

To gain more insight in the relation between the metal loading and the number of adsorption sites on the support, experiments were performed in which platinum was applied *via* the HDP method on differently activated and pretreated CNF. We compared the results obtained with this method with the characteristics of CNF-supported platinum catalysts prepared by ion exchange.

The effect of the number of oxygen-containing groups was investigated through samples PtCNF and PtCNF-A to PtCNF-D. PtCNF is prepared from CNF oxidized in HNO_3 for 2 h, while CNF in PtCNF-A and -B are only treated for 0.5 and 1 h respectively. From earlier work and from Table 2 it is known that a shorter oxidation time yields less (acidic) oxygen-containing groups [40]. The CNF used for the preparation of PtCNF-C are treated in HCl instead of in HNO_3, implying that no surface oxides have been introduced. For the synthesis of PtCNF-D, CNF are applied that are oxidized in HNO_3 for 2 h and are subsequently treated in N_2 at 973 K for 2 h to remove acidic oxygen-containing groups. The final platinum loadings of the various CNF-supported catalysts were determined with XRF (Table 1).

The effect of the number of acidic oxygen-containing surface groups (oxidation time) on the metal loading can be derived from Table 1. For PtCNF-A and –B platinum loadings of 2.7 respectively 3.6 wt% were found. PtCNF-C does not contain a significant amount of platinum and the loading of PtCNF-D is very small (0.5 wt%).

In Figure 3 the metal loading is plotted versus the number of acidic oxygen-containing groups on the CNF surface. This figure shows that as a first approximation a linear

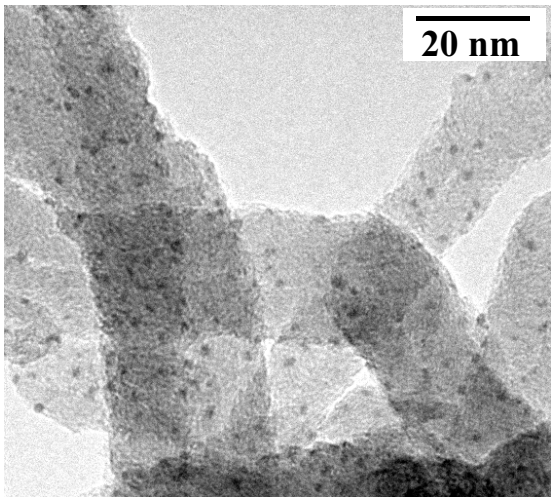

Figure 2. TEM image of PtCNF-10 after reduction at 473 K.

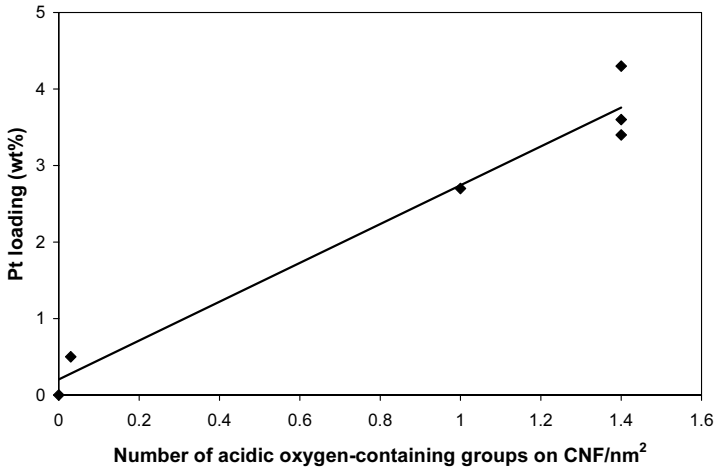

Figure 3. Relationship between number of acidic oxygen-containing surface groups on CNF support and the Pt loading of the catalyst.

correlation exists between the number of acid sites and the amount of platinum that can be deposited on the CNF using the HDP method. Therefore we conclude that the acidic oxygen groups on the CNF surface are not only necessary to increase the wettability using aqueous precursor solutions but also for the anchoring of the metal precursor.

TEM was used to investigate the average platinum particle size and the size distribution on the CNF support. For PtCNF-C and –D no platinum particles could be detected. TEM images of PtCNF-A (not-shown) and –B (Figure 4) demonstrate that in both catalysts, like we found with PtCNF (Figure 1), very small platinum particles (1-2 nm) are present well distributed over the CNF surface.

A remarkable finding is that HDP and ion exchange (performed at 293 and 363 K (PtCNF-IE-293/363)) gave different results with respect to the attainable loading. The loadings of these catalysts as determined with XRF analysis can be found in Table 1. The platinum loading of the catalysts prepared using ion exchange at 293 and 363 K is 1.4 and 1.8 wt% respectively, which is substantially smaller than 3.4-4.3 wt% found for the PtCNF catalysts prepared by the HDP method. This difference in loading will be discussed later on

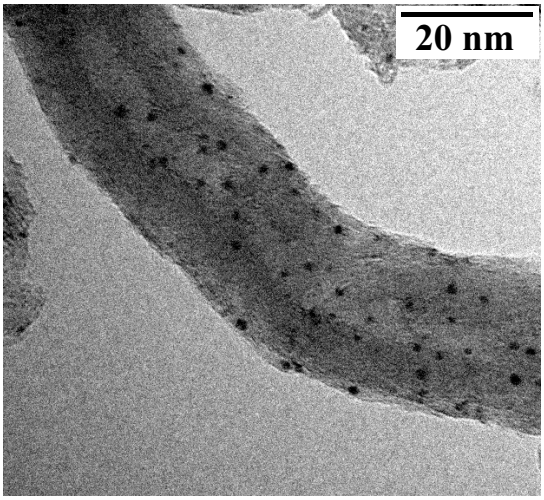

Figure 4. TEM image of PtCNF-B after reduction at 473 K.

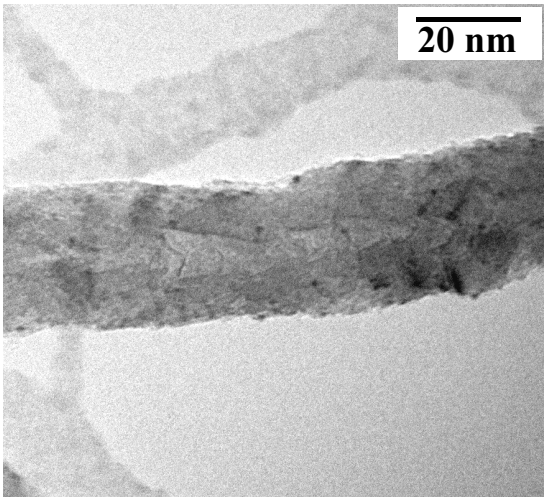

Figure 5. TEM image of PtCNF-IE-293 after reduction at 473 K.

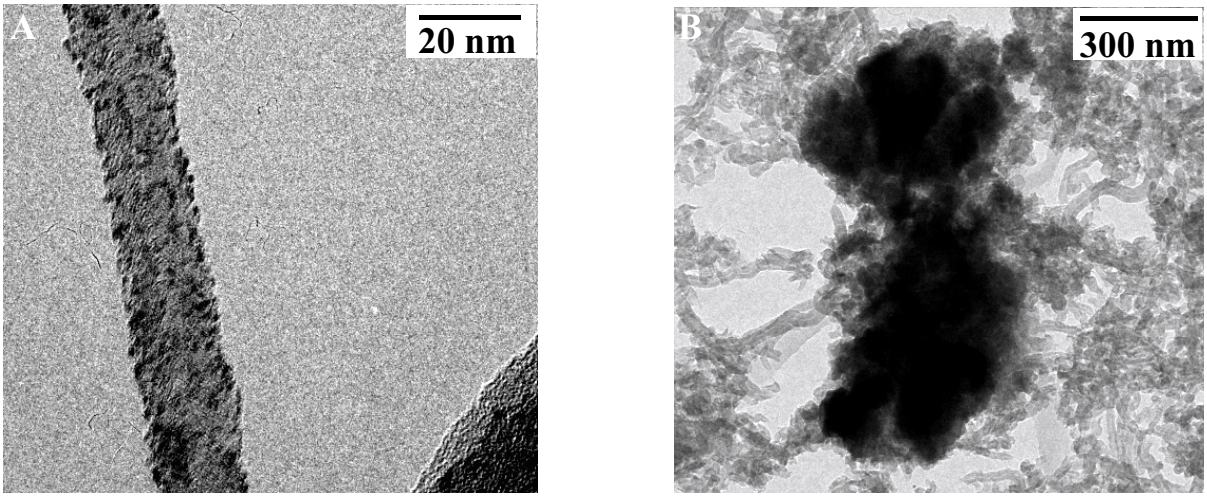

Figure 6. TEM images of dried RuCNFCl (5 wt%) prepared from rutheniumchloride using HDP.

together with the somewhat higher loading of the catalyst prepared by ion exchange at 363K. In Figure 5 a TEM image of PtCNF-IE-293 is shown. From this image it is clear that the platinum loading is indeed much lower than that of the catalysts prepared *via* the HDP method. From the TEM images a particle size distribution of 1-2 nm for PtCNF-IE-293 and of 1-4 nm for PtCNF-IE-363 was obtained. The average platinum particle sizes calculated from H_2-chemisorption are 0.8 and 1.5 nm respectively.

Synthesis and characterization of the Ru/CNF catalysts

We briefly investigated the HDP method for the preparation of CNF-supported ruthenium catalysts. Ruthenium (intake 5 wt%) was deposited on the fibers using two ruthenium precursors, *viz.* $RuCl_3$ and $RuNO(NO_3)_3(H_2O)_2$. In the majority of the studies reported in literature on the preparation of ruthenium-supported catalysts rutheniumchloride has been utilized as the precursor compound. Firstly, we explored the preparation of CNF supported ruthenium catalysts using this precursor salt (RuCNFCl). A catalyst with a relatively small average particle size of 3 nm was obtained, as can be seen in Figure 6A. SEM (not shown) and TEM images of the dried catalyst, however, revealed the presence of large lumps of ruthenium oxide next to the support (Figure 6B).

Apparently commercial ruthenium chloride is not a suitable precursor, since it may contain, as reported in the literature [41], as much as 80% Ru(IV) which is only soluble at a very low pH. We speculate that these Ru(IV) species precipitate and RuO_2 is formed next to the support, ultimately resulting in the large ruthenium lumps.

Secondly, $RuNO(NO_3)_3(H_2O)_2$ was used as precursor salt for the synthesis (RuCNF). TPR results showed that the CNF-supported ruthenium precursor was completely reduced at 473 K. Therefore this temperature was chosen as reduction temperature for the Ru/CNF catalysts. The metal loading of the Ru/CNF catalysts as established with ICP coincides with the intake ruthenium loading of 5 wt%. In Figure 7 two representative TEM images of

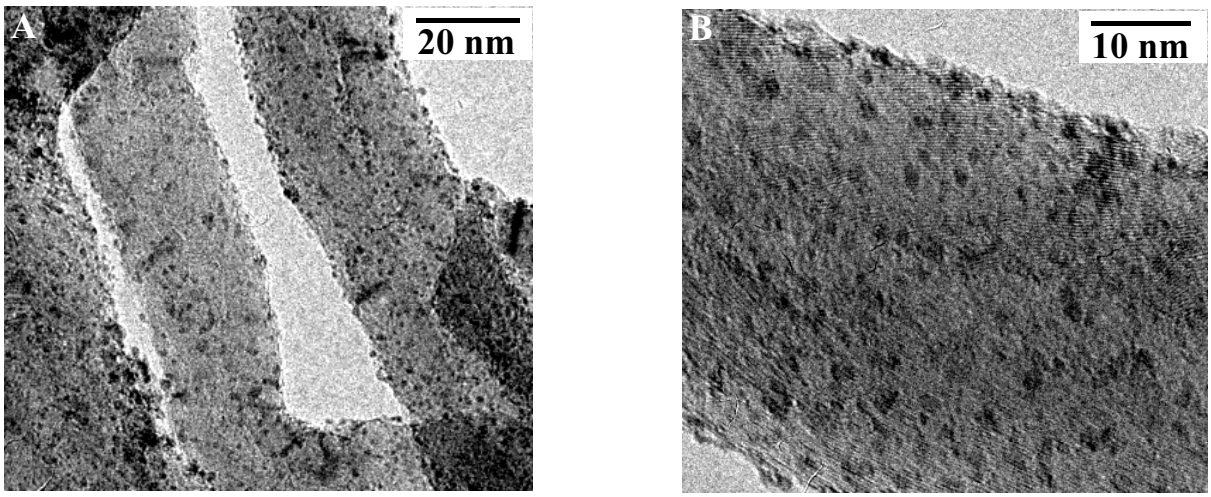

Figure 7. TEM images (A & B) of RuCNF (5 wt%) prepared from rutheniumnitrosylnitrate using HDP after reduction at 473 K.

RuCNF after reduction are shown. The ruthenium particles appear as dark dots on the fiber surface. In Figure 7B, at higher magnification, even the fishbone structure of the CNF is visible. The images show a homogeneous coverage with small ruthenium particles and no large ruthenium particles were observed. The ruthenium particle size distribution is very narrow; a size range of 1.1-2.2 nm has been established with an average particle size of 1.5 nm. The metal dispersion calculated from hydrogen chemisorption is 0.74, corresponding to ruthenium particles with an average size of 1.8 nm. The reproducibility of the HDP procedure using $RuNO(NO_3)_3(H_2O)_2$ was checked several times and always homogeneously distributed ruthenium particles were found in the 1-2 nm range.

Thermostability of RuCNF and PtCNF

To examine the stability of the catalysts (RuCNF and PtCNF) prepared by the HDP method, the reduced catalysts were treated in nitrogen at elevated temperatures. After this

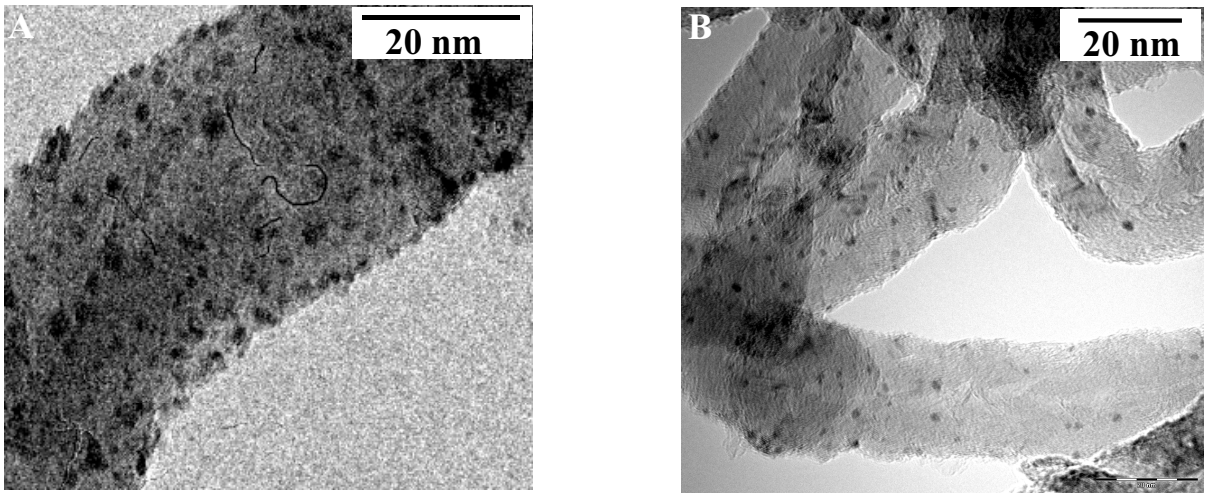

Figure 8. TEM images of A) RuCNF973 and B) PtCNF973 after reduction and subsequent heat treatment in N_2 at 973K.

Table 3. Dispersions and average particles sizes of PtCNF and RuCNF treated after reduction at 573, 773 and 973 K in N_2 for 2 h.

Sample	**TEM**	**H_2-chemisorption**	
	d (nm)	H_{total}/M	d (nm)
PtCNF	1-2	0.79	1.4
PtCNF573	1-2	1.06	1.1
PtCNF773	1-2	0.74	1.5
PtCNF973	1-3	0.49	2.3
RuCNF	1.5 ± 0.2	0.74	1.8
RuCNF573	n.d.	0.70	1.9
RuCNF773	2.2 ± 0.6	0.64	2.1
RuCNF973	1.8 ± 0.7	0.44	3.0

treatment the catalysts were characterized with TEM and hydrogen chemisorption. In Figure 8A and B TEM images of RuCNF973 and PtCNF973 are presented. Both the ruthenium and the platinum particle sizes remain (almost) unaltered after treatment up to 773 K. After treatment at 973K the particles have become slightly larger, however still also many small particles are present. Some sintering caused broadening of the particle size distribution and a small increase in the average particle size. The dispersions and the average particle sizes calculated from the hydrogen chemisorption data are listed in Table 3. These values are in close agreement with the estimated TEM values. This demonstrates the surprisingly strong bond between the CNF support and the metal particles. In literature it is well established that when activated CNF are heated in inert atmosphere, carboxyl and anhydride groups are already decomposed at temperatures beyond 473 K [17,18,40]. However, it is important to note that still non-acidic oxygen groups remain. The thermostability of these groups is rather high: decomposition under inert atmosphere starts at circa 873 K [17,18,40]. We speculate that these groups are key to stabilize the metal particles and prevent their sintering even at a temperature as high as 973 K.

Metal precursor / adsorption site ratio

Aim of this study was, next to the synthesis of highly dispersed and thermostable platinum and ruthenium on CNF catalysts, to find a relation between metal loading and the number of surface groups on CNF. For both preparation procedures we succeeded in the first aim. No inhomogeneities, as sometimes reported in the literature for porous oxidic support bodies [2,3], were found using ion exchange. However, we cannot exclude that at higher metal precursor concentrations results of the methods will differ. We speculate that using the HDP method, due to the controlled way of making adsorption sites available, a more homogeneous distribution can be obtained than with ion exchange.

The relation between the amount of platinum metal that could be deposited and the number of adsorption sites is less unequivocal. That such a relation exists is likely from Figure 3 in which a linear relationship is demonstrated between the number of acidic sites and the platinum loading. What still has to be explained is the difference in loading between the catalysts prepared by ion exchange and the HDP method. Factors that can influence the ultimate loading are amongst others the number and nature of the adsorption sites, the pH of the solution and the concentration and speciation of the metal precursor. These parameters will be discussed below.

In the literature concentrations of the metal precursor employed for ion exchange are usually in the range 10^{-1}-10^{-3} M [29,42-45]. In our work rather diluted precursor solution were utilized, especially for the preparation of the platinum catalysts (~10^{-3} M platinum and ~10^{-2} M ruthenium). When adsorption is reversible, low concentrations as used could have resulted in an incomplete utilization of the adsorption sites. However, this should hold not only for the ion exchange procedure but also for the HDP method if adsorption is not followed by nucleation and growth.

For PtCNF and RuCNF, catalysts prepared by the HDP method, the number of metal precursor molecules per nm^2 is 0.7 and 1.6, respectively. According to the Revised Physical Adsorption (RPA) model developed by Regalbuto *et al.* involving purely physical interactions also a maximum platinum loading can be derived [46]. Using $Pt(NH_3)_4^{2+}$ the expected maximum adsorption density would be 0.5 platinum precursor molecules/nm^2 based on a maximum coverage of a closed packed layer of $Pt(NH_3)_4^{2+}$ ions with two hydration shells. The adsorption density found for PtCNF is, taking into account the roughness of the estimations, in rather good agreement with the value predicted by the RPA model.

We also stated that the speciation of the metal precursor could affect the metal loading. For $Pt(NH_3)_4^{2+}$ no indication was found in the literature that hydrolysis or polymerization of the precursor can occur, so probably this precursor retains its 2+ charge irrespective the pH and needs as a consequence two neighboring adsorption sites as is often reported for oxidic supports [2,43]. Although the average active site density on CNF is relatively low, *i.e.* ~1.4 sites/nm^2, due to their presumable inhomogeneous distribution two-to-one adsorption might be possible. That this two-to-one adsorption is not to be excluded is emphasized by the fact that a Pt/acid site ratio of around 0.5 is found using HDP. Apparently, growth of the nuclei on the support by the formation of platinumhydroxide or some hydroxy compound does not occur, which is probably due to the high stability of the $Pt(NH_3)_4^{2+}$ complex. Precipitation of platinumhydroxide has never been observed in our experiments, not withstanding the low solubility product of $Pt(OH)_2$ (~10^{-33} mol^3/l^3) calculated from the relevant reduction potentials.

On the speciation of $[RuNO(NO_3)_3(H_2O)_2]$, on the other hand, somewhat more information can be found in the literature. Hydrolysis of this precursor in aqueous solutions is reported, resulting in species like $[RuNO(NO_3)_2(H_2O)_3]^+$ [47]. For RuCNF a Ru/acid site

ratio of circa 1.2 can be calculated, which ratio is close to the ratio expected for one-to-one adsorption.

To our judgment there is one, is it, speculative explanation for the deviating platinum loadings achieved with ion exchange and the HDP procedure. Ion exchange is performed at constant pH (~6) while when using the HDP method the support is exposed to an acidic environment for a long period of time during the procedure. We speculate that due to this treatment more adsorption sites become available, possibly by hydrolysis of carboxylic anhydrides. In the literature it is shown that during oxidative activation of CNF carboxyl groups are formed that upon removal of water during drying can be converted into carboxylic anhydride groups [18,31,48-51]. Hydrolysis of these anhydrides is an activated process: anhydrides are fairly stable, especially around neutral pH [52-54]. Since both with titration and with the HDP method a low starting pH is used, it is possible that in this environment more anhydrides are hydrolyzed to carboxylic groups than with ion exchange performed at a constant pH of around 6. Because this hydrolysis process is activated this might also explain the slightly higher loading found with PtCNF-IE-363 than with PtCNF-IE-293.

Conclusions

Carbon nanofiber (CNF)-supported platinum catalysts were prepared by an HDP method as well as by ion exchange. Using diluted precursor solutions with both techniques small uniform thermally stable platinum particles (1-2 nm) were obtained homogeneously distributed over the CNF. The HDP method, however, resulted in significantly higher platinum loadings than ion exchange. This difference could originate from the creation of additional adsorption sites in the acidic environment at which HDP is started, due to the hydrolysis of anhydridic carboxyl groups formed during drying of the activated CNF. With the HDP method also CNF-supported ruthenium catalysts were prepared successfully. We consider that the HDP method used for the preparation of CNF-supported platinum catalysts is an ion exchange procedure, in which in a controlled manner the acid sites slowly become available at increasing pH during the synthesis resulting in a high dispersion.

For HDP a linear relationship was found between the number of acidic oxygen groups on the CNF support and the obtained platinum loading. For the highest loaded catalyst a platinum/adsorption site ratio of 0.5 was established, corresponding to about 0.7 $Pt(NH_3)_4^{2+}$ molecules/nm^2. It is concluded that the acidic oxygen-containing groups do not only increase the wettability, but also function as anchoring sites of the metal precursor during the preparation. We suggest that the non-acidic oxygen groups avoid sintering of the metal particles, resulting in the high thermostability.

References

1. R. Schlögl, M. Che, O. Clause and C. Marchilly, Preparation of Solid Catalysts, Wiley VCH, Weinhein, (1999) Chapter 3 and 4.
2. J.W. Geus and J.A.R. van Veen, Stud. Surf. Sci. Catal. 123 (1999) 459.
3. J.W. Geus and P.B. Wells, Appl. Catal. 18 (1985) 231.
4. W.A. Spieker and J.R. Regalbuto, Chem. Eng. Sci. 56 (2001) 3491.
5. J.R. Regalbuto, M. Schrier, X. Hao, W.A.Spieker, J.G. Kim, J.T. Miller and A.J. Kropf, Stud. Surf. Sci. Catal. 143 (2002) 45.
6. J.-F. Lambert and M. Che, J. Mol. Catal. A Chem. 162 (2000) 5.
7. C. Lepetit and M. Che, J. Mol. Catal. A Chem. 100 (1995) 147.
8. A.J. van Dillen, J.W. Geus, L.A.M. Hermans and J. van der Meijden, J. Proc. 6th Int. Congr. Catal., 2 (1977) 677.
9. L.A.M. Hermans and J.W. Geus, Stud. Surf. Sci. Catal. 3 (1979) 113.
10. K.P. de Jong, Stud. Surf. Sci. Catal. 63 (1991) 19.
11. P. Burattin, M. Che and C. Louis, J. Phys. Chem. B 101 (1997) 7060.
12. P. Burattin, M. Che and C. Louis, J. Phys. Chem. B 102 (1998) 2722.
13. J.H. Bitter, M.K. van der Lee, A.G.T. Slotboom, A.J. van Dillen and K.P. de Jong, Catal. Lett. 89 (2003) 139.
14. K.P. de Jong and J.W. Geus, Catal. Rev. Sci. Eng. 42 (2000) 481.
15. F. Rodriguez-Reinoso, Carbon 36 (1998) 159.
16. R.J.J. Jansen, Ph.D. thesis, Delft University (1994).
17. H.P. Boehm, Adv. Catal. 16 (1966) 179.
18. T.G. Ros, A.J. van Dillen, J.W. Geus and D.C. Koningsberger, Chem. Eur. J. 8 (2002) 1151.
19. M.S. Hoogenraad, Ph.D. thesis, Utrecht University (1995).
20. A.B. Garcia, A. Cuesta, M.A. Montes-Moran, A. Martinez-Alonso and J.M.D. Tascon, J. Colloid Interface Sci. 192 (1997) 363.
21. Y.-H. Li, S. Wang, Z. Luan, J. Ding, C. Xu and D. Wu, Carbon 41 (2003) 1057.
22. A. Bismarck, C. Wuertz and J. Springer, Carbon 37 (1999) 1019.
23. J.P. Brunelle, Pure & Appl. Chem. 50 (1978) 1211.
24. Z. Zhou, S. Wang, W. Zhou, G. Wang, L. Jiang, W. Li, S. Song, J. Liu, G. Sun and Q. Xin, Chem. Comm. (2003) 394.
25. B. Yang, Q. Lu, Y. Wang, L. Zhuang, J. Lu, P. Liu, J. Wang and R. Wang, Chem. Mater. 15 (2003) 3552.
26. W. Li, C. Liang, W. Zhou, J. Qiu, Z. Zhou, G. Sun and Q. Xin, J. Phys. Chem. B 107 (2003) 6292.
27. C.A. Bessel, K. Laubernds, N.M. Rodriguez and R.T.K. Baker, J. Phys. Chem. B 105 (2001) 1115.
28. W.X. Chen, J.Y. Lee and Z. Liu, Chem. Comm. (2002) 2588.

29. M.A. Fraga, E. Jordão, M.J. Mendes, M.M.A. Freitas, J.L. Faria and J.L. Figueiredo, J. Catal. 209 (2002) 355.
30. C. Prado-Burguete, A. Linares-Solano, F. Rodriguez-Reinoso and C. Salinas-Martinez de Lecea, J. Catal. 128 (1991) 397.
31. A.E. Aksoylu, M. Madalena, A. Freitas, M. Fernando, R. Pereira and J.L. Figueiredo, Carbon 39 (2001) 175.
32. A.M. Fuente, G. Pulgar, F. Gonzalez, C. Pesquera and C. Blanco, Appl. Catal. A Gen. 208 (2001) 35.
33. L.B. Okhlopkova, A.S. Lisitsyn, V.A. Likholobov, M. Gurrath and H.P. Boehm, Appl. Catal. A Gen. 204 (2000) 229.
34. S.R. de Miguel, O.A. Scelza, M.C. Roman-Martinez, C. Salinas-Martinez de Lecea, D. Cazorla-Amoros and A. Linares-Solano, Appl. Catal. A Gen. 170 (1998) 93.
35. M.C. Roman-Martonez, D. Cazorla-Amoros, A. Linares-Solano, C. Salinas-Martinez-de Lecea, H. Yamashita and M. Anpo, Carbon 33 (1995) 3.
36. M.L. Toebes, J.H. Bitter, A.J. van Dillen and K.P. de Jong, Catal. Today, 76 (2002) 33 / Chapter 2 of this thesis.
37. J.J.F. Scholten, A.P. Pijpers and A.M.L. Hustings, Catal. Rev.-Sci. Eng. 27 (1985) 151.
38. O.L.J. Gijzeman, unpublished results.
39. H. He, J. Klinowski, M. Fortser and A. Lerf, Chem. Phys Lett. 287 (1998) 53.
40. M.L. Toebes, J.M.P. van Heeswijk, J.H. Bitter, A.J. van Dillen and K.P. de Jong, Carbon, in print / Chapter 3 of this thesis.
41. D.T. Sawyer, R.S. Gearge and J.B. Bagger, J. Am. Chem. Soc. 81 (1959) 5893.
42. G.C. Bond and P.B. Wells, Appl. Catal. 18 (1985) 225.
43. A. Goquet, M. Aouine, F.J. Cadete Santos Aires, A. De Mallmann, D. Schweich and J.P. Candy, J. Catal. 209 (2002) 135.
44. W.A. Spieker, J. Liu, J.T. Miller, A.J. Kropf and J.R. Regalbuto, Appl. Catal. A Gen. 232 (2002) 219.
45. E. Theodoridou, A.D Jannakoudakis, P.D. Jannakoudakis, N. Pagalos, J.O. Besenhard, C.I. Donner and M. Wicher, Electrochimica Acta 38 (1993) 793.
46. N. Santhanam, T.A. Conforti, W. Spieker and J.R. Regalbuto, Catal. Today 21 (1994) 141.
47. J.M. Fletcher, I.L. Jenkins, F.M. Lever, F.S. Martin, A.R. Powell and R. Todd, J. Inorg. Nucl. Chem. 1 (1955) 378.
48. H.P. Boehm, Carbon 40 (2002) 145.
49. M. Domingo-Garcia, F.J. Lopez Garzon and M.J. Perez-Mendoza, J. Colloid Interface Sci. 248 (2002) 116.
50. S. Haydar, C. Moreno-Castilla, M.A. Ferro-Garcia, F. Carrasco-Marin, J. Rivera-Utrilla, A. Perrard and J.P.Joly, Carbon 38 (2000) 1297.
51. J.M. Rosenfeld and C.B. Murphy, Talanta 14 (1967) 91.

52. S.P. Asprey, B.W. Wojciechowski, N.M. Rice and A. Dorcas, Chem. Eng. Sci. 51 (1996) 4681.
53. W. Liu and H.K. Lee, J. Chrom. A 805 (1998) 109.
54. A.V. Ferreira, H.J. van der Merwe and S.C. Slippers, Small Ruminant Res. 22 (1996) 79.

6

Influence of Oxygen-Containing Surface Groups on the Activity and Selectivity of Carbon Nanofiber-Supported Ruthenium Catalysts in the Hydrogenation of Cinnamaldehyde

Abstract

Carbon nanofiber-supported ruthenium catalysts were employed to study the influence of oxygen-containing surface groups on the catalytic performance in the liquid-phase hydrogenation of cinnamaldehyde. The carbon nanofibers were oxidized to introduce oxygen-containing groups and the metal precursor was applied using homogeneous deposition precipitation. After reduction the catalysts were heat-treated in nitrogen at different temperatures to tune the amount of surface oxygen functional groups. TEM and chemisorption studies showed the presence of a narrow and stable particle-size distribution (1-2 nm) even after heat treatment at 973 K. The overall specific activity increases by a factor of 22 after treatment at 973 K, which is related to the decreasing number of oxygen-containing groups. The cinnamyl alcohol selectivity decreases from 48% to 8% due to enhanced rate of hydrocinnamaldehyde production with increasing heat treatment. This unambiguously demonstrates the metal-support interaction, which involves support surface-oxygen functionalities that affect the metal activity and selectivity. The precise nature of this interaction has yet to be elucidated.

Introduction

Using the hydrogenation of cinnamaldehyde to cinnamyl alcohol as a test reaction we investigated the influence of the concentration of oxygen-containing surface groups on the activity and selectivity of carbon nanofiber (CNF)-supported ruthenium catalysts.

Catalytic hydrogenation of α,β-unsaturated aldehydes to their corresponding alcohols is attractive both for economical and scientific reasons [1-4]. Although hydrogenation of the C=C bond is thermodynamically more favorable, attempts have been made to enhance the selective hydrogenation of the C=O bond. With ruthenium as the active metal, high selectivities are attained only if titania and carbon, notably graphitic carbon, are used as support materials [1,3,5-7]. For example, in the liquid-phase hydrogenation of cinnamaldehyde with carbon nanotube-supported ruthenium catalysts [7-9] selectivities to cinnamyl alcohol up to 92% are observed, whereas alumina-supported ruthenium catalysts [6] give rise to selectivities of 20-30% and active carbon-supported ruthenium catalysts [10] to 30-40%. Often the increased selectivity to the unsaturated alcohol is explained in terms of a transfer of the π-electrons from the graphitic planes to the metal particles [7,8,11]. In this way the charge density on the metal increases, thus decreasing the probability for the C=C bond activation.

Although this explanation might be true, it is important to realize that at least two other factors direct the selectivity of carbon-supported catalysts too, namely the metal particle size and the presence of oxygen-containing surface groups. It is well established that the cinnamyl alcohol selectivity increases with increasing particle size and that this effect is particularly pronounced with particles larger than 3 nm [3]. Colomna *et al.* [12,13] emphasized the importance of oxygen-containing surface groups on carbon supports. In their study on the gas-phase hydrogenation of crotonaldehyde over platinum on activated carbon catalysts, they found an increased selectivity to the alcohol with a larger amount of oxygen-containing groups on the carbon surface. Later on, Bachiller-Baeza *et al.* [14] disputed the influence of the oxygen groups on the hydrogenation of crotonaldehyde over graphite-supported platinum and ruthenium catalysts. However, in both studies relatively large particles in the range of 3-10 nm were used and the particle sizes of the samples with different concentrations of oxygen-containing surface groups were different.

The above demonstrates, that more insight in the role of the oxygen-containing surface groups on the catalytic performance of carbon-supported catalysts can only be gained if a well-defined catalyst system is available. This requires a well-defined carbon support without contaminants and micropores, metal particles smaller than 3 nm with a narrow particle size distribution and a tunable number of surface oxygenates. Because of the importance of the features of the catalyst, we will report in detail on its preparation and characterization.

The catalyst system includes CNF of the fishbone type as the graphitic support material, activated by surface oxidation, and the homogeneous deposition precipitation (HDP)

technique is used to apply the metal precursor phase. Small-diameter CNF (10-50 nm) can be grown from decomposition of carbon-containing gases (CH_4, CO, C_2H_2) on small metal particles of similar sizes [15,16]. They have a relatively large and accessible external surface area (100 - 200 m^2/g), a well-defined graphitic structure, do not contain impurities, and are mechanically strong and chemically inert [15,16]. The fibers themselves contain no pores, but because they interweave during growth, larger mesoporous skeins are obtained. The hydrophobic and inert nature of the graphitic CNF brings along a problem: the application and anchoring of the catalytically active phase. However, the surface can be modified by treatment of the CNF in concentrated nitric acid. In this way oxygen-containing surface groups are introduced, enabling the anchoring of the active phase or its precursor and obtaining the wettable surface necessary for the aqueous solution of the metal precursor [17-20]. Moreover, concurrently, exposed nickel is extracted. The number of oxygen-containing groups on the CNF surface can be tuned by treatment in inert atmosphere at various temperatures, which (partly) removes the surface groups.

Several investigators have already demonstrated the great potential of CNF and related materials as support material. Metals such as Pt [21,22], Pd [15,23-25], Pt/Ru [26,27], Ru [8,28-30], Fe [31,32], Co [33] and Ni [34-38] have been applied on CNF and tested in various reactions, such as selective hydrogenations. In literature diverse methods have been presented to apply the active phase, mostly incipient wetness impregnation [23,30,33,37], but also adsorption [8], ion exchange [15] and electroless plating [38]. Unfortunately, it appears that these procedures do not result in both a relatively high dispersion and a narrow particle-size distribution. With ion exchange, for example, Hoogenraad *et al.* [15,25] applied palladium on CNF and found a maximum metal loading of 3 wt%. Using adsorption, Planeix *et al.* [8] applied 0.2 wt% ruthenium on carbon nanotubes, resulting in relatively large ruthenium particles in the range of 3-7 nm. Also when nickel, with a loading of 5 wt%, is deposited on CNF through incipient wetness impregnation substantially larger particles are found, in the range of 2-22 nm with an average of 8.1 nm [36]. We therefore explored the HDP technique as developed by Geus *et al.* and Che *et al.*, which is very successful in the production of highly loaded and well-dispersed catalysts on oxidic support materials [40-43].

In this paper we will demonstrate that the CNF-supported ruthenium catalysts thus prepared fulfill the formulated requirements of a well-defined catalyst system, which enables systematic study of the influence of oxygen-containing surface groups on activity and selectivity in the liquid-phase hydrogenation of cinnamaldehyde.

Experimental

Carbon nanofiber growth

For the growth of CNF, 20 wt% Ni/SiO_2 was prepared by homogeneous deposition precipitation (HDP) as described by van Dillen *et al.* [40] using silica (Degussa, Aerosil 200), nickel nitrate (Acros), and urea (Acros). After filtering, the catalyst precursor was dried at 393 K and calcined in static air at 873 K (heating rate 5 K/min) for 2 h.

One gram of the Ni-catalyst precursor was placed in a quartz reactor. Prior to the fiber growth the Ni-catalyst was reduced *in situ* for 2 h in a flowing stream of a mixture of H_2 (80 ml/min) and N_2 (320 ml/min) at 1 bar and 973 K (heating rate 5 K/min). Next, the CNF were grown at 823 K in a mixture of CO (80 ml/min), H_2 (28 ml/min), and Ar (292 ml/min) for 24 h.

The CNF were refluxed for 1 h in a 1 M KOH solution in order to remove the silica support. For the activation of the CNF and the removal of nickel, the CNF were refluxed in concentrated nitric acid for 2 h and washed thoroughly with demi-water.

Synthesis of carbon nanofiber-supported ruthenium catalyst

Ruthenium (5 wt%) was deposited on the fibers according to the HDP method. To an acidified suspension (pH=0.5) of 5 g CNF in 250 ml demi-water heated up to 363 K, 1.56 g urea (Acros) and 0.82 g (5 wt%) $RuNO(NO_3)_3.nH_2O$ (Acros) were added under vigorous stirring. The pH of the slurry was monitored, to follow the process and indicate its completeness. After 6 h the loaded CNF were filtered and washed thoroughly with demi-water, dried at 393 K, and reduced in H_2 at 473 K for 1 h (rate 5 K/min). Following reduction, the samples were exposed to air. In line with extensive experience in our lab [20], under ambient conditions further oxidation of the (graphite) CNF surface does not take place.

In order to introduce different concentrations of oxygen-containing groups on the CNF surface, samples of the freshly reduced catalyst were heat-treated in a nitrogen atmosphere for 2 h at 573, 773 and 973K, to remove (part of) the oxygen-containing groups. The catalyst samples together with their identification codes are listed in Table 1.

Table 1. Sample codes and treatment conditions of the various carbon nanofiber-supported ruthenium catalysts.

Sample name	Loading (wt %)	Gas-phase prereduction	Heat treatment in N_2
RuCNFnp[a]	5.0	-	-
RuCNF	5.0	473 K	-
RuCNF573	5.0	473 K	573 K
RuCNF773	5.0	473 K	773 K
RuCNF973	5.0	473 K	973 K

[a] np = no prereduction in the gas-phase

Catalyst and carbon nanofiber characterization

The numbers of acid sites of the oxidized CNF after the various heat-treatments were determined performing standard acid-base titrations. For this purpose 20-40 mg of oxidized CNF was stirred with 25 ml of a solution containing 0.1 M NaCl and 0.1 mM oxalic acid in demi-water, acidified to pH = 3 with HCl. While stirring, pure nitrogen was bubbled through the slurry and 10 mM NaOH was added dropwise from a buret until the endpoint had been reached. All acid sites with a $pK_a < 7.5$ were measured.

The CNF and the CNF-supported ruthenium catalysts were examined in a Philips CM-200 FEG TEM operated at 200 kV. Samples were prepared by suspending the fibers in ethanol under ultrasonic vibration. Some drops of the thus produced suspension were brought onto a holey carbon film on a copper grid.

TPR measurements were performed with a TPDRO 1100 instrument from Thermo Quest CE Instruments.

Specific surface areas (BET) were calculated from nitrogen physisorption data measured at 77K with a Micromeritics ASAP 2400 apparatus. Prior to the physisorption experiments the samples were evacuated at 473 K for at least 16 h. Ruthenium loadings were determined using inductively coupled plasma emission spectrometry on a Vista AZ CCD simultaneous ICP-AES.

XPS analyses were performed on a Quantum 2000 Scanning SK Microprobe instrument using Al Kα radiation. Before the analysis all samples were reduced again in hydrogen at 383 K (heating rate 4 K/min) for 30 minutes. Semi-quantitative data were calculated from the survey scans. The narrow scan data were used to determine the oxidation state and/or compounds for the Ru and C peaks. This was accomplished from a Gauss-Lorenzian peak fit of the appropriate photoelectron peaks.

Hydrogen chemisorption measurements were performed using a Micromeritics ASAP 2010C. Before the chemisorption measurements, each sample was dried in He at 393 K for 1 h, and reduced in flowing H_2 (50 ml/min STP) at 473 K for 2 h, heating rate 5K/min. After reduction the catalyst was degassed for 2 h at 0.1 Pa at the reduction temperature in order to eliminate chemisorbed hydrogen and water. The isotherms were measured at 308 K. The H/Ru ratios are based on the amounts adsorbed at zero pressure, found by extrapolation of the linear part of the isotherm. Calculations are made either with the total amount of adsorbed hydrogen or with the amount of strongly adsorbed hydrogen. Estimated average particle sizes and dispersions are based on spherical geometry and an adsorption stoichiometry of $H/Ru_s = 1$. The average Ru particle size, d, was calculated from:

$$d * D = 10^{21} \frac{M * 6 * \rho_{site}}{\rho_{metal} * N}$$

where d is the ruthenium particle size (nm), D is the dispersion, M is the molecular weight

(Ru = 101 g/mol), ρ_{site} is the ruthenium surface site density (16.3 Ru atoms/nm^2), ρ_{metal} is the metal density (Ru 12.3 g/cm^3) and N is the Avogadro number (6.022*10^{23} mol^{-1}) giving d=1.33/D (nm) [44].

Catalytic experiments

Hydrogenation of cinnamaldehyde was studied in batch-mode in a 200 ml autoclave equipped with a stirrer, a sample port, a reagent injection port, gas inlet and a vent. The sample tube was equipped with a filter at its end to prevent carry-over of catalyst particles while sampling.

The prereduced and heat-treated catalysts (0.5 - 1 g) were reactivated in *iso*-propanol (100 ml) at 383 K and 4.5 MPa H_2 pressure for 30 min in the autoclave (1250 rpm) prior to the introduction of cinnamaldehyde (~9 g). All the reactions were conducted under the above conditions. Micro samples were withdrawn periodically and analyzed on a gas chromatograph (Hewlett Packard 6890 Series with autosampler) using an HP5Cpsil8 capillary column (30 m x 0.32 mm). The calibration was done by using synthetic mixtures of pure compounds in *iso*-propanol. Methylbenzoate was used as internal standard.

The experimental cinnamaldehyde concentration versus time data are approximated by a rate law that is first order with respect to the reactant. Accordingly, catalytic activities are compared on the basis of the first-order rate constant from a regression fit of the experimental data in the expression:

$$\ln\left\{\frac{[CALD]_t}{[CALD]_0}\right\} = -kt$$

where $[CALD]_t$ = the cinnamaldehyde concentration at time t and $[CALD]_0$ = the cinnamaldehyde concentration at the beginning of the reaction.

Results

Characterization of the carbon nanofiber support

The CNF were of the fishbone type, *i.e.* with the graphite planes oriented at an angle to the central axis. After removal of the growth catalyst and the activation treatment with nitric acid the non-microporous fibers exhibited a surface area of 177 m^2/g. In Figure 1 an SEM image of an untreated CNF sample is shown. Clearly the mesoporous structure of the CNF skeins is visible. The lighter spots in the image, situated on top of the fibers, are nickel particles from which the fibers had been grown. X-ray diffraction and TEM images demonstrated that the graphitic structure had not been affected during activation. From SEM and TEM micrographs an average fiber diameter of 25 nm could be derived with a narrow diameter distribution.

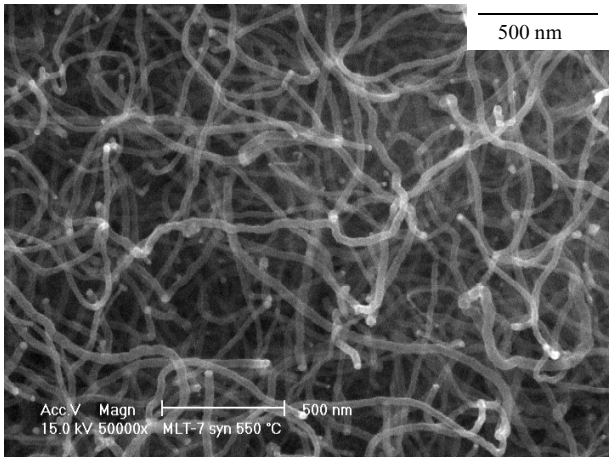

Figure 1. SEM image of untreated carbon nanofibers.

As stated earlier, the activation procedure in nitric acid is carried out to introduce various types of oxygen functional groups on the CNF and to remove non-encapsulated nickel from the growth catalyst. The remaining nickel (≤ 0.5 wt%, XRF analysis) is shown from TEM to be encapsulated by graphitic envelopes thus preventing interference in catalysis.

Table 2 lists the number of acid sites ($pK_a < 7.5$) of oxidized CNF treated at different temperatures, as determined by titration. Activation of the CNF resulted, after drying at 393 K, in 1.38 acid sites/nm^2 and heat treatment indeed in removal of part of the oxygen-containing groups: after treatment at 573 K 0.96 acid sites/nm^2 were present and after treatment at 773 K and 973 K only 0.20, respectively 0.03, acid sites/nm^2 remained.

Characterization of the carbon nanofiber-supported ruthenium catalysts

The metal loading of the Ru/CNF catalysts as established with ICP corresponded to the intended ruthenium loading of 5 wt%. TPR results (not shown) of the fresh catalyst demonstrated that the catalysts were completely reduced at 473 K. Therefore, all catalysts were reduced at this temperature. RuCNFnp was only reduced *in situ* at 383 K in the liquid-phase before the catalytic experiments to maintain a larger fraction of the oxygen-containing surface group on the catalyst. With XPS we checked the oxidation state of the reduced and heat-treated catalysts. In Table 3 the ruthenium $3p_{3/2}$ and $3d_{5/2}$ binding energies determined using Gauss-Lorenzian peak fits are displayed. The results showed that RuCNF, RuCNF573,

Table 2. Number of acid sites on CNF surface as a function of heat treatment temperature determined with acid-base titration.

Sample name	Number of acid site/nm^2
oxidized CNF	1.38
oxidized CNF - 573 K in N_2	0.96
oxidized CNF - 773 K in N_2	0.20
oxidized CNF - 973 K in N_2	~0.03

Table 3. Ruthenium $3p_{3/2}$ and $3d_{5/2}$ binding energies of the carbon nanofiber-supported ruthenium catalysts determined by XPS using Gauss-Lorenzian peak fits.

Sample name	Treatment in XPS	E_b (eV)	
		Ru $3p_{3/2}$	Ru $3d_{5/2}$
RuCNFnp	none	465	283.8
RuCNFnp	red 383 K	463.2	281.1
RuCNF	red 383 K	462.4	280.8
RuCNF573	red 383 K	462.1	280.9
RuCNF773	red 383 K	462.3	280.9
RuCNF973	red 383 K	462.8	281.1

RuCNF773 and RuCNF973 all show the same binding energy, indicating similar oxidation states for all samples. Only RuCNFnp is slightly shifted to higher binding energies. RuCNFnp is probably less reduced because some ionic Ru species might be present because of the mild reduction treatment.

In Figure 2a and b two representative TEM images of reduced RuCNF are shown. The ruthenium particles appear as dark dots on the surface of the CNF. The images show homogeneous coverage with small ruthenium particles. In Figure 2b the fishbone orientation of the graphitic planes is also visible. The ruthenium particle size distribution is very narrow. A range of 1.1-2.2 nm has been established with an average particle size of 1.5 nm. Using the HDP method we have prepared several CNF-supported ruthenium catalysts and the results convincingly demonstrate the reproducibility of the preparation method.

After heat treatment in inert atmosphere the catalysts are also characterized with TEM. In Figure 3a and b TEM images of RuCNF773 and RuCNF973 are displayed. The ruthenium particles are slightly larger after heat treatment, but many very small particles are still present too. Some sintering causes broadening of the particle size distribution and a small increase in the average particle size. The average particle sizes calculated from the TEM images are

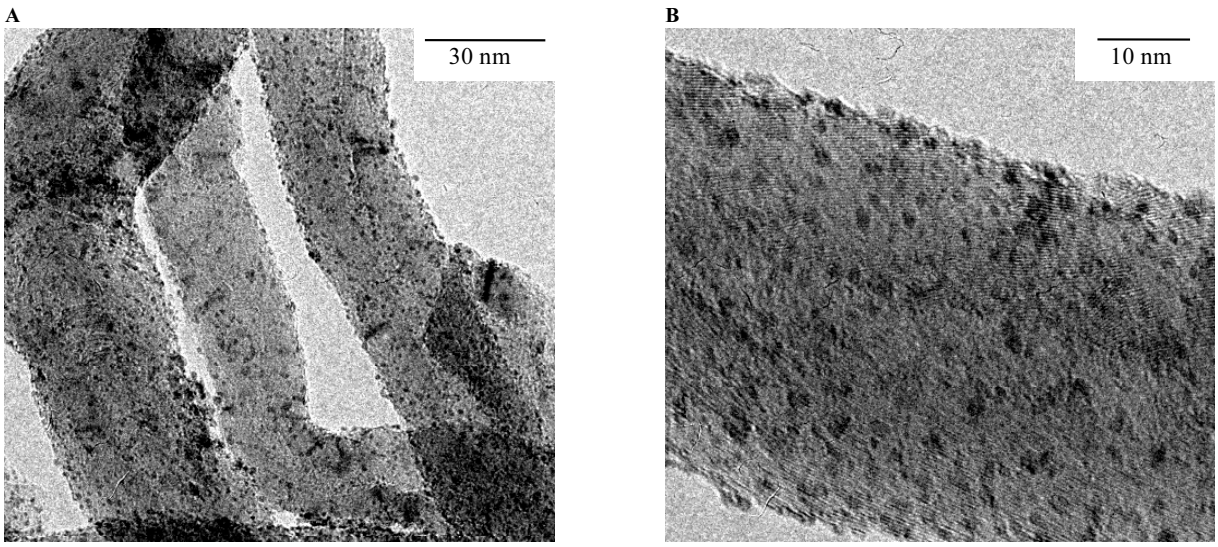

Figure 2. TEM images (A & B) of 5 wt% carbon nanofiber-supported ruthenium catalysts after reduction.

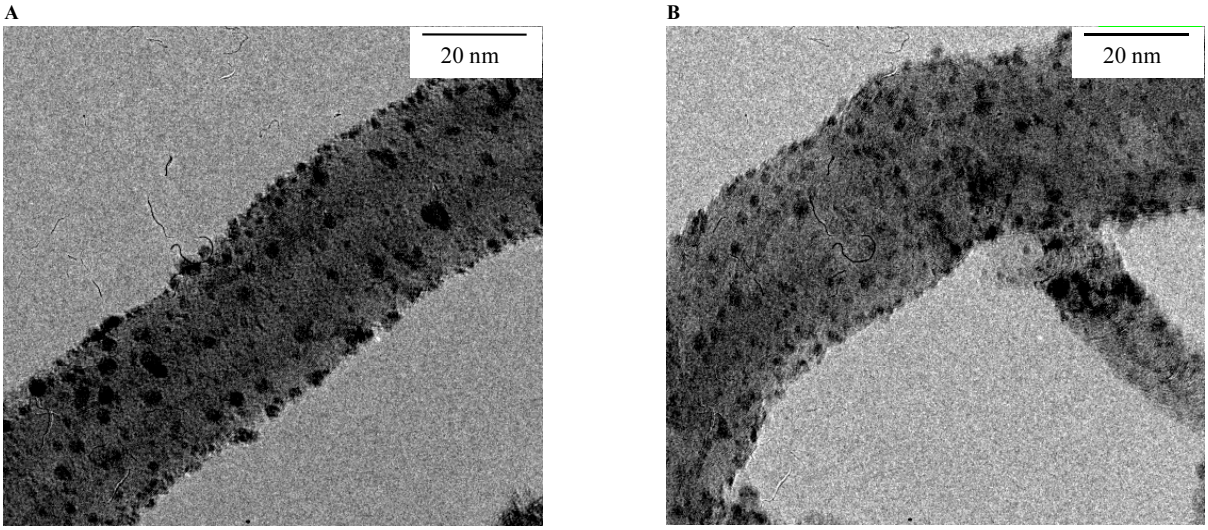

Figure 3. TEM images of 5 wt% carbon nanofiber-supported ruthenium catalysts after reduction and heat treatment in N_2 at (A) 773K and (B) 973K.

Table 4. TEM and hydrogen chemisorption results on the different carbon nanofiber-supported ruthenium catalysts.

Sample	**TEM**	**H_2-chemisorption**			
		irreversible		total	
	d (nm)	H/Ru	d (nm)	H/Ru	d (nm)
RuCNF	1.5 ± 0.2	0.40	3.4	0.74	1.8
RuCNF573	n.d.	0.45	3.0	0.70	1.9
RuCNF773	2.2 ± 0.6	0.38	3.5	0.64	2.1
RuCNF973	1.8 ± 0.7	0.25	5.3	0.44	3.0

n.d. = not determined

presented in Table 4, along with the average particle sizes calculated from the hydrogen chemisorption data. These last values are in close agreement with the estimated TEM values if the total amount of adsorbed hydrogen is used for the calculations. Also, hydrogen chemisorption shows a small decrease in H/Ru ratio for the catalysts heat-treated under inert atmosphere.

Hydrogenation of cinnamaldehyde

The hydrogenation of cinnamaldehyde can be presented by a simplified reaction pathway, as shown in Figure 4. Additionally, various side-reactions can occur. For instance, in this study in some cases 3-propoxy-1-propenyl-benzene is formed (Table 6). This product forms *via* the reaction between β-methylstyrene, a hydrogenolysis product of cinnamyl alcohol, and the solvent *iso*-propanol.

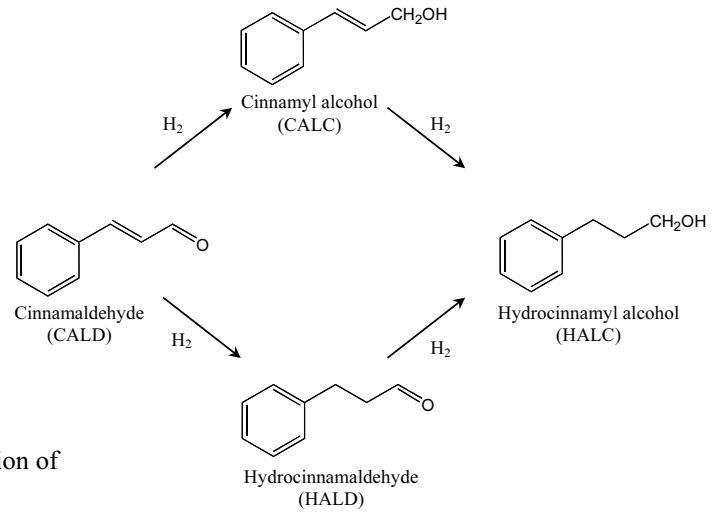

Figure 4. Reaction pathway of the hydrogenation of cinnamaldehyde.

The reproducibility of the catalytic experiments and the absence of gas-liquid diffusion limitations were checked by varying the amount of catalyst used for the catalytic measurements. In Figure 5 the decrease in reactant concentration (mole %) is displayed versus time for 0.5 and 1 g of RuCNF773 and in the small inserted graph the first order rate constants are plotted versus catalyst weight. A linear relation is observed between the amount of catalyst and the volume-based rate constant, demonstrating the reliability of the catalytic tests.

Figure 6 shows product distributions obtained with RuCNF and RuCNF973. For reasons of clarity only the amounts of cinnamaldehyde (CALD) and the primary reaction products hydrocinnamaldehyde (HALD) and cinnamyl alcohol (CALC) are plotted. An exponential decrease in the cinnamaldehyde concentration is observed as a function of time with a concurrent increase in the concentrations of the reaction products. This shows that the reaction is first order with respect to cinnamaldehyde. In Table 5 the calculated rate constants, the relative rate constants compared to the measured rate with RuCNFnp, and the TOF values are given. From Figure 6 and Table 5 the large difference in catalytic performance as a function of treatment temperature is distinct. A significant increase in total activity is

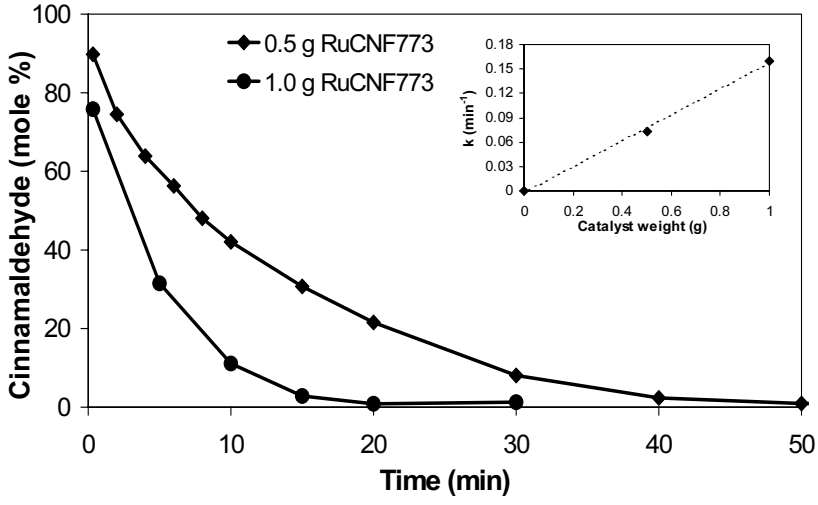

Figure 5. Catalytic activity of RuCNF773 for cinnnamaldehyde hydrogenation; effect of the catalyst amount.

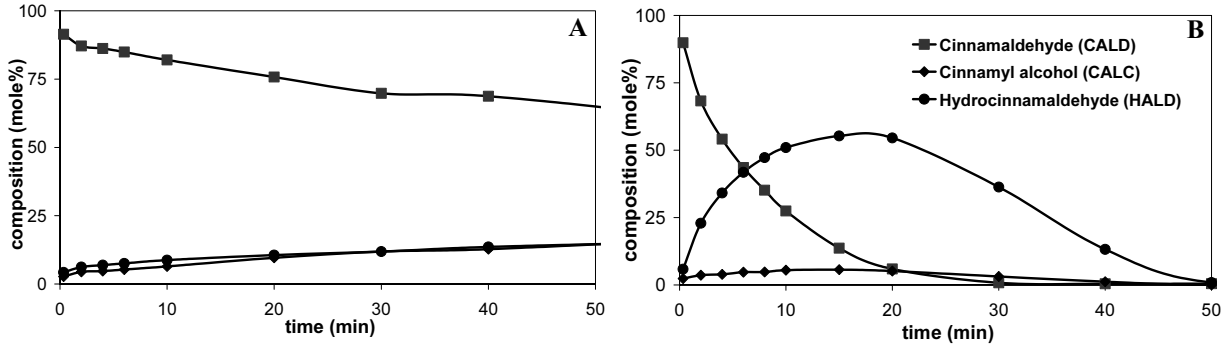

Figure 6. Cinnamaldehyde conversion and product distribution as a function of time on stream obtained at 383K and 4.5 MPa hydrogen over carbon nanofiber-supported ruthenium catalysts (A) RuCNFnp and (B) RuCNF973.

observed with increasing treatment temperature of the CNF-supported ruthenium catalysts. The activity is enhanced by a factor of 22 when the treatment temperature is increased from 383 K, the reduction temperature of RuCNFnp, to 973 K (RuCNF973). The same trend is noticed with the TOF values. This increase in activity can mainly be ascribed to a large increase in aldehyde (HALD) formation, as can be seen in Figure 7. The activity for cinnamyl alcohol formation increases only slightly as a function of the catalyst treatment temperature. Apparently, hydrogenation of the C=C bond is enhanced when less oxygen-containing groups are present on the surface.

The selectivities for the different reaction products at 60% conversion are represented in Table 6. From this table it is clear that not only the activity but also the selectivity highly depends on the pretreatment temperature of the Ru/CNF catalysts. RuCNFnp gives a S_{HALD} of 34% and a S_{CALC} of 48%. At higher treatment temperatures S_{CALC} drops and S_{HALD} increases. RuCNF973 is very selective to hydrocinnamaldehyde with S_{HALD} > 70%. This large change in selectivity is mainly caused by the increased activity for C=C hydrogenation.

Table 5. Activity for cinnamaldehyde hydrogenation with carbon nanofiber-supported ruthenium catalysts, calculated from the time needed to obtain 60% conversion.

Sample name	Rate constant (min^{-1})	Rel. rate constant[b]	TOF (s^{-1})[a]
RuCNFnp	$6.2 * 10^{-3}$	1.0	n.d.
RuCNF	$8.2 * 10^{-3}$	1.3	0.03
RuCNF573	$1.7 * 10^{-2}$	2.7	0.08
RuCNF773	$7.4 * 10^{-2}$	12	0.31
RuCNF973	$1.4 * 10^{-1}$	22	0.83

[a] Results are given in mole CALD hydrogenated per mole of ruthenium surface atoms in the catalyst per second. The number of ruthenium surface atoms is calculated from the catalyst weight, the metal loading and the H/Ru (total H) ratio.

[b] Relative rate constant is the rate constant divided by the rate constant of RuCNFnp.

n.d. Not determined because the H/Ru ratio is not known for this sample.

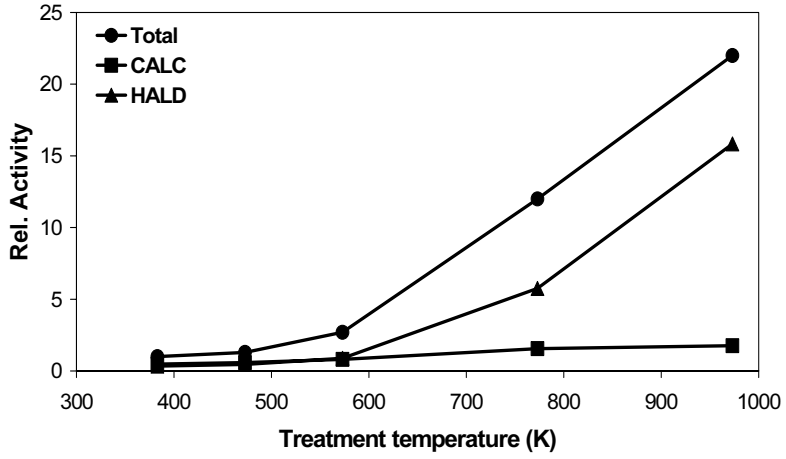

Figure 7. Relative activity for CALD hydrogenation (●), for production of CALC (■), and for production of HALD (▲) after different pretreatment temperatures of Ru/CNF.

Discussion

Aim of our study was to reveal the effect of oxygen-containing surface groups of CNF-supported ruthenium catalysts on the catalytic performance in the selective hydrogenation of cinnamaldehyde. From literature it is known that, to be able to discriminate the effect of the surface groups from the effect of the particle size of the active metal, it is necessary to use a catalyst with a narrow and constant size distribution and a high dispersion with, preferably, a mean particle size < 3 nm [3]. The presented results demonstrate that we, using the HDP procedure, succeeded in the design of such a catalyst with a mean size in the range of 1-2 nm.

The CNF used for this study are entirely graphitic and very uniform as shown in the SEM images in Figure 1. By treatment in boiling nitric acid, oxygen-containing surface groups were introduced, while the graphitic character of the CNF was maintained. It turned out that the number of oxygen-containing surface groups could be tuned by treatment in nitrogen at different temperatures, as was established with titration experiments (Table 2).

Table 6. Selectivity to cinnamyl alcohol (CALC), hydrocinnamaldehyde (HALD), hydrocinnamyl alcohol (HALC) and a byproduct for cinnamaldehyde hydrogenation with carbon nanofiber-supported ruthenium catalysts (determined at 60% conversion).

Sample name	Products			Byproduct
	S_{CALC} (%)	S_{HALD} (%)	S_{HALC} (%)	3-propoxy-1-propenyl benzene
RuCNFnp	48	34	18	-
RuCNF	43	33	16	8
RuCNF573	30	33	14	23
RuCNF773	13	48	13	26
RuCNF973	8	73	12	7

Using ion exchange the number of acidic groups of the freshly activated fibers could have given rise, taking 1.38 groups/nm^2, to a ruthenium loading of at most 3-4 wt%, which is close to the experimental results of Hoogenraad *et al.*[15,25]. For this calculation we assumed one ruthenium-precursor molecule per acidic site. These authors used ion exchange to apply palladium on CNF and found a metal loading of around 3 wt% at most. This implies that an alternative method had to be used to obtain a 5 wt% CNF supported ruthenium catalyst.

We applied the HDP technique to deposit ruthenium on the oxidized CNF. TEM images (Figure 2 and 3) and chemisorption data (Table 4) demonstrate that with this technique reproducibly highly dispersed catalysts with narrow particle size distributions could be prepared. In the procedure the precipitating agent, in this case hydroxyl ions, is introduced slowly and homogeneously *via* urea hydrolysis at 363K. Production and consumption of hydroxyl ions is balanced in such a way that nucleation of the ruthenium-precursor in the liquid-phase is avoided and exclusively is anchored to the support. Under these conditions oxidic support materials form a surface compound [40-43]. On carbon supports no surface compounds are formed [39] and probably the interaction is confined to that of the precursor ions with a relatively low number of surface sites. However, the results clearly show the applicability of the HDP technique to the preparation of CNF supported metal catalyst.

When the average particle sizes calculated from TEM images and derived from H_2-chemisorption are compared (Table 4) it appears that the particle sizes based on the total amount of adsorbed hydrogen correspond best to the TEM results. In literature often only the strongly adsorbed hydrogen is taken to calculate the dispersion, but XAFS results of Oudenhuijzen *et al.* with Pt/Al_2O_3 catalysts unambiguously show the presence of a Pt-H antibonding state for both weakly and strongly bonded hydrogen [45]. This demonstrates that with this type of metals weakly bonded hydrogen is also chemisorbed to the metal particles and should be taken into account for the determination of the dispersion and the mean particle size.

Upon heating under inert atmosphere some sintering occurs (Table 4). The average particle sizes become slightly larger after heating at 973 K and the particle size distributions somewhat broader. Nevertheless the sintering is very limited, taking into account the treatment temperatures up to 973 K. This demonstrates the very high thermostability of the catalysts and the surprisingly strong bond between the CNF support and the ruthenium metal particles. The exact nature of the metal-support interaction is not yet clear.

It is well established that when oxygen-containing groups on a carbon support are heated under inert atmosphere, carboxyl groups are already decomposed at temperatures beyond 473 K [19,20]. However, the largest influence on the catalytic performance is expected from oxygen groups other than carboxylic groups that are still present and are in direct contact with the ruthenium particles. The titration results presented in Table 2 also show that simply by heating at different temperatures CNF can be obtained with a varying and well-defined number of acidic oxygen-containing surface groups, enabling our study on the effect of these groups on catalysis. It is important to note that upon activation of CNF, besides oxygen-

containing groups on the surface, ether-type oxygen groups are also formed in between the graphitic layers [20]. The thermostability of these groups is rather high: decomposition under inert atmosphere starts at circa 873 K. These groups are not probed with titration, but they can also have an influence on the catalytic system.

In the hydrogenation of cinnamaldehyde large differences are found between the differently pretreated catalysts in the activity and the selectivity. The total activity strongly increases with increasing treatment temperature of the Ru/CNF catalysts (Table 5). This large increase in activity is mainly caused by a rise in the activity for the hydrogenation of the C=C bond, yielding hydrocinnamaldehyde, while the activity for the hydrogenation of the carbonyl bond increases only slightly (Figure 7). Consequently, the selectivity for cinnamylalcohol drops and the hydrocinnamaldehyde selectivity rise with increasing pretreatment temperature.

From TPR and XPS results it appears that RuCNF, RuCNF573, RuCNF773 and RuCNF973 are completely reduced. Very small numbers of ionic ruthenium species can still be present in these samples, but their occurrence is not obvious from the XPS data. RuCNFnp can still contain larger amounts of ionic ruthenium; however, the largest changes in activity and selectivity are found for the samples treated at higher temperature, meaning that a variance in oxidation state most likely does not bring about the observed effects.

Also, a particle size effect cannot account for the observed changes in selectivity. The ruthenium particle sizes of the catalysts hardly differ, notably not with RuCNFnp, RuCNF, RuCNF573 and RuCNF773, and all catalysts have particles < 3nm (Table 6). Besides, it is well established that the cinnamyl alcohol selectivity increases with increasing ruthenium particle size and this effect is particularly pronounced with ruthenium particles larger than 3 nm [3]. Here, the trend is opposite. We therefore conclude that, because the particle size effect has to be excluded, the change in catalytic performance is related to the difference in the concentration of oxygen-containing surface groups.

The best illustration to this is given in Figure 8, in which the relative total activity for cinnamaldehyde hydrogenation is plotted versus the amount of acidic surface groups/nm^2 present on the CNF surface. Because determination of the oxygen-containing groups of the Ru/CNF catalysts themselves could not be effectuated because of disturbance of the titration experiments by the ruthenium phase, we have taken in this figure as second-best choice the values found with the freshly activated CNF support. A nice correlation is observed between the activity and the acidity of the support. When only few acidic groups are present the activity is high and with increasing surface acidity the activity drops. This correlation is not a direct cause-and-effect relation. Besides the acidic groups also other oxygen-containing surface groups are present on the CNF surface. But the measured shift in activity gives a strong indication that the amount of oxygen incorporated in the CNF plays an important role in the catalytic performance.

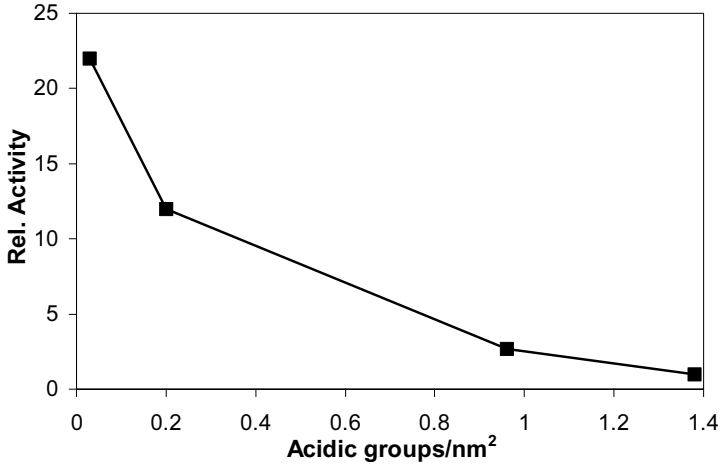

Figure 8. Relative total activity for cinnamaldehyde hydrogena-tion as a function of the amount of acidic groups/nm^2 on the bare carbon nanofiber surface.

The most current explanation for the effect of the oxygen-containing surface groups on the catalytic performance is the effect of the polarity of the CNF support. At increasing treatment temperatures, the CNF surface changes gradually from polar to non-polar due to the removal of the oxygen-containing surface groups. This change in polarity can change the preferential adsorption mode of cinnamaldehyde and, thus, a shift in selectivity. English *et al.* [46] found an enhanced selectivity to crotonalcohol for Pt/TiO_2 after high-temperature reduction due to an increased polarity at the metal surface. This increased polarity was caused by a decoration of titania suboxides (TiO_x) of the surface of the Pt crystallites that act as relatively strong electron pair acceptor sites for the free electron pairs at the oxygen of the carbonyl group. Thus, the increased polarity leads to an activation of the C=O bond of crotonaldehyde and enhances the rate of C=O bond hydrogenation. This model cannot fully explain our results with respect to the hydrogenation of cinnamaldehyde. Although it accounts for the shifts in selectivity, it does not clarify the significant increase in the hydrogenation rate of C=C bond and the slight increase in C=O bond hydrogenation with decreasing polarity.

An alternative explanation implies the influence of the oxygen-containing groups present on the CNF surface on the electronic state of ruthenium. This model is based on the work of Koningsberger *et al.* and concerns metal-oxidic support interaction [47-49]. These authors state that, due to the effect of the support, the density of states (DOS) and thereby the Fermi level of the metal particles shifts to a higher binding energy with decreasing electron density of the support oxygen atoms. For the here studied CNF-supported ruthenium catalysts this model suggests that lower amounts of (more electronegative) oxygen in the carbon support would give rise to lowering of the DOS of the metal. This could result in stronger bonding between the metal and the reactant, thereby enhancing its rate of hydrogenation.

At the moment we cannot conclude which explanation holds or if a combination of the two effects causes the changes in activity and selectivity. Further studies using XPS, EXAFS, XANES are in progress to further clarify the influence of the oxygen-containing groups on the hydrogenation of cinnamaldehyde over metal CNF catalysts.

Conclusions

Using homogeneous deposition precipitation, carbon nanofiber-supported ruthenium catalysts were prepared with a narrow and constant size distribution, a high dispersion and a mean particle size < 3 nm. By treatment of carbon nanofibers in nitric acid and, subsequently, heat treatment under nitrogen atmosphere, the number of oxygen-containing groups on the carbon nanofiber surface was tuned.

A clear trend was observed in activity and selectivity in the liquid-phase hydrogenation of cinnamaldehyde with a decreasing number of oxygen-containing surface groups. The rate of cinnamaldehyde conversion was enhanced with a factor of 22 after removal of the oxygen groups. This enhanced activity is mainly caused by a strong increase in hydrogenation rate of the C=C bond, while only a slightly increased C=O bond hydrogenation occurs. Due to this a large shift in selectivity towards hydrocinnamaldehyde was observed. This unambiguously demonstrates the important influence of the surface-oxygen functionalities on the catalytic performance. The exact mechanism of this influence is currently under investigation.

References

1. P. Kluson and L. Cerveny, Appl. Catal. A Gen.128 (1995) 13.
2. V. Ponec, Appl. Catal. A Gen. 149 (1997) 27.
3. B. Coq and F. Figueras, Coord. Chem. Rev. 178-180 (1998) 1753.
4. P. Gallezot and D. Richard, Catal. Rev.-Sci. Eng. 40 (1998) 81.
5. A. Giroir-Fendler, D. Richard and P. Gallezot, Stud. Surf. Sci. Catal. 41 (1988) 171.
6. B. Coq, P.S. Kumbhar, C. Moreau, P. Moreau and M.G. Warawdekar, J. Mol. Catal. 85 (1993) 215.
7. P.S. Kumbhar, B. Coq, C. Moreau, P. Moreau, J.M. Planeix and M.G. Warawdekar, Catalysis: Modern Trends, Narosa Publishing House, New Delhi (1995).
8. J.M. Planeix, N. Coustel, B. Coq, V. Brotons, P.S. Kumbhar, R. Dutartre, P. Geneste, P. Bernier and P.M. Ajayan, J. Am. Chem. Soc. 116 (1994) 7935.
9. M. Lashdaf, A. Hase, E. Kauppinen and A.O.I. Krause, Catal. Lett. 52 (1998) 199.
10. S. Galvagno, G. Capanelli, G. Neri, A. Donato and R. Pietropaolo, J. Mol. Catal. 64 (1991) 237.
11. T. Vergunst, F. Kapteijn and J.A. Moulijn, Catal. Today 66 (2001) 381.
12. F. Coloma, A. Sepúlveda-Escribano and F. Rodríguez-Reinoso, Appl. Catal. A Gen. 123 (1995) L1.
13. F. Coloma, A. Sepúlveda-Escribano, J.L.G. Fierro and F. Rodríguez-Reinoso, Appl. Catal. A Gen. 150 (1997) 165.

14. B. Bachiller-Baeza, A. Guerrero-Ruiz and I. Rodríguez-Ramos, Appl. Catal. A Gen. 192 (2000) 289.
15. M.S. Hoogenraad, Ph.D. thesis, Utrecht University (1995).
16. K.P. de Jong and J.W. Geus, Catal. Rev.-Sci. Eng. 42 (2000) 482.
17. F. Rodriguez-Reinoso, Carbon 36 (1998) 159.
18. R.J.J. Jansen, Ph.D. thesis, Delft University (1994).
19. H.P. Boehm, Adv. Catal. 16 (1966) 179.
20. T.G. Ros, A.J. van Dillen, J.W. Geus and D.C. Koningsberger, Chem. Eur. J. 8 (2002) 1151.
21. R.T.K. Baker, K. Laubernds, A. Wootsch and Z. Paál, J. Catal. 193 (2000) 165.
22. C.A. Bessel, K. Laubernds, N.M. Rodriguez and R.T.K. Baker, J. Phys. Chem. B 105 (2001) 1115.
23. C. Pham-Huu, N. Keller, L.J. Charbonniere, R. Ziessel and M.J. Ledoux, Chem. Commun. (2000) 1871.
24. C. Pham-Huu, N. Keller, G. Ehret, L.J. Charbonniere, R. Ziessel and M.J. Ledoux, J. Mol. Catal. A Chem. 170 (2001) 155.
25. M.S. Hoogenraad, R.A.G.M.M. van Leeuwarden, G.J.B. van Breda Vriesman, A. Broersma, A.J. van Dillen and J.W. Geus, Stud. Surf. Sci. Catal. 91 (1995) 263.
26. E.S. Steigerwalt, G.A. Deluga, D.E. Cliffel and C.M. Lukehart, J. Phys. Chem. B 105 (2001) 8097.
27. S. Hermans, J. Sloan, D.S. Shephard, B.F.G. Johnson and M.L.H. Green, Chem. Commun. (2002) 276.
28. B. Coq, J.M. Planeix and V. Brotons, Appl. Catal. A Gen. 173 (1998) 175.
29. T. Braun, M. Wohlers, T. Belz, G. Nowitzke, G. Wortmann, Y. Uchida, N. Pfänder and R. Schlögl, Catal. Lett. 43 (1997) 167.
30. M. Lashdaf, A. Hase, E. Kauppinen and A.O.I. Krause, Catal. Lett. 52 (1998) 199.
31. N.M. Rodriguez, M.-S. Kim and R.T.K. Baker, J. Phys. Chem. 98 (1994) 13108.
32. E. van Steen and F.F. Prinsloo, Catal. Today 71 (2002) 327.
33. Z.-J. Liu, Z.-Y. Yuan, W. Zhou, L.-M. Peng and Z. Xu, Phys. Chem. Chem. Phys. 3 (2001) 2518.
34. S.K. Shaikhutdinov, L.B. Avdeeva, B.N. Novgorodov, V.I. Zaikovskii and D.I. Kochubey, Catal. Lett. 47 (1997) 35.
35. F. Salman, C. Park and R.T.K. Baker, Catal. Today 53 (1999) 385.
36. A. Chambers, T. Nemes, N.M. Rodriguez and R.T.K. Baker, J. Phys. Chem. B 102 (1998) 2251.
37. C. Park and R.T.K. Baker, J. Phys. Chem. B 102 (1998) 5168
38. L.M. Ang, T.S.A. Hor, G.Q. Xu, C.H. Tung, S.P. Zhao and J.L.S. Wang, Carbon 38 (2000) 363.

39. B.L. Mojet, M.S. Hoogeraad, A.J. van Dillen, J.W. Geus and D.C. Koningsberger, J. Chem. Soc., Faraday Trans 93 (1997) 4371
40. A.J. van Dillen, J.W. Geus, L.A.M. Hermans and J. van der Meijden, Stud. Surf. Sci. Catal. 2 (1977) 677.
41. L.A.M. Hermans and J.W. Geus, Stud. Surf. Sci. Catal. 3 (1979) 113.
42. P. Burattin, M. Che and C. Louis, J. Phys. Chem. B 101 (1997) 7060.
43. P. Burattin, M. Che and C. Louis, J. Phys. Chem. B 102 (1998) 2722.
44. J.J.F. Scholten, A.P. Pijpers and A.M.L. Hustings, Catal. Rev.-Sci. Eng. 27 (1985) 151.
45. M.K. Oudenhuijzen, J.H. Bitter and D.C. Koningsberger, J. Phys. Chem. B 105 (2001) 4616.
46. M. English, A. Jentys and J.A. Lercher, J. Catal. 166 (1997) 25.
47. D.E. Ramaker, J. de Graaf, J.A.R. van Veen and D.C. Koningsberger, J. Catal. 203 (2001) 7.
48. D.C. Koningsberger, J. de Graaf, B.L. Mojet, D.E. Ramaker and J.T. Miller, Appl. Catal. A Gen. 191 (2000) 205.
49. B.L. Mojet, J.T. Miller, D.E. Ramaker and D.C. Koningsberger, J. Catal. 186 (1999) 373.

7

Support Effects in the Hydrogenation of Cinnamaldehyde over Carbon Nanofiber-Supported Platinum Catalysts

Part I: Catalysis and Characterization

Abstract

Carbon nanofiber-supported platinum catalysts were studied to establish the influence of the support surface composition on their performance in the liquid-phase hydrogenation of cinnamaldehyde. By acid-base titration, XPS and TGA-MS the amount of oxygen-containing surface groups was determined in activated carbon nanofiber samples and in the platinum catalysts pretreated at various temperatures. TEM, EXAFS and H_2-chemisorption studies showed the presence of a narrow and stable platinum particle-size distribution (1-2 nm). The overall catalytic activity increased by a factor of 25 after treatment at 973 K, which is related to the decreasing amount of oxygen on the fibers. The differences in intrinsic activity upon thermal treatment are even larger, since internal diffusion limitation slowed down the reaction for the most active catalysts as will be shown in part II. With XPS and H_2-chemisorption experiments carried out at 308 K no clear evidence was found for a change in the electronic structure of the platinum particles induced by the oxygen-containing groups present on/in the surface of the carbon nanofibers. A model involving the effect of the support surface composition on the mode of adsorption of cinnamaldehyde is discussed in Chapter 8.

Introduction

The selective hydrogenation of α,β-unsaturated aldehydes to unsaturated alcohols is a key step especially in the preparation of various fine chemicals [1-4]. In the literature often titania- and graphitic carbon- noble supported metals are used either with or without a promoter, to obtain a high alcohol selectivity [1,3,5-9]. Recently several publications have appeared in which carbon nanofibers (CNF) or carbon nanotubes (CNT) are examined as catalyst support [10]. For this type of reactions promising results were found. For example, in the liquid-phase hydrogenation of cinnamaldehyde with CNT-supported ruthenium catalysts [7,11,12] selectivities to cinnamyl alcohol up to 92% have been observed, whereas alumina-supported ruthenium catalysts gave rise to selectivities of 20-30% [6]. With activated carbon-supported ruthenium catalysts selectivities upto 30-40% have been obtained [13]. Often the increased selectivity towards the unsaturated alcohol is explained in terms of transfer of π-electrons from the graphitic planes to the metal particles [7,11,14]. In this way the charge density on the metal increases, leading to better π^*_{CO} backbonding and thus increasing probability for the C=O bond hydrogenation.

Earlier we reported on the influence of oxygen-containing surface groups in the liquid-phase hydrogenation of cinnamaldehyde using CNF-supported ruthenium catalysts [15]. In that study we used well-defined Ru/CNF catalysts with highly dispersed and uniform ruthenium particles of 1-2 nm. A clear trend was observed in activity and selectivity with the number of oxygen-containing surface groups. The rate of cinnamaldehyde conversion was enhanced by a factor of 22 after removal of the majority of the surface oxygenates which was mainly due to a strong increase in hydrogenation rate of the C=C bond.

A possible explanation for a direct effect of the oxygen-containing surface groups can be found in the adsorption of the organic reactant [16-18]. After increasing treatment temperatures, the CNF surface gradually changes from polar to non-polar due to the removal of the oxygen-containing surface groups. This change in polarity might change the preferential adsorption mode of cinnamaldehyde and enables adsorption of the reactant on the CNF support, thereby influencing the activity and selectivity. An alternative explanation implies the indirect influence of the oxygen-containing groups on catalysis *via* the electronic state of the metal. This model is based on the work of Koningsberger *et al.* and concerns the interaction between small (<2 nm) metal particles and oxidic supports [19-21]. With decreasing electron density of the support oxygen atoms, the density of states (DOS) and the Fermi level of the metal particles shift to a higher binding energy. This effect has been observed with XPS, FTIR and XAFS. Koningsberger *et al.* state explicitly that in their model the electron density distribution and the Fermi-level in the metal particles are changed, without the need for electron transfer from or to the support [22]. For carbon-supported noble metal catalysts this model suggests that lower amounts of (more electronegative) oxygen in the carbon support would give rise to lowering of the DOS of the metal. This could result in

stronger bonding between the metal and the reactant, thereby enhancing its rate of hydrogenation.

To get more insight in the nature of the distinct influence of oxygen-containing surface groups, we report on the influence of these groups in CNF-supported platinum catalysts in the liquid-phase hydrogenation of cinnamaldehyde. This investigation is performed on well-defined Pt/CNF catalysts with metal particles of 1-2 nm with a narrow particle size distribution and a tunable amount of support surface oxygen. A well-defined catalyst with small and uniform metal particles is needed to enable observation of the electronic support effect at all [23]. In the current study we discuss the characteristics of the CNF and the type and number of oxygen-containing surface groups present after activation and heat treatment in N_2. With XPS and H_2-chemisorption experiments we investigate whether the catalytic performance of the Pt/CNF system is related to an electronic effect, similar to that described for oxide-supported catalysts. The influence of the oxygen groups on the adsorption of the reactant on the CNF support is dealt with in Chapter 8.

Experimental

Carbon nanofiber growth

For the growth of CNF, 20 wt% Ni/SiO_2 was prepared by homogeneous deposition precipitation (HDP) as described by van Dillen *et al.* [24] using silica (Degussa, Aerosil 200), nickel nitrate (Acros) and urea (Acros). After filtering the catalyst precursor was dried at 393 K and calcined in static air at 873 K (heating rate 5 K/min) for 2 h. One gram of the Ni-catalyst precursor was placed in a quartz reactor. Prior to the fiber growth the Ni-catalyst precursor was reduced *in situ* for 2 h in a stream of a mixture of H_2 (80 ml/min) and N_2 (320 ml/min) at 1 bar and 973 K (heating rate 5 K/min). Next, the CNF were grown at 823 K in a mixture of CO (80 ml/min), H_2 (28 ml/min), and Ar (292 ml/min) for 24 h. A more detailed description of the growth catalyst and the growth of the CNF can be found elsewhere [25]. The CNF were refluxed for 1 h in a 1 M KOH solution in order to remove the silica support. For activation by surface oxidation and removal of nickel, the CNF were refluxed in concentrated nitric acid for 2 h and washed thoroughly with demi-water.

Synthesis carbon nanofiber-supported platinum catalyst

Platinum (intake 5 wt%) was deposited on the fibers according to a homogeneous deposition precipitation method. To an acidified suspension (pH=3) of 5 gram CNF in 250 ml demi-water heated up to 363 K under inert atmosphere, 0.41 g urea (Acros) and 0.52 g $Pt(NH_3)_4(NO_3)_2$ (Aldrich) were added under vigorous stirring. The pH of the slurry was monitored, to follow the process and to indicate its completeness. After 18 h the loaded CNF were filtered and washed thoroughly with demi-water, dried at 353 K in an N_2 flow and

reduced in flowing H_2 at 473 K for 1 h (heating rate = 5 K/min). Next the samples were exposed to air at RT.

In order to obtain different concentrations of oxygen-containing surface groups on the CNF, samples of the freshly reduced catalyst were heat-treated in an N_2 flow for 2 h at 573, 773 and 973K [26]. The catalyst samples together with their identification codes are listed in Table 1.

Catalyst characterization

The numbers of acid sites of the oxidized CNF after the various heat-treatments were determined by standard acid-base titrations. For this purpose 20-40 mg of oxidized CNF was stirred with 25 ml of a solution containing 0.1 M NaCl and 0.1 mM oxalic acid in demi-water, acidified to pH =3 with HCl. While stirring, pure nitrogen was bubbled through the slurry and 10 mM NaOH was added drop wise from a buret until the endpoint (pH = 7.5) had been reached.

The total number of thermally removable oxygen-containing groups was measured using thermogravimetric analysis on a Netzsch STA-429 thermobalance. The gases evolved were monitored by a Fisons Thermolab quadropole mass spectrometer through a capillary situated directly above the sample cup. Samples (20-100 mg) were heated in Ar (60 ml/min) at a rate of 5 K/min up to 1123 K and maintained at that temperature for one hour.

The CNF-supported platinum catalysts were examined in a Philips CM-200 FEG TEM and a Tecnai 20 FEG TEM both operated at 200 kV. After suspending in ethanol under ultrasonic vibration, samples were brought onto a holey carbon film on a copper grid.

Platinum loadings were determined by means of XRF on a Philips PW 1480. Before analysis the Pt/CNF samples were pressed into a tablet using a methyl methacrylate binder.

XPS analyses were performed on a Fisons ESCALAB 210I-XL and a Vacuum Generators XPS system. Al Kα X-ray radiation was utilized, employing an anode current of 20 mA at 15 and 10 keV, respectively. The pass energy of the analyzer was set at 70 eV for the Fisons apparatus and 50 eV for the Vacuum Generators XPS. Before analysis the Pt/CNF catalysts were reduced (again) by H_2 in the apparatus at 383 K (heating rate 5 K/min) for 30 min and were measured without grinding of the CNF skeins.

Table 1. Sample codes, loadings and pretreatment conditions of the various CNF-supported platinum catalysts.

Sample	Loading (wt %) XRF	Gas-phase pre-reduction	Heat treatment in N_2
PtCNFnp[a]	3.6	-	-
PtCNF	3.6	473 K	-
PtCNF573	3.6	473 K	573 K
PtCNF773	3.6	473 K	773 K
PtCNF973	3.6	473 K	973 K

[a] np = not pre-reduced in the gas-phase.

Hydrogen chemisorption measurements were performed using a Micromeritics ASAP 2010C. Each sample was dried in He at 393 K for 1 h, and reduced in flowing H_2 (flow rate = 50 ml/min STP) at 473 K for two hours, heating rate 5K/min. After reduction the samples were degassed for two hours at 10^{-1} Pa at the reduction temperature in order to remove chemisorbed hydrogen and water. The isotherms were measured at 308 K. The presented H/Pt ratios are based on the amounts adsorbed at zero pressure found by extrapolation of the linear part of the isotherm. Calculations have been made with the total amount of adsorbed hydrogen, because XAFS results of Oudenhuijzen *et al.* with Pt/Al_2O_3 catalysts unambiguously show that also "weakly" bonded hydrogen is chemisorbed and must be taken into account [27]. Estimated average particle sizes and dispersions are based on spherical geometry and an adsorption stoichiometry of $H/Pt_s = 1$. The average Pt particle size, d, was calculated from:

$$d * D = 10^{21} \frac{M * 6 * \rho_{site}}{\rho_{metal} * N}$$

where d is the average platinum particle size (nm), D is the dispersion (H/Pt), M is the atomic weight (Pt = 195.09 g/mol), ρ_{site} is the platinum surface site density (12.5 Pt atoms/nm^2), ρ_{metal} the metal density (21.45 g/cm^3) and N the Avogadro constant ($6.022*10^{23}$ mol^{-1}) giving d=1.13/D (nm) [28].

XAFS experiments

XAFS spectra at the Pt L_3 edge were taken at the HASYLAB (Hamburg, Germany) synchotron beamline X1.1, equipped with a Si(311) double crystal monochromator. The monochromator was detuned to 50% of the maximum intensity to avoid higher harmonics present in the X-ray beam. The measurements were done in transmission mode using ion chambers filled with an Ar/N_2 mixture to have a μx of 20% in the first and a μx of 80% in the second ionization chamber. The energy of the X-ray beam was calibrated by using a Pt foil between the second and third ionization chamber.

The powdered catalysts were diluted with boron nitride and pressed into a self-supporting wafer (calculated to have an absorbance of 2.5) mounted in a stainless steel *in situ* cell equipped with Be-windows. The samples were re-reduced *in situ* at 473 K for 30 min (5 K/min) in flowing H_2 and cooled down in an H_2 atmosphere. The reduced samples are considered to be fully covered with hydrogen and are further denoted by (RED). Next the EXAFS data for the L_3 edge were collected (T = 77 K).

Extraction of the EXAFS data from the measured absorption spectra was performed with the XDAP code [29]. Three scans were averaged and the pre-edge was subtracted using a modified Victoreen curve. The background was subtracted employing cubic spline routines with a continuously adjustable smooth parameter. Normalization was performed by dividing the data by the edge-step at 50 eV after the adsorption edge.

Data for phase shifts and backscattering amplitudes for Pt-Pt and Pt-C were obtained from FEFF7 and FEFF8 calculations respectively and calibrated by the experimental data of Pt foil and $[Rb_2Pt(CN)_4]1.5H_2O$. Data analysis of the CNF-supported platinum catalysts was performed by multiple shell fitting using the difference file technique in R space ($1.6 < R < 3.2$ Å) with the XDAP code [30,31].

Both high Z (Pt-Pt) and low Z (Pt-C/O) contributions are present in the EXAFS data collected on CNF-supported platinum. In this study, the EXAFS fits have been checked by applying k^1 and k^3 weightings in order to be certain that the results are the same for all weightings. The variances of the magnitude and imaginary part of the Fourier transforms of fit and data were calculated according to:

$$\text{Variance} = \frac{\int\left[FT^n_{model}(R) - FT^n_{exp}(R)\right]^2 dR}{\int\left[FT^n_{exp}(R)\right]^2 dR} * 100$$

with $FT^n = FT[k^n \chi(k)]$. In this study the statistical significance of a contribution has been checked by a comparison of the amplitude of $(Fit)_j$ with the noise level present in the difference file (the noise in the difference file is essentially the same as the noise in the experimental data).

Catalytic experiments

Liquid-phase hydrogenation of cinnamaldehyde was studied in a 500 ml stirred semi-batch reactor equipped with a sample port, reagent injection port, gas inlet and vent.

The catalysts (0.2 gram) were (re)-activated in suspension in *iso*-propanol (220 ml) at 383 K with H_2 at a total pressure of 3.0 MPa for 30 minutes in the stirred autoclave (1500 rpm) prior to the introduction of cinnamaldehyde (3.0 g). All reactions were executed at 383 K using a total pressure of 5.0 MPa. Samples were withdrawn periodically and analyzed on a gas chromatograph (Hewlett Packard 5890 Series with autosampler) using an HP5 capillary column (30 m x 0.32 mm x 0.25 μm ID).

After the hydrogenation experiments the changes in platinum particle size of the spent catalysts were investigated with TEM. For PtCNF to PtCNF973 no significant modification in size and shape of the platinum particles was observed. The platinum particles in PtCNFnp, however, had sintered to 2-10 nm during the reaction under the rather severe conditions (5.0 MPa and 383K).

To investigate whether the catalysts became irreversibly deactivated, three consecutive experiments with one catalyst batch of PtCNF were executed. Between the runs the catalyst was washed repeatedly with *iso*-propanol and dried. The activity of the catalysts in the three runs was comparable, thus proving the absence of irreversible deactivation.

Duplicate experiments were performed with both PtCNF and PtCNF973 showing rates and selectivities to the various products to be within an error margin of around 5%, indicating excellent reproducibility.

Results and Discussion

Characterization of the CNF support

The CNF are of the fishbone type *i.e.* with the graphite planes oriented at an angle to the central axis and the fibers are interwoven into porous skeins. After removal of the growth catalyst and the activation treatment with nitric acid for 2 h the non-microporous fibers exhibited a specific surface area of 177 m^2/g. X-ray diffraction and TEM-images demonstrated that the graphite-like structure of the CNF had not been affected during activation. From SEM and TEM micrographs an average fiber diameter of 25 nm could be derived with a narrow diameter distribution.

As stated earlier the activation procedure in nitric acid is carried out to introduce various types of oxygen functional groups on the CNF and to remove non-encapsulated nickel from the growth catalyst. TEM images show that the remaining nickel (≤ 0.5 wt%, XRF analysis) is encapsulated by graphitic envelopes, thus preventing interference in catalysis.

Table 2 lists the number of acid sites ($pK_a < 7.5$) of oxidized CNF treated at different temperatures in N_2 as determined by titration, as well as the number of oxygen atoms/nm^2 calculated from XPS and TGA-MS results. After activation and drying of the CNF 1.4 acid sites/nm^2 were present. Heat treatment resulted in a gradual removal of the majority of the acidic oxygen-containing groups to 0.03 acid sites/nm^2 after treatment at 973 K. XPS

Table 2. Number of oxygen atoms/nm^2 on CNF surface as a function of treatment temperature determined with acid-base titration, XPS and TGA-MS.

Sample	Titration		XPS		TGA-MS	
	Number of acid site/nm^2	O atoms/nm^2	O/C atomic ratio	O atoms/nm^2	Weight loss (%)	O atoms/nm^2
CNFox	1.4 ± 0.1	2.8 ± 0.2	0.069	9.6 ± 1.4	5.7	9.8 ± 0.8
CNFox - N_2 573 K	1.0 ± 0.1	2.0 ± 0.2	0.038	5.3 ± 0.8	3.7	6.3 ± 0.5
CNFox - N_2 773 K	0.2 ± 0.02	0.4 ± 0.04	0.032	4.4 ± 0.7	3.3	5.6 ± 0.5
CNFox - N_2 973 K	~0.03 ± 0.003	0.06 ± 0.01	0.017	2.3 ± 0.3	1.8	3.0 ± 0.3
PtCNFnp			0.044	6.1 ± 0.9	5.1	7.7 ± 0.6
PtCNF			0.038	5.3 ± 0.8	3.8	6.5 ± 0.5
PtCNF573			0.037	5.1 ± 0.8	3.7	6.2 ± 0.5
PtCNF773			0.026	3.6 ± 0.5	2.7	4.5 ± 0.5
PtCNF973			0.016	2.2 ± 0.3	1.5	2.6 ± 0.3

measurements were done to establish the amount of oxygen in the outer layer of 2-3 nm of the CNF. After oxidation and drying an O/C atomic ratio of 0.069 was found. A gradual decrease in the O/C ratio from 0.069 to 0.017 with increasing heat-treatment temperature was observed. Using a model the O/C ratios can be converted into a number of oxygen atoms/nm^2 [32]. These results (Table 2) show that fibers oxidized in HNO_3 for 2 h contain 9.6 O atoms/nm^2. Since oxygen-containing surface groups often contain one or two oxygen atoms, this implies that about 5-10 oxygen-containing surface groups would be present when it is assumed that all oxygen is located at the outer surface. Values up to 1-3 groups/nm^2, as earlier proposed by Boehm and as we found by titration, seem to be more realistic [33]. An explanation for this discrepancy can be found in the assumption that oxygen atoms are not exclusively present at the surface, but also are built in in the subsurface (2-3 nm) graphene sheets [34,35]. TGA-MS up to 1123 K was used to establish the number of thermally removable oxygen atoms from the surface and the bulk of the CNF. Also TGA-MS results show the presence of oxygen-containing groups in the oxidized CNF and the partial removal of these groups with increasing heat treatment. The number of oxygen atoms as determined using XPS and TGA-MS are comparable when the error margins are taken into account. From these results and earlier work [26] it is concluded that oxygen is not present throughout the carbon support, but is mainly located in the outer 2-3 nm of the fibers with 2-30% present in acidic groups at the exterior surface, *i.e.* accessible for titration. It is noted that with increasing treatment temperature the ratio of (acidic oxygen at exterior)/(total oxygen) drops largely. For a more detailed investigation on the effect of oxidation of CNF we refer to [26].

Characterization of the CNF-supported platinum catalysts

The metal loading of the Pt/CNF catalysts as established with XRF was 3.6 wt% (Table 1). TPR results (not shown) of the freshly loaded sample demonstrated that all catalysts were completely reduced at 473 K. Therefore all catalysts were reduced at this temperature, is it

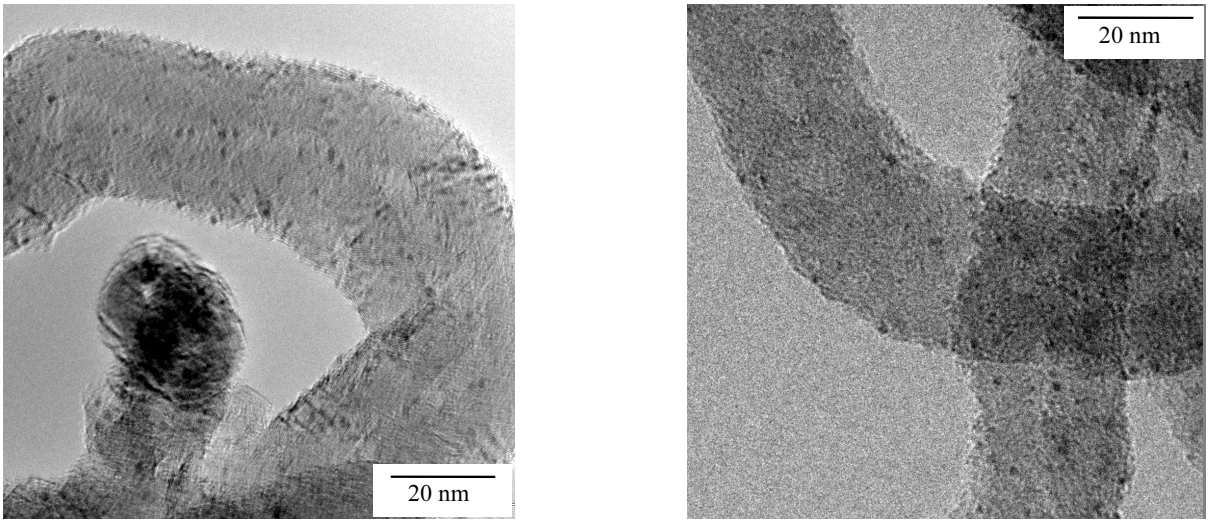

Figure 1. TEM images of CNF-supported platinum catalysts after reduction (PtCNF).

Table 3. TEM and hydrogen chemisorption results at 308 K on the different CNF-supported platinum catalysts.

Sample	TEM d (nm)	H_2-chemisorption				
		irreversible		total		H_{irr}/H_{tot}
		H/Pt	d (nm)	H/Pt	d (nm)	
PtCNF	1-2	0.37	3.1	0.79	1.4	0.45
PtCNF573	1-2	0.63	1.8	1.06	1.1	0.60
PtCNF773	1-2	0.33	3.5	0.74	1.5	0.42
PtCNF973	1-3	0.21	5.4	0.49	2.3	0.43

that PtCNFnp was only reduced *in situ* at 383 K preceding the catalytic experiments, this to maintain a support oxygen concentration as large as possible.

The amount of support oxygen still present on the platinum catalysts after the different treatments is assessed using XPS and TGA-MS (Table 2). Unfortunately, titration experiments could not be performed, since the presence of metallic platinum interfered with the measurements. This table shows that due to the application of platinum on the CNF the

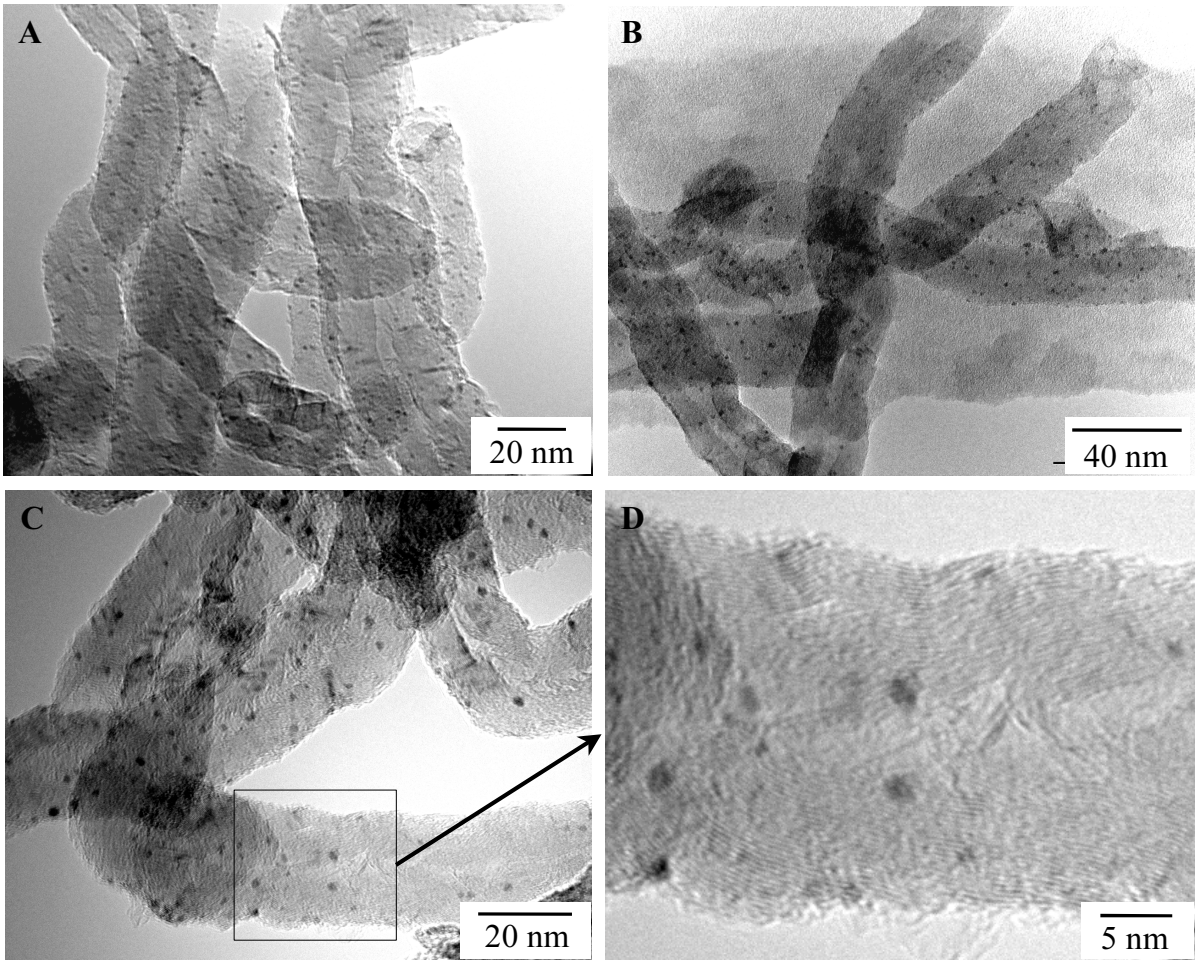

Figure 2. TEM images of CNF-supported platinum catalysts after reduction and heat-treatment in N_2 A) PtCNF573, B) PtCNF773 and C and D) PtCNF973.

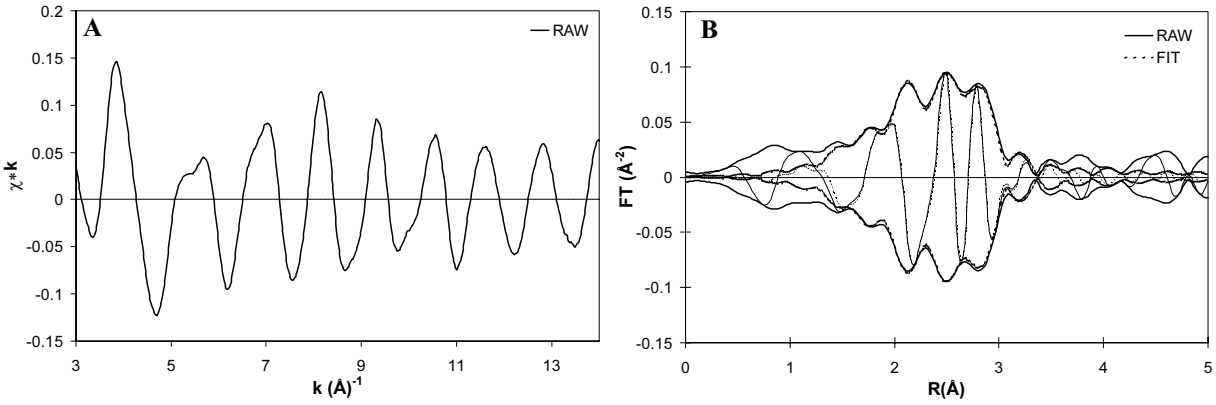

Figure 3. A) The EXAFS raw data (k^1-weighted, Δk = 3-14 Å) of PtCNF (RED). B) The corresponding Fourier transforms (k^1-weighted, Δk = 3-14 Å) of the EXAFS raw data (solid line) and the total fit (dotted line).

average number of oxygen atoms/nm^2 has decreased from about 9.7 (CNFox) to about 6.9 (PtCNFnp). A more detailed investigation on the relation between the oxygen groups and the metal loading can be found elsewhere [36]. Subsequent reduction and heat treatments resulted in a further gradual decrease in the amount of support oxygen to ultimately around 2-3 oxygen atoms/nm^2 for PtCNF973, very similar to the values observed with unloaded CNF.

In Figure 1 two representative TEM images of PtCNF are shown. The platinum particles are small and homogeneously distributed over the CNF surface. The particles size distribution is very narrow; particles of 1-2 nm are observed. The average particle size and H/Pt ratio calculated from hydrogen chemisorption data are presented in Table 3. Using the total amount of adsorbed hydrogen an H/Pt of 0.79 an average platinum particle size of 1.4 nm was calculated for PtCNF.

After reduction the platinum catalysts were treated in N_2 at 573, 773 and 973 K to remove part of the support oxygen-containing groups. From the TEM images (Figure 2 A-D) it is clear that treatment at 573 and 773 K did not affect the platinum particle size, while treatment at 973 K resulted in a small increase in particle size. In Figure 2D the graphene sheets of the fishbone CNF covered with some platinum particles are visible. Hydrogen chemisorption results (Table 3) show an unexpected and up to now unexplained increase in H/Pt from 0.79 for PtCNF to 1.06 for PtCNF573. After treatment at 773 and 973 K H/Pt ratios of 0.74 and 0.49 were found, indicating average particle sizes of 1.5 and 2.3 nm, respectively, thereby confirming TEM results.

EXAFS was used as an additional method to determine the structural parameters of the platinum particles in PtCNF and PtCNF773. Figure 3A shows the experimental EXAFS data (k^1 weighted, Δk = 3-14 Å^{-1}) of PtCNF (RED) in a hydrogen atmosphere. The signal to noise ratio at k = 4.4 Å^{-1} amounts to approximately 150 on both the PtCNF and PtCNF773 spectra, showing the data to have an excellent quality.

Table 4. Fit parameters of EXAFS spectra (Δk: 3-14 $Å^{-1}$, ΔR:1.6-3.2 Å) and variances for model spectra of PtCNF (RED) and PtCNF773 (RED).

Catalyst (treatment)	**Scatter**	**N** ± 10%	**R (Å)** ± 0.02 Å	**$\Delta\sigma^2$ ($Å^2$)** ± 5%	**ΔE_0 (eV)** ± 10%	**k^1-variance (%)** Im.	Abs.
PtCNF	$C(O)_s$	0.7	2.02	$2.0*10^{-3}$	1.2	0.39	0.14
(RED)	$C(O)_l$ Pt	1.6	2.65	$2.2*10^{-3}$	-0.3		
		5.2	2.77	$1.1*10^{-3}$	2.1		
PtCNF773	$C(O)_s$	0.3	2.01	$1.3*10^{-3}$	3.2	0.34	0.12
(RED)	$C(O)_l$ Pt	2.0	2.62	$1.4*10^{-3}$	1.5		
		5.5	2.76	$1.6*10^{-3}$	1.3		

The corresponding k^1-Fourier transform of the raw EXAFS data of PtCNF (RED) is displayed in Figure 3B. This is a typical example of the Fourier transform of small supported platinum particles using k^1-weighing. It contains both Pt-Pt and Pt-C(O) contributions. In this study, the separation of Pt-C and Pt-O contributions is not carried out, because it is difficult to identify O and C as different backscatterers since they are neighboring elements in the Periodic Table. The sum of Pt-C and Pt-O contributions is denoted as Pt-C(O). The parameters used to fit the experimental EXAFS data of PtCNF (RED) and PtCNF773 (RED) are given in Table 4. As an example Figure 3B enables the comparison of the Fourier transforms of the raw EXAFS data (solid line) and the fit (dotted line) of PtCNF (RED) using the parameters listed in Table 4. This comparison demonstrates the excellent fit quality of all the EXAFS data. The C(O)and Pt backscatterers were identified using the difference file technique. The variances in imaginary and absolute parts were used to determine the fit quality. Fits with variances below 1% have been considered to represent good models for the experimental data.

The EXAFS results in Table 4 show a Pt-Pt bond distance in PtCNF and PtCNF773 of 2.77 and 2.76 Å respectively, which is typical for metallic platinum particles in a hydrogen atmosphere [37]. The Pt-Pt coordination numbers found are 5.2 (PtCNF) and 5.5 (PtCNF773). This shows that in both samples very small Pt particles with an average size of around 1 nm are present [38,39]. The other parameters of PtCNF and PtCNF773 differ only slightly or not at all. A full EXAFS study dealing with the structure of the metal-support interface in the Pt/CNF catalysts, the shortening of the Pt-C distance upon evacuation and the role of oxygen-containing groups in stabilizing the platinum particles is published in a separate paper [40].

Hydrogenation of cinnamaldehyde

The hydrogenation of cinnamaldehyde can be presented by a simplified reaction pathway as shown in Figure 4. In this study the main by-products before complete conversion of cinnamaldehyde were cinnamyl *iso*-propylether and the di-*iso*-propylacetal of hydrocinnam

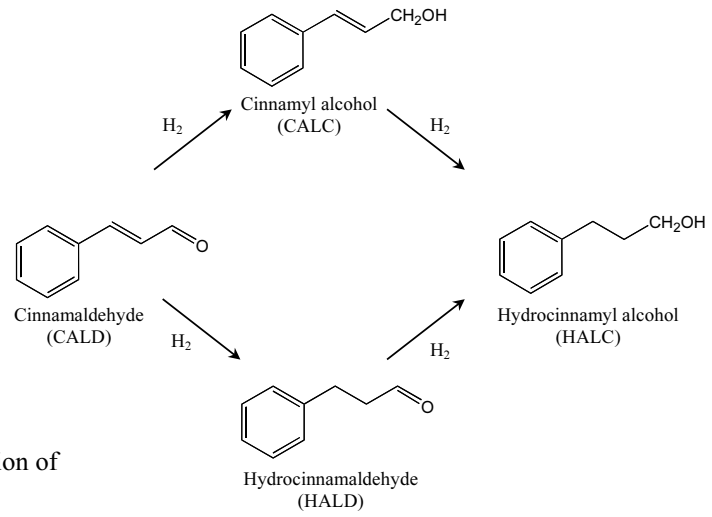

Figure 4. Reaction pathway of the hydrogenation of cinnamaldehyde.

aldehyde. These products form *via* a reaction between cinnamaldehyde or hydrocinnamaldehyde and the solvent *iso*-propanol.

For PtCNF and PtCNF973 Figure 5 shows, as a function of time, the molar composition of the reaction mixture for cinnamaldehyde (CALD), the primary reaction products hydrocinnamaldehyde (HALD) and cinnamyl alcohol (CALC) and the secondary product hydrocinnamyl alcohol (HALC). First of all, from these graphs the large difference in hydrogenation activity between PtCNF and PtCNF973 is striking. Using PtCNF after 600 min only 80% conversion is obtained, while using PtCNF973 cinnamaldehyde is completely converted within 20 min. The difference in activity will be dealt with in more detail below.

It is clear that the selectivities to the main products are dependent on the catalyst. PtCNF produces cinnamyl alcohol and hydrocinnamaldehyde in comparable amounts. On the other hand, with PtCNF973 hydrocinnnamaldehyde is the main product. In Figure 6 the selectivities to cinnamylalcohol (CALC) and hydrocinnamaldehyde (HALD) are plotted as a function of the conversion and in Table 5 the selectivities at 60% conversion to the various

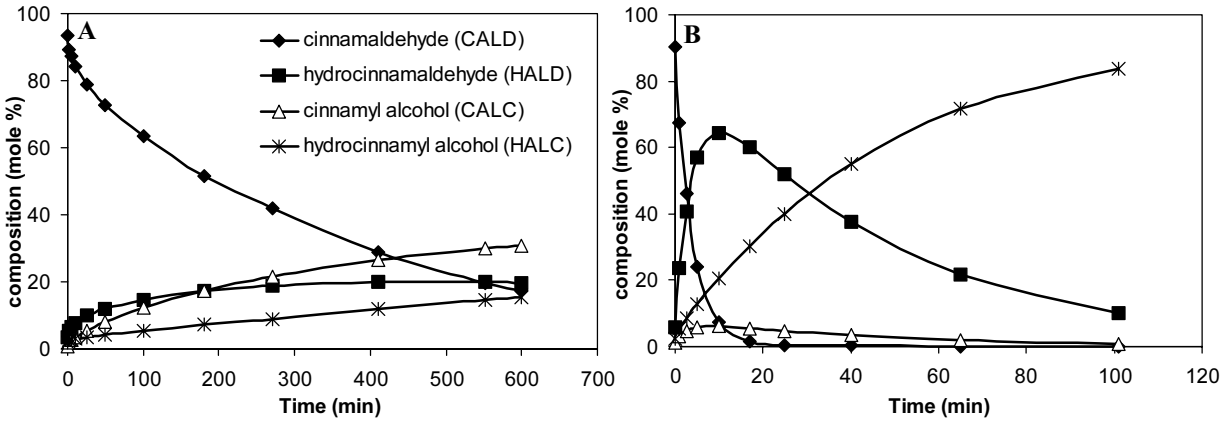

Figure 5. Cinnamaldehyde conversion and product distribution as function of time on stream obtained at 383K and 5.0 MPa hydrogen over CNF-supported platinum catalysts A) PtCNF and B) PtCNF973.

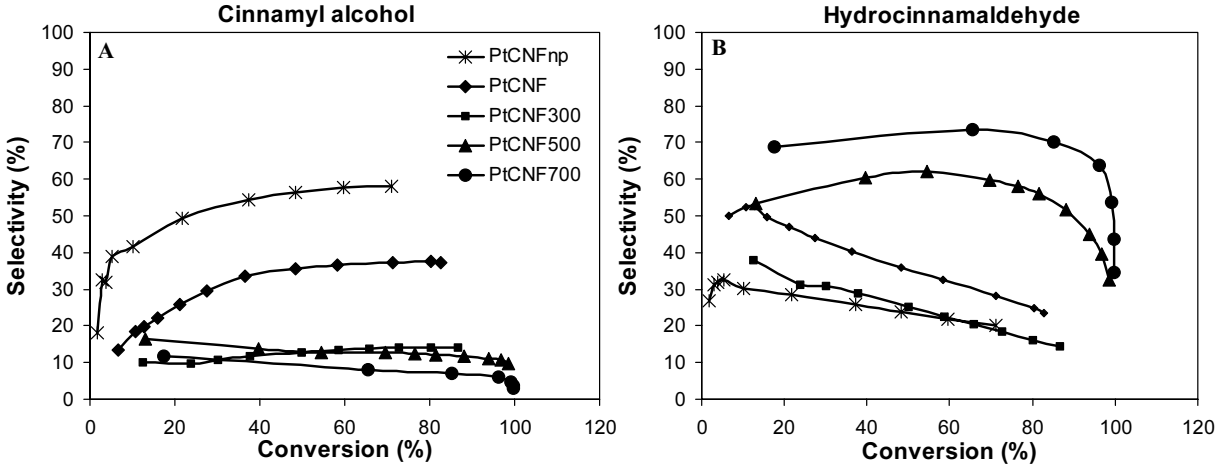

Figure 6. Selectivities of different CNF-supported Pt catalysts as a function of conversion to A) cinnamyl alcohol and B) hydrocinnamaldehyde.

reaction products and the two main byproducts are represented. For PtCNFnp S_{CALC} = 58% and S_{HALD} = 22% is found. With increasing treatment temperature the selectivity towards the alcohol gradually declines and the selectivity to hydrocinnamaldehyde rises. For PtCNF973 S_{CALC} = 8 %, while S_{HALD} = 74 %. Obviously the rate of C=C hydrogenation of cinnamaldehyde is strongly enhanced with heat treatment of the catalyst, while the rate of hydrogenation of the C=O is only slightly increased. Figure 5 demonstrates, however, that the secondary hydrogenation of hydrocinnamaldehyde to hydrocinnamyl alcohol is also much faster on PtCNF973, *i.e.* the C=O hydrogenation rate seems dependent on the substrate molecule.

Figure 6 shows that the selectivities to the primary and secondary products depend on the conversion of cinnamaldehyde. Beyond 5% conversion the selectivity of the heat-treated catalysts remains fairly constant. Another striking feature is the strong dependence of the amount of formed by-products with the treatment of the catalyst (Table 5): PtCNFnp,

Table 5. Selectivity to cinnamyl alcohol, hydrocinnamaldehyde, hydrocinnamyl alcohol and two by-products for cinnamaldehyde hydrogenation with CNF-supported platinum catalysts determined at 60% conversion.

Sample name	**Products**			**By-products**	
	S_{CALC} (%)	S_{HALD} (%)	S_{HALC} (%)	Cinnamyl *iso*-propylether	Di-*iso*-propylacetal of hydrocinnamaldehyde
PtCNFnp	58	22	13	1	1
PtCNF	37	32	15	2	6
PtCNF573	13	23	12	11	19
PtCNF773	13	61	17	1	2
PtCNF973	8	74	18	0	0

Table 6. Initial activities, relative activities and TOF for cinnamaldehyde hydrogenation with CNF-supported platinum catalysts at 383 K and 5.0 MPa.

Sample name	Initial activity ($mmol*min^{-1}*g_{cat}^{-1}$)	Rel. activity[b]	TOF (s^{-1})[a]
PtCNFnp	0.60	1.0	n.d.
PtCNF	1.9	3.2	0.23
PtCNF573	4.0	6.7	0.39
PtCNF773	11	19	1.6
PtCNF973	15	25	3.3

[a] Results are given in mole CALD hydrogenated per mole of platinum surface atoms in the catalyst per second. The amount of platinum surface atoms is calculated from the catalyst weight, the metal loading and the H/Pt (total H) ratio.

[b] Relative activity is the initial activity divided by the initial activity of PtCNFnp.

n.d. Not determined because the H/Pt ratio is not known for this sample.

PtCNF773 and PtCNF973 produce only minor amounts of the *iso*-propanol ether and acetal, while PtCNF (2 and 6%) and especially PtCNF573 (11 and 19%) form large amounts of these products. It is well known that these type of reactions are acid catalyzed [41]. Therefore, it is expected that with increasing heat treatment of the catalyst and thus with decreasing support acidity the amount of by-products drops. However, the low amount of by-products formed using PtCNFnp is unexpected.

Although the data show many interesting phenomena, we will in this study mainly focus on the effect of the oxygen-containing groups on the strongly enhanced activity for C=C hydrogenation in cinnamaldehyde. From the decrease in the concentration of cinnamaldehyde with time (Figure 5) initial activities were calculated for all samples. These values are given in Table 6 together with the relative activity compared to the activity of PtCNFnp and the related TOF. Both Figure 5 and Table 6 show the clear differences in catalytic behavior as a function of treatment temperature of the catalysts. With increasing treatment temperature a strong increase in the total activity was found. The activity of PtCNF973 was measured almost 25 times larger than that of PtCNFnp and almost 8 times larger than that of PtCNF. The TOFs differ even somewhat more due to a small increase in mean particle size in PtCNF973. This increase in total activity is mainly caused by a large increase in hydrocinnamaldehyde formation as can be concluded from Figure 5.

Calculations of the Weisz-Prater criterion of PtCNF and PtCNF973 and calculated concentration profiles in the catalyst particles of these catalysts using a kinetic model, which includes mass transfer inside the catalyst particles, demonstrate that with PtCNF internal diffusion limitations are not apparent. In contrast, with PtCNF973 the increase in activity is such that diffusion of the organic compounds in the catalyst bodies limits the reaction rate [42]. From the latter calculation the ratio of the intrinsic activity of PtCNF and PtCNF973 is much larger than the factor of 8 in observed activities.

Electronic structure of platinum

The hydrogenation results presented here using the Pt/CNF catalysts and the results reported in an earlier study on RuCNF catalysts [15] show that the catalytic behavior of CNF-supported noble metals is strongly dependent on the heat treatment and thus on the amount of oxygen groups present in/at the support surface. In order to investigate whether the oxygen-containing groups influence the electronic structure of the platinum particles, we executed XPS and H_2-chemisorption measurements. Using XPS a shift in platinum binding energy is expected and with hydrogen chemisorption the H_{strong}/H_{total} ratio should change if an electronic effect of the support is effective.

In Table 7 the platinum $4f_{7/2}$ and $4f_{5/2}$ binding energies are displayed as determined for the CNF-supported platinum catalysts after reduction using Gauss-Lorenzian peak fits. For metallic platinum, binding energies of 70.9 ($4f_{7/2}$) and 74.3 eV ($4f_{5/2}$) have been reported [43]. The results show that in PtCNF, PtCNF573, PtCNF773 and PtCNF973 the platinum binding energy is equal for all samples and around 71.4 and 74.6 eV, respectively, indicating that platinum in all the CNF-supported catalysts is in the metallic state. The binding energy of PtCNFnp is slightly shifted to higher values, as ionic Pt species might be present because of the mild reduction conditions.

With oxides change of the electron density of the support was found greatly to influence the metal binding energies of noble metal particles, *i.e.* higher binding energies when applied on supports with a relatively low oxygen electron density. Mojet *et al.*, for instance, found a shift in binding energies of about 1.4 eV for both Pd $3d_{3/2}$ and Pd $3d_{5/3}$ in a Pd/LTL with a K/Al atomic ratio ranging from 0.55 to 1.10 [44]. Our results, however, indicate that the varying concentration of oxygen groups on the carbon support does not influence the electronic properties of platinum as determined with XPS.

In Table 3 the H_{irr}/H_{total} ratios of the various Pt/CNF catalysts are given. Oudenhuijzen *et al.* [45] observed that for small LTL-supported platinum particles the hydrogen coverage and binding strength depend on the support properties. Nevertheless, for the various Pt/CNF catalysts no clear trend can be observed in the H_{strong}/H_{total} ratios.

Since we did not observe changes in the platinum binding energy and H_2-chemisorption

Table 7. Platinum $4f_{7/2}$ and $4f_{5/2}$ binding energies of the CNF-supported platinum catalysts determined by XPS using Gauss-Lorenzian peak fits.

Sample name	Treatment in XPS	E_b (eV)	
		Pt $4f_{7/2}$	Pt $4f_{5/2}$
PtCNFnp	red 383 K	73.4	76.2
PtCNF	red 383 K	71.4	74.6
PtCNF573	red 383 K	71.4	74.7
PtCNF773	red 383 K	71.4	74.7
PtCNF973	red 383 K	71.6	74.6

we think that changes in electron density of the CNF support by partly removing the oxygen groups are much smaller than the changes in the electron density in oxidic-supported catalysts with for example varying K/Al ratios.

Oxygen content of the support

In Figure 7A the relative total activity is plotted versus the amount of acidic oxygen-containing groups/nm^2 of the various CNF surfaces. Because titrimetric determination of the acidic groups on the Pt/CNF catalysts could not be effectuated due to the interfering action of platinum, we used the values found with the unloaded CNF support (see Table 2). An almost linear relation, especially for the PtCNFnp to PtCNF773 catalysts, is observed between the total activities and the concentration of acidic oxygen groups of the support. When only few acidic groups are present the activity is high and with increasing surface acidity the activities drop. The line between PtCNF773 and PtCNF973 is dotted, since the activity measured using PtCNF973 is influenced by internal diffusion limitation. Besides the acidic groups also other oxygen-containing surface groups are present on the CNF surface. Therefore, in Figure 7B the relative total activities are plotted versus the number of oxygen atoms. For the number of oxygen atoms the values found with XPS are used. The correlation between activity and oxygen concentration is not as clear as between the activity and the number of acidic support surface groups. The shape of the two curves is not the same, since the number of the acidic oxygen-containing groups is not linearly proportional to the total amount of oxygen on/in the fibers (Table 2). These curves suggest that catalysis is directly influenced by the acidic oxygen-containing groups at the exterior surface of the CNF support. The strong increase in activity could be brought about by the removal of these support surface groups. A model in which the hydrogenation is assisted by adsorption of the cinnamaldehyde on the CNF support after removal of the oxygen surface groups is discussed in Chapter 8.

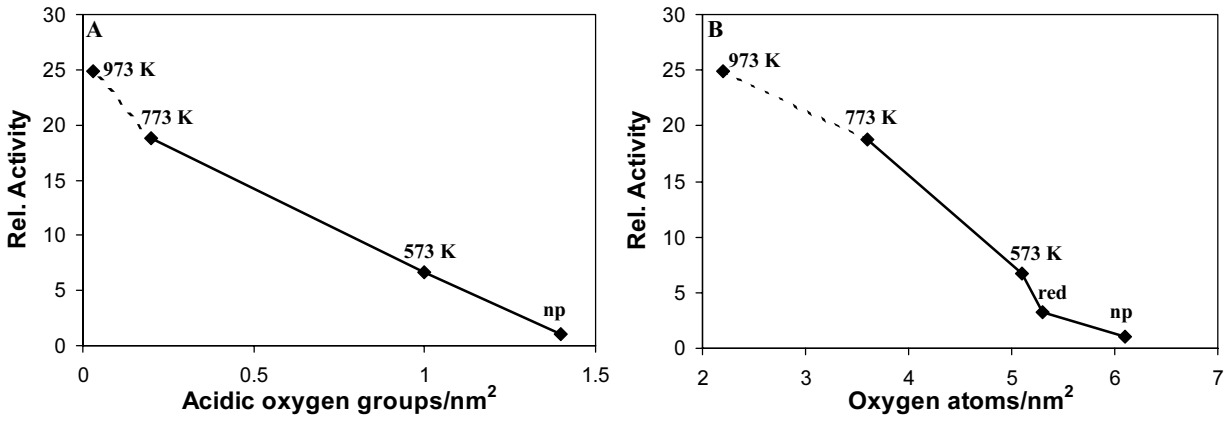

Figure 7. Relative total activity for cinnamaldehyde hydrogenation as a function of the amount of acidic groups (A) and as a function of the amount of oxygen (XPS) on the CNF-supported platinum catalysts (B).

Conclusions

Well-defined carbon nanofiber-supported platinum catalysts were prepared with a narrow size distribution, and a mean particle size of 1-2 nm, both features being prerequisites for performing studies on the electronic support effect. By treatment of carbon nanofibers in nitric acid and subsequent loading, reduction and heat treatment under nitrogen atmosphere, the concentration of oxygen-containing groups on the carbon nanofiber surface was varied without a significant change in platinum particle size.

The activity and selectivity in the liquid-phase hydrogenation of cinnamaldehyde was found to be dependent on the amount of oxygen of the CNF support. The rate of cinnamaldehyde conversion was enhanced with a factor of 25 after removal of the oxygen groups. The differences in intrinsic activities are even much larger, since with the catalyst treated at high temperature internal diffusion limits the reaction rate as will be shown in part II. This enhanced activity is mainly caused by a strong increase in hydrogenation rate of the C=C bond, while only a slight increase in C=O bond hydrogenation is observed.

Using XPS and H_2-chemisorption up to now no evidence has been found that the amount of oxygen in the support influences the electronic properties of the platinum particles. So, apparently modification of the electronic properties of the metal is not the first cause of the large changes in catalytic behavior of the catalysts. A model in which the hydrogenation is assisted by adsorption of the cinnamaldehyde on the CNF support after removal of the oxygen surface groups is discussed in Chapter 8.

Acknowledgements

Staff and personnel of beamline X1.1 at Hasylab (Hamburg, Germany) are kindly acknowledged. The European Union program for Large Scale Facilities (Contract ERBFMGECT950059) is acknowledged for financial support.

References

1. P. Kluson and L. Cerveny, Appl. Catal. A Gen. 128 (1995) 13.
2. V. Ponec, Appl. Catal. A Gen. 149 (1997) 27.
3. B. Coq and F. Figueras, Coord. Chem. Rev. 178-180 (1998) 1753.
4. P. Gallezot and D. Richard, Catal. Rev.-Sci. Eng. 40 (1998) 81.
5. A. Giroir-Fendler, D. Richard and P. Gallezot, Stud. Surf. Sci. Catal. 41 (1988) 171.
6. B. Coq, P.S. Kumbhar, C. Moreau, P. Moreau and M.G. Warawdekar, J. Mol. Catal. 85 (1993) 215.

7. P.S. Kumbhar, B. Coq, C. Moreau, P. Moreau, J.M. Planeix and M.G. Warawdekar, Catalysis: Modern Trends (N.M. Gupta and D.K. Chakrabarty, Eds.) Narosa Publishing House, New Delhi 1995.
8. A.B. da Silva, E. Jordoa, M.J. Mendes and P. Fouilloux, Appl. Catal. A Gen. 148 (1996) 253.
9. C.M.G. van de Moesdijk and M.A.R. Bosma, US patent 4745234 (1988).
10. P. Serp, M. Corrias and P. Kalck, Appl. Catal. A Gen. 253 (2003) 337.
11. J.M. Planeix, N. Coustel, B. Coq, V. Brotons, P.S. Kumbhar, R. Dutartre, P. Geneste, P. Bernier and P.M. Ajayan, J. Am. Chem. Soc. 116 (1994) 7935.
12. M. Lashdaf, A. Hase, E. Kauppinen and A.O.I. Krause, Catal. Lett. 52 (1998) 199.
13. S. Galvagno, G. Capanelli, G. Neri, A. Donato and R. Pietropaolo, J. Mol. Catal. 64 (1991) 237.
14. T. Vergunst, F. Kapteijn and J.A. Moulijn, Catal. Today 66 (2001) 381.
15. M.L. Toebes, F.F. Prinsloo, J.H. Bitter, A.J. van Dillen and K.P. de Jong, J. Catal. 214 (2003) 78 / Chapter 6 of this thesis.
16. R. Burch and A.R. Flambard, J. Catal. 78 (1982) 389.
17. M. Haruta, S. Tsubota, T. Kobayashi, M.J. Genet and B. Delmon, J. Catal. 144 (1993) 175.
18. J.H. Bitter, K. Seshan and J.A. Lercher, J. Catal. 171 (1997) 279.
19. D.E. Ramaker, J. de Graaf, J.A.R. van Veen and D.C. Koningsberger, J. Catal. 203 (2001) 7.
20. D.C. Koningsberger, J. de Graaf, B.L. Mojet, D.E. Ramaker and J.T. Miller, Appl. Catal. A Gen. 191 (2000) 205.
21. B.L. Mojet, J.T. Miller, D.E. Ramaker and D.C. Koningsberger, J. Catal. 186 (1999) 373.
22. V. Ponec and G.C. Bond, Stud. Surf. Sci. Catal. 95 (1995) 234.
23. A. Yu. Stakheev and L.M. Kustov, Appl. Catal. A Gen. 188 (1999) 3.
24. A.J. van Dillen, J.W. Geus, L.A.M. Hermans and J. van der Meijden, Stud. Surf. Sci. Catal. 2 (1977) 677.
25. M.L. Toebes, J.H. Bitter, A.J. van Dillen and K.P. de Jong, Catal. Today 76 (2002) 33 / Chapter 2 of this thesis.
26. M.L. Toebes, J.M.P. van Heeswijk, J.H. Bitter, A.J. van Dillen and K.P. de Jong, Carbon, in print / Chapter 3 of this thesis.
27. Oudenhuijzen, M.K., Bitter, J.H., and Koningsberger, D.C., J. Phys. Chem. B 105 (2001) 4616.
28. J.J.F. Scholten, A.P. Pijpers and A.M.L. Hustings, Catal. Rev.-Sci. Eng. 27 (1985) 151.
29. M. Vaarkamp, J.C. Linders and D.C. Koningsberger, Physica B 208 & 209 (1995) 159.
30. D.C. Koningsberger, B.L. Mojet, G.E. van Dorssen and D.E. Ramaker, Top. Catal. 10 (2000) 143.

31. D.C. Koningsberger, J. de Graaf, B.L. Mojet, D.E. Ramaker, and J.T. Miller, Appl. Catal. A Gen. 191 (2000) 205.
32. O.L.J. Gijzeman, unpublished results.
33. H.P. Boehm, Adv. Catal. 16 (1966) 179.
34. T.G. Ros, A.J. van Dillen, J.W. Geus and D.C. Koningsberger, Chem. Eur. J. 8 (2002) 1151.
35. H. He, J. Klinowski, M. Fortser and A. Lerf, Chem. Phys Lett. 287 (1998) 53.
36. M.L. Toebes, J.H. Bitter, A.J. van Dillen and K.P. de Jong, J. Phys. Chem. B, submitted / Chapter 5 of this thesis.
37. M.K. Oudenhuijzen, J.H. Bitter and D.C. Koningsberger, J. Phys. Chem. B. 105 (2001) 4616.
38. B.J. Kip, F.B.M. Duivenvoorden, D.C. Koningsberger and R. Prins, J. Catal. 105 (1987) 26.
39. J. de Graaf, A.J. van Dillen, K.P. de Jong and D.C. Koningsberger, J. Catal. 203 (2001) 307.
40. Y. Zhang, M.L. Toebes, W.E. O'Grady, A. van der Eerden, K.P de Jong and D.C. Koningsberger, J. Phys. Chem. B, submitted.
41. R.T. Morrison and R.N. Boyd, Organic Chemistry, Prentice Hall Int, New Jersey 1992.
42. M.L. Toebes, T.A. Nijhuis, J. Hájek, J.H. Bitter, A.J. van Dillen, D.Yu. Murzin, and K.P. de Jong, in preparation / Chapter 8 of this thesis.
43. C.D. Wagner, W.M.Riggs, L.E. Davis, J.F. Moulder and G.E. Muilenberg (Eds), Handbook of X-Ray Photoelectron Spectroscopy, Perkin-Elmer Corporation, Minnesota 1978.
44. B.L. Mojet, M.J. Kappers, J.C. Muijsers, J.W. Niemantsverdriet, J.T. Miller, F.S. Modica and D.C. Koningsberger, Stud. Surf. Sci. Catal. 84 (1994) 909.
45. M.K. Oudenhuijzen, Ph.D. thesis, Utrecht University, 2002.

8

Support Effects in the Hydrogenation of Cinnamaldehyde over Carbon Nanofiber-Supported Platinum Catalysts

Part II: Kinetic Study

Abstract

Carbon nanofiber-supported platinum catalysts with a narrow and stable platinum particle size distribution (1-2 nm) were prepared, one with a considerable amount of oxygen support surface groups (PtCNF, 2.8 acidic O atoms/nm^2) and one with a much smaller amount (PtCNF973, 0.06 acidic O atoms/nm^2). Their catalytic performance was compared in the liquid-phase hydrogenation of cinnamaldehyde in a semi-batch reactor at 383 K using hydrogen pressures of 2.8-6.8 MPa and a cinnamaldehyde concentration in the range 14-345 mol/m^3. The observed overall catalytic activity increased by a factor of 8 with the removal of the oxygen support groups. The observed activity of PtCNF973 is one of the highest reported in literature for platinum catalysts in this reaction. The differences in intrinsic activity upon thermal treatment are much larger, since internal diffusion limitation slows down the reaction rate for the most active catalyst. Using a model including both Langmuir-Hinshelwood kinetics and mass transfer effects we found that the intrinsic reaction rate increased up to a factor of 120 with the removal of the oxygen-containing surface groups. These results suggest that hydrogenation is assisted by adsorption of the benzene ring of cinnamaldehyde on the non-polar CNF support surface after removal of the oxygen-containing groups.

Introduction

The selective hydrogenation of α,β-unsaturated aldehydes to unsaturated alcohols is a key step especially in the preparation of various fine chemicals and is often used in the literature as a sensitive test reaction [1-5]. Important factors influencing the activity and selectivity are amongst others, the active metal, the catalyst support properties, the metal particle size and the presence of promoters such as a second metal or alkaline solutions. A very commonly used catalyst system for this type of reactions is platinum supported on graphitic carbon [3,6-9].

Our study of a series of carbon nanofiber (CNF)-supported platinum catalysts [10] and earlier work on Ru/CNF catalysts [11] have shown a continuous trend in activity and selectivity in the liquid-phase hydrogenation of cinnamaldehyde with decreasing numbers of oxygen-containing support surface groups. The observed rate of cinnamaldehyde conversion was enhanced by a factor of 22 (Ru) and 25 (Pt) as the number of acidic oxygen-containing groups per nm^2 decreased from 2.8 to 0.06, mainly due to a strong increase in hydrogenation rate of the C=C bond. Only a slight increase in C=O bond hydrogenation rate was observed, resulting in a large shift in selectivity towards hydrocinnamaldehyde.

A possible explanation for the change in catalytic properties involves an indirect support effect on catalysis *via* the electronic state of the metal particles. The density of states of the metal particles may shift to a higher binding energy with decreasing electron richness of the support atoms, which influences the catalytic behavior [12-14]. However, we have shown that with the Pt/CNF catalytic system the electronic properties of the platinum particles do not change to a large extent with a varying number of oxygen-containing groups [10]. Therefore, it is not likely that the changes in catalytic performance with decreasing numbers of oxygen-containing support groups are primarily brought about by an electronic effect.

An alternative explanation for a support effect on the catalytic performance can be found in its direct involvement in the catalytic action, *e.g. via* adsorption of the substrate molecules. A few examples for this are reported in the literature. Burch *et al.* [15,16] observed that titania-supported nickel particles exhibited a fifty times higher specific activity for the formation of methane from CO/H_2 than silica-supported nickel catalysts due to active sites at the metal-titania interface. Also with gold on titania catalysts the metal-support interface plays a essential role in the CO oxidation by O_2. In this reaction probably oxygen adsorbs on oxygen vacancy sites in the titania surface while CO adsorbs on gold [17,18]. For CO_2/CH_4 reforming over zirconia-supported platinum catalysts, Bitter *et al.* [19] proposed that CO_2 is activated on the support by formation of carbonate species that react with methane adsorbed on platinum.

We studied to what extent oxygen-containing surface groups on CNF influence the catalytic performance of CNF-supported noble metal catalysts in the hydrogenation of cinnamaldehyde. We found that at increasing treatment temperatures of Pt/CNF, the CNF

surface changes gradually from polar to non-polar due to the removal of oxygen-containing surface groups, which might affect the adsorption location or mode of the organic compound and thus affect the role of the support in the reaction. We have used kinetic modeling to quantify the impact of the support on the catalytic action.

Often a first order rate law has been used to model the cinnamaldehyde hydrogenation experiments, however, this simple rate equation does not describe the cinnamaldehyde kinetics satisfactory [20-24]. Tronconi *et al.* [25], Neri *et al.* [26] and Vergunst *et al.* [27] provide a more extensive kinetic model for this complex reaction. Tronconi *et al.* and Neri *et al.* studied the effect of the temperature using Langmuir-Hinshelwood kinetics. They assumed that adsorption of reactants and products is reversible and competitive while hydrogen is activated on a different site and does not compete with the organic compounds. The rate-determining step is considered to be the reaction between atomic hydrogen and the adsorbed organic compound. A two-site model is assumed, one type of site for hydrogenation of the carbonyl bond (C=O) and another type of site for olefinic bond (C=C) hydrogenation. They found that other models (using one type of site only or using competitive hydrogen adsorption) gave less satisfactory results. Vergunst *et al.* [27] compared three different kinetic models for the hydrogenation of cinnamaldehyde over Pt/C/monolithic catalysts. A single-site and a two-site model with the surface reactions as rate-controlling steps were unable to fit the experimental data satisfactory. They concluded that a single-site model in which both adsorption, surface reaction and desorption are all rate determining steps gives the best results. However, the effect of hydrogen pressure and initial cinnamaldehyde concentration on the activity and selectivity could not be included in the model successfully.

In the current study two CNF-supported platinum catalysts with small and uniform metal particles (1-2 nm) were investigated, one with a considerable amount of oxygen support surface groups (PtCNF) and one with a much smaller amount (PtCNF973). Their catalytic performance was measured in the liquid-phase hydrogenation of cinnamaldehyde in a semi-batch reactor at 383 K. Kinetic models were used to fit the experimental results obtained with varying concentrations of cinnamaldehyde ($[CALD]_0$ = 14-345 mol/m^3) and hydrogen pressures (P_{H2} = 2.8-6.8 MPa). Reaction rate constants for the different steps and adsorption constants were derived from the model fits taking into account internal diffusion limitation with the most active catalyst PtCNF973. An explanation for the enhanced activity and shifted selectivity with decreasing oxygen-containing surface groups based on the kinetic modeling results is proposed.

Experimental

Catalyst preparation

A detailed description of the growth of the CNF from silica-supported nickel can be found in Chapter 2 of this thesis and [28]. The CNF with an average diameter of 25 nm were refluxed for 1 h in a 1 M KOH solution in order to remove the silica support. For removal of nickel and introduction of oxygen-containing groups, the CNF were refluxed in concentrated nitric acid for 2 h and washed thoroughly with demi-water.

Platinum (intended 5 wt%) was deposited on the fibers according to a homogeneous deposition precipitation method [29,30]. A suspension of 1 g CNF in 250 ml demi-water was acidified (pH=3) and heated up to 363 K under inert atmosphere. Subsequently, 0.41 g urea (Acros) and 0.52 g $Pt(NH_3)_4(NO_3)_2$ (Aldrich) were added under vigorous stirring. The pH was monitored to follow the process and to indicate its completeness. The loaded CNF were filtered and washed thoroughly with demi-water, dried at 353 K in an N_2 flow and reduced in H_2 at 473 K for 1 h (heating rate = 5 K/min). Following reduction the samples were exposed to air.

A sample of the freshly reduced catalyst (PtCNF) was heat-treated in an N_2 flow for 2 h at 973K (PtCNF973), to remove (part of) the oxygen-containing groups from the CNF surface.

Catalytic experiments

The liquid-phase hydrogenation of cinnamaldehyde was studied in a 500 ml stirred semi-batch reactor equipped with a sample port, a reagent injection port, gas inlet and vent.

The catalyst samples (0.2 gram), consisting of spherical catalyst particles with an average radius of 60 μm as determined on the basis of SEM images, were re-reduced in *i*-propanol (220 ml) at 383 K and 2.8 MPa H_2 pressure for 30 minutes in the autoclave (1500 rpm) prior to the introduction of cinnamaldehyde (CALD) (0.40-10.0 g = 14-345 mol/m^3). All reactions were conducted at 383 K using total pressures of 3.0, 5.0 and 7.0 MPa(g). These total pressures result, after correction for the vapor pressure of *iso*-propanol at 383 K, in hydrogen partial pressures of 2.8, 4.8 and 6.8 MPa. Also experiments with the two primary products, hydrocinnamaldehyde (HALD) and cinnamyl alcohol (CALC), were performed at 383 K and a hydrogen pressure of 4.8 MPa. Samples of the reaction mixture were withdrawn periodically and analyzed on a gas chromatograph (Hewlett Packard 5890 Series with autosampler) using an HP5 capillary column (30 m x 0.32 mm; 0.25 μm film thickness).

Results and Discussion

CNF-supported platinum catalysts

The metal loading of the PtCNF and PtCNF973 catalysts as determined with XRF was found to be 3.6 wt%. In Figure 1 TEM images of PtCNF and PtCNF973 are shown. The platinum particles of PtCNF are small (1-2 nm) and homogeneously distributed over the support surface. For PtCNF973 the platinum particles are slightly larger, ranging from 1-3 nm. From H_2-chemisorption measurements, platinum dispersions of 0.79 and 0.49 were derived corresponding with an average particle size of 1.4 nm for PtCNF and 2.3 nm for PtCNF973. EXAFS data of PtCNF confirm the TEM and H_2-chemisorption results; from the measured coordination number of 5.2, an average particle size of 1.0 nm could be calculated. TEM examination of the spent catalysts demonstrated that during the hydrogenation experiment no significant change in the platinum particle size and distribution had occurred. Although a slight increase in average platinum particle size is observed after heat treatment at 973 K it is highly unlikely that this change in particle size is the main cause of the large increase in activity and the shift in selectivity. First of all, in Chapter 7 we have demonstrated that a continuous trend was observed in the activity with decreasing numbers of acidic oxygen groups while the average particle sizes of the catalysts treated at 573 and 773 K were similar to the platinum particle size found with PtCNF [10]. Secondly, a particle size effect is unlikely to bring about such huge changes in catalytic performance.

The amount of oxygen present on the CNF support and the Pt/CNF catalysts after the different treatments was assessed using XPS and TGA-MS. With the unloaded supports also acid-base titrations were performed to establish the number of carboxylic sites at the exterior surface of the CNF. PtCNF contains a total number of 6 O atoms/nm^2 while the number of acidic sites corresponds to 2.8 O atoms/nm^2. All techniques showed a much lower level of the total number of oxygen (2.4 O atoms/nm^2) and the number of acidic oxygen-containing groups (0.06 O atoms/nm^2) on the catalyst after treatment in nitrogen at 973 K. Our elaborate investigation on the size of the platinum particles of the Pt/CNF catalysts and change in number of (surface) oxygen groups with the pretreatment can be found elsewhere [10,31].

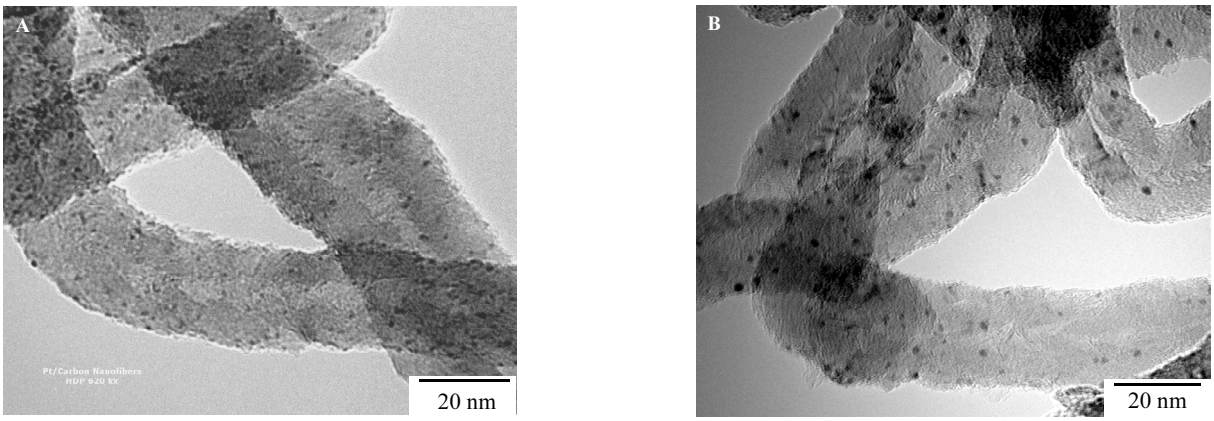

Figure 1. TEM images of 3.6 wt% CNF-supported platinum catalysts A) PtCNF and B) PtCNF973.

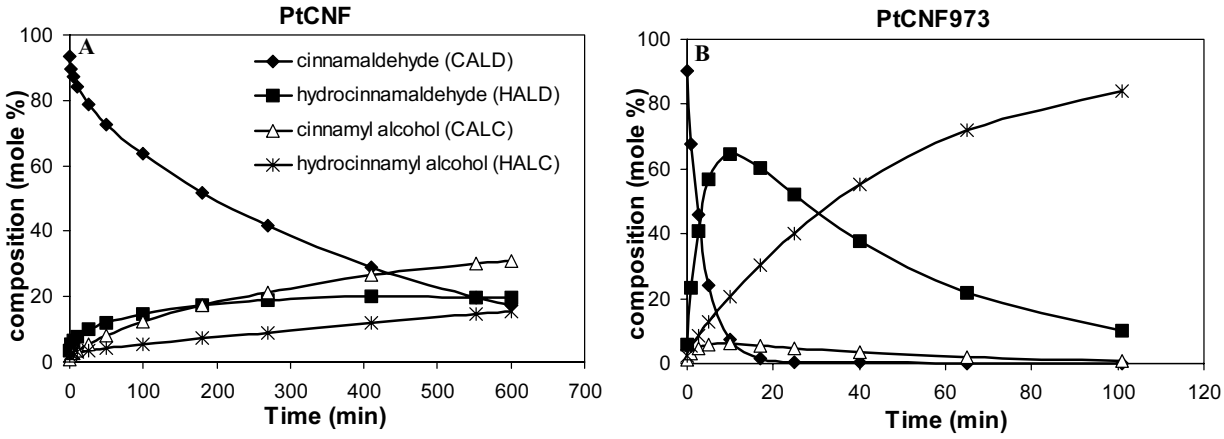

Figure 2. Cinnamaldehyde conversion ($[CALD]_0$ = 103 mol/m^3) and product distribution as function of time on stream obtained at 383K and a hydrogen pressure of 4.8 MPa over A) PtCNF and B) PtCNF973.

Catalytic results

General

Typical concentration-time plots of cinnamaldehyde hydrogenation experiments with both PtCNF and PtCNF973 under standard reaction conditions (103 mol/m^3 CALD, hydrogen pressure 4.8 MPa, T = 383 K) are displayed in Figure 2. Especially for the most active catalyst (PtCNF973) the consecutive reaction is evident, *i.e.* the primary products HALD and CALC are hydrogenated to hydrocinnamyl alcohol (HALC). The concentration-time plots of PtCNF973 in Figure 2 point towards Langmuir-Hinshelwood (LH) type kinetics. Strong adsorption of the reactant CALD occurs, due to which the primary products (HALD and CALC) react only slowly to the final product (HALC) as long as CALD is still present. With PtCNF the LH kinetic mechanism is less clear, since all three products are formed in significant amounts from the start of the experiment. For an adsorption type mechanism this implies that the relative adsorption strength of CALD is not much higher than that of the products.

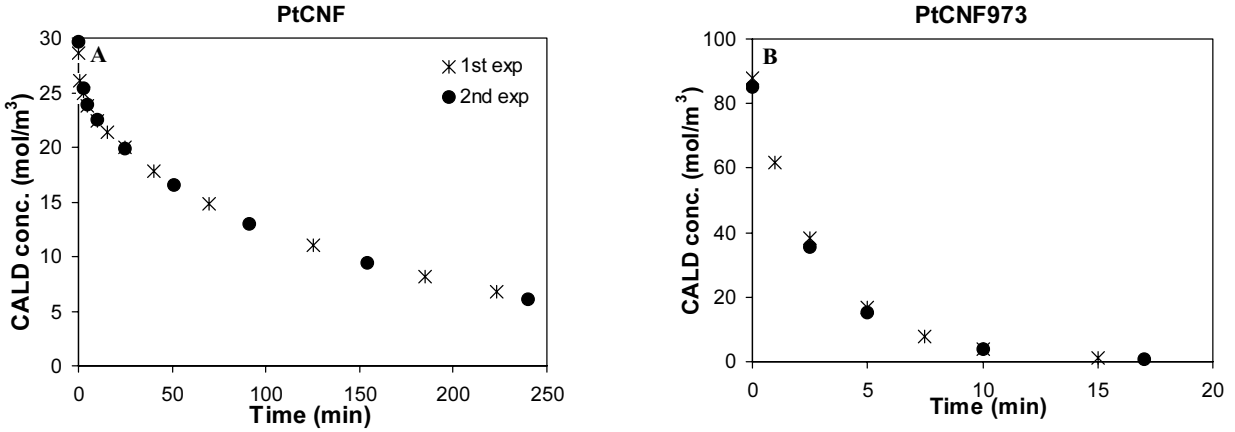

Figure 3. The reproducibility of results of the cinnamaldehyde hydrogenation over A) PtCNF ($[CALD]_0$ = 34 mol/m^3) and B) PtCNF973 ($[CALD]_0$ = 103 mol/m^3), measured at standard conditions (T = 383 K and P_{H2} = 4.8 MPa).

From the decrease in the concentration of CALD with time an initial activity was calculated. Under standard reaction conditions for PtCNF the initial activity is 1.9 mmol $*min^{-1}*g_{cat}^{-1}$ and for PtCNF973 14.9 $mmol*min^{-1}*g_{cat}^{-1}$. TOFs of respectively 0.23 s^{-1} and 3.3 s^{-1} were found, calculated as mole CALD hydrogenated per mole of platinum surface atom per second. The increased activity of PtCNF973 is mainly caused by a large increase in HALD formation rate as can be seen in Figure 2. Apparently the rate of hydrogenation of the C=C bond is strongly enhanced when most of the oxygen-containing groups are removed from the CNF surface. The selectivities towards CALC and HALD determined at 60% conversion are 37% and 32% for PtCNF and 8% and 74% for PtCNF973, respectively.

Duplicate experiments were performed with both PtCNF and PtCNF973 (Figure 3) showing rates and selectivities (not shown) to the various products to be the same, indicating excellent reproducibility. To investigate whether the catalysts became irreversibly deactivated, three consecutive experiments with one batch of catalyst PtCNF were executed. Between the runs the catalyst was washed repeatedly with *iso*-propanol and dried. The activity of the catalysts in the three runs was comparable, thus proving the absence of irreversible deactivation.

Influence H_2 pressure

Figure 4 displays the effect of hydrogen pressure on the activity of PtCNF ($[CALD]_0$ = 103 mol/m^3) and PtCNF973 ($[CALD]_0$ = 345 mol/m^3). From a comparison of the activities measured at 2.8 and 4.8 MPa for PtCNF it may be concluded that the rate is almost pressure independent, which might indicate that for this pressure range and catalyst hydrogen is not involved in the rate-determining step. However, the activity at a hydrogen pressure of 6.8 MPa is significantly higher, which point to a hydrogen order >0. For PtCNF973 the influence of the hydrogen pressure is more pronounced, however, the order in hydrogen is <1. The precise orders in hydrogen cannot be established from these data, for that more experiments would be required. With both catalysts no influence of the hydrogen pressure on the selectivities was observed.

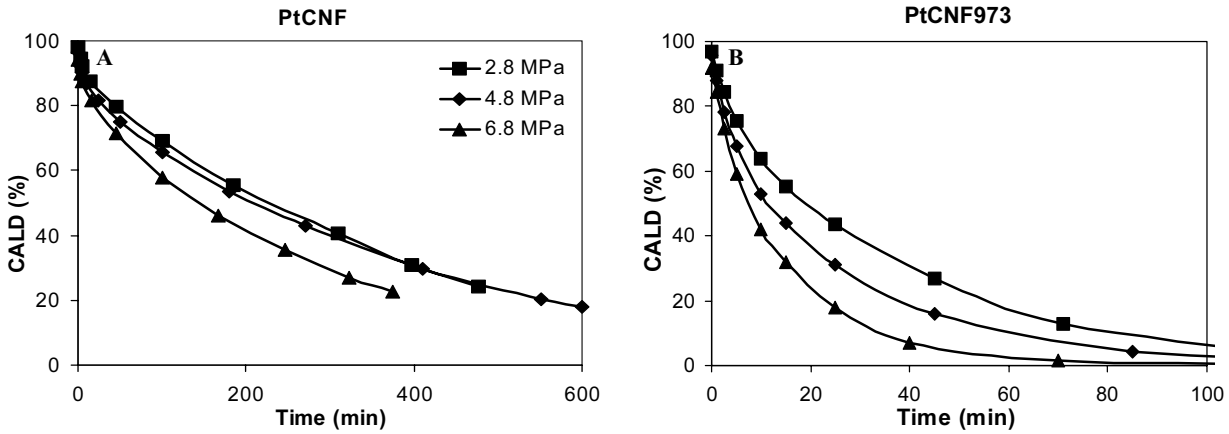

Figure 4. Effect of hydrogen pressure on cinnamaldehyde conversion at 383 K over A) PtCNF ($[CALD]_0$ = 103 mol/m^3) and B) PtCNF973 ($[CALD]_0$ = 345 mol/m^3).

Influence initial CALD concentration

In Figure 5 the initial hydrogenation rates for both catalysts are plotted versus the initial CALD concentration ($[CALD]_0$) measured at 4.8 MPa and 383 K. First, especially for PtCNF973, a strong increase in the initial activity with increasing $[CALD]_0$ is observed which levels off at higher concentrations. This, again, is in accordance with LH adsorption kinetics, in which at low reactant concentrations the fractional occupancy of the catalyst surface increases linearly with the concentration in the solution and, with this, the activity. At higher reactant concentrations, however, the surface is almost fully occupied and the activity becomes independent of $[CALD]_0$.

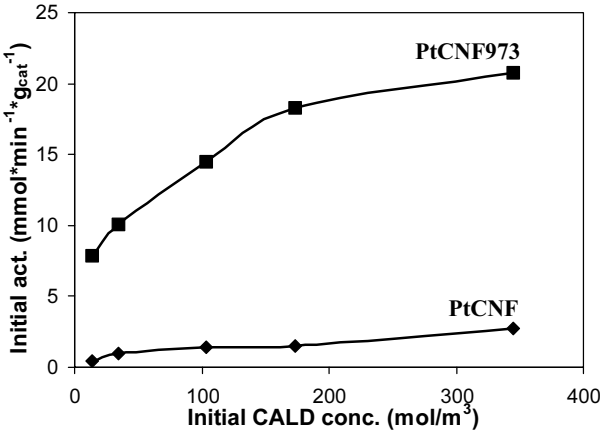

Figure 5. Effect of initial CALD concentration on initial activity at 383 K and hydrogen pressure of 4.8 MPa for PtCNF and PtCNF973.

The results collected in Figure 6 show that not only the activity but also the selectivity is a function of the initial CALD concentration. For PtCNF S_{CALC} increases with increasing

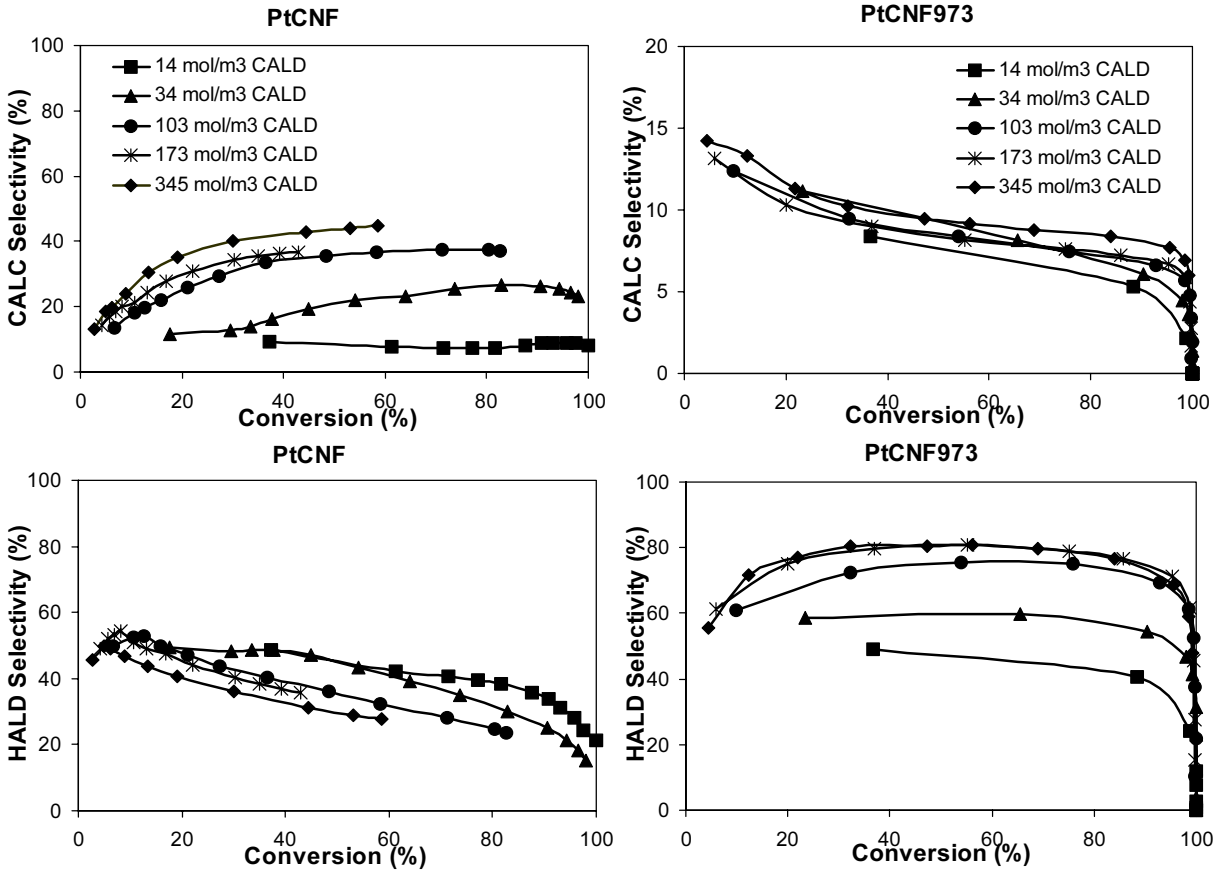

Figure 6. Effect of initial CALD concentration on CALC and HALD selectivities for PtCNF and PtCNF973 (T = 383 K and P_{H2} = 4.8 MPa).

CALD concentration at the expense of S_{HALD} and S_{HALC} (not shown). With PtCNF973 S_{CALC} is very small and practically independent of the initial CALD concentration. Nevertheless, S_{HALD} changes drastically with $[CALD]_0$: the higher the initial CALD concentration, the higher S_{HALD}, although, beyond a CALD concentration of 173 mol/m^3 no further increase in S_{HALD} is observed. In literature a shift in selectivity for the CALD hydrogenation is ascribed to a change in adsorption mode with varying initial CALD concentration [32,33]. At high concentrations the CALD molecules are supposed to adsorb perpendicular to the platinum surface with the aromatic rings in a parallel arrangement, thereby enhancing the hydrogenation rate of the carbonyl group. At low initial CALD the molecules are supposed to adsorb flat on the surface. For PtCNF an increase in S_{CALC} is observed with increasing $[CALD]_0$, which is in agreement with this model. However, in our study very small platinum particles are used, making the parallel arrangement of CALD molecules on the metal surface less probable. For PtCNF973, on the other hand, S_{CALC} does not change and mainly S_{HALD} is increasing with the $[CALD]_0$. The shift in S_{HALD} is in the other direction, as one would expect from the model with the changing adsorption arrangement. An alternative explanation for the shift in selectivity with the concentration has been proposed by Nijhuis *et al.* [34] who ascribed the dependency of the selectivities on the initial reactant concentration for the selective hydrogenation of 3-methyl-1-pentyn-3-ol to internal diffusion limitation of the organic reactant at the lowest concentrations.

Gas-liquid diffusion limitation

In the type of autoclave used, with a self inducing stirrer at 1500 rpm, a conservative estimate for the G-L mass transfer rate of hydrogen is $k_L.a$ =0.1 s^{-1}. With a hydrogen concentration of 260 mol.m^{-3} (P_{H2} = 4.8 MPa [35]), a hydrogen transfer rate of about 26 mol.m^{-3}.s^{-1} can be obtained. The highest measured rate is 0.31 mol.m^{-3}.s^{-1}. It can be calculated that in this case the bulk liquid would be 99% saturated with hydrogen, making G-L mass transfer limitation highly unlikely.

Intra-particle diffusion limitation

We stated as a possibility that the observed influence of the initial CALD concentration on the product selectivities could point towards internal diffusion limitations, especially with PtCNF973 since this catalyst is much more active than PtCNF. To evaluate the presence of internal diffusion limitations, we use the Weisz-Prater number (Equation (1)).

$$\Phi = \eta\phi^2 = \frac{\rho_p \cdot r_{v,obs} \cdot d_p^{\,2}}{36 \cdot D_{eff} \cdot c_s}\left(\frac{n+1}{2}\right) < 0.15 \qquad (1)$$

In Table 1 the parameters used for the calculations are given. The diffusion coefficients for the organic compounds and hydrogen were estimated using the approximation method of

Table 1. Weisz-Prater numbers (Φ) for hydrogen and CALD in the reaction performed under standard conditions (T = 383 K, P_{H2} = 4.8 MPa and $[CALD]_0$ = 14 mol/m^3) with PtCNF and PtCNF973 and the parameters used for the calculations.

Parameter	PtCNF	PtCNF973
ρ_p (kg/m^3)	1100	1100
$r_{w,obs}$ (mol/(kg$_{cat}$.s)	0.007	0.132
d_p (m)	$120 \cdot 10^{-6}$	$120 \cdot 10^{-6}$
$D_{eff,CALD}$ (m^2/s)	$2.0 \cdot 10^{-9}$	$2.0 \cdot 10^{-9}$
$D_{eff,H2}$ (m^2/s)	$8.4 \cdot 10^{-9}$	$8.4 \cdot 10^{-9}$
c_{CALD} (mol/m^3)	14	14
c_{H2} (mol/m^3)	260	260
n	0-1	0-1
Φ_{CALD}	0.05-0.11	1.1-2.1
Φ_{H2}	0.0007-0.0013	0.013-0.027

Wilke and Chang [36]. In view of the Langmuir-Hinshelwood type of kinetics Weisz-Prater numbers were calculated for both an order of 0 and an order of 1.

The Weisz-Prater numbers (Φ) were calculated for hydrogen and CALD in the reaction performed under standard conditions (T = 383 K, P_{H2} = 4.8 MPa). In these calculations the initial CALD concentration was used at which internal diffusion limitation is most probable ($[CALD]_0$ = 14 mol/m^3). The results for both catalysts are given in Table 1. For PtCNF and PtCNF973 the Weisz-Prater numbers for hydrogen are smaller than 0.15, indicating the absence of internal diffusion limitations. For CALD, on the other hand, using PtCNF a value close to 0.15 was found. Using PtCNF973 a value larger than 0.15 was obtained, pointing towards internal mass transport effects. These calculations are only an indication since the limit of 0.15 is not strict and the calculations are partly based on roughly estimated parameters. Therefore, intra-particle mass transfer is taken into account in the kinetic modeling.

Kinetic modeling

The kinetic experiments were modeled using the Athena Visual Workbench package (v. 8.0, Stewart & Associates Engineering Software). Based on the concentration-time results (Figure 2) and the activity versus initial CALD concentration plot (Figure 5) LH adsorption kinetics were chosen, which is in agreement with literature [25-27]. We assumed that hydrogen adsorption is dissociative and non-competitive with the organic molecules (*i.e.* on a separate site) and follows a LH type of adsorption behavior. Amongst others Tronconi *et al.* and Neri *et al.* found that this gave the best results [25,26]. For PtCNF973 an experimental order in hydrogen of approximately 0.5 is observed. This 0.5 order implies that the rate-

determining step (r.d.s.) involves a reaction with one adsorbed hydrogen atom. For the PtCNF catalyst the experiments pointed towards an order in hydrogen close to 0, meaning that over this catalyst the reaction is almost independent of the hydrogen concentration. By using a large hydrogen adsorption constant (K_H) in the kinetic model an order in hydrogen of zero is obtained, while using a much smaller K_H will result in an order in hydrogen of 0.5. These values for K_H result in pseudo reaction orders of the model in agreement with the experimental observed reaction orders.

Both a one- and a two-site model were investigated. In the one-site model C=C and C=O are hydrogenated on the same type of site and in the latter model two different types of sites for C=C and C=O hydrogenation are used. The best results were obtained with the one-site model, therefore we focused on this type of model for fitting our data. Other kinetic rate expressions (*e.g.* competitive hydrogen adsorption and a model for PtCNF973 without internal diffusion limitation) were also explored, but these expressions did not lead to satisfactory results.

Summarizing, the assumptions made to derive our kinetic model are:

- LH adsorption type kinetics
- Only one type of site for the organic molecules is present. The hydrogenation of C=C and C=O occurs at the same site.
- The surface reactions are rate determining, adsorption and desorption are considered to be in quasi-equilibrium.
- Hydrogen shows non-competitive and dissociative adsorption.
- Hydrogenation reactions using the primary products have shown that reactions are irreversible as is found in the literature [27,33].
- Spherical catalyst particles of uniform size
- No G-L mass transfer limitations.
- R.d.s: reaction between an adsorbed organic species and one adsorbed hydrogen atom.

A scheme of the elementary steps considered is depicted in Figure 7. Since adsorption and desorption steps are in quasi-equilibrium a simplified scheme with the elementary hydrogenation steps can be utilized (Figure 8). According to the assumptions described above we have defined the reaction rate of the hydrogenation of CALD to HALD (reaction 1) as:

$$r_{1,I} = k_1 \cdot \theta_{CALD} \cdot \theta_H \tag{8}$$

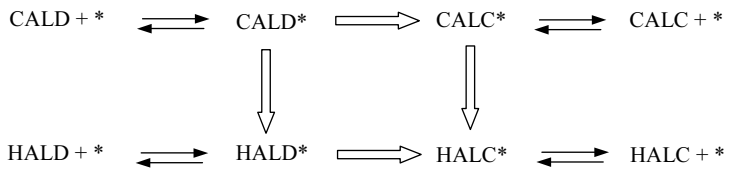

Figure 7. The elementary steps in cinnamaldehyde hydrogenation.

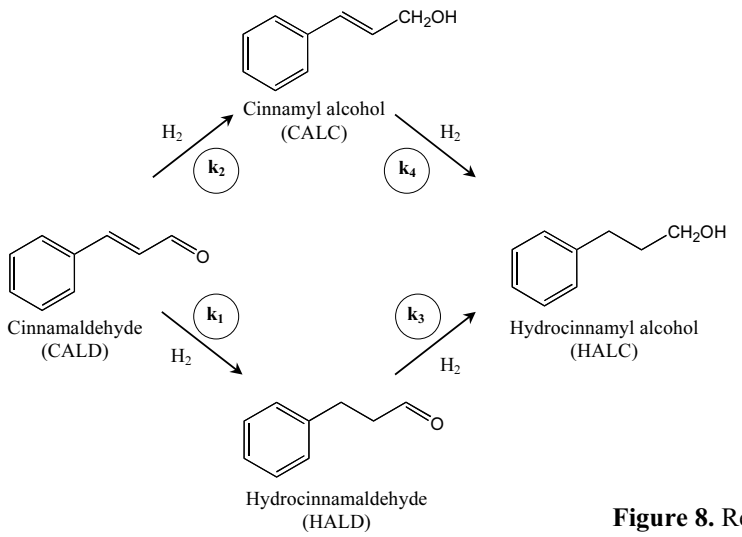

Adsorption and desorption of reactants and products:

$H_2 + 2\,\theta_{\#} \rightleftharpoons 2\,\theta_H$ [3]

$CALD + \theta_* \rightleftharpoons \theta_{CALD}$ [4]

$HALD + \theta_* \rightleftharpoons \theta_{HALD}$ [5]

$CALC + \theta_* \rightleftharpoons \theta_{CALC}$ [6]

$HALC + \theta_* \rightleftharpoons \theta_{HALC}$ [7]

Figure 8. Relevant steps of the proposed kinetic model.

The number of active sites is included in the rate constant. From equation (3) of the scheme (Figure 8) it follows that:

$$K_H = \frac{\theta_H^2}{\theta_{\#}^2 \cdot c_{H_2}} \longrightarrow \theta_H = \theta_{\#} \cdot \sqrt{c_{H_2} \cdot K_H} \quad \text{and with} \quad \theta_{\#} + \theta_H = 1 \quad \text{this results in:}$$

$$\theta_H = \frac{\sqrt{c_{H_2} \cdot K_H}}{1 + \sqrt{c_{H_2} \cdot K_H}} \tag{9}$$

And from equation (4) we can derive:

$$K_{CALD} = \frac{\theta_{CALD}}{\theta_* \cdot c_{CALD}} \qquad \theta_{CALD} = c_{CALD} \cdot K_{CALD} \cdot \theta_* \tag{10}$$

Equation (5), (6) and (7) give respectively:

$$\theta_{HALD} = c_{HALD} \cdot K_{HALD} \cdot \theta_* \tag{11}$$

$$\theta_{CALC} = c_{CALC} \cdot K_{CALC} \cdot \theta_* \tag{12}$$

$$\theta_{HALC} = c_{HALC} \cdot K_{HALC} \cdot \theta_* \tag{13}$$

The site balance is as follows:

$$\theta_* + \theta_{CALD} + \theta_{HALD} + \theta_{CALC} + \theta_{HALC} = 1 \tag{14}$$

Combining (9) to (13) in the site balance equation results in

$$\theta_* = \frac{1}{1 + c_{CALD} \cdot K_{CALD} + c_{HALD} \cdot K_{HALD} + c_{CALC} \cdot K_{CALC} + c_{HALC} \cdot K_{HALC}} \tag{15}$$

Using equation (8)-(10) the rate expression for the hydrogenation of CALD to HALD (reaction 1) can be derived:

$$r_1 = k_1 \cdot \left(c_{CALD} \cdot K_{CALD} \cdot \theta_*\right) \cdot \theta_H \tag{16}$$

And with (9) and (15) this results in:

$$r_1 = \frac{k_1 \cdot c_{CALD} \cdot K_{CALD}}{\left(1 + c_{CALD} \cdot K_{CALD} + c_{HALD} \cdot K_{HALD} + c_{CALC} \cdot K_{CALC} + c_{HALC} \cdot K_{HALC}\right)} \cdot \frac{\sqrt{c_{H_2} \cdot K_H}}{1 + \sqrt{c_{H_2} \cdot K_H}} \tag{17}$$

Analogously, the rate expressions of the hydrogenation of CALD to CALC (reaction 2), HALD to HALC (reaction 3) and CALC to HALC (reaction 4) are:

$$r_2 = \frac{k_2 \cdot c_{CALD} \cdot K_{CALD}}{\left(1 + c_{CALD} \cdot K_{CALD} + c_{HALD} \cdot K_{HALD} + c_{CALC} \cdot K_{CALC} + c_{HALC} \cdot K_{HALC}\right)} \cdot \frac{\sqrt{c_{H_2} \cdot K_H}}{1 + \sqrt{c_{H_2} \cdot K_H}} \tag{18}$$

$$r_3 = \frac{k_3 \cdot c_{HALD} \cdot K_{HALD}}{\left(1 + c_{CALD} \cdot K_{CALD} + c_{HALD} \cdot K_{HALD} + c_{CALC} \cdot K_{CALC} + c_{HALC} \cdot K_{HALC}\right)} \cdot \frac{\sqrt{c_{H_2} \cdot K_H}}{1 + \sqrt{c_{H_2} \cdot K_H}} \tag{19}$$

$$r_4 = \frac{k_4 \cdot c_{CALC} \cdot K_{CALC}}{\left(1 + c_{CALD} \cdot K_{CALD} + c_{HALD} \cdot K_{HALD} + c_{CALC} \cdot K_{CALC} + c_{HALC} \cdot K_{HALC}\right)} \cdot \frac{\sqrt{c_{H_2} \cdot K_H}}{1 + \sqrt{c_{H_2} \cdot K_H}} \tag{20}$$

The catalytic experiments have indicated that especially for PtCNF973 internal diffusion limitation is present; therefore we have included a term in our model for the diffusion of reactants and products in the catalyst particle. The differential equation for diffusion combined with reaction in a spherical catalyst particle is:

$$\frac{\partial c}{\partial t} = D\left(\frac{\partial^2 c}{\partial z^2} + \frac{2}{z}\frac{\partial c}{\partial z}\right) - r_x \tag{21}$$

Equations are solved in a spherical coordinate system (with radius z), for hydrogen and the organic reactant and products (each with their appropriate diffusivity). The reaction rate r_x, in

which *x* is one of the organic compounds, is defined for CALD as r_1+r_2, for HALD as $-r_1+r_3$, for CALC as $-r_2+r_4$ and for HALC as $-r_3-r_4$. The corresponding boundary conditions are:

$$z = 0 \longrightarrow \frac{\partial c}{\partial z} = 0 \tag{22}$$

$$z = r_p \longrightarrow c = c_s \tag{23}$$

For hydrogen the bulk concentration is assumed to remain constant. The change in the bulk concentrations of the organic reactants/products is equal to the flux in/out of the catalyst particles. This can be described by the following differential equation for CALD:

$$\frac{\partial c_x}{\partial t} = -\frac{3}{r_p} \cdot \frac{c_{cat}}{\rho_{cat}} \cdot D_x \left.\frac{\partial c}{\partial z}\right|_{z=r_p} \tag{24}$$

with for all equations as starting values:

$$t = 0, \qquad c_{H_2} = c_{H_2,sat}, \qquad c_x = c_{x,0}$$

The differential equations were numerically solved and fitted to the experimental observations. The parameters that were fitted to the experiments are: k_1, k_2, k_3, k_4, K_{CALD}, K_{HALD}, K_{CALC}, K_{HALC}. Using PtCNF the K_H was assumed large ($1.0*10^3$) to represent the observed zero order in hydrogen and for PtCNF973 a small K_H ($1.0*10^{-4}$) was used to get the observed order in hydrogen of 0.5. In the experiments no inhibition of HALC was observed. To reduce the number of parameters, therefore the adsorption of the final product (HALC) was assumed to be zero. The diffusion coefficients for the organic compounds and for hydrogen used in the model amounted to $D_{eff,CALD} = 2 \cdot 10^{-9}$ m^2/s and $D_{eff,H2} = 8 \cdot 10^{-9}$ m^2/s. A set of nine (PtCNF973) respectively eleven (PtCNF) experiments were modeled simultaneously to determine the rate parameters and adsorption constants. The first two experimental points were not used for the fitting, since because of the high initial rate the relative uncertainty in the GC-analyses was considered too large (as a result of small deviations in the sampling time or the need for longer flushing of the sampling line). Consequently the time axis was shifted by 3-5 minutes. Weighing factors were used in the fitting inversely proportional to $[CALD]_0$ so that all experiments were taken into account in the fitting process equally.

Some of the resulting fits (including the experimental data) for PtCNF are plotted in Figure 9. From Figure 9 it can be concluded that the model fits the experimental data fairly well. In Figure 10 part of the fit results of PtCNF973 are plotted. In the experiment using 14 mol/m^3 CALD, the reactant is so rapidly converted that only the primary products (CALC and HALD) and the final product (HALC) are apparent in Figure 10a. Also for this catalyst the fits are satisfactory.

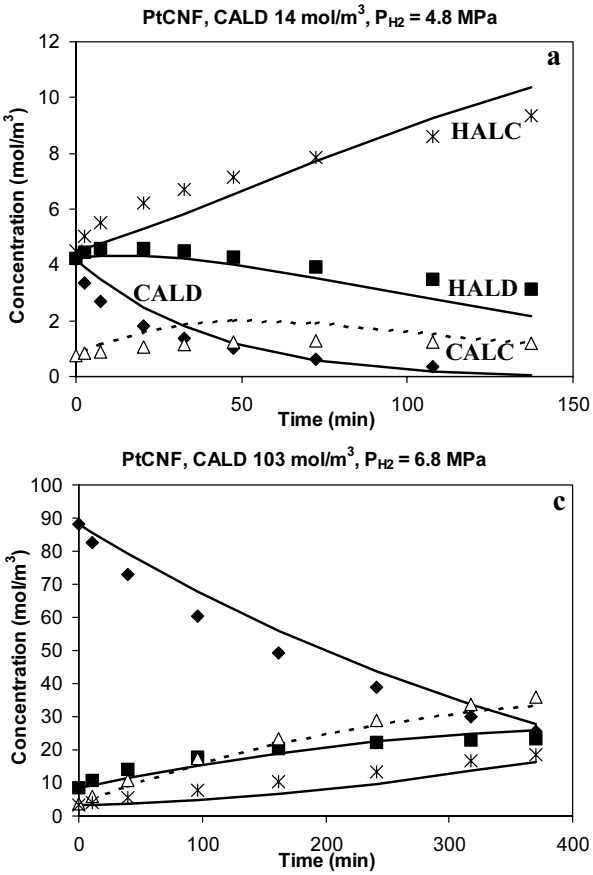

Figure 9. Experimental and model results of some of the cinnamaldehyde hydrogenation reactions over PtCNF (T = 383 K). Line: Fitted according to the model, dotted line is CALC. Markers: Experimental data ◆ CALD, ■ HALD, ∆ CALC and ✳ HALC.

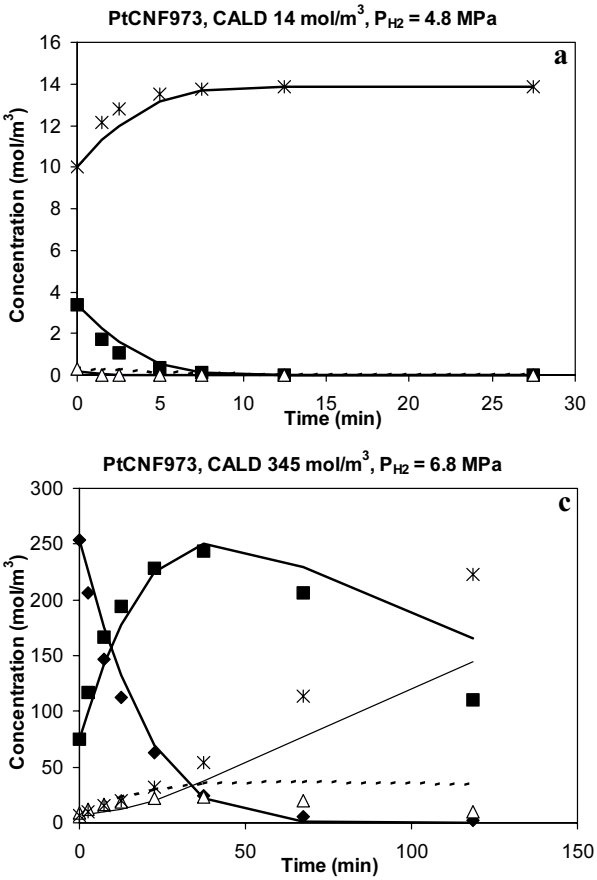

Figure 10. Experimental and model results of some of the cinnamaldehyde hydrogenation reactions over PtCNF973 (T = 383 K). Line: Fitted according to the model, dotted line is CALC. Markers: Experimental data ◆ CALD, ■ HALD, ∆ CALC and ✳ HALC.

Table 2. The values of the estimated parameters in the kinetic models.

Parameter	Units	PtCNF		PtCNF973	
			95% confidence interval		95% confidence interval
k_1	mol/(m_{cat}^3*s)	2.0	1.7-2.3	1600	1400-1800
k_2	mol/(m_{cat}^3*s)	3.3	3.0-3.6	210	150-280
k_3	mol/(m_{cat}^3*s)	34	29-39	260	170-350
k_4	mol/(m_{cat}^3*s)	1.5	1.1-1.9	16	1.6-30
K_{CALD}	m^3/mol	0.21		18	
K_{HALD}	m^3/mol	0.0078		5.7	
K_{CALC}	m^3/mol	0.21		18	
K_{HALC}	m^3/mol	0		0	
K_H	m^3/mol	1000		$1.0*10^{-4}$	
SSRES		$8.9*10^4$		$1.0*10^5$	

SSRES = Sum of squared residuals.

The rate constants and adsorption constants of reactants and products are given in Table 2. The sum of the residual squares that is also shown in Table 2 gives information about the quality of the fit. Since the values are almost the same, the quality of the fits for PtCNF and PtCNF973 are comparable. From this table it is clear that changes of two to three orders of magnitude in reaction rate constants are obtained from the model for PtCNF and PtCNF973. For these parameters the 95% confidence intervals are given, demonstrating that these changes in the reaction rate constants are highly significant.

However, it is difficult to directly compare the reaction rate constants for the two catalysts, since they have a strong correlation with the adsorption constants, which are also changing. Therefore, a better comparison is made by calculating the intrinsic reaction rates from these parameters according to equations (17)-(20). These intrinsic rates are given in Table 3. When comparing the results obtained, especially the differences in r_1 and r_2 are striking. r_1 increases by a factor of about 120 with the removal of most of the oxygen groups from the CNF and r_2 increases by a factor of around 9. r_3 and r_4 also increase, is it to a lower extent.

Table 3. Intrinsic reaction rates calculated from the modeled kinetic parameters (c_{H2} = 260 mol/m^3, c_x = 103 mol/m^3, T = 383 K).

Intrinsic reaction rate (mol/(m_{cat}^3*s))	PtCNF	PtCNF973
r_1	1.9	220
r_2	3.2	29
r_3	15	36
r_4	1.4	2.2

The increases in intrinsic reaction rate can be caused by an increase in the catalyst activity, by an increase of the total number of active sites since this is included in the reaction rate constants, or by a combination of the two. Also an increase with a factor of up to 700 in the various adsorption constants is found going from PtCNF to PtCNF973. This indicates that after heat treatment the nature of the active sites has changed due to the removal of oxygen-containing groups. A working hypothesis based on the modeling results that can explain these differences in reaction rate and adsorption constants will be discussed in the last paragraph.

Concentration profiles in the catalyst particle

Using the parameters of the model we report the calculated concentrations profiles inside the catalyst particles in the course of the various cinnamaldehyde hydrogenation experiments (Figure 11a-d). In Figure 11c and d the concentration profiles of H_2 of around 260 mol/m^3 have been omitted. For both PtCNF and PtCNF973 the hydrogen concentration throughout the particle remains practically constant. In PtCNF973 during reaction large concentration gradients of the organic compounds exist, especially when low $[CALD]_0$ are used, giving rise to internal transport limitations. In Figure 11d the concentration profiles in a PtCNF particle are shown after 5 min reaction time when started with 14 mol/m^3 CALD. The concentration profiles here are much flatter than in 11 c, demonstrating that with catalyst PtCNF internal

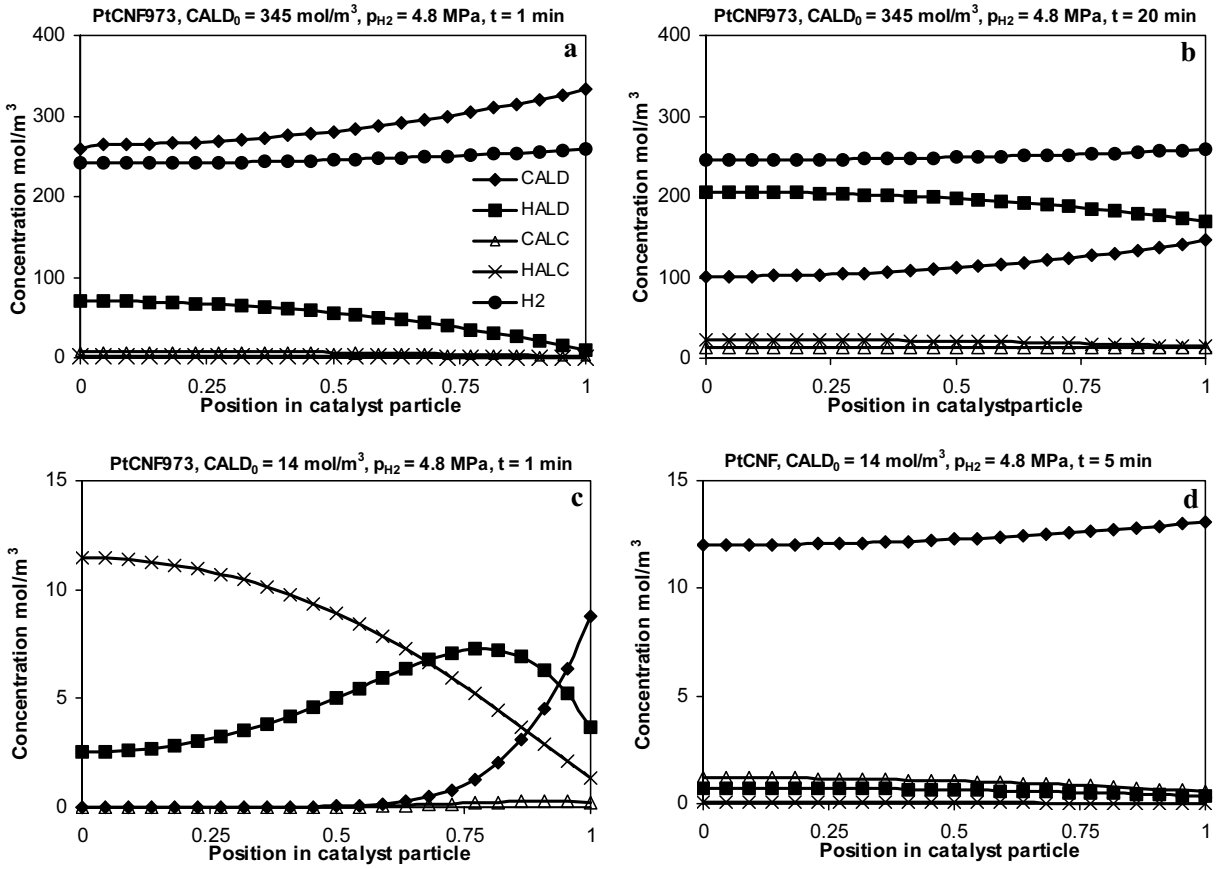

Figure 11. Calculated concentration profiles in catalyst particles during cinnamaldehyde hydrogenation reaction performed at 383 K and a hydrogen pressure of 4.8 MPa.

diffusion limitation is hardly apparent. For PtCNF973 internal diffusion limitation implies that the observed activity is much lower than the intrinsic activity. This is confirmed by ratios up to 120 in the intrinsic reaction rates found using kinetic modeling, much larger than the factor 8 of the observed reaction rates of PtCNF973 versus PtCNF.

Comparison of cinnamaldehyde hydrogenation activity with the literature

When we compare our results with those reported in the literature [37-39] for the hydrogenation of cinnamaldehyde over highly-dispersed platinum catalysts, we conclude that the activity we found with PtCNF973 is high (Table 4). The same conclusion can be drawn for our earlier reported RuCNF973 catalyst [11] when its performance is compared with that presented in literature. Also the TOF value for PtCNF973 is one of the highest, namely 3.3 s^{-1}. Only for a few catalysts with relatively large particles somewhat higher TOFs have been reported [37]. It is important to note that the conditions used for the measurements in the literature deviate ($\Delta T \sim 50$ K) from our own conditions. Therefore a straightforward comparison between the activities and TOFs is difficult. If the observed activity of PtCNF973 is recalculated to 333 K using an E_a of 34 kJ/mol [40] an activity of $14*10^{-4}$ $mol.s^{-1}.g_{Pt}^{-1}$ is found. However, the activity of our platinum catalyst treated at 973 K (PtCNF973) reported in Table 4 is the observed activity and since we demonstrated that internal mass transfer constraints limit the reaction rate of PtCNF973 the intrinsic activity and the related TOF are at least an order of magnitude larger.

Table 4. Comparison of observed activity in the selective hydrogenation of cinnamaldehyde at high pressure using *iso*-propanol as solvent over various unpromoted supported catalyst systems.

Catalyst	Loading (wt %)	d_{Pt} (nm)	P (MPa)	T (K)	C_{CALD} ($mol.l^{-1}$)	Solvent	Activity ($mol.s^{-1}.g_{Pt}^{-1}$)	TOF (s^{-1})	Ref.
Pt/AC	3.8	1.3	4.0	333	2.0	*i*-prop	$7.5*10^{-4}$	0.02	[39]
Pt/Graphite	3.6	1.3	4.0	333	2.0	/H_2O/Na -acetate	$7.8*10^{-4}$	0.02	
Pt/Graphite	3.6	1.3	4.0	333	2.0	*i*-prop	$7.7*10^{-4}$	0.19	[37]
Pt/Graphite	1.1	1.3	4.0	333	2.0	/H_2O/Na	$35*10^{-4}$	0.80	
Pt/Graphite	1.1	1-5	4.0	333	2.0	-acetate	$23*10^{-4}$	3.6	
Pt/AC	11.4	1.3	4.0	333	2.0		$6.7*10^{-4}$	0.17	
Pt/AC	1.1	1.3	4.0	333	2.0		$7.5*10^{-4}$	0.18	
Pt/AC	4.7	8	4.0	333	2.0		$1.9*10^{-4}$	0.36	
Pt/K-10	5	3.8	5.0	323	0.002	*i*-prop	$0.9*10^{-4}$	-	[38]
Pt/K-10	5	3.8	0.4	368	0.002		$0.4*10^{-4}$	-	
Pt/CNF	3.6	1.4	4.8	383	0.10	*i*-prop	**$8.8*10^{-4}$**	**0.23**	This
Pt/CNF973	3.6	2.3	4.8	383	0.10		**$69*10^{-4}$**	**3.3**	work

AC = activated carbon

K-10 = montmorillonite clay

Support effects on catalytic performance

In part I of our study on the influence of the oxygen-containing support surface groups on the performance of CNF-supported platinum catalysts in the hydrogenation of cinnamaldehyde we demonstrated that the amount of oxygen in the support does not influence the electronic state of the supported platinum to a large extent. Therefore we concluded that the changes in catalytic properties are not primarily induced by an electronic effect [10]. Our kinetic investigation reveals that with the removal of the oxygen from the graphite-like support the intrinsic reaction rates increase with a factor up to 120. It is difficult to discriminate whether this increase originates from an increase in the number of active sites or from an increase in intrinsic activity. This is because the reaction rate constants include the total number of active sites. H_2-chemisorption measurements and TEM demonstrate that the number of platinum sites is slightly smaller with PtCNF973, so it is impossible that an increase in the number of platinum active sites accounts for the strong increase in the reaction rate constants. However, if adsorption of the organic reactant with PtCNF973 can occur on the carbon support then the total number of adsorption sites may be enhanced. Nevertheless, it is unlikely that the total number of adsorption sites is increased by a factor of >100. Therefore we tentatively assign the increase in intrinsic reaction rates to both an increase in the total number of adsorption sites and an increase in the intrinsic activity.

Above observations and considerations are the basis for a model which can explain the enhanced activity for the high temperature treated catalyst. In Figure 12 a schematic representation of our working hypothesis is depicted. It is assumed that on a CNF-supported platinum catalyst with a large amount of oxygen-containing surface groups (PtCNF) adsorption and dissociation of hydrogen and adsorption of the organic reactants all have to take place on the platinum particles. In other words the adsorption of CALD on the polar carbon surface is weak. On the platinum particles hydrogenation sites are present and apparently the hydrogenation of CALD on the platinum is rather difficult. On the other hand,

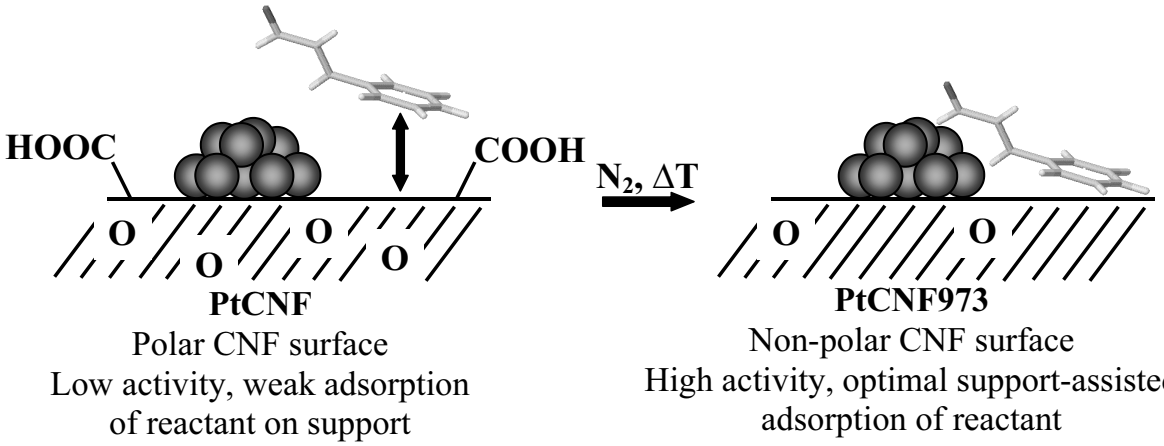

Figure 12. Schematic representation of CALD adsorption explaining the enhanced activity for the CNF-supported platinum catalyst after the removal of the majority of the oxygen-containing groups, by support-assisted catalysis.

when hardly oxygen groups are present (PtCNF973), reactant molecules adsorb with the benzene ring on the non-polar surface of the carbon nanofibers. We speculate that on the carbon surface other sites are present that can very efficiently hydrogenate C=C bonds. Hydrogen dissociation in all cases has to take place on the platinum particles. However, the organic reactants adsorbed in the vicinity of the platinum particles might easily and rapidly react with the hydrogen atoms adsorbed on the metal, resulting in an increased hydrogenation activity. So, hydrogenation is probably assisted by the CNF support due to adsorption of the substrate molecules on the surface. Theoretical calculations on the optimal geometrical configuration of CALD on the CNF surface, *cf.* [41], are needed to further study this proposition. Measurements of the heat of adsorption of CALD on the two catalysts can contribute to this discussion too.

Conclusions

Carbon nanofiber (CNF)-supported platinum catalysts with different concentrations of oxygen-containing surface groups on the support were employed to study the influence of these groups on the performance in the liquid-phase hydrogenation of cinnamaldehyde. The activity in this reaction was found to be strongly dependent of the amount of oxygen in/on the CNF support. The observed overall activity increased by a factor of 8 after removal of the majority of the oxygen groups by treatment at 973 K in inert atmosphere. This PtCNF973 catalyst exhibits a high activity compared to data reported in literature. The intrinsic activity of this catalyst is even at least an order of a magnitude larger, since internal diffusion limitations slows down the reaction rate.

As results of our earlier study demonstrated that the amount of oxygen in the support does not influence the electronic state of the supported platinum to a large extent, we concluded that the changes in catalytic behavior are not primarily caused by an electronic effect. Using a two-site model based on Langmuir-Hinshelwood kinetics and taking into account mass transfer constraints with respect to the organic compounds we found that the intrinsic reaction rates increase up to a factor of 120 when the oxygen groups are removed from the CNF surface. These results suggest that hydrogenation is assisted by adsorption of the cinnamaldehyde on the non-polar CNF support surface.

Notation

a mass transfer area per reactor volume, $m^2/m^3_{reactor}$
c concentration, mol/m^3
c_{cat} catalyst concentration, $g/m^3_{reactor}$
c_s bulk concentration, $mol/m^3_{reactor}$

D diffusion coefficient of diffusing compound in liquid, m^2/s
D_{eff} effective diffusivity, m^2/s
d_p catalyst particle diameter, m
k reaction rate constant, $mol/(m^3.s)$
k_L mass transfer constant, m/s
K adsorption equilibrium constant for compound on catalyst, m^3/mol
n reaction order, dimensionless
r reaction rate, $mol/(m^3_{cat}.s)$
r_p radius of the catalyst particle, m
$r_{w,obs}$ observed reaction rate, $mol/(s.kg_{cat})$
t time, s
z radial position in catalyst particle, m

Greek letters

Φ Weisz-Prater number
θ fractional occupation, dimensionless
ρ_{cat} catalyst density, g/m^3_{cat}
ρ_p catalyst particle density, kg/m^3

Subscripts

* empty organic compound site
\# empty hydrogen site
CALD cinnamaldehyde
CALC cinnamyl alcohol
cat catalyst
H_2 molecular hydrogen
HALC hydrocinnamyl alcohol
HALD hydrocinnamaldehyde
s bulk
sat saturation
x organic compound

References

1. P. Kluson and L. Cerveny, Appl. Catal. A Gen. 128 (1995) 13.
2. V. Ponec, Appl. Catal. A Gen. 149 (1997) 27.
3. B. Coq and F. Figueras, Coord. Chem. Rev. 178-180 (1998) 1753.
4. P. Gallezot and D. Richard, Catal. Rev.-Sci. Eng. 40 (1998) 81.

5. J. Hájek, N. Kumar, T. Salmi, D.M. Murzin, H. Karhu, J. Vayrynen, L. Cerveny and I. Paseka, Ind. Eng. Chem. Res. 42 (2003) 295.
6. A. Giroir-Fendler, D. Richard and P. Gallezot, Stud. Surf. Sci. Catal. 41 (1988) 171.
7. B. Coq, P.S. Kumbhar, C. Moreau, P. Moreau and M.G. Warawdekar, J. Mol. Catal. 85 (1993) 215.
8 . P.S. Kumbhar, B. Coq, C. Moreau, P. Moreau, J.M. Planeix and M.G. Warawdekar, Catalysis: Modern Trends (N.M. Gupta and D.K. Chakrabarty, Eds.) Narosa Publishing House, New Delhi 1995.
9. C.M.G. van de Moesdijk and M.A.R. Bosma, US Patent 4745234 (1988).
10. M.L. Toebes, Y. Zhang, J. Hájek, T.A. Nijhuis, J.H. Bitter, A.J. van Dillen, D.Yu. Murzin, D.C. Koningsberger and K.P. de Jong, in preparation / Chapter 7 of this thesis.
11. M.L. Toebes, F.F. Prinsloo, J.H. Bitter, A.J. van Dillen and K.P. de Jong, J. Catal. 214 (2003) 78 / Chapter 6 of this thesis.
12. D.E. Ramaker, J. de Graaf, J.A.R. van Veen and D.C. Koningsberger, J. Catal. 203 (2001) 7.
13. D.C. Koningsberger, J. de Graaf, B.L. Mojet, D.E. Ramaker and J.T. Miller, Appl. Catal. A Gen. 191 (2000) 205.
14. B.L. Mojet, J.T. Miller, D.E. Ramaker and D.C. Koningsberger, J. Catal. 186 (1999) 373.
15. R. Burch and A.R. Flambard, J. Catal. 78 (1982) 389.
16. R. Burch and A.R. Flambard, Stud. Surf. Sci. Catal. 11 (1982) 193.
17. M. Haruta, S. Tsubota, T. Kobayashi, M.J. Genet and B. Delmon, J. Catal. 144 (1993) 175.
18. J.-D. Grunwaldt and A. Baiker, J. Phys. Chem. B 103 (1999) 1002.
19. J.H. Bitter, K. Seshan and J.A. Lercher, J. Catal. 171 (1997) 279.
20. S. Galvagno, G. Capannelli, G. Neri, A. Donato and R. Pietropaolo, J. Mol. Catal. 64 (1991) 237.
21. Z. Poltarzewski, S. Galvagno, R. Pietropaolo and P. Staiti, J. Catal 102 (1986) 190.
22. L. Cerveny, Z. Belohlav and M.N.H. Hamed, Res. Chem. Intermed. 22 (1996) 15.
23. L. Zhang, J.M. Winterbottom, A.P. Boyes and S. Raymahasay, J. Chem. Technol. Biotechnol. 72 (1998) 264.
24. A.J. Marchi, D.A. Gordo, A.F. Trasarti and C.R. Apesteguia, Appl. Catal. A Gen. 249 (2003) 53.
25. E. Tronconi, C. Crisafulli, S. Galvagno, A. Donato, G. Neri and R. Pietropaolo, Ind. Eng. Chem. Res. 29 (1990) 1766.
26. G. Neri, L. Bonaccorsi, L. Mercadante and S. Galvagno, Ind. Eng. Chem. Res. 36 (1997) 3554.
27. T. Vergunst, F. Kapteijn and J.A. Moulijn, Catal Today 66 (2001) 381.

28. M.L. Toebes, J.H. Bitter, A.J. van Dillen and K.P. de Jong, Catal. Today 76 (2002) 33 / Chapter 2 of this thesis.
29. A.J. van Dillen, J.W. Geus, L.A.M. Hermans and J. van der Meijden, Stud. Surf. Sci. Catal. 2 (1977) 677.
30. M.L. Toebes, L.M. Tang, M.H. Huis in 't Veld, J.H. Bitter, A.J. van Dillen and K.P. de Jong, J. Phys. Chem. B, submitted / Chapter 5 of this thesis.
31. M.L. Toebes, J.M.P. van Heeswijk, J.H. Bitter, A.J. van Dillen and K.P. de Jong, Carbon, in print / Chapter 3 of this thesis.
32. R.J. Berger, E.H. Stitt, G.B. Marin, F. Kapteijn and J.A. Moulijn, Cattech 5 (2001) 30.
33. P. Gallezot and D. Richard, Catal. Rev.-Sci. Eng. 40 (1998) 81.
34. T.A. Nijhuis, G. van Koten, F. Kapteijn and J.A. Moulijn, Catal. Today 79-80 (2003) 315.
35. C.L. Young, R. Battino and R.W. Cargill, IUPAC Solubility data series Vol. 5/6 Hydrogen and Deuterium, Pergamon Oxford 1981.
36. C.R. Wilke and P. Chang, AIChE Journal 1 (1955) 4057.
37. D. Richard, P. Fouilloux and P. Gallezot, Proc. Int. Congr. Catal., 9th 3 (1988) 1074.
38. G. Szollosi, B. Torok, L. Baranyi and M. Bartok, J. Catal. 179 (1998) 619.
39. A. Giroir-Fendler, D. Richard and P. Gallezot, Stud. Surf. Sci. Catal. 41 (1998) 171.
40. J. Hájek, J. Wärnå and D.Yu. Murzin, Ind. Eng. Chem. Res., submitted.
41. F. Delbecq and P. Sautet, J. Catal. 220 (2003) 115.

9A

Summary and Concluding Remarks

In the quest for new and well-defined support materials for heterogeneous catalysts we explored the potential of carbon nanofibers (CNF). CNF belongs to the by now extensive family of synthetic graphite-like carbon materials with advantageous and tunable physico-chemical properties. Other members of this family are carbon nanotubes (CNT), single-walled carbon nanotubes (SWNT) and highly ordered pyrolytic graphite (HOPG). CNF can be obtained in a reproducible way by catalytic decomposition of a carbon-containing gas over small transition-metal particles from which the fibers grow due to deposition of carbon as a specific stacking of graphene sheets.

Aim of the work described in this thesis has been the exploration of the potential of CNF as catalyst support material, notably for platinum and ruthenium, and to reveal its role in the performance of these catalysts in hydrogenation reactions. A prerequisite for such a study was to synthesize well-defined CNF-supported catalysts. Therefore, very pure CNF were produced with a uniform diameter. For the application of the noble metals a reproducible preparation procedure has been designed resulting in a homogeneous distribution of small metal particles with a narrow particle size distribution. For investigating the effect of the surface properties of the CNF on the catalytic behavior a sensitive test reaction was needed in which both the influence of the catalyst properties on activity and selectivity could be observed. We have chosen for the selective hydrogenation of cinnamaldehyde.

In **Chapter 2** research aiming at a further extension of our knowledge on the formation of uniform CNF using various nickel catalysts was described. A systematic study has been

carried out on the influence of the metal particle size of the growth catalyst and the nature of the carbon-containing gas on the CNF growth and the microscopic and mesoscopic structure of the materials. CNF were catalytically grown by the decomposition of carbon-containing gases (CH_4, CO/H_2 or C_2H_4/H_2) over a silica-supported nickel catalyst and an unsupported nickel catalyst at 823 K. It turned out that both the nickel particle size and the nature of the carbon-containing gas significantly affected the CNF growth process. A continuous production of CNF was only possible when carbon deposition, diffusion and growth were in a subtle balance. We demonstrated that at the chosen temperature (823 K) small supported nickel particles (5-10 nm) exposing high-index planes needed a carbon-containing gas with a relatively low reactivity, like CH_4 or CO/H_2, to produce CNF. The resulting fishbone CNF had a uniform and small average diameter (25 nm). However, large unsupported nickel particles exposing low index-planes that are less efficient to dissociate CH_4 and CO/H_2, only produced CNF from a reactive carbon-containing gas, like C_2H_4/H_2. The CNF thus obtained showed a variety of morphologies with a large range of diameters (50-500 nm). These results underline that the quality of the CNF material firmly is connected to the properties of the growth catalyst.

Before applying the active phase the inert and non-polar CNF had to be activated in order to introduce oxygen-containing groups on the CNF surface, thus enhancing the wettability and making the surface more reactive. **Chapter 3** focused on the effects of this acid treatment on the graphite-like structure and texture of the CNF. The total number of oxygen groups and the number of acidic oxygen-containing groups introduced were determined using acid-base titration, TGA-MS and XPS. Oxidation was performed by refluxing the nanofibers in HNO_3 and mixtures of HNO_3/H_2SO_4 for different times. It was demonstrated that the graphite-like structure of the treated fibers remained intact, however, specific surface area and pore volume increased with the severity of the oxidation treatment. For the first time it was shown that the most predominant effect that gives rise to these textural modifications is the opening of the inner tubes of the fibers. Also we demonstrated that both the total oxygen content as well as the number of acidic surface groups introduced by the activation procedure depended strongly on the type of oxidizing agent used and the treatment time. Besides acidic oxygen groups (1-3.3 groups/nm^2) at the CNF exterior surface, oxygen was also built in in subsurface layer (2-3 nm) of the fibers. Moreover from the results it was clear that heat treatment of oxidized CNF in inert atmosphere at 973 K led to almost complete decomposition of the acidic oxygen-containing groups, while non-acidic oxygen groups remained present on/in the CNF.

We reviewed the literature on the synthesis of supported palladium catalysts in **Chapter 4**. Special attention has been paid to the interplay of relevant properties of (oxidic and carbon) supports and that of the appropriate precursor compounds. With oxide and carbon supports sol-gel, deposition-precipitation, deposition-reduction, ion exchange and impregnation methods have been reported in the literature. In general it turned out that irrespective the chosen application procedure the thermal treatment often dominated the ultimate metal dispersion. Thermal treatment in an inert atmosphere at temperatures not exceeding 773 K

prior to reduction was beneficial for the palladium dispersion. Gas-phase reduction led to smaller Pd particles than liquid-phase reduction. In our opinion large progress can be made in the development of highly loaded thermostable palladium catalysts by utilizing deposition-precipitation techniques in combination with anchoring sites on the support.

The results of this literature survey on carbon supports had given direction to our approach to solve the key problem in the synthesis of CNF-supported platinum and ruthenium catalysts. In **Chapter 5** we described the preparation of CNF-supported platinum and ruthenium catalysts by two different ion exchange techniques, one at a constant pH of ~ 6 (ion exchange) and one in which the pH is gradually increased from 3 to 6 by the hydrolysis of urea (HDP method). Using diluted precursor solutions with both synthesis techniques homogeneously distributed, highly dispersed and thermally stable metal particles were obtained with an average particle size of 1-2 nm. A striking finding was that with the HDP method substantially higher metal loadings (~ +100 %) could be obtained than with the ion exchange method. We speculated that this difference originated from the creation of additional adsorption sites due to hydrolysis of anhydridic carboxyl groups in the acidic environment at which the HDP procedure has been started. A linear relationship was found between the number of acidic oxygen groups on the CNF support and the obtained platinum loading using HDP. For the highest loaded catalyst a platinum/adsorption site ratio of 0.5 was established, corresponding to about 0.7 $Pt(NH_3)_4^{2+}$ molecules/nm^2. It was concluded that the acidic oxygen-containing groups do not only increase the wettability, but also act as anchoring sites for the metal precursor ions in the first step of the preparation. We suggested that the non-acidic oxygen groups avoid sintering of the metal particles, resulting in the high thermostability.

The results of Chapter 2 to 5 showed that our efforts to prepare well-defined CNF-supported catalysts with uniform small (1-2 nm) platinum or ruthenium particles with a narrow diameter distribution, in combination with a tunable number of support surface oxygenates has been successful. Using these systems we tried to gain more insight in the role of the oxygen-containing surface groups on their catalytic performance in the cinnamaldehyde hydrogenation. In **Chapter 6** we reported on the surprisingly strong influence of oxygen-containing surface groups on the activity and selectivity of carbon nanofiber (CNF)-supported ruthenium catalysts. For this study CNF were oxidized to introduce oxygen-containing groups and the metal precursor was applied using HDP. After reduction the catalysts were heat-treated in nitrogen at different temperatures to tune the amount of surface oxygen functional groups without significantly affecting the metal particle sizes. We found the overall activity strongly to increase after treatment at 973 K, which could be related to the decreasing number of oxygen-containing groups. Also a shift in selectivity from cinnamyl alcohol to hydrocinnamaldehyde was observed. Two models to explain the effect of the oxygen-containing groups were proposed; one implies an indirect influence *via* the metal while in the other model the oxygen groups directly influence catalysis by changing

the location and/or the mode of reactant adsorption. Both hypotheses were investigated in this work.

In **Chapter 7** we extended this work to CNF-supported platinum catalysts in the hydrogenation of cinnamaldehyde. For this catalyst system the effect of the surface oxygenates appeared even more pronounced than for the ruthenium catalysts. The observed overall catalytic activity increased by a factor of 25 with decreasing amount of oxygen on the fibers. The observed activity for the catalyst treated at 973 K is one of the highest reported in literature for this reaction and the intrinsic activity was even larger, since internal diffusion limitation slowed down the reaction rate for the most active catalyst. In order to shed more light on the exact nature of the influence of oxygen-containing surface groups XPS and H_2-chemisorption experiments were conducted. With these techniques no clear evidence has been found for a change in the electronic properties of the platinum particles. Therefore, we concluded that modification of the electronic properties of the metal is not the first cause of the large changes in catalytic behavior.

An alternative explanation involving a direct effect of the support surface composition on the mode and/or location of adsorption of cinnamaldehyde was discussed in **Chapter 8**. A model including both Langmuir-Hinshelwood kinetics and mass transfer effects was used to determine whether the changes in the catalyst support due to heat treatment could be quantified by relevant kinetic parameters. Two CNF-supported platinum catalysts with a narrow and stable platinum particle size distribution (1-2 nm) were used, one with a considerable amount and one with a much smaller amount of oxygen support surface groups. The performance of both catalysts was measured in the liquid-phase hydrogenation of cinnamaldehyde in a semi-batch reactor at 383 K using hydrogen pressures of 2.8–6.8 MPa and an initial CALD concentration in the range 14-345 mol/m^3. The intrinsic reaction rates increase up to factor 120 with the removal of the oxygen-containing surface groups. These results support the model in which hydrogenation is assisted by adsorption of the benzene ring of cinnamaldehyde on the non-polar CNF support surface after removal of the oxygen surface groups.

Summarizing, the results described in this thesis have shown the potential of CNF as catalyst support material for liquid-phase reactions. We succeeded in the production of well-defined CNF and the development of a method to reproducibly apply small, uniform and thermally stable ruthenium or platinum particles. These CNF-supported catalysts displayed unique high activities in the selective hydrogenation of cinnamaldehyde. Moreover, spectacular effects of support oxygen have been observed on catalysis; the intrinsic reaction rates increase with a factor of up to 120 with the removal of the oxygen-containing groups from the CNF surface probably by substrate adsorption on the support. Future research in this area could amongst others be devoted to the mode of adsorption of cinnamaldehyde on the CNF and to tuning of the CNF-supported catalysts in such a way that a high selectivity to the desired product (cinnamylalcohol) can be obtained.

9B

Samenvatting en Conclusies

In de zoektocht naar nieuwe en goedgedefinieerde dragermaterialen voor heterogene katalysatoren hebben we de mogelijkheden van het gebruik van kooldraden (‘carbon nanofibers’, CNF) bestudeerd. Kooldraden behoren bij de inmiddels omvangrijke familie van synthetische koolstofmaterialen, die verwant zijn met grafiet, met gunstige en instelbare fysisch-chemische eigenschappen. Koolstofnanobuizen (CNT), enkelwandige koolstofnanobuizen (SWNT) en geordend grafiet (HOPG) zijn andere leden van deze familie. Kooldraden kunnen reproduceerbaar gesynthetiseerd worden door het katalytisch ontleden van koolstofhoudende gassen op kleine overgangsmetaaldeeltjes waaruit de draden groeien door afzetting van koolstof in een specifieke stapeling van grafietvlakken.

Doel van dit onderzoek was het bestuderen van de gebruiksmogelijkheden van kooldraden als dragermateriaal voor onder meer platina en ruthenium en de rol van de drager op de activiteit en selectiviteit van deze katalysatoren in hydrogeneringsreacties. De beschikbaarheid van goedgedefinieerde kooldraadgedragen katalysatoren was een voorwaarde voor dergelijk onderzoek. Om die reden werden er kooldraden geproduceerd met een smalle diameter-verdeling. Voor het afzetten van edelmetalen moest een reproduceerbare methode ontwikkeld worden waarmee een homogene verdeling van kleine metaaldeeltjes met een smalle deeltjes-grootteverdeling kon worden verkregen. Er was tevens een gevoelige testreactie nodig waarmee het effect van de eigenschappen van de katalysator op zowel de activiteit als de selectiviteit waargenomen kan worden. Wij hebben gekozen voor de selectieve hydrogenering van kaneelaldehyde.

In **Hoofdstuk 2** is het onderzoek beschreven naar de synthese van uniforme kooldraden uit verschillende nikkelkatalysatoren. Een systematische studie is uitgevoerd naar de invloed van de deeltjesgrootte van het metaal van de groeikatalysator, alsmede de aard van het

koolstofhoudende gas op de kooldraadgroei en de fysisch-chemische eigenschappen van de resulterende kooldraden. De kooldraden werden katalytisch geproduceerd door middel van de ontleding van koolstofhoudende gassen (CH_4, CO/H_2 of C_2H_4/H_2) op een silicagedragen nikkelkatalysator en op een ongedragen nikkelkatalysator bij 823 K. Uit dit onderzoek is gebleken dat zowel de deeltjesgrootte van het nikkel als de aard van het koolstofhoudende gas een belangrijke rol spelen tijdens het kooldraadgroeiproces. Continue groei van kooldraden is alleen mogelijk wanneer de vorming van koolstofatomen, diffusie en groei in balans zijn. Wij hebben laten zien dat bij de gekozen temperatuur kleine gedragen nikkeldeeltjes met hoge indexvlakken slechts kooldraden groeien uit een weinig reactief gas, zoals CH_4 en CO/H_2. De resulterende kooldraden zijn uniform en hebben een kleine gemiddelde diameter (25 nm). De grote ongedragen nikkeldeeltjes met voornamelijk lage indexvlakken aan de buitenkant blijken minder goed in staat om CH_4 en CO/H_2 te ontleden. Met deze katalysator kunnen alleen kooldraden geproduceerd worden met behulp van een reactief gas, zoals C_2H_4/H_2. Deze kooldraden vertonen een verscheidenheid aan morfologieën en hebben een brede diameterverdeling (50-500 nm).

Voordat op de inerte en apolaire kooldraden een actieve fase aangebracht kon worden werden de kooldraden geactiveerd, d.w.z. er werden zuurstofgroepen ingebouwd om het oppervlak reactiever en hydrofieler te maken. **Hoofdstuk 3** richt zich op het effect van deze behandeling op de textuur en grafietachtige structuur van kooldraden. De totale hoeveelheid zuurstof en het aantal zure zuurstofgroepen dat aanwezig was in/op de kooldraden na de oxidatie werden bepaald door middel van zuur-base titraties, TGA-MS en XPS. In dit onderzoek zijn de kooldraden geoxideerd door ze gedurende verschillende tijden te refluxen in HNO_3 en mengsels van HNO_3/H_2SO_4. Gebleken is dat de grafietachtige structuur van de kooldraden tijdens de activering intact blijft. Het specifiek oppervlak en het porievolume neemt daarentegen toe met de sterkte van de oxidatiebehandeling. Als eersten hebben we laten zien dat de voornaamste oorzaak voor deze veranderingen in de textuur het openen van de binnenbuizen van de kooldraden is. Ook is aan het licht gekomen dat zowel de totale hoeveelheid zuurstof als het aantal zure zuurstofgroepen een functie zijn van het type zuur dat gebruikt wordt voor de oxidatie en de duur van de oxidatie. Naast zure zuurstofgroepen (1-3.3 groepen/nm^2), wordt er ook zuurstof ingebouwd in de oppervlaktelaag (2-3 nm) van de kooldraden. Bovendien lieten de resultaten zien dat een hittebehandeling van geactiveerde kooldraden in een inerte atmosfeer resulteert in een bijna volledige ontleding van de zure zuurstofgroepen, terwijl de niet-zure zuurstofgroepen aanwezig blijven in/op de kooldraden.

In **Hoofdstuk 4** worden de resultaten van een literatuurstudie naar de synthese van gedragen palladiumkatalysatoren weergegeven. In het bijzonder is aandacht besteed aan het samenspel van de relevante eigenschappen van de (oxidische en koolstof) dragermaterialen en van de geschikte precursors. Voor het afzetten van palladium op koolstof en op oxidische dragermaterialen zijn in de literatuur onder andere sol-gel-, depositie-precipitatie-, depositie-reductie-, ionenuitwisseling- en impregnatiemethodes toegepast. In het algemeen kan gezegd worden dat onafhankelijk van de gekozen methode een hittebehandeling een belangrijke invloed heeft op de uiteindelijke metaaldispersie. Een behandeling in een inerte atmosfeer tot 773 K voor de reductie blijkt bevorderlijk voor de palladiumdispersie. Bovendien blijkt gasfasereductie te leiden tot kleinere

palladiumdeeltjes dan een reductie in de vloeistoffase. Wij stellen voor dat grote vooruitgang geboekt kan worden in de ontwikkeling van hoog beladen, thermisch stabiele palladiumkatalysatoren door gebruik te maken van depositie-precipitatie technieken in combinatie met een dragermateriaal waarop voldoende ankerplaatsen voor de metaalprecursor aanwezig zijn.

De resultaten van het literatuuronderzoek naar koolstofdragermaterialen zijn gebruikt om een plan van aanpak op te stellen voor de synthese van kooldraadgedragen platina- en rutheniumkatalysatoren. In **Hoofdstuk 5** beschreven we de bereiding van kooldraadgedragen platina- en rutheniumkatalysatoren d.m.v. twee verschillende ionenuitwisselingsmethodes, één bij constante pH ~ 6 (ionenuitwisseling) en één waarbij de pH geleidelijk toeneemt van 3 naar 6 door de ontleding van ureum (HDP methode). Gebruikmakend van verdunde precursoroplossingen kunnen met beide methodes homogeen verdeelde, hoog disperse en thermisch stabiele metaaldeeltjes verkregen worden met een gemiddelde deeltjesgrootte van 1-2 nm. Opvallend is dat met HDP aanzienlijk hogere metaalbeladingen (~ +100 %) verkregen kunnen worden dan met ionenuitwisseling. Wij vermoeden dat dit verschil veroorzaakt wordt door het ontstaan van extra adsorptieplaatsen door het hydrolyseren van anhydridegroepen bij de lage pH waarbij HDP gestart wordt. Voor de platinakatalysatoren bereid met HDP werd een lineair verband waargenomen tussen het aantal zure zuurstofgroepen op de kooldraden en de uiteindelijke platinabelading. Tevens werd voor de katalysator met de hoogste belading een verhouding platina/adsorptieplaats vastgesteld van 0.5 wat overkomt met 0.7 $Pt(NH_3)_4^{2+}$ moleculen/nm^2. De zure zuurstofgroepen verbeteren niet alleen de bevochtiging, maar dienen ook als ankerplaatsen voor de metaalprecursorionen in de eerste stap van de bereiding. Zeer waarschijnlijk voorkomen de niet-zure zuurstofgroepen sintering van de metaaldeeltjes en hebben de katalysatoren daardoor een hoge thermische stabiliteit.

De resultaten gepresenteerd in Hoofdstuk 2 t/m 5 tonen aan dat we er in geslaagd zijn om goedgedefinieerde kooldraadgedragen katalysatoren te synthetiseren met uniforme kleine (1-2 nm) platina- of rutheniumdeeltjes met een smalle deeltjesgrootteverdeling in combinatie met een variabele hoeveelheid zuurstofgroepen op de drager. Gebruikmakend van deze katalysatoren hebben we geprobeerd meer inzicht te krijgen in de rol van de zuurstofgroepen op de hydrogenering van kaneelaldehyde. In **Hoofdstuk 6** wordt de verrassend grote invloed van de zuurstofgroepen op de activiteit en selectiviteit van kooldraadgedragen rutheniumkatalysatoren besproken. In dit onderzoek hebben we de kooldraden geoxideerd om zuurstofhoudende groepen te introduceren en m.b.v. HDP werd de metaalprecursor aangebracht. Na reductie werden de katalysatoren behandeld in stikstof bij verhoogde temperatuur om de hoeveelheid zuurstofgroepen te variëren zonder een noemenswaardige verandering in de deeltjesgrootte van het metaal. De resultaten tonen aan dat na behandeling bij 973 K de totale activiteit sterk toe nam, waarschijnlijk door een afnemend aantal zuurstofhoudende groepen. Tevens werd een verschuiving in de selectiviteit van kaneelalcohol naar hydrokaneelaldehyde waargenomen. Twee modellen zouden het effect van de zuurstofgroepen kunnen verklaren. In het eerste model oefent de zuurstof indirect invloed uit via het metaal en in het andere model beïnvloedt de zuurstof de katalyse rechtstreeks door de plaats en/of manier van adsorptie van de reactant. Beide hypothesen zijn bestudeerd in dit werk.

In **Hoofdstuk 7** wordt werk beschreven met kooldraadgedragen platinakatalysatoren in de hydrogenering van kaneelaldehyde. Het effect van de zuurstofgroepen is voor deze katalysatoren zelfs nog sterker dan voor de rutheniumkatalysatoren. De waargenomen totale katalytische activiteit nam met een afnemende hoeveelheid zuurstofgroepen toe met een factor 25. De waargenomen activiteit voor de katalysator behandeld bij 973 K is één van de hoogst gerapporteerde waarden in de literatuur voor deze reactie. De intrinsieke activiteit blijkt zelfs nog hoger: diffusie van kaneelaldehyde binnen de deeltjes limiteert de reactiesnelheid van de meest actieve katalysator. Om meer duidelijkheid te krijgen over de exacte aard van de invloed van de zuurstofhoudende groepen werden XPS- en waterstofchemisorptie-experimenten uitgevoerd. Met deze technieken werd geen bewijs gevonden voor een sterke verandering van de elektronische eigenschappen van de platinadeeltjes. Daarom kan geconcludeerd worden dat de grote veranderingen in activiteit en selectiviteit van de katalysatoren waarschijnlijk niet veroorzaakt worden door veranderingen in de elektronische eigenschappen van het metaal.

Een alternatieve verklaring waarin de samenstelling van het oppervlak van de kooldraden een directe invloed heeft op de plaats en/of manier van adsorptie van kaneelaldehyde wordt besproken in **Hoofdstuk 8**. Een model dat zowel Langmuir-Hinshelwood kinetiek- en transporteffecten beschrijft is gebruikt om de veranderingen in het katalysatordragermateriaal, veroorzaakt door de temperatuurbehandeling, te kwantificeren in relevante kinetische parameters. Twee kooldraad-gedragen platinakatalysatoren met een smalle en stabiele deeltjesgrootteverdeling (1-2 nm) werden gebruikt, één met een grote hoeveelheid zuurstofgroepen en één met een aanzienlijk lager aantal zuurstofgroepen op het kooldraadoppervlak. De prestatie van beide katalysatoren werd gemeten in de vloeistoffasehydrogenering van kaneelaldehyde in een semibatch reactor bij 383 K met een waterstofdruk van 2.8-6.8 MPa en een initiële kaneelaldehyde concentratie van 14-345 mol/m^3. De intrinsieke reactiesnelheden namen toe (tot factor 120) met het verwijderen van de zuurstofgroepen van de kooldraden. De resultaten ondersteunen een model waarin de hydrogenering bevorderd wordt door adsorptie van de benzeenring van het kaneelaldehyde op het niet-polaire kooldraadoppervlak na verwijderen van de zuurstofgroepen.

De resultaten van het onderzoek beschreven in dit proefschrift laten zien dat kooldraden een veelbelovend katalysatordragermateriaal zijn voor vloeistoffasereacties. We zijn erin geslaagd om goedgedefinieerde kooldraden te synthetiseren en om een methode te ontwikkelen om op een reproduceerbare manier kleine uniforme en thermisch stabiele ruthenium- en platinadeeltjes aan te brengen. Deze kooldraadgedragen katalysatoren vertonen hoge activiteiten in de selectieve hydrogenering van kaneelaldehyde. Bovendien is het effect van zuurstofgroepen op de drager, waargenomen in de hydrogenering van kaneelaldehyde spectaculair; de intrinsieke reactiesnelheden namen met een factor tot 120 toe door het verwijderen van de zuurstofgroepen van het oppervlak van de kooldraden waarschijnlijk vanwege adsorptie van het substraat op het oppervlak. Verder onderzoek op dit gebied zou zich onder andere kunnen richten op de manier waarop het kaneelaldehyde adsorbeert op de kooldraden en op het optimaliseren van de eigenschappen van de kooldraadgedragen katalysatoren zodat een hoge selectiviteit naar het gewenste product (kaneelalcohol) verkregen kan worden.

List of Publications and Presentations

Publications

M.L. Toebes, A.J. van Dillen and K.P. de Jong 'Synthesis of Supported Palladium Catalysts - A Review' J. Mol. Catal. A Chemical 173 (2001) 75-98.

M.L. Toebes, J.H. Bitter, A.J. van Dillen and K.P. de Jong 'Impact of the Structure and Reactivity of Nickel Particles on the Catalytic Growth of Carbon Nanofibers' Catal. Today 76 (2002) 33-42.

M.L. Toebes, F.F. Prinsloo, J.H. Bitter, A.J. van Dillen and K.P. de Jong 'Synthesis and Characterization of Carbon Nanofiber-Supported Ruthenium Catalysts' Stud. Surf. Sci. Catal. 143 (2002) 201-208.

M.L. Toebes, F.F. Prinsloo, J.H. Bitter, A.J. van Dillen and K.P. de Jong 'Influence of Oxygen-Containing Surface Groups on the Activity and Selectivity of Carbon Nanofiber-Supported Ruthenium Catalysts in the Hydrogenation of Cinnamaldehyde' J. Catal. 214 (2003) 78-87.

M.L. Toebes, J.M.P. van Heeswijk, J.H. Bitter, A.J. van Dillen and K.P. de Jong 'The Influence of Oxidation on the Texture and the Number of Oxygen-Containing Surface Groups of Carbon Nanofibers' Carbon, in print.

M.L. Toebes, L.M. Tang, M.H. Huis in 't Veld, J.H. Bitter, A.J. van Dillen and K.P. de Jong 'Preparation of Carbon Nanofiber-Supported Platinum and Ruthenium Catalysts - Comparison of Ion Exchange and Homogeneous Deposition Precipitation' J. Phys. Chem. B, submitted.

Y. Zhang, M.L. Toebes, A. van der Eerden, W.E. O'Grady, K.P. de Jong and D.C. Koningsberger 'Metal Particle Size and Structure of the Metal-Support Interface of Carbon-Supported Platinum Catalysts as Determined with EXAFS Spectroscopy' J. Phys. Chem. B, submitted.

M.L. Toebes, Y. Zhang, J. Hájek, T.A. Nijhuis, J.H. Bitter, A.J. van Dillen, D.Yu. Murzin, D.C. Koningsberger and K.P. de Jong 'Support Effects in the Hydrogenation of Cinnamaldehyde over Carbon Nanofiber-Supported Platinum Catalysts - Part I: Catalysis and Characterization' in preparation.

M.L. Toebes, T.A. Nijhuis, J. Hájek, J.H. Bitter, A.J. van Dillen, D.Yu. Murzin, and K.P. de Jong 'Support Effects in the Hydrogenation of Cinnamaldehyde over Carbon Nanofiber-Supported Platinum Catalysts - Part II: Kinetic Study' in preparation.

E. Crezee, B.W. Hoffer, P.R.M. Mooijman, B. van der Linden, J.C. Groen, M.L. Toebes, K.P. de Jong, F. Kapteijn and J.A. Moulijn 'Selective Hydrogenation of D-Glucose over Ruthenium Catalysts' in preparation.

Oral Presentations

M.L. Toebes, F.F. Prinsloo, J.H. Bitter, A.J. van Dillen and K.P. de Jong 'Selective Hydrogenation of Cinnamaldehyde over Carbon Nanofiber-Supported Ruthenium Catalysts' 3rd Netherlands' Catalysis and Chemistry Conference, Noordwijkerhout, The Netherlands, March 2002.

M.L. Toebes, F.F. Prinsloo, J.H. Bitter, A.J. van Dillen and K.P. de Jong 'Synthesis and Characterization of Carbon Nanofiber-Supported Ruthenium Catalysts' 8th International Symposium on the Scientific Bases for the Preparation of Heterogeneous Catalysts, Louvain-la-Neuve, Belgium, September 2002.

M.L. Toebes 'Platinum on Carbon Nanofibers - Support-Assisted Catalysis?' NIOK Symposium the Future of the Dutch Catalysis Institute, Utrecht, The Netherlands, September 2003.

M.L. Toebes, J. Hájek, T.A. Nijhuis, J.H. Bitter, A.J. van Dillen, D.Yu. Murzin and K.P. de Jong 'Platinum on Carbon Nanofibers - Support-Assisted Catalysis?' 5th Netherlands' Catalysis and Chemistry Conference, Noordwijkerhout, The Netherlands, March 2004.

Poster Presentations

M.L. Toebes, J.H. Bitter, A.J. van Dillen and K.P. de Jong 'Tailoring of Carbon Nanofibers for Use as Catalyst Support' 2nd Netherlands' Catalysis and Chemistry Conference, Noordwijkerhout, The Netherlands, March 2001.

M.L. Toebes, J.H. Bitter, A.J. van Dillen and K.P. de Jong 'Catalytic Synthesis of Carbon Nanofibers – Tuning of the Physico-Chemical Properties' 5th European Congress on Catalysis, Limerick, Ireland, September 2001.

M.L. Toebes, Y. Zhang, J.H. Bitter, A.J. van Dillen, D.C. Koningsberger and K.P. de Jong 'Influence of Oxygen-Containing Surface Groups in Carbon Nanofiber-Supported Platinum Catalysts' 4th Netherlands' Catalysis and Chemistry Conference, Noordwijkerhout, The Netherlands, March 2003.

M.L. Toebes, F.F. Prinsloo, J.H. Bitter, A.J. van Dillen and K.P. de Jong 'Selective Hydrogenation of Cinnamaldehyde over Carbon Nanofiber-Supported Ruthenium and Platinum Catalysts' 18th North American Catalysis Society Meeting, Cancun, Mexico, June 2003.

Dankwoord

Met de laatste bladzijden van dit boekje nadert ook het einde van mijn promotietijd. Het is een ontzettend leuke, onvergetelijke en leerzame periode geweest, die ik nooit alleen had kunnen/willen volbrengen. Ik wil daarom ook iedereen bedanken die op enige wijze heeft bijgedragen aan dit proefschrift.

Krijn, ik heb onze samenwerking als bijzonder prettig ervaren. Jouw grenzeloze enthousiasme, je goede begeleiding en het vertrouwen dat je mij gegeven hebt, hebben mij zeker geholpen om gemotiveerd en positief te blijven. Ik ben blij dat ik de kans heb gehad om van jouw kennis en ervaring te leren. Diek, ook jij bedankt voor je samenwerking. Onze levendige discussies zullen me zeker bijblijven. Jos, de hoeveelheid correctiewerk die je (zonder ooit te mopperen) voor mij verricht hebt is enorm. Ik kon altijd even binnenlopen om een vraag te stellen, je wat resultaten te laten zien of om incidenteel even wat stoom af te blazen. Ik heb je grote inzet en interesse zeer gewaardeerd. Harry, jij hebt dan geen officiële functie binnen mijn promotieonderzoek, toch heb jij ook een belangrijke rol gespeeld bij het tot stand komen van dit proefschrift. We hebben heel wat uurtjes gediscussieerd over wetenschap en over meer onnozele zaken. Ook wil ik alle leden van de CW/STW-gebruikerscommissie bedanken voor hun nuttige suggesties en opbouwende kritiek.

Verder wil ik de studenten die aan mijn onderzoek meegewerkt hebben niet onvermeld laten. Ferry, jouw scriptie vormde de basis voor een gedeelte van het inleidende hoofdstuk. Bastiaan, de door jouw bereide uniforme nikkelkatalysatoren, waren erg waardevol. Jürgen, ik verwacht dat jouw titratie-methode (hoofdstuk 3) ook nog door andere kooldraadcollega's gebruikt gaat worden. Kees, aanbrengen van ijzer op kooldraden was moeilijker dan verwacht. Bedankt voor je pogingen. Lai Mei en Marije, jullie hebben heel wat platina op kooldraden af moeten zetten, maar het is gelukkig niet voor niets geweest (hoofdstuk 5).

Daarnaast gaat mijn dank uit naar alle mensen buiten de Universiteit Utrecht waarmee ik in de afgelopen periode heb mogen samenwerken. Frans Prinsloo (Sasol), your work on the deposition of ruthenium on carbon nanofibers and the first hydrogenation experiments have been of great importance for my research. Shell (Heiko Oosterbeek en Gert Jonkers) wil ik bedanken voor het uitvoeren van XPS experimenten. De katalyseresultaten zoals beschreven in hoofdstuk 6 heb ik gemeten bij DSM Research. Hiervoor gaat mijn speciale dank uit naar Henk Oevering en Martin Zilverstand. I would also like to express my thanks to Jan Hájek and Prof. Murzin of the Åbo Akademi University (Finland) for helping with the hydrogenations and for their valuable comments. The excellent quality of the data is displayed in chapter 7 and 8.

Binnen de universiteit en de sectie ben ik ook ontzettend veel mensen dank verschuldigd. Yihua, thank you for the pleasant cooperation. Xander, zonder jou was hoofdstuk 8 nooit tot stand gekomen. Je hebt me met een oneindig geduld geïntroduceerd in de wereld van het kinetisch modelleren. Verder heb ik alle hulp en metingen van Cor (TEM), Prof. Geus (TEM), Marjan (SEM), Vincent (H_2-chemisorptie), Ad^M (XPS en N_2-physisorptie), Leendert (burn-off proeven),

Onno (XPS) en Fred (TGA-MS) erg gewaardeerd. Ad^{vE}, Jeroen, Harry, Laurens, Pieter, Yaying en Yihua, bedankt voor jullie medewerking en gezelligheid tijdens de EXAFS metingen in Hamburg. Prof. van Egmond en Ruud Dijkman (sectie Membraan Enzymologie) worden bedankt voor het beschikbaar stellen van de titratie-apparatuur en het meedenken over de experimenten. De medewerkers/sters van de glasblazerij, elektronica, de werkplaats en de AV-dienst: alle hand- en spandiensten die jullie in de jaren voor mij verricht hebben, heb ik erg geapprecieerd. Verder zou ik nog graag langs deze weg Ans, Thea^{vO}, Dymph, Monique en Thea^{P} willen bedanken voor allerlei (zeker niet onbelangrijke) organisatorische zaken.

De afgelopen jaren heb ik het geluk gehad mijn kantoor te mogen delen met andere 'kooldraad-fielen'. Marije (o.a. voor de af en toe noodzakelijke vrouwenpraat), Tijmen (zowel voor een goed gesprek als een leuke grap), Leendert (wijnexpert en gasbelteller) en Stefan (mijn partner in crypto's), jullie zijn alle vier compleet verschillende persoonlijkheden, maar ik heb jullie allemaal erg leren waarderen. Ik heb de sfeer op onze kamer altijd als zeer prettig ervaren en ik hoop dat ik jullie met mijn geklets niet te veel van het werk gehouden heb.

Naast het werk was er op de vakgroep ook altijd ruimte voor de nodige ontspanning. Ik wil daarom ook alle collega's hartelijk bedanken voor de gezelligheid tijdens de pauzes, LIITs, BBQs, congressen, vrijdagmiddagborrels, vakgroepsuitjes, cursussen en spontane terrasbezoekjes /etentjes. Ook heb ik erg genoten van de diverse sport- en spelactiviteiten, zoals de Toerpool, de Teammaster en Topcoach (ik ben nog hopeloos op zoek naar een nieuwe strategie). De squashers (Harry, Bibi, Rudy en Gerbrand) mijn excuses voor alle blauwe plekken. Marije, Sander, Michiel, Jules en Tijmen (de 'Catanners') binnenkort weer een potje Steden en Ridders? Ries, Dennis, Gerbrand, Karen, Marije en Jules (de 'Pub Quizzers') het is de hoogste tijd om bij Mr. Balls die Life Size Furby (voor Dennis) te winnen. Ik hoop dat jullie je niet gestoord hebben aan mijn (soms misschien iets te) competitieve instelling.

Moniek, bedankt dat ik, toen ik nog niet in Utrecht woonde, altijd bij je kon logeren als we eens een feestje hadden. Kom je binnenkort weer een keer eten? Dennis, voor jouw is ook een mooie toekomst weggelegd. Probeer de zon eens wat vaker in het water te zien schijnen. Bert, New Wave is echt niet mijn ding, ik hou het toch bij Heather Nova en Coldplay ;-). Jules, je hebt op de belangrijke momenten laten zien dat je een echte vriend bent. Harry en Helma (mijn Nico en Mirna), ik wil jullie heel erg bedanken voor jullie fijne vriendschap.

Mijn paranimfen, Inge en Nicole, ik ken jullie allebei al meer dan 25 jaar en jullie hebben me altijd door dik en dun gesteund. Inge, vroeger konden we nog wel eens flink ruzie maken, maar sinds we allebei uit huis zijn is er een hechte vriendschap ontstaan die ik erg waardeer (Thomas, jij bent ook een lieverd). Nicole, als buurmeisjes zijn we samen opgegroeid en hebben we veel (zowel leuke als minder leuke dingen) meegemaakt. Je bent een geweldige vriendin!

Oma, bedankt voor alle gezellige logeerpartijtjes en zaterdagmiddagen. Je bent de allerliefste oma die ik me kan wensen.

De allerlaatste regels wil ik gebruiken om mijn ouders te bedanken. Papa en Mama, jullie hebben mij altijd onvoorwaardelijk gesteund en heel veel liefde gegeven. Ik kom nog altijd ontzettend graag thuis om weer eens lekker bij te praten, samen koffie te drinken bij 'de Vleugel' of om Papa te helpen met een PS2 probleem. Ik hou van jullie!

Marjolein

Curriculum Vitae

Marjolein Toebes werd geboren op 23 juli 1975 te Winterswijk. In 1993 behaalde zij het VWO diploma aan de Rijksscholengemeenschap Hamaland te Winterswijk. In september van datzelfde jaar begon zij met de studie Hoger Laboratorium Onderwijs (HLO) aan de Hogeschool Enschede met als specialisatie Analytische Chemie. Een stage en afstudeeronderzoek werden gedurende tien maanden uitgevoerd bij Akzo Nobel Central Research in Arnhem op de afdeling Chromatografie (Dr. M.A.H. de Zwart). Het diploma werd in juni 1997 *met lof* behaald. Vervolgens begon zij in augustus 1997 met de verkorte studie Scheikunde aan de Universiteit Utrecht. Het doctoraal examen, met als hoofdvak Anorganische Chemie en Katalyse (Prof. J.W. Geus), werd afgelegd *met genoegen* in augustus 1999. Vanaf oktober 1999 was zij werkzaam als Assistent in Opleiding (AIO) in de sectie Anorganische Chemie en Katalyse (Prof. K.P. de Jong, Prof. D.C. Koningsberger en Dr. A.J. van Dillen) van de Universiteit Utrecht. De verkregen onderzoeksresultaten staan beschreven in dit proefschrift.